METASOMATISM ASSOCIATED WITH THE NORTH QOROQ CENTRE, SOUTH GREENLAND

DAVID ALEXANDER RAE

Doctor of Philosophy

ASTON UNIVERSITY

November 1988

METASOMATISM ASSOCIATED WITH THE NORTH QOROQ CENTRE, SOUTH GREENLAND

by
David Alexander Rae

Submitted for the degree of Doctor of Philosophy
November 1988

Summary

This thesis describes the alkali metasomatism and fenitisation associated with the North Qoroq nepheline syenite centre in the Gardar alkaline igneous province of South Greenland.

Alkali metasomatism occurs both within the syenite centre and in the country rocks of granite-gneiss, quartzitic sandstones and basalt lavas. Within the syenite centre the metasomatism produces distinctive petrographic textures. The mafic minerals develop a characteristic poikilitic texture, a feature seen less commonly in the felsic phases which tend to recrystallise to a fine grained feldspathoidal matrix.

The metasomatic activity produces significant changes in whole-rock chemistry and a detailed discussion is given of computational methods in the representation of whole-rock chemical change. One approach is adopted for the examination of the metasomatic changes and it is shown that the metasomatism took place at near constant volume and was dominated by desilicification coupled with addition of sodium.

Examination of the felsic phases in the syenite centre demonstrates the usefulness of cathodoluminescence microscopy in studying textural changes during the metasomatism of the feldspars. The causes of luminescence are examined and it is shown that the presence of red luminescent albite is indicative of fluid activity in the rock. Where reaction with the metasomatising fluid is most intense, nepheline and sodalite are formed at the expense of K-feldspar while albite remains in the rock and occurs in a granular mosaic with the feldspathoids.

Modification of mafic silicate compositions indicates that the metasomatism in the syenites was initially under the influence of Na- and volatile-rich fluids at relatively high temperature and low oxygen fugacity. Differences in magmatic mineral assemblages and localised reactions in micro-environments gave rise to a patchy and variable metasomatism. Decreasing temperature and increasing oxygen fugacity led to the later formation of acmitic pyroxene. The mafic mineralogy developed in the country rocks shows that higher oxygen fugacities prevailed, and with decreasing temperature produced riebeckite, acmite and haematite.

Fluid inclusion studies indicate that more than one fluid phase was active in and around the North Qoroq centre and mixing between magmatic and meteoric fluids is suggested. Apatite chemistry demonstrates that the rare earth elements are mobile during the metasomatism and were probably transported in fluorine and/or carbonate complexes.

It is proposed that maximum temperatures of metasomatism were no higher than 650^{oc} in the syenites and quartzite and less than 500^{oc} in the granite-gneiss and fluid activity persisted to at least 100^{oc}. The fluids emanating from the syenites were initially very sodium-rich, silica-poor and had low oxygen fugacity. Fluid evolution from the syenites was by continuous fractionation to a fluorine-rich magmatic residue.

Comparisons are drawn with other Gardar centres and alkaline igneous centres around the world and suggestions are made for future research topics.

Key Words - alkali-metasomatism, Gardar, syenite, mineralogy, fluid-phase

Acknowledgements

I thank Dr. A.D. Chambers for encouragement and supervision throughout the project and for acting as field assistant during the summer of 1986. The Greenland Geological Survey are thanked for considerable logistical assistance with fieldwork and the transportation of rock samples. Financial support was provided by a Natural Environment Research Council grant (No. GT4/85/GS/5) and is gratefully acknowledged. Professor D.D. Hawkes provided research facilities at the University of Aston.

The following people are all thanked for valuable assistance with the analytical work in the thesis : Dr P.G. Hill, Dr D.M. Russell and Dr. J.A. Craven for assistance with electron microprobe analysis at the Grant Institute of Geology, University of Edinburgh ; B. Kamalludin and Dr G. Walker for running cathodoluminescence spectra in the Department of Pure and Applied Physics, UMIST ; Dr R.A. Mason for running ion probe analyses of feldspars at the Department of Geology, Cambridge University ; A. Warren and J. Barker for assistance with the inductively coupled plasma spectrometry analysis at the Department of Geology, RHBNC ; J. Kinnaird and Dr P. Bowden for assistance with fluid inclusion analysis at the Department of Geology, University of St Andrews.

The technical staff in the Department of Geology, University of Aston are thanked for their assistance. J. Coundon and B. Brueton prepared the thin sections and probe sections, R. Wightman assisted with XRF analysis and A. Mistry assisted with the photography. R.G. Howell in the Department of Metallurgy gave help and tuition in the use of electron microprobes.

Thanks go to the postgraduates in the department, whose friendship throughout the course of study is greatly appreciated, especially A. Swarbrick and H. Dorans for moral support when it was most needed.

Finally, I am very grateful to my parents for considerable moral and financial support and for always being there when needed.

Contents

List of Figures

List of Plates

List of Tables

CHAPTER 1

Introduction

1.1 Aims and objectives

The thesis continues research on the Igaliko nepheline syenite complex. The specific aims of this project are to look at metasomatism associated with the intrusion of the syenites of the North Qoroq centre and determine how this has affected pre-existing rocks of varying chemistry and mineralogy.

The objectives of the project are to : (a) produce criteria for the recognition of metasomatic influences in pre-existing alkaline igneous rocks, (b) characterise in detail the whole-rock chemical variation associated with the metasomatism of the syenites and country rocks, (c) examine the chemical variation in the major mineral phases (feldspar, pyroxene, amphibole and biotite) of the syenites and country rocks, (d) from the magmatic and metasomatic mineral chemistry 'trends' evaluate the significance of possible controlling factors such as fugacity of oxygen and peralkalinity and (e) study the mobility of 'residual' trace elements (eg. rare earth elements, Zr, Y, Nb) in the metasomatic fluids.

The various lines of evidence allow conclusions to be drawn on the changes occuring during the metasomatism, the nature of the metasomatising fluid and ultimately on the late-stage crystallisation and fluid evolution in the North Qoroq syenites.

1.2 Previous investigations

The nepheline syenites of the Igaliko Complex were known from the late nineteenth century and are mentioned by early workers such as Steenstrup and Kornerup (1881) and Flink (1898) but the first detailed mapping of the syenites was undertaken by Ussing and Boggild (Ussing 1894, 1912). Wegmann visited the area between Qoroq and Narsarsuaq in the 1930's (Wegmann 1938), but the most detailed systematic mapping was done by the Greenland Geological Survey (G.G.U.). The Igaliko Complex was mapped by Emeleus and Harry in the summer field seasons of 1961,

1962, 1963 and 1966 (Emeleus and Harry 1970). During the 1970's detailed geochemical and mineralogical studies were carried out on all four of the Igaliko nepheline syenite centres. Stephenson (1972, 1974, 1976) examined the South Qoroq centre, Chambers (1976) the North Qoroq centre, Powell (1978) the Igdlerfigssalik centre and Jones (1980) the Motzfeldt centre. The work on North Qoroq examined in detail the petrogenesis and crystallisation history of the syenites and made some preliminary observations on the effects of metasomatism associated with the centre. This thesis continues that research and makes a detailed investigation of the metasomatic activity.

1.3 Alkali metasomatism (fenitisation)

The definition of the term 'fenitisation' has changed significantly since it was first introduced by Brogger (1921). He first gave the name 'fenite' to rocks that were originally of granitic composition and had been metasomatically altered towards rocks of an alkali-syenitic composition by solutions emanating from an ijolite-melteigite magma. McKie (1966) noted that the term had since acquired a wider meaning and was generally used to cover the whole spectrum of widespread metasomatism of rocks of varied composition closely associated with carbonatite complexes. Fenitisation, as it is used at the present day, has even wider applicability and is defined as the alkali metasomatism of country rocks surrounding intrusions of carbonatite and/or alkaline rocks. Fenitisation is a specific example of metasomatism, which has the more general definition of the alteration of pre-existing rocks by a fluid phase, involving net chemical changes in the rock. For the purpose of this thesis, a distinction is made between the two terms in which fenitisation refers specifically to the alteration of the country rocks whereas metasomatism is used as a general term for the alteration of all rock types.

Historically, any metasomatic alteration of the igneous rocks from which the fenitising fluids emanate has been neglected while there have been numerous studies of the fenitisation itself. von Eckermann's account of Alno (1948) remains a classic study of the process of fenitisation while the general review by McKie (1966) gave the first detailed discussion of mineral chemistry. A method for the representation of whole-rock chemical

change was also proposed which is still used to the present day (see Chapter 3). Gresens (1967) derived a general metasomatic equation for the recalculation of chemical analyses and the quantitative assessment of mass transfer during metasomatism (see Chapter 3). The study of amphibole and pyroxene variations in fenites from East Africa by Sutherland (1969) is an important account of mineral chemistry and one of the first attempts to relate the observed assemblages to experimentally defined P-T-X stability fields. Recent work includes that of Kresten and Morogan (1986) and Kresten (1988) who re-examined fenitisation at the type locality of Fen, Norway.

1.4 Techniques

Various techniques and approaches have been adopted in the study of the metasomatism and fenitisation associated with the North Qoroq centre. Chapter 2 gives an account of the summer field season of 1986 during which over 300 samples were collected. A selected number of these were used in further laboratory studies and Chapter 2 also describes the petrography of the altered rocks and summarises the main features of the unaltered rocks. The geochemical and mineralogical evidence necessary to prove metasomatism is presented in later chapters and the whole-rock chemical variation associated with the metasomatism is examined in Chapter 3 where a comprehensive discussion is given of computational methods in the recalculation of chemical analyses and the representation of mass balance. The samples were all analysed for 10 major and 18 trace elements by standard X-ray fluorescence techniques (see appendix 2). Chapter 4 studies the mineral chemistry and textures of the alkali feldspars in the metasomatised syenites. The uses of cathodoluminescence microscopy in the study of metasomatic processes is discussed in detail and some implications for the nature of the fluid phase are drawn from the feldspar alteration. All mineral analyses were carried out by electron probe microanalysis (EPMA). The luminescence was examined by spectral techniques and this was related to chemistry using these and with the aid of ion probe analyses of Ti in the feldspars. The modification of the mafic silicate compositions is discussed in Chapter 5 and again all analyses are by standard EPMA methods. Conclusions are drawn on the

significance of parameters such as oxygen fugacity, temperature and peralkalinity. A combination of EPMA, inductively coupled plasma spectrometry (ICPS) and fluid inclusion studies are used in Chapter 6 to examine the rare earth element chemistry of apatites, whole-rock rare earth element variations and temperatures and salinities of the metasomatic fluids. Conclusions are reached on the anion content of the fluids and the role of complexing in material transfer. The results of the thesis are drawn together and discussed in Chapter 7. Some speculation is given on the late-stage evolution of the syenites and comparisons are drawn both with other Gardar centres and alkaline igneous centres around the world. A review is given of some previous work on metasomatism and fenitisation and, finally, a brief model is presented to account for the metasomatism and fenitisation seen in and around the North Qoroq centre.

References

Brogger, W.C. 1921. Die eruptivgesteine des Kristianiagebietes, IV., Das Fengebiet in Telemark. NORSK VIDENSK SELSK SKRIFTER I, MATH NATURV K1 **No 9**, 408pp.

Chambers, A.D. 1976. The petrology and geochemistry of the North Qoroq centre, Igaliko Complex, South Greenland. UNPUBL PhD THESIS, UNIV OF DURHAM.

Emeleus, C.H. & Harry, W.T. 1970. The Igaliko Nepheline Syenite Complex: general description. MEDDEL OM GRON **Bd 186 Nr 3.**

Flink, G. 1898. Berattelse om en Mineralogisk Resa i Syd-Gronland sommaren 1897. MEDDEL OM GRON **Bd 14 Nr 2.**

Gresens, R.L. 1967. Composition-volume relationships of metasomatism. CHEM GEOL **2**, 47-65.

Jones, A.P. 1980. The petrology and structure of the Motzfeldt Centre, Igaliko, South Greenland. UNPUBL PhD THESIS, UNIV OF DURHAM.

Kresten, P. 1988. The chemistry of fenitisation : examples from Fen, Norway. CHEM GEOL **68**, 329-51.

Kresten, P. & Morogan, V. 1986. Fenitisation at the Fen complex, southern Norway. LITHOS **19**, 27-42.

McKie, D. 1966. Fenitisation. *In* Tuttle, O.F. & Gittins, J. (eds) *Carbonatites*, 261-94. New York: Wiley-Interscience.

Powell, M. 1978. The crystallization history of the Igdlerfigssalik nepheline syenite intrusion, Greenland. LITHOS **11**, 99-120.

Steenstrup, K.J.V. & Kornerup, A. 1881. Beretring om expeditionen til Julianehaabs distrikt; 1876. MEDDEL OM GRON **Bd 2 Nr 1**.

Stephenson, D. 1972. Alkali clinopyroxenes from nepheline syenites of the South Qoroq Centre, South Greenland. LITHOS **5**, 187-201.

Stephenson, D. 1974. Mn and Ca enriched olivines from nepheline syenites of the South Qoroq Centre, South Greenland. MINERAL MAG **46**, 283-300.

Stephenson, D. 1976. The South Qoroq nepheline syenites, South Greenland: petrology, felsic mineralogy and petrogenesis. BULL GRONLANDS GEOL UNDERS **118**.

Sutherland, D.S. 1969. Sodic amphiboles and pyroxenes from fenites in East Africa. CONTRIB MINERAL PETROL **24**, 114-35.

Ussing, N.J. 1894. Mineralogisk-petrografiske Undersogelser af Gronlandske Nefelinsyeniter og beslaegtede Bjaergarter. Anden del: De Kiselsyrefattige Hovedminerdles. MEDDEL OM GRON **Bd 14 Nr 1**.

Ussing, N.V. 1912. Geology of the country around Julianehaab, Greenland. MEDDEL OM GRON **Bd 38**.

von Eckermann, H. 1948. The alkaline district of Alno Island. SVER GEOL UNDERS **Ca 36**, 176pp.

Wegmann, C.E. 1938. On the structural divisions of southern Greenland. MEDDEL OM GRON **Bd 133 Nr 2**.

CHAPTER 2

General Geology, Fieldwork and Petrography

2.1 General Setting and Geology

2.1.1 The Igaliko Complex

The Igaliko complex is one of a number of major complexes to be found in the Gardar province of South Greenland. Reviews of the Proterozoic alkaline province have been produced by Upton (1974), Emeleus and Upton (1976) and Upton and Emeleus (1987) and a detailed account of the Igaliko complex is given by Emeleus and Harry (1970). Only a brief summary, therefore, will be given here of the general setting of Gardar magmatism and the place of the Igaliko complex within this activity.

The Gardar igneous province (Figure 2.1) is the result of intra-plate alkaline magmatism in southern Greenland in the period 1320-1120Ma, related to rifting of the supercontinent that comprised North America, Greenland and Europe (Upton and Emeleus 1987). Gardar igneous rocks occur as relict lava successions, dyke swarms and central intrusive complexes. Typical Gardar dykes consist of transitional or mildly alkaline olivine basalt and hawaiite and more evolved compositions such as trachyte, phonolite and carbonatite, whereas the central complexes comprise salic alkaline rocks. There are about ten central complexes varying from alkali granite through to foyaite. Augite syenite is common, and probably played a parental role in most of the central complexes, which then evolved along a silica-undersaturated or a silica-oversaturated trend.

The Igaliko complex consists of four major syenite centres, all of which are undersaturated. The four centres cover almost the full time-span of Gardar activity, with the North Qoroq and Motzfeldt centres representing early Gardar activity and the South Qoroq and Igdlerfigsalik centres middle to late activity. The age relationship between North Qoroq and Motzfeldt is uncertain as the age difference determined by Rb-Sr isotopes is covered by the error bars (Blaxland *et al.* 1978). All four centres are made up of a number of generally concentric units.

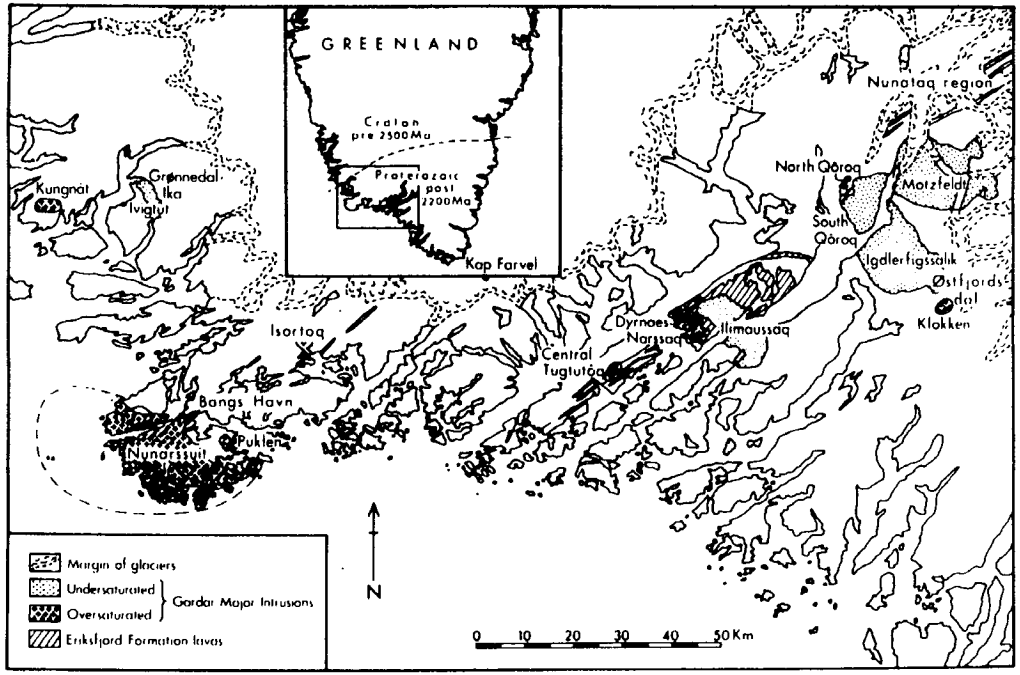

Figure 2.1 General geological map of the Gardar alkaline igneous province, showing the location of the Igaliko Complex and the North Qoroq centre. Reproduced from Upton and Emeleus (1987).

2.1.2 The North Qoroq Centre

The North Qoroq centre, situated adjacent to the airport of Narsarsuaq (Figure 2.2), is the smallest and most north-westerly of the four centres and has been dated at 1295±61Ma (Blaxland *et al.* 1978). To the north the centre cuts the gneissose granites and granodiorites of the Julianehab Granite complex dated at ~1800Ma (van Breemen *et al.* 1974) and to the west the early Gardar sediments and lavas of the Eriksfjord formation. The southern boundary, partly intrusive and partly faulted, is formed by the younger South Qoroq centre (1185±8Ma, Blaxland *et al.* 1978). To the east the contacts are obscured by Qoroq fjord and the steep cliffs bounding the fjord, though a reconnaisance survey in summer 1986 suggested that the North Qoroq centre may be cut by the outer unit of the Motzfeldt centre in this area.

The North Qoroq centre consists of six major units designated SN1A to SN5 in order of emplacement (Figure 2.3). The unit originally numbered SN3 (Emeleus and Harry 1970) is now thought to be an altered variant of SN1B. The syenites were intruded at a high crustal level and all show undersaturated character. Emplacement of the bodies was probably by ring fracture and block subsidence, combined with a degree of stoping. The outer contacts of the syenites are steep and outward dipping where lower levels are exposed (Plate 2.1) but become flatter and more complex in the roof zones. Petrographic, mineralogical and geochemical studies (Chambers 1976) have demonstrated that in situ crystal fractionation accounts for the bulk of the variation in rock types. The most important fractionating phase was alkali feldspar, the crystallisation and separation of which resulted in the syenites becoming increasingly peralkaline and undersaturated. An alkali-rich fluid phase appears to have been active during the late-stage evolution of the most fractionated North Qoroq syenitic magmas, resulting in metasomatism within the centre, at times masking and overprinting the magmatic crystal fractionation effects.

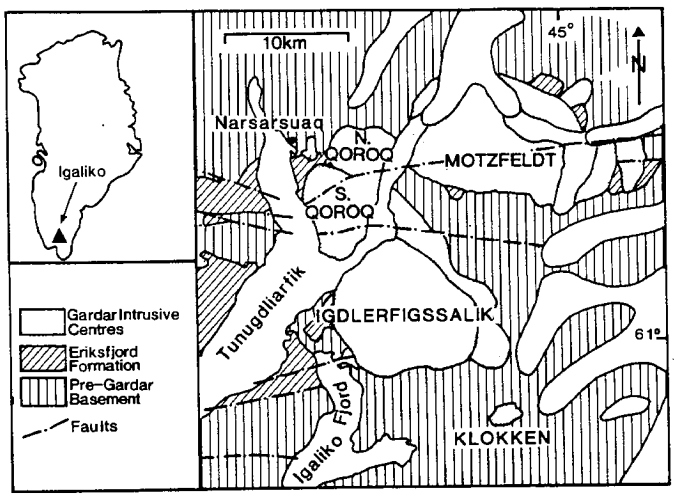

Figure 2.2 Simplified map of the Igaliko nepheline syenite complex, showing the four centres: North Qoroq, South Qoroq, Motzfeldt and Igdlerfigssalik.

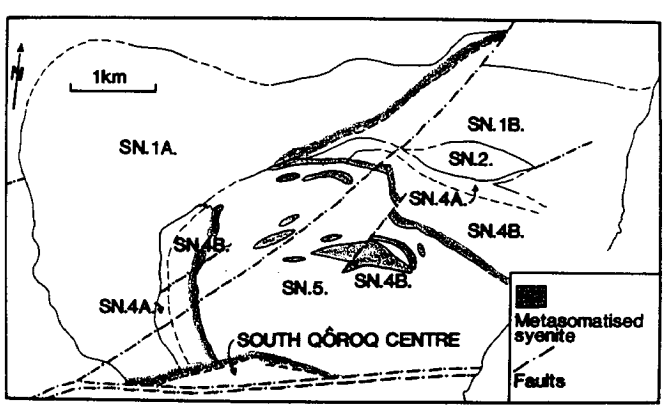

Figure 2.3 Geological map of the North Qoroq centre, showing the individual units constituting the centre and the principal areas of metasomatised syenite.

Plate 2.1 The steep, outward dipping outer contact of the North Qoroq nepheline syenite centre viewed from the neighbouring Motzfeldt centre.

2.2 Fieldwork

2.2.1 Introduction and Logistics

A concise account of the field relations found in North Qoroq, and in the Igaliko Complex as a whole, was given by Emeleus and Harry (1970). Chambers (1976) detailed further observations on the North Qoroq centre. This section gives an account of the summer field season of 1986 and introduces observations relevant to the metasomatism within and around the centre.

An excellent base camp was established near the old hospital site at the Narsarsuaq road end and a second camp was established on the plateau of the North Qoroq centre. This enabled four or five days fieldwork to be carried out from the plateau before the samples collected were taken down to the base camp and fresh provisions were taken back up. In this way the steep and arduous climbs out of the valley were kept to a minimum, resulting in more work time and the completion of the fieldwork in only four and a half weeks. The excellent weather also contributed with only one day being lost due to low cloud. Both the mosquitoes and black fly, though, remain a constant problem and irritation.

The fieldwork was carried out using aerial photographs rather than maps due to the poor quality of the latter. The photographs covered the Narsarsuaq area and the corresponding map is sheet V.3 of the Danish Geodetic Institute's maps. The vast majority of equipment was provided by the Greenland Geological Survey who also provided sample boxes and arranged for the collection of the rock samples from Narsarsuaq and their delivery to Britain. Basic provisions were obtainable from the store at Narsarsuaq.

The aim of the field season was to sample metasomatised and recrystallised material from the North Qoroq syenites and the surrounding country rocks. The major sampling areas, therefore, were along syenite-syenite contacts and around the margins of the intrusion. Where possible systematic traverses were taken away from contacts.

2.2.2 The Julianehab Granite

The Julianehab Granite is the basement rock in the Narsarsuaq area and forms the majority of the country rocks to the syenites (Emeleus and Harry 1970). The main area of sampling was in the area to the west of the long lake at 550m and from there along the contact towards Narsarsuaq (Figure 2.4). Traverses were also taken in the Narsarsuaq valley and one at locality 18. West of the long lake the contact appears to be shallow and is very complex, indicating exposure near the roof zone of the outer syenite, SN1A. The syenite veins the granite and there are several granite xenoliths that have been included in the syenite. As the granite/gneiss syenite contact is followed away from the long lake increasingly lower levels are exposed and the contact becomes steeper and much less complex with a simple cross-cutting relationship to the granite. Metasomatic alteration is characterised by a cloudy, recrystallised appearance of the felsic minerals, a reduction in the quartz content, an increased abundance of biotite and the growth of small needles of mafic minerals.

2.2.3 The Eriksfjord Formation

The Eriksfjord Formation comprises an interbedded sequence of sediments and lavas. The sedimentary rocks are marked simply as one unit on the geological map but they are in fact a very varied sequence of conglomerates, sandstones (some quartzitic) and siltstones. The metasomatic alteration varies depending on the nature of the rock being altered. Massive, coarse-grained quartzites are characterised by a very patchy alteration in which some areas can be quite unaffected while other areas are extensively veined and recrystallised with numerous pods of mafic minerals. The more impure sediments tend to preserve original sedimentary features such as conglomerate bands, large scale cross bedding, fine lamination and load structures. The alteration of these rocks is more pervasive, commonly with a spotted growth of new mafic minerals. The main areas of sampling were in the Narsarsuaq valley adjacent to both the North and

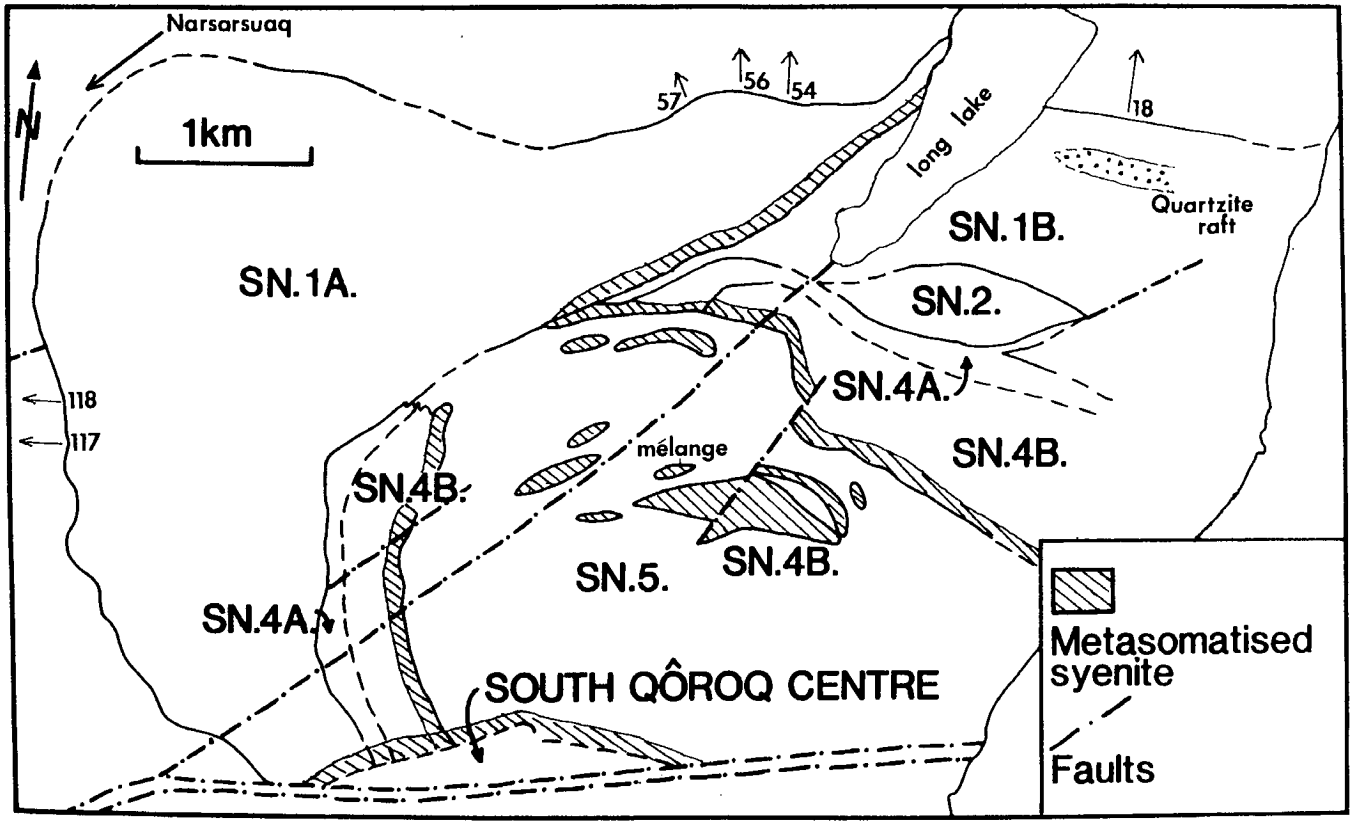

Figure 2.4 Geological map of the North Qoroq centre, showing localities of granite-gneiss traverse sampling (numbered arrows), the quartzite raft, the melange and the long lake.

South Qoroq syenites and from a large quartzite raft stoped into unit SN1B east of the long lake at 550m (see Figure 2.4). In the vicinity of the contact with the South Qoroq centre the syenite intrudes the Eriksfjord formation sediments along bedding planes in the form of sills and veins. Where the veining is extensive, banding is formed with some bands resulting from the apparent syenitisation of the sediment. These complex contact relationships and the presence of rafts of sedimentary material in the syenites indicate that the roof zone of the North Qoroq centre was close to, and possibly controlled by, the contact between the basement Julianehab Granite and the overlying Eriksfjord formation.

2.2.4 The Syenites

Metasomatic effects are not restricted to the country rocks but occur within the centre, where a later unit intrudes an earlier one. Metasomatic alteration is characterised in hand specimen by the recrystallised, saccharoidal appearance of the feldspars and the spotted growth of poikilitic mafic minerals. The best developments of metasomatised rocks occur where the South Qoroq centre cuts the outer syenite, unit SN1A of North Qoroq, where SN5 intrudes SN4 and where SN1B intrudes SN1A. In addition, less fractionated parts of the outer syenite (SN1A) display patchy auto-metasomatism. Sampling of the syenites was therefore restricted to these areas. The area within SN5 termed 'the melange' (Emeleus and Harry 1970) was also sampled (see Figure 2.4). The melange is a complex area of rafts of SN4 included in SN5, indicating exposure at a high structural level. Where SN4 is metasomatised by SN5 the original phenocrysts are recrystallised and at the contacts mixing between the two units often imparts a very streaky appearance to the rock. The contact between SN1B and SN1A runs close to the west side of the long lake and covers a zone some 50m wide from the first appearance of xenoliths of SN1A in SN1B to the last appearance of SN1B. This broad contact zone again suggests that the contact is relatively flat lying and exposed near the roof zone of SN1B. Some of the xenoliths of SN1A are themselves xenolithic and comprise coarsely recrystallised syenite with small finer-grained syenite inclusions. It is possible that the latter are original roof chill pendants in SN1A which later collapsed into the still molten core of the unit. Most of the xenoliths

are irregularly shaped, but rounded, indicating a degree of resorption. Fluorite is common as patches and veins along the contact between SN1A and SN1B and also associated with unit SN5 as late cross-cutting veins or small plugs.

The field studies on the North Qoroq centre provide abundant evidence that many units are exposed near their roof zones (eg. abundance of xenoliths, flat-lying complex contact zones and sill- and dyke-like bodies of syenite extending into the country rock). As any late fluids generated within a unit are likely to rise upwards it is this feature that makes the centre suited to the study of metasomatism.

2.2.5 Sample Selection

All the areas described above were extensively sampled during the field season and over 300 samples were collected. Of these only a selected number could be used in further laboratory studies and certain areas of metasomatism were concentrated on. Within the syenite centre, the contact zones between units SN1B and SN1A and between units SN5 and SN4 were studied. The study of the Julianehab Granite was restricted largely to samples taken as traverses in the area to the west of the long lake, near the roof zone of the outer syenite unit, SN1A. Examination of the Eriksfjord Formation was restricted to the massive, pure quartzites which provided a tight control on protolith composition. The sequence of impure sediments and lavas adjacent to the North and South Qoroq centres provide an area for future work.

2.3 Petrography

2.3.1 Introduction

Chambers (1976) gave detailed petrographic descriptions of the unaltered syenites of the North Qoroq centre and an introduction to the petrography of the recrystallised rocks. In the following section a brief summary will be given of the major features of the unaltered rocks, for comparison with the descriptions of the textures and mineralogy produced during the metasomatism. The petrographic observations described

here will be of a general nature and features relevant to a specific mineral group will be emphasised at the start of the appropriate chapter.

2.3.2 Unit SN1A

2.3.2.1 Primary Magmatic Variation

The outer syenite of North Qoroq, SN1A, is a large unit with a present outcrop area of about 10km^2. Prior to the intrusion of adjacent centres and younger units within the North Qoroq centre it would have been of much greater aerial extent. The syenite body shows substantial variation with a progressive and gradational change from a narrow marginal augite syenite, only mildly undersaturated, through to a highly evolved, thoroughly undersaturated, peralkaline interior.

The mafic phases in the marginal augite syenite are fayalitic olivine rimmed by magnetite, pale green ferro-augite and brown titanian hastingsitic hornblende. These phases occur in mafic clusters together with titanomagnetite and apatite. Biotite, where present, rims magnetite and probably formed by sub-solidus reaction. Towards the more fractionated interior of the unit the assemblage rapidly changes. Olivine disappears and the dominant pyroxene is now aegerine-augite or in the most evolved rocks aegerine. Amphibole is a green pleochroic katophorite or a blue arfvedsonitic alkali amphibole. The pyroxene becomes highly interstitial, occuring as anhedral wedges between the felsic phases.

The felsic mineralogy shows similar changes although alkali feldspar is the dominant phase throughout the unit. In the marginal augite syenite it occurs as irregular crystals with interlocking rims and is crypto- or micro-perthitic. Towards the centre of the unit the feldspars are tabular and more coarsely perthitic. Nepheline, only present as small interstitial areas in the marginal rocks, occurs as abundant large euhedral crystals and is joined by significant quantities of sodalite, analcite and cancrinite.

2.3.2.2 Secondary Variation Associated with the Fluid Phase

Rocks of the outer part of SN1A have been subject to the action of a late-stage fluid and as a result mafic and felsic phases developed characteristic textures. The textures and mineralogy vary from section to section but there are general features common to all the metasomatic rocks. The most striking feature is the pronounced development of a poikilitic texture. The mafic phases can form large poikilitic crystals up to 1cm across with a euhedral outline. In the incipient stages of metasomatism the mafic clusters, typical of the unaltered syenite, are still present and the effects of the fluid phase are less obvious. Ferro-augite is embayed or corroded and is sometimes rimmed by aegerine-augite which also occurs interstitially between the alkali feldspars. Both the ferro-augite and the brown amphibole are rimmed by green pleochroic amphibole.

In the sections showing advanced metasomatism the mafic clusters have disappeared and the rock is dominated by the large poikilitic mafic minerals. This growth appears to take one of two forms, either dominated by alkali amphibole or by pyroxene. Some sections show large poikilitic crystals of blue/green alkali amphibole rimmed by aggregates of acmite or poikilitic acmite (Plate 2.2). Intergrown with the acmite are numerous small crystals of biotite and some small aenigmatites. Also, intimately associated with the other mafic minerals is poikilitic aenigmatite. Poikilitic aggregates of acmite and biotite are found, formed by the complete alteration of amphibole, and poikilitic aenigmatite occurs in the groundmass. The felsic groundmass in these sections is usually rich in feldspathoids such as sodalite and analcite. Alternatively, the section is dominated by large poikilitic crystals of aegerine-augite (Plate 2.3). There are occasional cores of poikilitic alkali amphibole. Enclosed in the aegerine-augite there are crystals of biotite and opaques and aggregates of alkali pyroxene+biotite+opaques are common. Small crystals of aegerine-augite and biotite are also occasionally found in the groundmass. There is only minor aenigmatite. The felsic mineralogy in these sections is dominated by relict perthite, albite and nepheline. The textures developed in the felsic mineralogy in response to the fluid phase are described in detail in Chapter 4. They range from the initial coarsening of the perthitic alkali feldspar to its complete

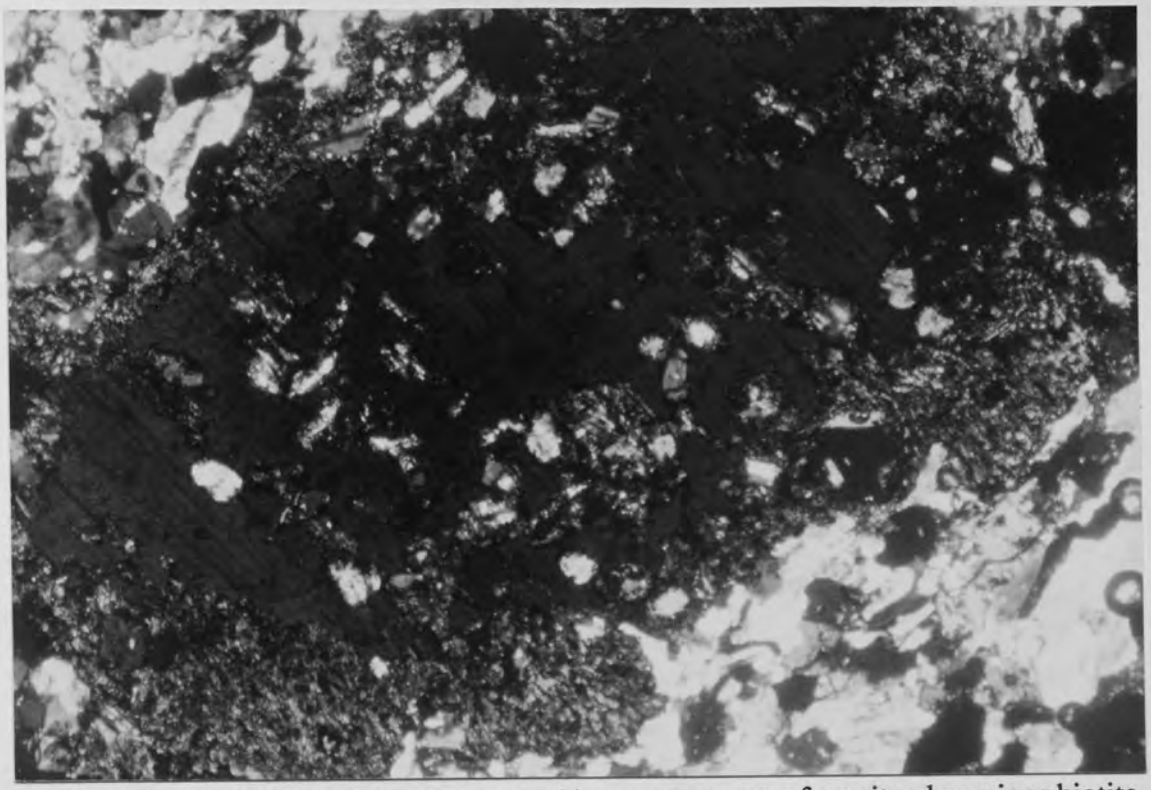

Plate 2.2 Poikilitic amphibole rimmed by an aggregate of acmite plus minor biotite in metasomatised SN1A. Sample taken from the SN1A/SN1B contact zone. Width of field of view = 0.89mm.

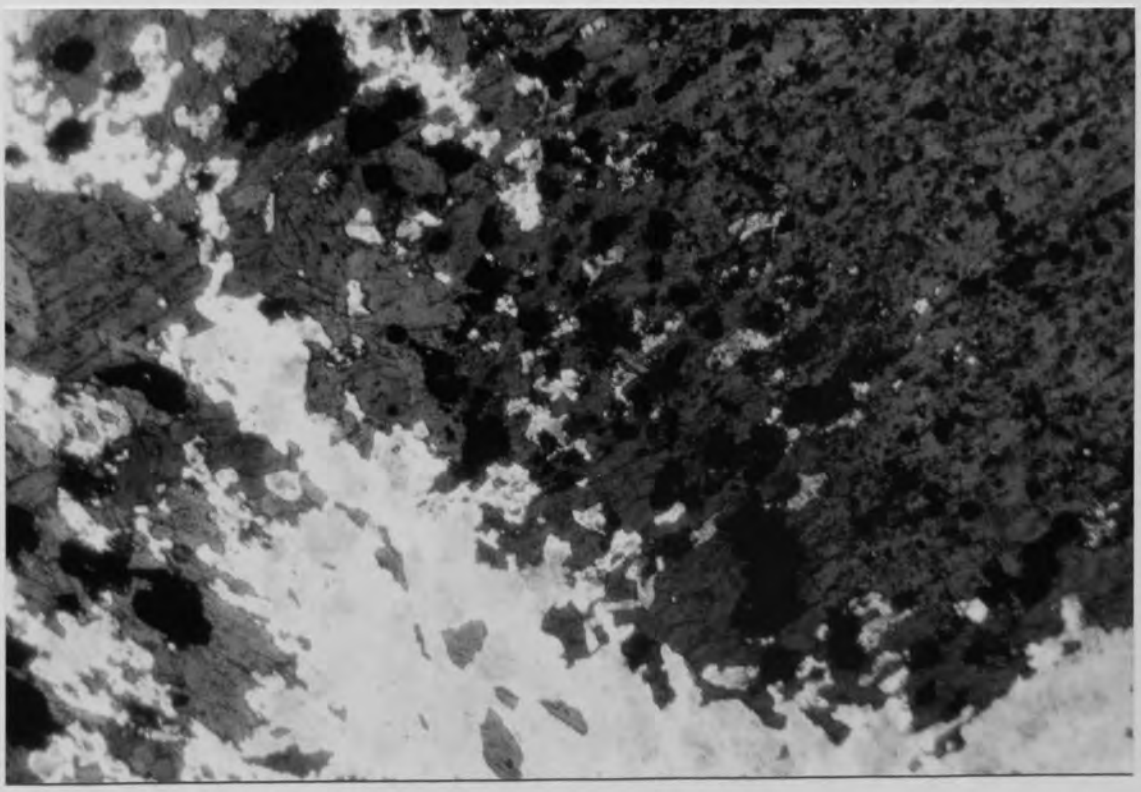

Plate 2.3 Assemblage of aegerine-hedenbergite plus magnetite and biotite in metasomatised SN1A. Sample taken from the SN1A/SN1B contact zone. Width of field of view = 0.89mm

breakdown and the formation of a fine-grained, granular, fedspathoid-rich matrix. Common accessory minerals in the metasomatised rocks are sodalite, fluorite, analcite and cancrinite. These become more abundant as the metasomatism becomes more intense. Also present are Zr-rich phases, tentatively identified by Chambers (1976) as members of the rinkite-mosandrite series, and apatite. The 'rinkite' occurs in significant quantities in a few sections.

2.3.3 Unit SN4B

2.3.3.1 Primary Magmatic Variation

This unit is characterised by having numerous feldspar phenocrysts, up to 2cm in length, set in a generally fine- to medium-grained groundmass. There is a marginal fine-grained phase which is strongly porphyritic and an inner coarser-grained phase. The feldspar phenocrysts are the largest and most numerous but there are also phenocrysts of apatite, Fe/Ti oxides, pyroxene and olivine. The pyroxenes are euhedral pale pink augites with pale green ferro-augite rims and the olivine is anhedral and rimmed by opaques. Towards the centre of the unit there is a decrease in the phenocryst content of the rock. Apatite, pyroxene, Fe/Ti oxide and olivine phenocrysts decrease in abundance and eventually disappear towards the units centre. Feldspar phenocrysts, though, persist. There are compositional changes in the groundmass with thick rims of aegerine-augite on the augitic pyroxene and an increase in the abundance of amphibole. The mafic minerals and opaques occur together in clusters , as in SN1A. Although much of the interior of the unit has been lost by the intrusion of SN5 nepheline, sodalite, analcite and occasionally cancrinite are more prominent.

2.3.3.2 Secondary Variation Associated with the Fluid Phase

The metasomatic features seen in unit SN4B are broadly similar to those described for unit SN1A. There are large poikilitic crystals of blue/green alkali amphibole that enclose feldspar and nepheline (Plate 2.4). Aegerine-augite occurs as small subhedral/anhedral grains disseminated through the groundmass. Biotite is also

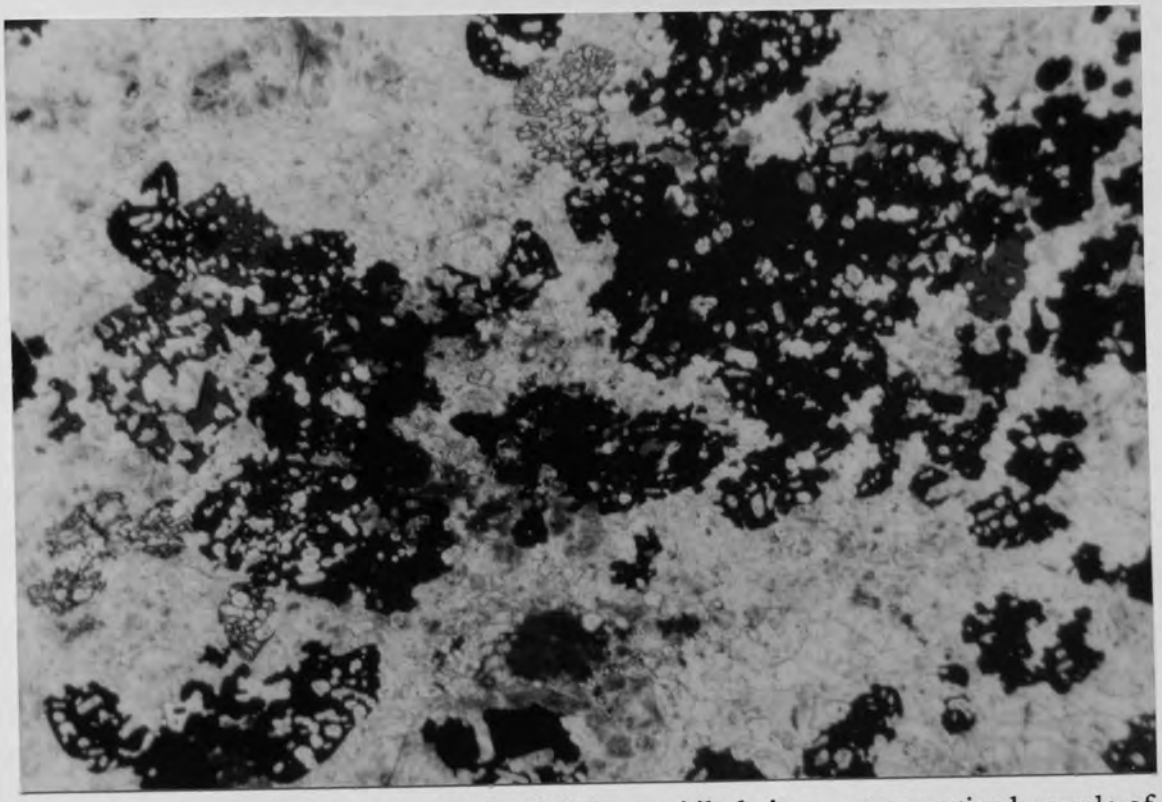

Plate 2.4 Typical occurence of poikilitic amphibole in a metasomatised sample of unit SN4B. Width of field of view = 8.3mm

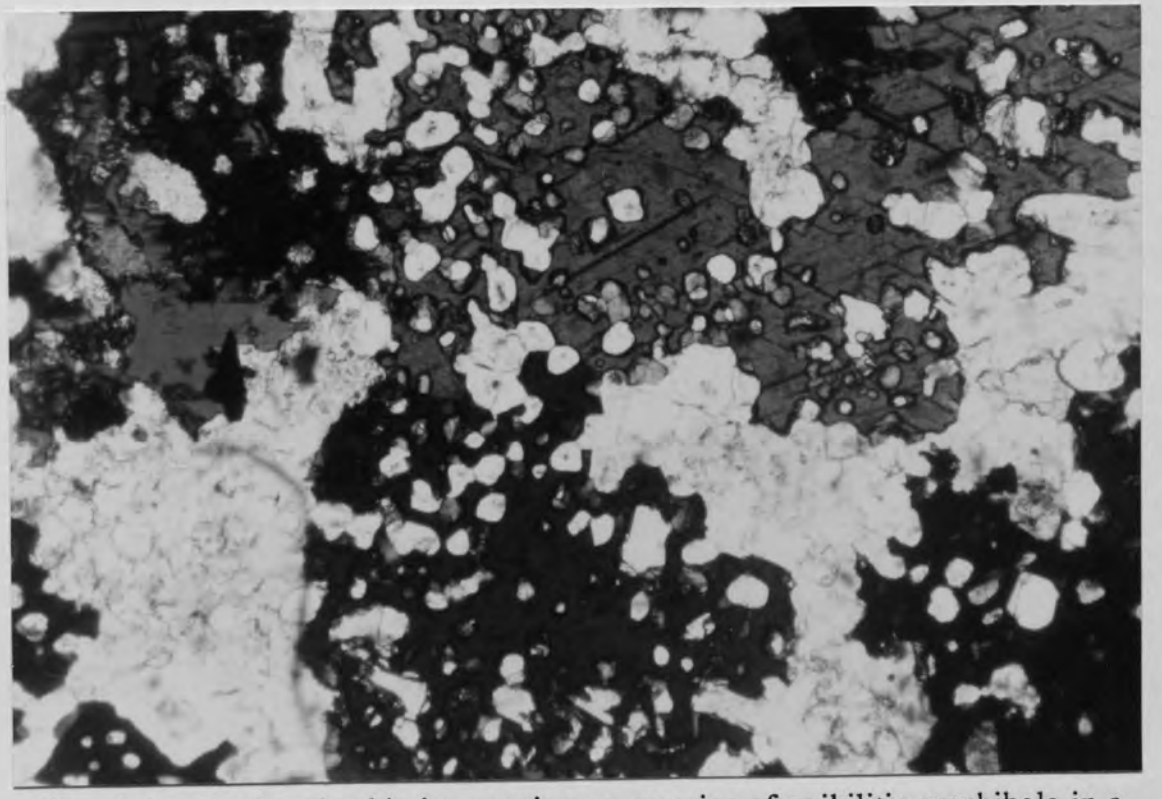

Plate 2.5 Acmite plus biotite growing on margins of poikilitic amphibole in a metasomatised sample of unit SN4B. Width of field of view = 0.89mm

found as small embayed crystals in the groundmass and is associated with opaques. The mafic clusters of opaques+pyroxene+biotite are still present in the less heavily metasomatised sections. As metasomatism becomes more extensive the alkali feldspars completely breakdown and the felsic groundmass is totally recrystallised to a fine-grained granular matrix. This is composed largely of albite, nepheline, sodalite and analcite with sodalite, and more occasionally nepheline, occuring as major poikilitic phases. There is a more extensive development of poikilitic blue/green amphibole and aegerine and biotite become occasional poikilitic phases (Plate 2.5), often associated with the amphibole. Poikilitic aenigmatite is present possibly pseudomorphing amphibole. Interstitial calcite and fluorite occur in the groundmass and apatite is common as small euhedral crystals. The Zr-rich phase 'rinkite' is an occasional minor phase.

2.3.4 The Julianehab Granite

The Julianehab Granite is a two feldspar granite gneiss. Microcline, showing well developed cross-hatched twinning, partly sericitised plagioclase feldspar and quartz form the bulk of the mode (Plate 2.6). The quartz shows strained, undulose extinction. Biotite, amphibole and opaques are present in minor amounts with the former often being chloritised. Apatite is present as an accessory phase. Fenitisation results in the reduction and eventual disappearance of quartz and microcline while plagioclase becomes very heavily sericitised. There is extensive growth of fibrous blue amphibole and large flakes of biotite, often associated in clusters (Plate 2.7). These appear to be joined by a network of fine-grained interconnecting pathways of biotite and amphibole. Brown pleochroic amphibole is also commonly developed and minor opaques are associated with the mafic minerals. In the most heavily fenitised rocks apatite becomes common, occuring as large euhedral grains, usually found in association with the mafic minerals (Plate 2.8). Calcite occurs as patches and veins in the groundmass and in the immediate contact with the syenite centre there is often extensive albitisation.

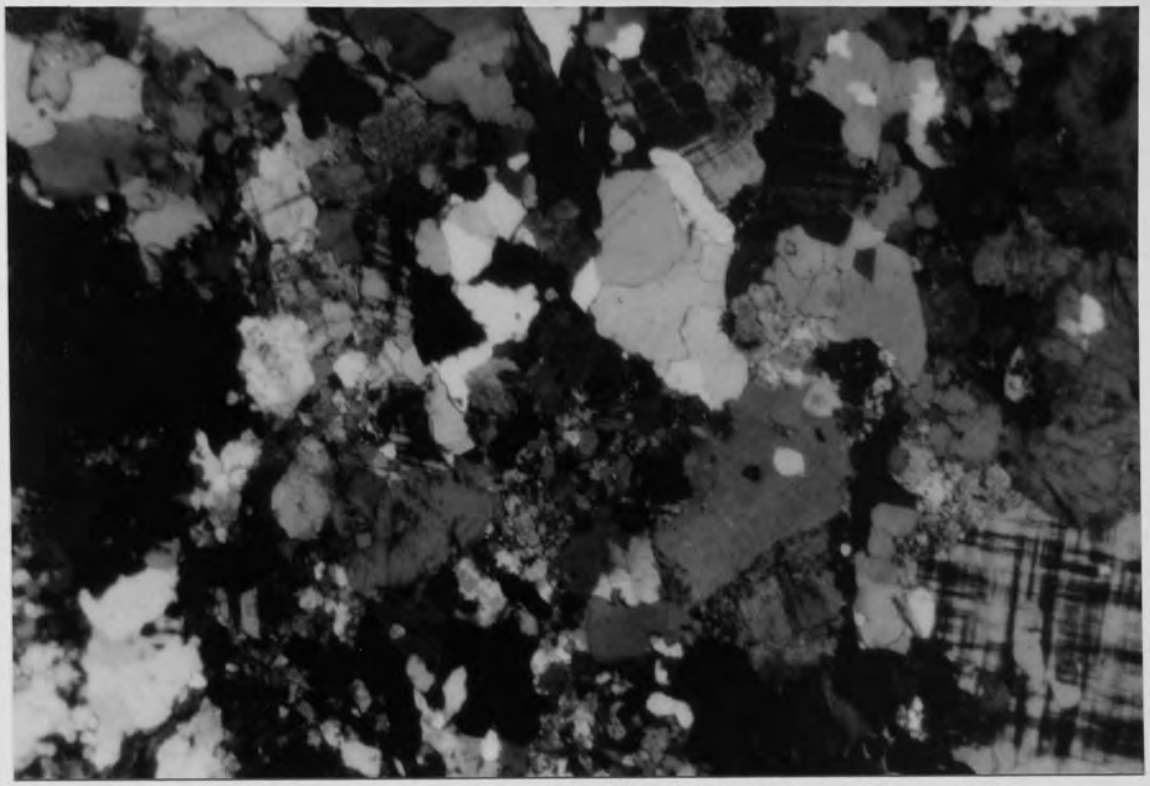

Plate 2.6 Typical section of the unfenitised basement granite-gneiss. Width of field of view = 8.3mm

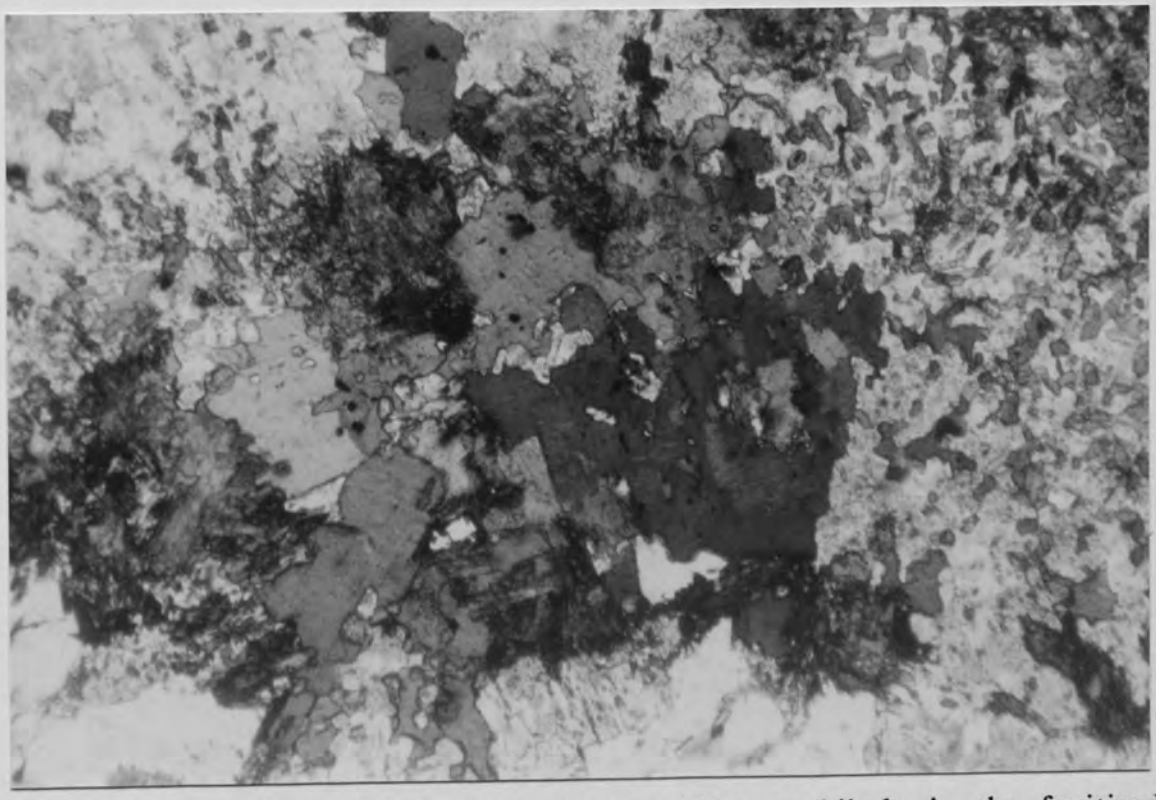

Plate 2.7 Growth of biotite and riebeckitic amphibole in the fenitised granite-gneiss. Width of field of view = 3.4mm

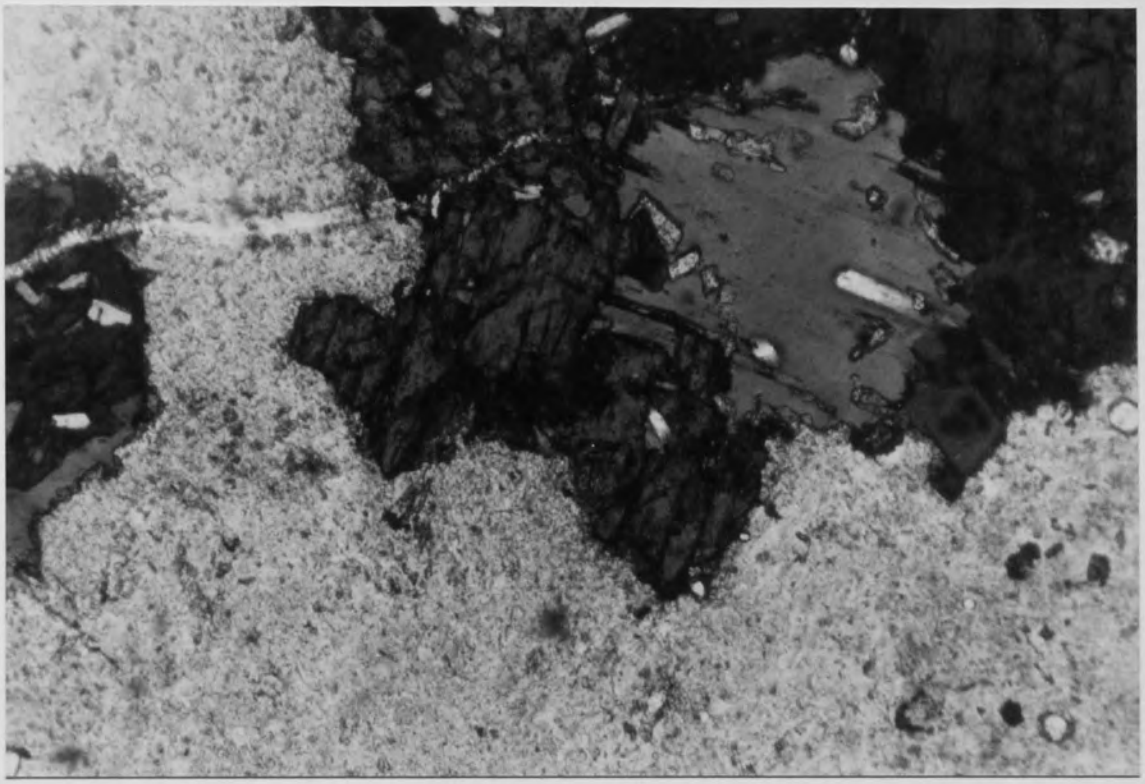

Plate 2.8 The close association of apatite and mafic minerals (amphibole and biotite) in the fenitised granite-gneiss. Width of field of view = 3.4mm

2.3.5 The Quartzite

The samples of quartzite studied are from a raft included in the syenite unit SN1B east of the long lake. The raft, which has been stoped into the syenite, is approximately 400m long by about 70m wide and probably represents a large displaced roof pendant. The least altered areas within the raft are coarse-grained, pure quartzite showing a well developed granoblastic texture. Metasomatic effects are patchy and variable. Rocks in which there is still abundant quartz show the irregular development of laths of euhedral albite enclosed in the quartz grains and the coating of grain boundaries with haematite (Plate 2.9a). This coating is sometimes extensive enough to give the rock a black, metallic appearance in hand specimen. Minor fluorite and aggregates of opaques are present. This alteration can progress to the formation of a fine-grained matrix dominated by albite with irregular grain boundaries and often poorly developed twinning (Plate 2.9b). There is sporadic growth of aegerine-augite and poikilitic or fibrous arfvedsonite and occasional irregular patches of heavily sericitised feldspar, which may represent minor amounts of original detrital feldspar. Apatite is absent from these albitised areas. The metasomatic alteration can also lead to the more extensive patchy growth of alkali mafic minerals. Large clusters or pods are formed which are suggestive of oblique cross-sections of veins. These are dominated by euhedral to subhedral aegerine-augite crystals (Plate 2.10). Alkali amphibole is present in lesser amounts and is usually interstitial between the pyroxene grains. Associated with the mafic minerals are veins of fluorite and calcite which both also occur as interstitial patches and distinct grains. Apatite is disseminated throughout these patches and takes the form of small equant grains included in pyroxene, amphibole, calcite and fluorite. Large clusters of apatite are formed along the contacts between the pods or veins of alkali mafic minerals and the surrounding albitised matrix (see Chapter 6), giving a thick rim of apatite between the two areas (Plate 2.11). The development of apatite is restricted to the areas where there is growth of mafic clusters.

Plate 2.9a Initial development of albite within quartz grains in the quartzite raft enclosed in unit SN1B. Width of field of view = 3.4mm

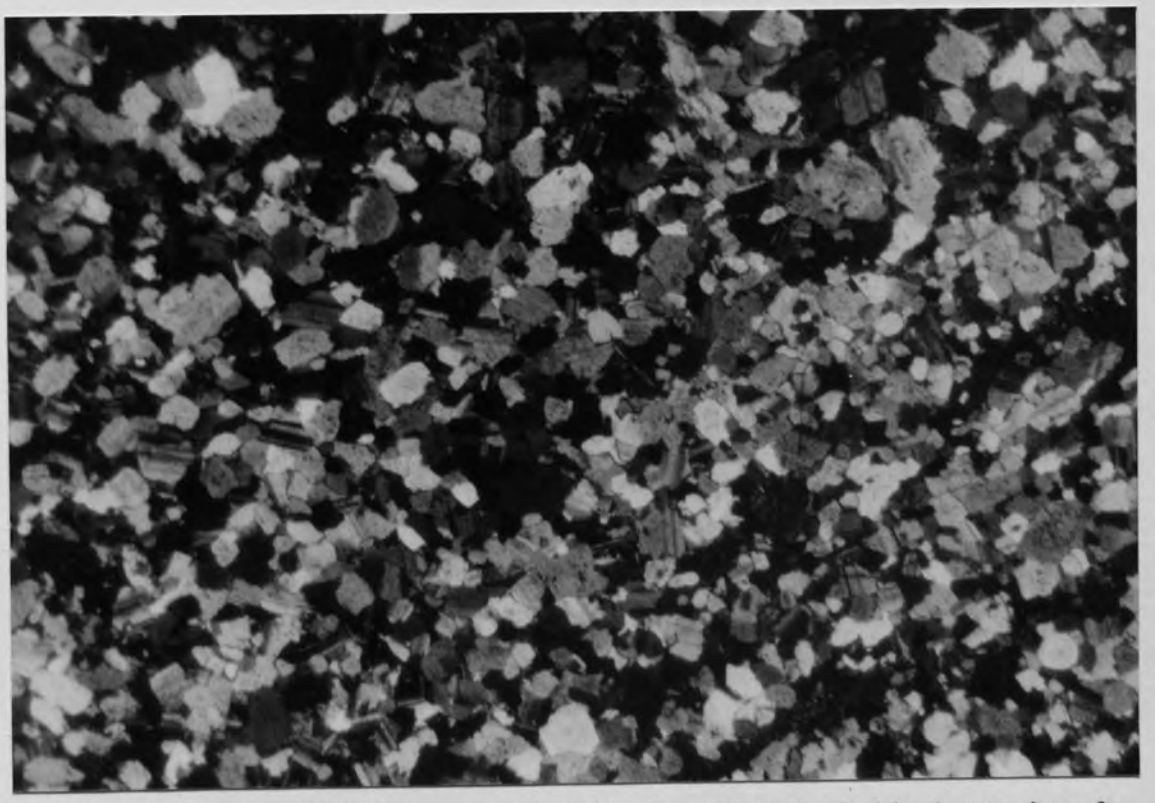

Plate 2.9b A completely albitised matrix in the fenitised quartzite raft. Width of field of view = 3.4mm

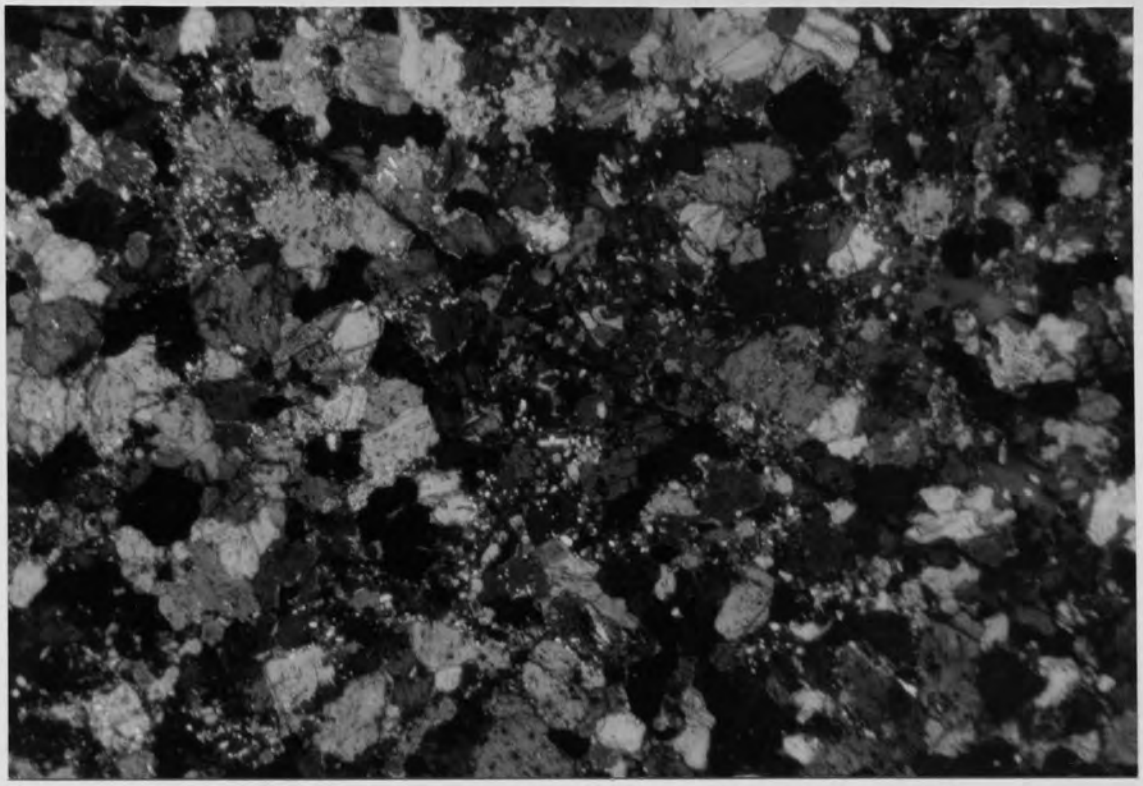

Plate 2.10 Subhedral aegerine-augite and interstitial alkali amphibole forming a mafic cluster in the fenitised quartzite raft.
Width of field of view = 8.3mm

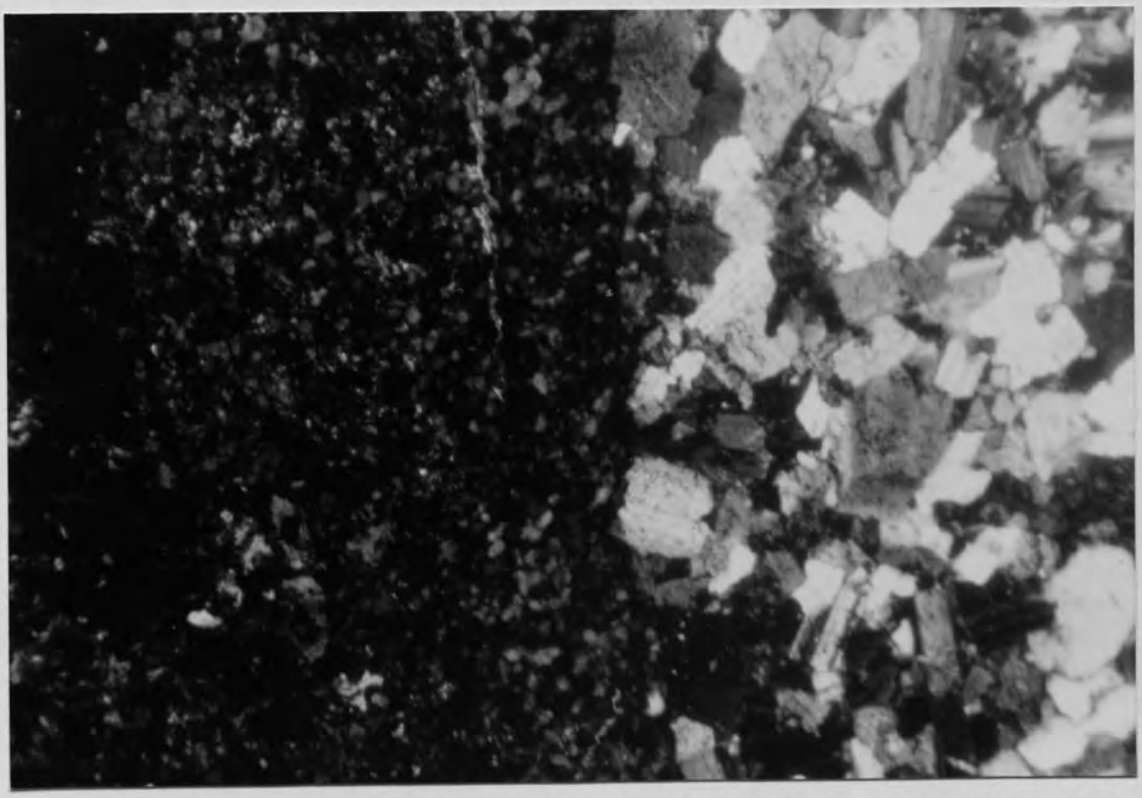

Plate 2.11 Apatite rim between the albitised matrix and a mafic mineral pod in the fenitised quartzite raft. Width of field of view = 0.89mm

2.3.6 Conclusions

Extensive discussion will be deferred until mineralogical and geochemical evidence has been presented but some general conclusions based solely on the petrography can be made.

Within the syenite centre the metasomatism produces distinctive textures. These can be traced, especially in the felsic mineralogy (Chapter 4), from the initial stages of metasomatism to a completely recrystallised and metasomatically altered rock. Whereas the felsic minerals tend to form a fine-grained granular mosaic the mafic minerals develop a characteristic poikilitic texture, although these textures are seen less commonly in the felsic phases. While the textural effects produced are similar from section to section there are significant differences in the mineralogy.

Two differing assemblages of mafic minerals are formed which are found adjacent to each other on a microscopic scale. The first is poikilitic alkali amphibole+poikilitic aenigmatite+acmite/biotite set in a sodalite- and analcite-rich groundmass and the second is poikilitic aegerine-augite+opaques+ biotite+acmite set in an albite- and nepheline-rich groundmass. Chambers (1976) noted primary magmatic variations in the syenite units, especially SN4, in the relative proportions of amphibole and pyroxene in the rock. It is possible that this initial variation is preserved through the metasomatism to produce the different assemblages or that there were local variations in pH_2O during the metasomatic process. Alternatively, local variations and fluctuations through time in fO_2 in the fluids, initiated by localised reactions in separate and limited microenvironments, could be responsible with the alkali amphibole+aenigmatite representing a lower oxygen fugacity environment than acmite+opaques+biotite (Ernst 1962).

Whatever the details it is clear, from the mineralogical changes, that there has been considerable addition of sodium to and loss of silica from the metasomatic rocks. The fluids must also have carried the halogens F and Cl leading to the formation of fluorite and sodalite. The breakdown of augite released calcium which may have been

used in the formation of fluorite and the breakdown of perthite could have produced the potassium needed for the growth of biotite. The occurence of minerals such as 'rinkite' and apatite indicate that the fluids carried quantities of the rare earth elements, presumably in the form of complexes (see Chapter 6). This feature is clearly seen in the metasomatic quartzites where there are significant quantities of apatite. The relatively pure quartzitic country rocks provide a much tighter control on the initial rock composition than do the syenites and it is clear from the common development of aegerine-augite, alkali amphibole, apatite, fluorite and calcite that the fluids introduced Na, Fe, Mg, Ca and F. The growth of acmite indicates the presence of Fe^{3+} as opposed to Fe^{2+}. There is considerable development of biotite in the Julianehab Granite close to the contact with the syenite which must require the transport of significant quantities of potassium. The presence of free quartz in the country rocks prohibits the growth of feldspathoids such as nepheline.

Whole rock and mineralogical variations in composition will be discussed in the following chapters and the preliminary observations and implications for the fluid activity will be examined in detail.

References

Blaxland, A.B., Van Breemen, O., Emeleus, C.H., & Anderson, J.G. 1978. Age and origin of the major syenite centres in the Gardar province of South Greenland : Rb-Sr studies. BULL GEOL SOC AM **89**, 231-44.

Chambers, A.D. 1976. The petrology and geochemistry of the North Qoroq centre, Igaliko Complex, South Greenland. UNPUBL PhD THESIS, UNIV OF DURHAM.

Emeleus, C.H. & Harry, W.T. 1970. The Igaliko Nepheline Syenite complex : general description. MEDDEL OM GRON **BD.186 NR.3.**

Emeleus, C.H. & Upton, B.G.J. 1976. The Gardar period in southern Greenland. *In* Escher, A. & Watt, W.S. (eds) *Geology of Greenland*, 152-81. Copenhagen : Gronlands Geologiske Undersogelse.

Ernst, W.G. 1962. Synthesis, stability relations, and occurence of riebeckite and riebeckite-arfvedsonite solid solutions. J GEOL **70**, 689-736.

Upton, B.G.J. 1974. The alkaline province of south-west Greenland. *In* Sorenson, H. (ed) *The Alkaline Rocks,* 221-37. New York : Wiley-Interscience.

Upton, B.G.J. & Emeleus, C.H. 1987. Mid Proterozoic alkaline magmatism in southern Greenland: the Gardar province. *In* Fitton, J.G. & Upton, B.G.J. (eds) *Alkaline Igneous Rocks,* 449-71. Geological Society Special Publication No.30.

van Breemen, O., Aftalion, M. & Allart, J.H. 1974. Isotopic and geochronological studies on granites from the Ketilidian Mobile Belt of South Greenland. BULL GEOL SOC AM **85**, 403-12.

CHAPTER 3

Whole-rock Geochemistry

3.1 Introduction

The definition of metasomatism is the alteration of pre-existing rocks by a fluid phase, involving net chemical changes in the rocks. Fenitisation is a specific example of this process and is defined as the in situ alkali metasomatism of country rocks surrounding intrusions of carbonatites and/or alkaline rocks. So, by definition, metasomatism requires whole-rock chemical change. It is vital, therefore, that a study of whole-rock chemistry, demonstrating the nature and extent of the chemical changes taking place, should form the framework on which all studies of fenitisation are based.

To provide an effective study of metasomatic processes the gains and losses of chemical components in a given rock must be examined. There is a large body of literature dealing with the chemistry of fenitisation and metasomatism (eg. Kresten 1988, Rubie 1982),and examining the problems involved in accurately representing the mass exchange in a rock. It has long been recognised that a simple comparison of the chemistry of altered and unaltered rocks in terms of the oxide weight percents is unsatisfactory. The addition of one element will produce a false apparent decrease in the weight percents of all the other elements even without any real exchange taking place.

Barth (1948) proposed that chemical analyses should be recalculated to 160 oxygens. This "standard cell" was regarded as being constant during metasomatism, which involved dominantly cationic exchange. This scheme was modified by McKie (1966) who suggested an oxygen framework of 100 oxygens, simply to standardise the calculation to a convenient number. Si-cations are then used as a baseline against which other cations are plotted on simple X-Y variation diagrams.

Gresens (1967) derived a general metasomatic equation which includes an expression for the relative specific gravities of the parent rock (protolith) and metasomatic rock (metasomite). This allows the chemical exchange to be calculated in terms of grams/100grams or moles/100ml and in relation to possible volume changes

during metasomatism. It is this method that has been adopted by most authors post-1967 (eg. Babcock 1973, Hoeve 1978) and, while it has remained basically unchanged since, several subtle variations in approach and in the plots produced have been developed.

This chapter will give an up to date review of the computational methods used in the study of metasomatism and one approach will be selected for the study of the North Qoroq area. The granite-gneiss is used to examine this approach in detail before it is applied to the other rock types in the area. The whole-rock chemical changes produced by the metasomatism are presented and the implications for the nature of the fluid discussed.

3.2 Computational Methods

All the methods of calculating and quantifying the mass exchange in a rock involve at least one important assumption or constraint on the process. The gains and losses of chemical components are calculated for a unique and assumed metasomatic condition. The approach of McKie (1966) assumes that the anion framework (treated as solely an oxygen framework) remains constant throughout the metasomatism. The assumption of constant oxygen is unlikely to be universally valid and is probably only applicable in specific situations. The work of Taylor (1971) has clearly shown that considerable oxygen exchange takes place between circulating fluids and cooling igneous plutons and this must introduce some doubt as to whether the oxygen framework does in fact remain constant. Treating the anion content solely as oxygen, while probably being valid for rocks of granitic composition, becomes increasingly dubious in the more evolved alkaline systems. The presence of sodalite and fluorite testify to the increased abundance and influence of the halogens on the anion exchange in the rock. Also inherent in the process is the assumption of constant volume, as no account is taken of the relative specific gravities of the protolith and the metasomite. This restriction to constant volume means that mass exchange is only quantifiable under very limited geological conditions. The net implication is that recalculating data to a 100-oxygen standard cell will give, in general, only qualitative information and so

definitive statements on mass balance should only be made if the assumptions involved are supported by independent evidence. Despite these drawbacks this method will reveal general trends and give a first approximation of the gains and losses in the rock.

The general metasomatic equation of Gresens (1967) allows the mass exchange in a rock to be related to volume change. The equation is :

$$Xn = 100[Fv(g^B/g^A)Xn^B - Xn^A]$$

where

Xn = the gain or loss of element n in producing metasomatic rock B from parent rock A

Fv = the volume factor, defined as the ratio between the final and initial volumes (ie. V_B/V_A)

$Xn^{A,B}$ = the weight fractions of component n in the parent and metasomatic rock

$g^{A,B}$ = the specific gravity of the parent and metasomatic rock

The equation contains two unknown variables, Xn and Fv. This means that Xn cannot be quantified until a value for Fv has been decided upon or vice versa, and so an assumption must be made about one of the unknowns. It could be assumed that one component had remained immobile (and therefore Xn=0) allowing a unique value of Fv to be calculated, and hence the gains and losses of all the other elements. Alternatively a value of Fv could be assumed eg. constant volume.

The usual procedure is to substitute a range of set values of Fv into the equation, producing a linear series of Xn values for each element. Composition-volume factor (Xn-Fv) graphs are then plotted to display changing component gains and losses with changing volume. Gresens proposed that if the lines for several elements crossed the gain-loss zero line at the same Fv value (ie. form a cluster) it suggests that those elements constitute a group of immobile elements and the unique Fv value deduced can be applied to the other mobile elements to calculate the gains and losses in the rock. The

basis for this is simply that it is unlikely that a group of elements would behave identically if they were all mobile.

Although the Gresens' equation is the only method that displays all the possibilities there remain several drawbacks and uncertainties in quantifying the mass balance which must be recognised. The identification of clustering on an Xn-Fv diagram is a very subjective process and where the clustering is not absolutely clear it is open to the prejudices of the author. Only small changes in the Fv value arrived at can lead to differences in the interpreted behaviour of mobile elements, even to the extent of changing gains into losses or vice versa. The presence of a cluster on one Xn-Fv diagram is not sufficient evidence to deduce a volume factor as it is possible that in some instances a group of elements will behave in an identical fashion (Appleyard 1980). The same cluster must be shown to persist in all the samples. To avoid drawing numerous Xn-Fv diagrams, clustering is best identified by plotting histograms of Fv values corresponding to zero mass change for each element. These can then be combined into one histogram that includes all elements in all samples (Kresten 1988) and if a well defined large peak is formed then that volume factor can be read off.

In a lot of cases no clustering can be identified on an Xn-Fv diagram and so no element can be assumed to be immobile. In these instances an alternative method for defining Fv must be found and in a study of fenitisation at Fen, Norway, Kresten (1988) proposed a new method to tackle this problem. He stated :

"One may assume that the sums of components supplied and depleted during fenitisation roughly balance ie. that the total mass change of the rock during fenitisation will be at minimum."

He therefore proposed that :

"The value for zero mass change of the total rock can be used in order to estimate Fv."

The advantage of this method is that it is less sensitive to minor variations in protolith composition than the single element lines. The total rock line for each sample is plotted on an Xn-Fv diagram and the appropriate volume factor read off. The idea that a

rock will balance gains and losses also implies that volume will be kept as near constant as possible, with any volume changes being due to density differences between the protolith and the metasomite. As realistic density changes are limited to about $\pm 0.5 \times 10^3 kg/m^3$ of the original (a density change equivalent to the difference between a granitic rock and a basaltic rock), the volume changes within which the total rock line can give a feasible estimate of Fv are also limited to near constant volume. If there is independent (eg. field or petrographic [deformation structures, veining]) evidence for a volume factor not corresponding to the measured density difference between the metasomite and the protolith then it is likely that the total rock line will give a false estimate of Fv and if a large volume change is suspected then the estimated Fv will almost certainly be wrong.

These drawbacks in no way invalidate the method but only serve to highlight the fact that assumptions are made in an attempt to constrain the metasomatic process and independent evidence should be sought to support those assumptions. Kresten (1988) recognised this when he said :

"The calculation of total rock curves . . . . is merely another, and possibly more comprehensive, way of treating Gresens' (1967) equation."

If other evidence indicates a near constant volume process then the estimate of Fv by use of the total rock line will be at least as reliable as any other method.

The Gresens' (1967) equation only contrasts one protolith with one metasomite and interpretation is susceptible to variations in the protolith composition. In rocks such as the basement gneiss and quartzite in the North Qoroq area this is not a major problem as they are of approximately constant composition. In the syenite units, though, the choice of suitable, typical, unaltered parent material and metasomatised product is complicated in that, prior to metasomatic alteration, the syenite units possessed a primary variation due to crystal fractionation processes. An advantage of recalculating the analyses to 100 oxygens and plotting on a variation diagram, is that in contrast to the Gresens' Xn-Fv plots all samples can be compared and any trends with increasing fenitisation identified. It is therefore desirable to produce a fenitisation index

for the variation diagrams that will allow representation of gains and losses against increasing fenitisation. For all the fenitised rocks analysed, granite-gneiss, quartzite and syenite there is unquestionably in the vast majority of cases an overall increase in Na and decrease in Si.

It seems reasonable to choose as a fenitisation index a parameter reflecting these changes and cations Na-Si has been selected. This index shows a progressive increase with increasing grade of fenitisation and allows the behaviour of other elements to be evaluated. It must be stressed that for altered country rock quartzite and granite-gneiss, both of which show little primary variation (ie.constant protolith composition) this index reflects well changes during fenitisation. It is less effective for the fenitised syenites which display a primary variation due to crystal fractionation processes. This may not pose severe problems with unit SN4B, which shows limited primary variation, but is much more of a problem with SN1A where primary variation is extensive.

Kresten (1988) also addressed this problem of a fenitisation index and decided upon using the total mass gains of a sample, as calculated from Gresens equation at the deduced volume factor, as the chemical index of fenitisation. The basis for this is that a higher grade fenite will have had more material added to it than a lower grade fenite, which will ultimately grade into unaltered rock with no mass exchange. This index was tested for the North Qoroq samples and was found to be generally applicable. An alteration to this index, though, is proposed to give a still more widely applicable baseline against which gains and losses can be represented. If a metasomatic process dominantly leaches the rock then an index based solely on gains may not be representative and so it is suggested that the losses from the rock should also be taken into account. This is done by taking the absolute value of the total losses and adding this figure to the total gains to give the total 'absolute' mass exchange in the rock and this figure will be used as the new fenitisation index.

In the same way as for Na-Si, the total mass exchange baseline is effective for the country rocks but is less useful for the syenite units which, as stated previously,

show a primary magmatic variation. When compared to a single protolith parent most syenite samples will have gains and losses solely due to crystal fractionation processes and without any fenitisation.

A summary, therefore, of the various methods of quantitatively and graphically representing the fenitisation process is as follows :-

1. Recalculation of analyses to 100 oxygens and the use of plots of cations against a fenitisation index of Na-Si to show variation involving a range of samples.
2. The use of Gresens' general metasomatic equation to produce compositional change-volume factor (Xn-Fv) graphs applicable to all possibilities, but restricted to one parent (protolith) and one metasomatised sample (metasomite) per graph.
3. The use of Gresens' equation to plot histograms of Fv values corresponding to zero mass change for each element to look for clustering and the combination of these into a histogram for all elements. The presence of a marked peak suggests an appropriate value for volume factor (Fv).
4. The application of Gresens' equation as advocated by Kresten (1988) to produce Xn-Fv graphs for total rock change. It is suggested that a zero mass change situation indicates the appropiate volume factor (Fv).
5. The assumption that a component such as oxygen is fixed and the use of it in Xn-Fv plots to fix a value for Fv.
6. The plotting of gains and losses of major and trace elements for this volume factor.
7. The plotting of major and trace element variation against a fenitisation index of gains and losses (ie. total mass exchange).

A summary of some of the most important factors involved in using Gresens' equation is also appropriate at this stage.

It is clear that the densities of the protolith and the metasomite play an important role in the calculations and two methods were used to calculate the rock densities. A computer programme was written (see Appendix 5) to process the XRF chemical analyses through Gresens' equation, in which the density is calculated using the method of Bottinga and Weill (1970).This method is designed specifically for silicate liquids and so, when

applied to rock analyses, some minor discrepancies in absolute values are inevitable. However, rock and mineral analyses taken from Cox *et al.* (1979) were used to test this approach and realistic values were obtained. The densities of all samples used by Rae and Chambers (1988) were measured directly by suspending rock chips in a measuring cylinder of water and while absolute values differ slightly from those computed by the programme, the ratios of density of protolith to density of metasomite remain the same. In using Gresens' equation (see p.44) it is only the ratio that is important and so no discrepancies are introduced by using the computer programme. This is borne out by the identical conclusions arrived at in the current and the following chapters, as regards the chemistry of unit SN1A, in which the densities were calculated by different methods.

Gresens' equation is a simple way of relating the change in weight fraction of any given component in a rock to the change in density of the rock, so allowing an estimate of volume change during metasomatism to be made. Only once a unique value for the volume change, or volume factor (Fv) in the equation, has been decided on can the gain or loss of a given component be calculated (see p.44). In order to represent all possible volume changes, ie. all possible metasomatic conditions, a series of volume factors are substituted into the equation hence producing a linear series of Xn values for each component. The Xn values of all the components are added together at each Fv value to give a set of values for the total gain or loss of material in the rock at each Fv value. Xn-Fv graphs are then constructed to represent total gains or losses in the rock against all possible volume changes. Assuming that the rock balances mass by changing density, the volume factor corresponding to zero mass change can be read off as the unique volume factor. This is put back into Gresens' equation to recalculate the gains and losses of each component which are then represented on barcharts.

The methods discussed above will be examined in detail in the next section, using North Qoroq data, and a standard routine for the treatment of whole-rock analyses in the study of fenitisation will be suggested.

3.3 Chemistry of the granite gneiss

3.3.1 Introduction

The granite-gneiss has been chosen as the rock type to be used for a detailed examination of the computational methods described above. The reason for this choice is that the problem of compositional variation in the parent material is not significant in the basement granite-gneiss. Variations in the granite-gneiss are minor compared to those produced by the metasomatism and will not affect the major gains and losses. The following procedure is based largely on that adopted by Kresten (1988) but with some amendments introduced by the author. All samples were analysed on a Phillips PW1400 X-ray spectrometer and representative analyses are listed in Table 3.1. Analytical techniques are detailed in Appendix 2.

3.3.2 Recalculation to a 100 oxygen cell

The recalculation of oxide wt% values into cations per 100 oxygens is the first step in the treatment of the data. All elements are plotted against the baseline of Na-Si. Increases in the values in this baseline reflect increased fenitisation and several clear differences between unaltered and fenitised rocks can be seen.

The average protolith is plotted along with the metasomatised samples on the cation plots (Figure 3.1), on which clear trends are seen for most elements. Si shows an obvious decrease and Ti, Al, FeT, Mn, Ca and Na increase. The trends for Mg and K are not clear as, although they are gained, there is poor correlation with increasing Na-Si. The two series of samples DAR70-79 and 279-281, which form two of the traverses in the granite-gneiss away from the syenite contact, all cluster around the average parent, showing little chemical change. They also show little petrographic alteration and so the tight grouping highlights the relative homogeneity in the original composition of the granite-gneiss. The gains and losses described in the more highly fenitised samples are the changes expected from the alteration of a granitic rock by a fluid in equilibrium with an undersaturated syenitic rock, but it is possible that Si remained constant and the fenitisation was a purely additive process or Al remained

Table 3.1 Representative whole-rock XRF analyses.
Sample nos. DAR142, DAR191 - unit SN4B ; nos. DAR107, DAR123 - unit SN1A ; nos. DAR324, DAR163, DAR175 - granite-gneiss ; nos. DAR291, DAR65 - quartzite raft.

Sample No.	DAR142	DAR191	DAR107	DAR123	DAR324	DAR163	DAR175	DAR291	DAR65
SiO2	56.678	57.046	53.736	54.839	73.473	57.214	56.545	98.880	58.518
TiO2	0.340	0.341	0.266	0.216	0.150	0.367	1.000	0.194	0.522
Al2O3	19.166	19.730	20.051	20.582	14.192	19.227	18.703	1.084	6.784
Fe2O3	7.302	6.556	7.063	4.733	1.366	4.557	5.661	1.218	9.826
MnO	0.276	0.225	0.197	0.145	0.061	0.122	0.166	0.020	0.425
MgO	0.187	0.229	0.170	0.170	0.311	1.057	1.054	0.084	1.772
CaO	1.619	1.607	1.633	1.332	1.264	2.646	3.144	0.189	9.636
Na2O	8.574	8.008	8.089	9.847	3.891	5.323	5.891	0.063	6.116
K2O	5.650	6.033	5.457	5.483	4.056	5.749	4.532	0.176	0.669
Total	99.792	99.775	96.662	97.347	98.764	96.262	96.696	101.908	94.268
Zn	219	146	115	89	29	137	120	22	103
Cu	5	2	2	4	0	5	12	3	69
Ni	24	15	17	17	57	12	20	198	38
Rb	277	249	366	317	160	192	90	4	23
Sr	61	56	23	38	289	580	1465	20	1046
Y	105	60	15	23	12	30	31	15	102
Zr	1496	845	433	598	93	533	664	133	371
Nb	281	257	129	95	12	109	110	33	50
Ba	203	210	60	112	469	1309	2480	54	85
U	4	3	0	3	7	5	3	2	2
Th	18	10	2	4	22	10	5	7	50
Pb	20	14	4	5	35	24	23	8	14
TiO2	2773	2832	1982	1563	1299	4277	10187	1719	4611
V	2	5	2	2	11	32	13	20	156
Cr	-3	-2	13	-2	38	7	16	27	39
La	144	116	16	27	22	60	54	49	436
Ce	330	277	41	67	46	131	115	92	809
Nd	146	139	21	25	17	60	55	41	345

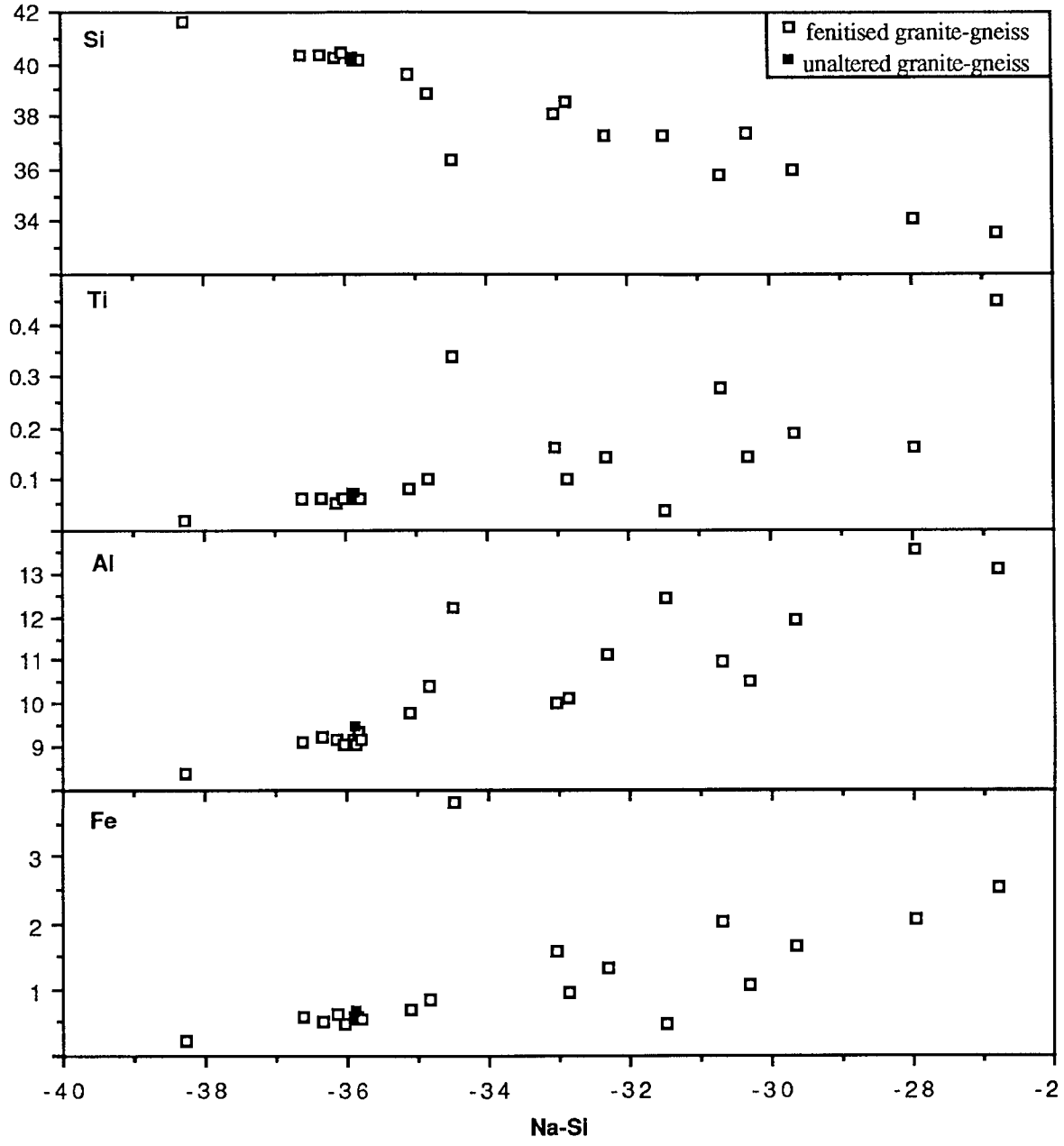

Figure 3.1 (two pages) - Whole-rock chemical variation in the granite-gneiss. Cations per 100 oxygens versus the baseline Na-Si, in which increasing numerical value corresponds to increasing fenitisation.

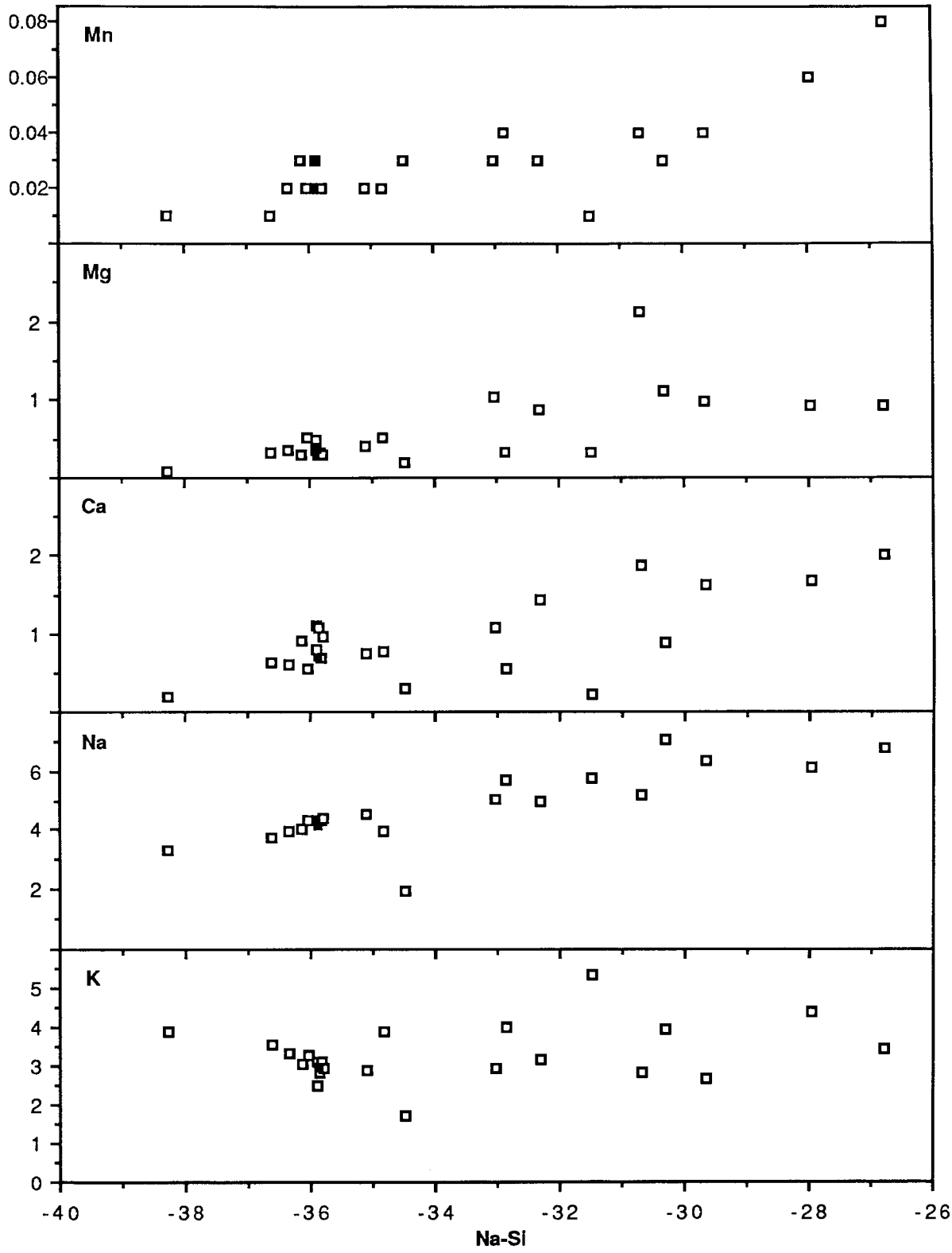
Mn
0.08
0.06
0.04
0.02
Mg
2
1
Ca
2
1
Na
6
4
2
K
5
4
3
2
1
0
-40
-38
-36
-34
-32
-30
-28
-26
Na-Si

constant. The gains and losses of the other elements could be adjusted accordingly, but it is this sort of consideration with which the 100 oxygen cell cannot cope. The gains and losses indicated by this method should now be examined more closely using the Gresens (1967) composition-volume equation.

3.3.3 Composition-volume relationships

3.3.3.1 Estimation of the volume factor (Fv)

The first thing that must be decided is the composition of parent rock to be used in the calculations. The 100 oxygen cell allows the representation of all samples whereas the Gresens equation requires a single parent. Two samples of unaltered granite-gneiss were taken at some distance from the contact with the syenite centre and, as the granite-gneiss has been shown to be originally homogeneous, these values were averaged to produce one average parent rock (protolith) which will be used in all the subsequent calculations.

The Xn-Fv relations of each element are now calculated at set volume factors of 0.6, 0.8, 1.0, 1.2 and 1.4, corresponding to a range in volume change from 60% of the original volume up to 140% of original volume and one example of an Xn-Fv graph that would be produced is given as Figure 3.2. The volume factors for zero mass change of each element in each sample are calculated and a series of histograms produced (Figure 3.3). The appearance of significant peaks in the same place for different elements is taken as an indication of the relative immobility of those elements and hence an indication of the volume factor. Although most elements show a peak near constant volume there is a considerable spread, suggesting that they were mobile, to varying degrees, during the fenitisation process. Ti, Mg, Ca and Na tend to show zero mass change at volume factors less than 1 and this probably indicates that they were dominantly added during the fenitisation.

The series of histograms is grouped into one plot of all the elements in all the samples (Figure 3.4) which shows a much clearer peak near constant volume, though this tails down to lower values of Fv due to the large number of elements being

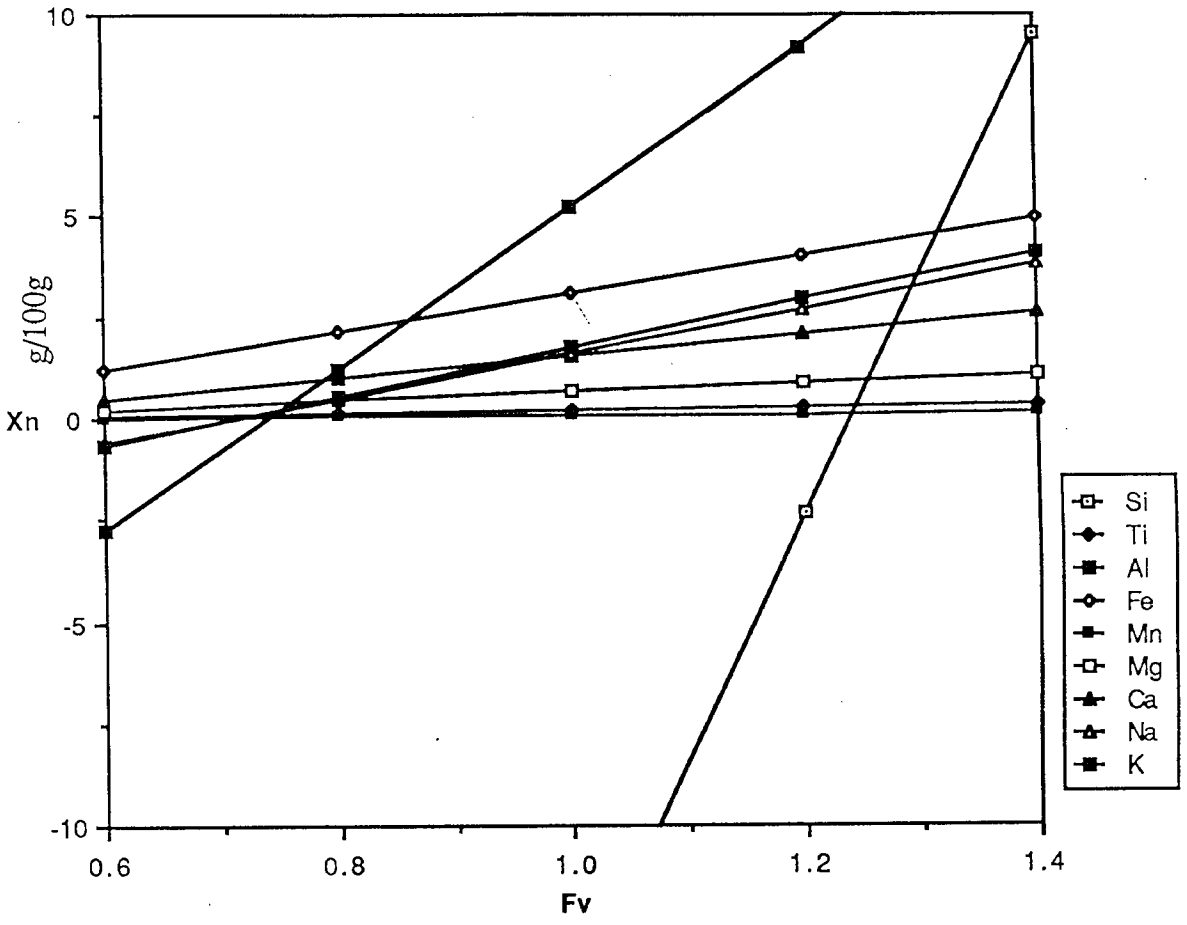

Figure 3.2 Sample compostion-volume (Xn-Fv) plot using sample DAR163 from the granite-gneiss. Fv values of 0.6, 0.8, 1.0, 1.2 and 1.4 are substituted into Gresens' equation and corresponding values of Xn are calculated for each component. A straight line can then be drawn through the points for each component and so all possible metasomatic conditions are represented on one graph. Note the lack of clustering making it very difficult to decide on a unique value for Fv

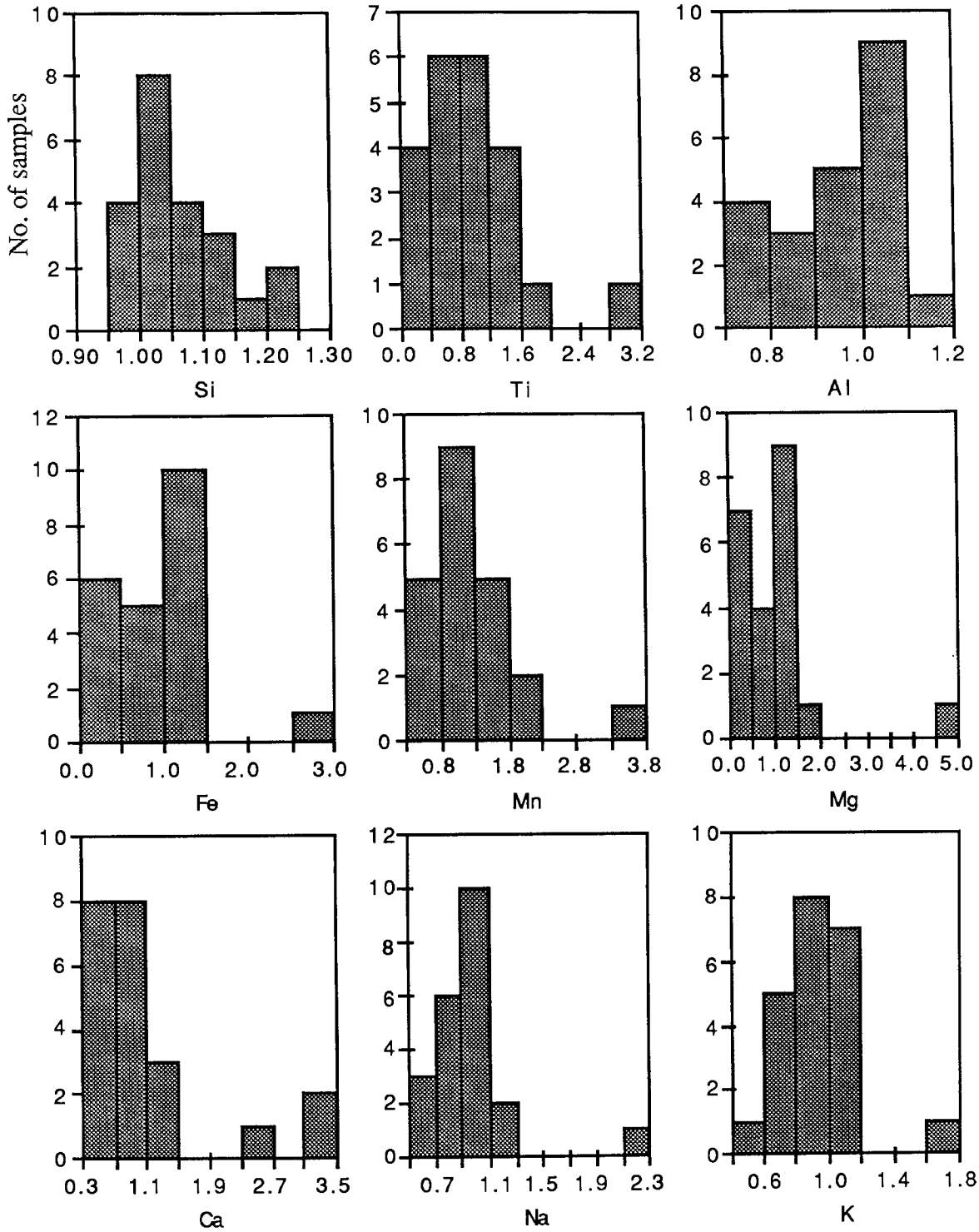

Figure 3.3 Series of histograms showing the Fv values that correpond to zero mass change for each element. If a group of elements show a significant peak at a similar value of Fv it is taken to indicate the relative immobility of those elements.

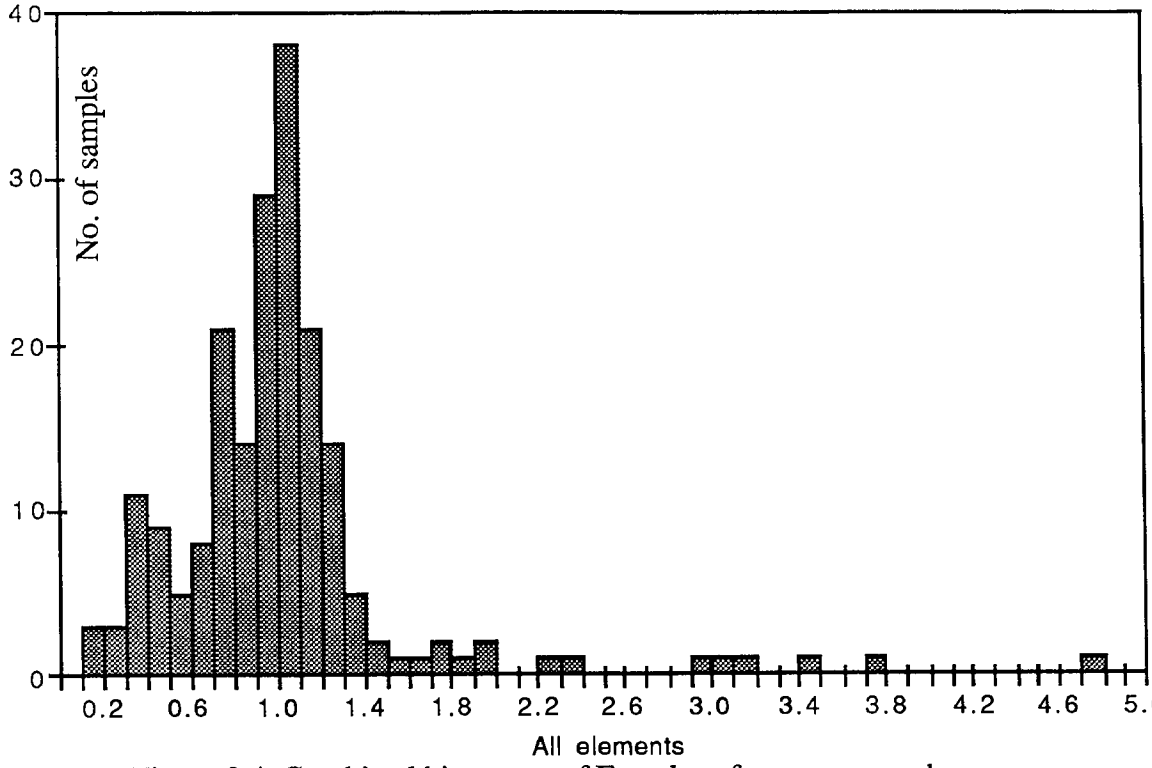

Figure 3.4 Combined histogram of Fv values for zero mass change for all elements in all the samples., granite-gneiss, ie. a compilation of Fig. 3.3 into one histogram.

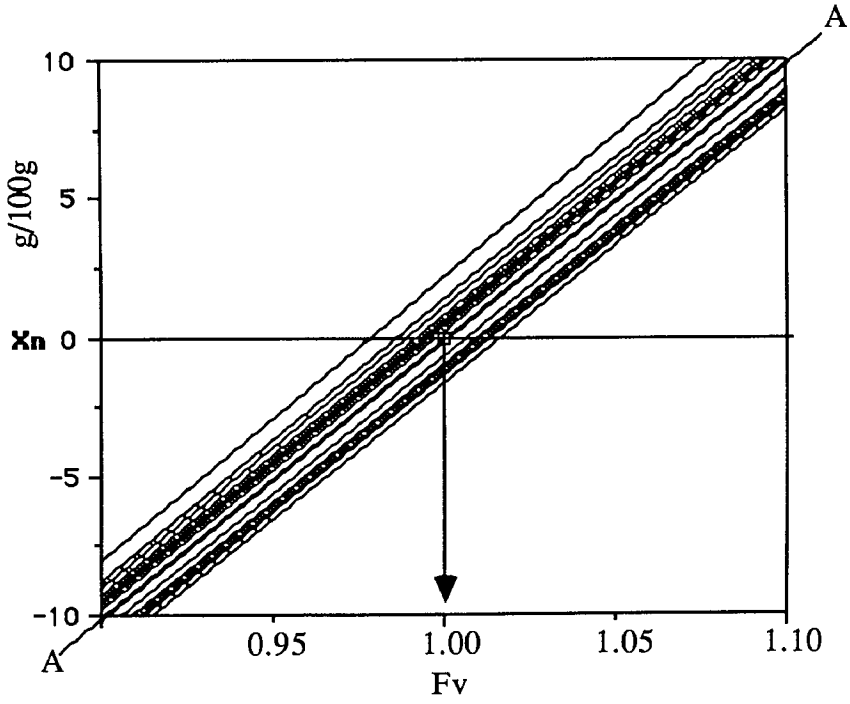

Figure 3.5 Total rock lines for the granite-gneiss plotted on an Xn-Fv graph. The gains and losses of each component are calculated at set values of Fv and these are then added together to produce the Xn values for the total rock. This is done for each sample and the values plotted on the above Xn-Fv graph.

added and hence crossing the gain-loss zero line at low volume factors. Despite the apparent mobility of most of the major elements during the fenitisation of the granite-gneiss an approximate value of Fv=1 (ie. constant volume) can be deduced.

This is, of course, only one line of evidence for the volume change and needs to be supported if possible. Given that only small volume changes are indicated by the histogram, the assumption that total mass change of the rock will be at minimum (Kresten 1988) is probably valid. The mass balance for the total rock (using the oxides SiO_2, TiO_2, Al_2O_3, Fe_2O_3 (total iron), MnO, MgO, CaO, Na_2O and K_2O) was calculated at the same range of volume factors as above (ie. 0.6-1.4) and the total rock lines plotted on an Xn-Fv diagram (Figure 3.5).These show a tight grouping from Fv=0.98 up to Fv=1.02 with an average of 1.00 or constant volume.

The only other assumption that can be used to estimate Fv is that a single component remained immobile. The two commonest components used for this purpose are Al and O. As a final check on the validity of the volume factor so far deduced the mass balance of oxygen was calculated at the same range of volume factors. Using the assumption of constant oxygen, values of Fv can be deduced and a unique solution arrived at. The range of volume factors is again limited and once more the average value is close to 1.00. The excellent agreement between all three lines of evidence, based on independent assumptions, allows Fv to be set at close to constant volume with some confidence.

It was shown in the previous section that the sort of evidence just used to deduce the volume factor is only valid in processes that involve small volume changes (approximately in the range 0.85-1.15). Inherent in these calculations is the attempt to balance mass and hence move to constant volume. Therefore, independent field and/or petrographic evidence is needed. For instance, the presence of veins and pods of new material, breccias, cracks or cavities and strain textures would all indicate volume change, casting doubt on the Fv chosen. Although the gneiss is veined in places and there are some patches of new mafic minerals developed in thin section, there is no

evidence to support a large volume change in the rock and so gains and losses were calculated at the Fv values deduced from the total rock lines for each sample.

3.3.3.2 Calculation of gains and losses

The gains and losses of each element in each sample are presented as barcharts (Figure 3.6).These emphasise the features shown on the cation plots of decreasing Si at the expense of most other elements and emphasise the unaltered and homogeneous nature of the samples DAR70-79 and 279-281. For the other samples, 162-179, for Si to be held constant, and the process made purely additive, volume increases of up to 25% would be needed in the most altered rocks, a change that would be seen unequivocally in hand specimen and thin section. Rubie (1982) favoured the assumption of constant Al for the fenitisation of granitic rocks but for this to be the case at North Qoroq then volume decreases of up to 25-30% would be required, Na would become near constant and gains in FeT would become greatly reduced, results that are inconsistent with the introduction of new alkali mafic minerals.

The barcharts only show which elements are gained or lost but the use of a fenitisation index allows trends with increasing fenitisation to be identified. Plotted against the fenitisation index (Fen.I.) the gains and losses show similar trends to the cation plots (Figure 3.7). There is a clear decrease in Si and obvious increases in Al, Ti, Fe and Na. The increases in Ca and Mn are not as clear as on the cation plots and Mg and K again show no clear trend, though it should be noted that all these elements are dominantly added in the more highly fenitised samples. The major process affecting the gneiss, therefore, appears to be desilicification concurrent with the addition of other elements, maintaining near constant volume. It should be remembered that on all these graphs the parent rock will always plot at the origin or point 0-0 ie. no mass exchange.

3.3.3.3 Trace elements

The trace element variations have been calculated using Gresens equation. The element ppm values were converted into oxide wt% values and the gains and losses

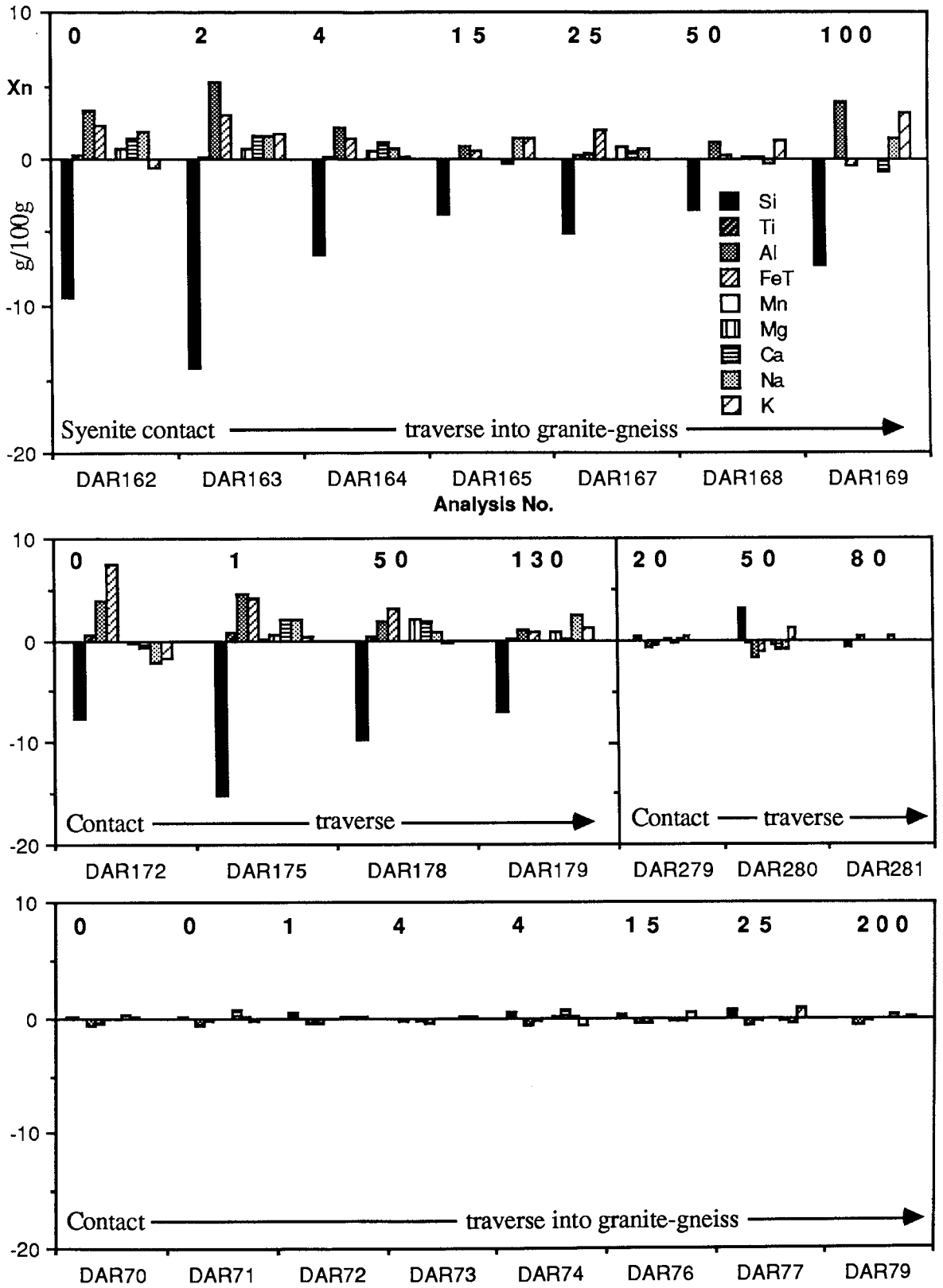

Figure 3.6 Major element variation in the granite gneiss presented on barcharts of gains and losses calculated from Gresens' equation at the value of Fv deduced from the total rock line for each sample (see Fig. 3.5). Symbols are the same for each plot and arrowed lines indicate the direction of traverses. The order of elements down the legend is the same as the order across each sample for this and all subsequent barcharts presented in the thesis. Numbers in bold are the distance from the syenite/gneiss contact in metres.

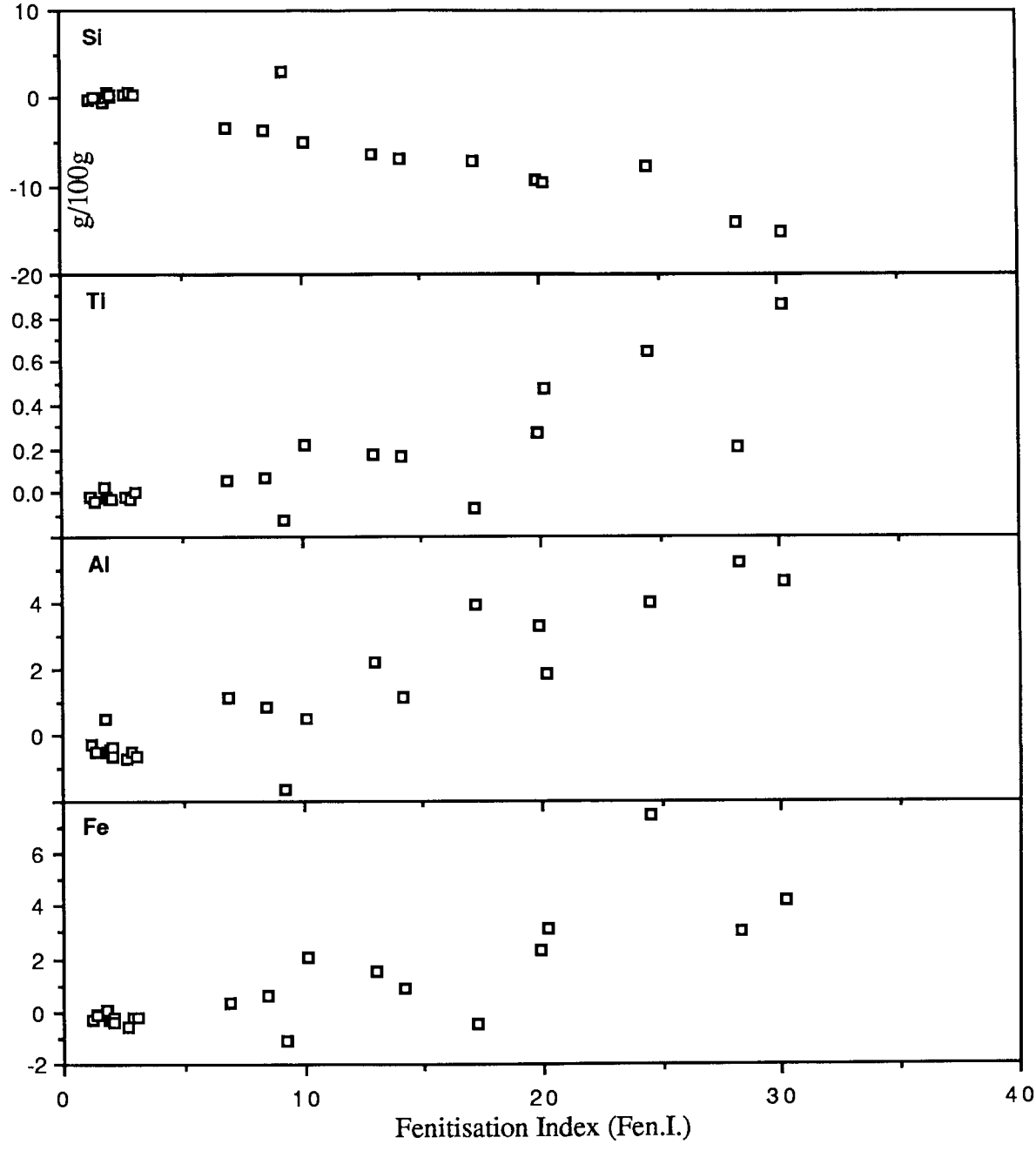

Figure 3.7 (two pages) Major element variation in the granite-gneiss
Gains and losses (g/100g) as calculated from Gresens' equation plotted against the fenitisation index in order to identify trends with increasing fenitisation.

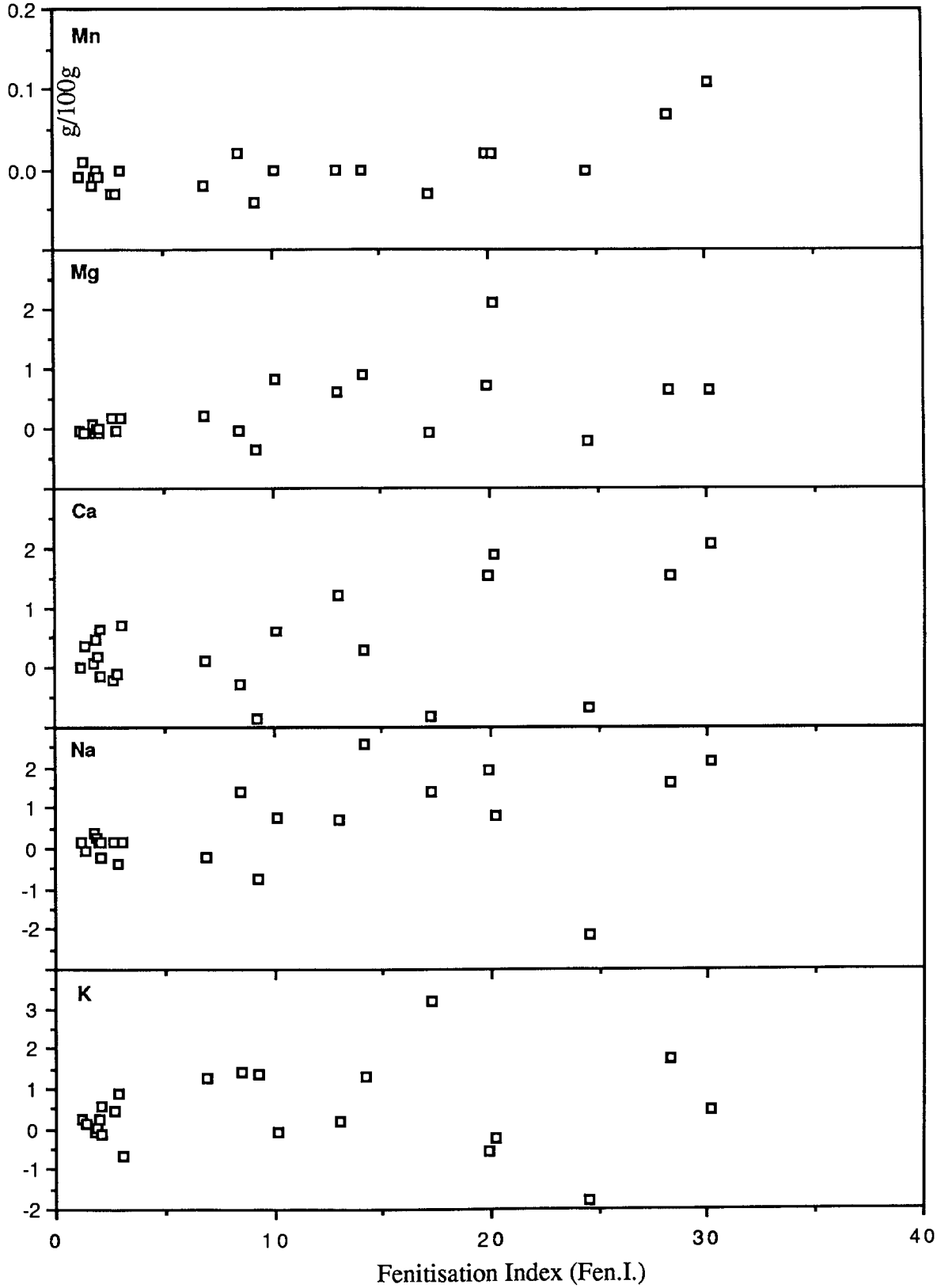
Mn
g/100g
0.2
0.1
0.0
Mg
2
1
0
Ca
2
1
0
Na
2
1
0
-1
-2
K
3
2
1
0
-1
-2
0
10
20
30
40
Fenitisation Index (Fen.I.)

were then calculated. The results were multiplied by 100 to give sensible numbers and so they are in units of grams/10000grams rather than the g/100g of the major elements. The most important factor is not the absolute amounts added or removed but the identification of patterns of consistent gains or losses in certain elements. The variations are represented on barcharts to show relative changes between elements (Figure 3.8).

The trace element barcharts again emphasise the unaltered and homogeneous nature of the samples 70-79 and 279-281 though there is a minor but consistent loss of Ba. In contrast, the samples which show strong alteration with the development of biotite, alkali amphibole and apatite show large increases in Ba and Sr, and Zr, Y, Nb and La. The two samples furthest from the syenite contact (DAR169,179) show Ba and Sr depletions. The other trace elements show only minor and irregular changes in comparison to these elements. It can be seen that the dominant process in the granite-gneiss is one of trace element addition which will be contrasted later with the syenites (sections 3.5 and 3.6) in which trace elements are often leached from the rocks.

These six trace elements are then plotted against the fenitisation index to identify trends with increasing fenitisation (Figure 3.9). The same features apparent on the barcharts are highlighted on these graphs. Ba, Sr and Zr tend to increasing gains with increasing fenitisation and Y, Nb and La are dominantly gained but show no clear trend. As the distributions of Y, Nb and La are controlled by minor phases a fenitisation index based on the major elements is unlikely to reveal clear trends and the regular variation in Zr may reflect its incorporation in one of the major phases such as amphibole. It is interesting to note that the two trace elements that show the biggest gains, Ba and Sr, are the elements that are most consistently lost from the syenites (sections 3.5 and 3.6) and a process could be envisaged of a fluid scouring elements from the syenite and redepositing them on reaction with the surrounding country rocks. The nature of these fluids, and whether we are looking at a single or more likely multiple fluid phase activity, is discussed in Chapter 6.

The systematic treatment given above to both the major and trace element data will now be employed to examine the mass balance relations in the quartzite and

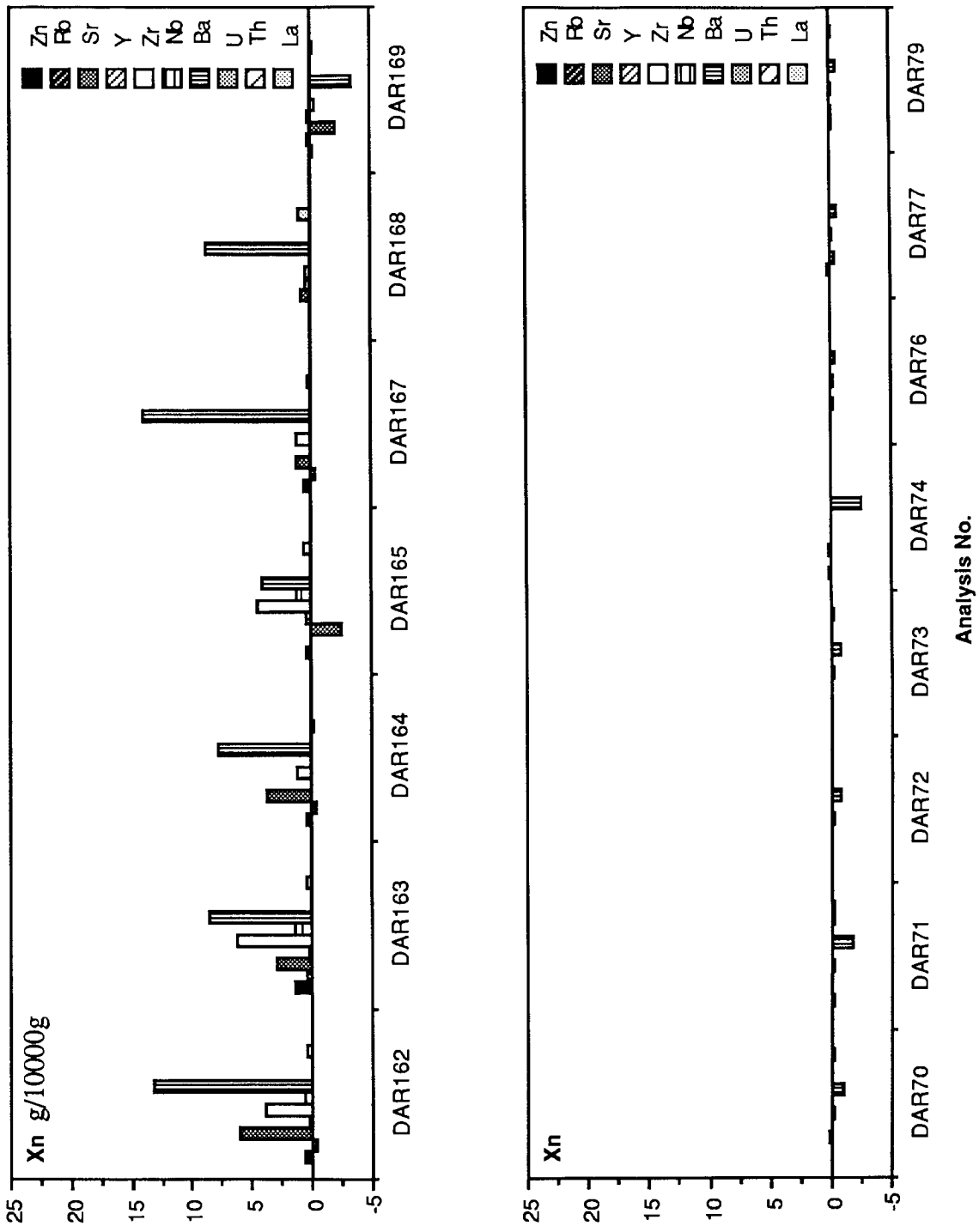

Figure 3.8 (two pages) Trace element variation in the granite-gneiss presented on barcharts of gains and losses calculated from Gresens' equation. Units are g/10000g.
The traverses are the same as those shown on Figure 3.6

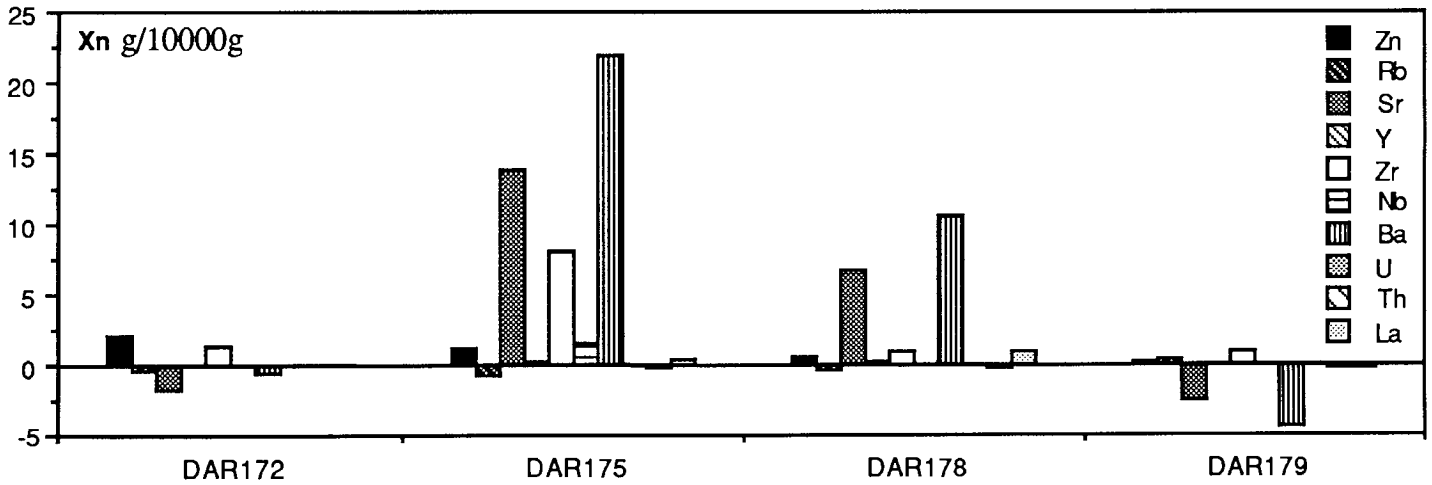
Xn g/10000g
25
20
15
10
5
0
-5
Zn
Pb
Sr
Y
Zr
Nb
Ba
U
Th
La
DAR172
DAR175
DAR178
DAR179

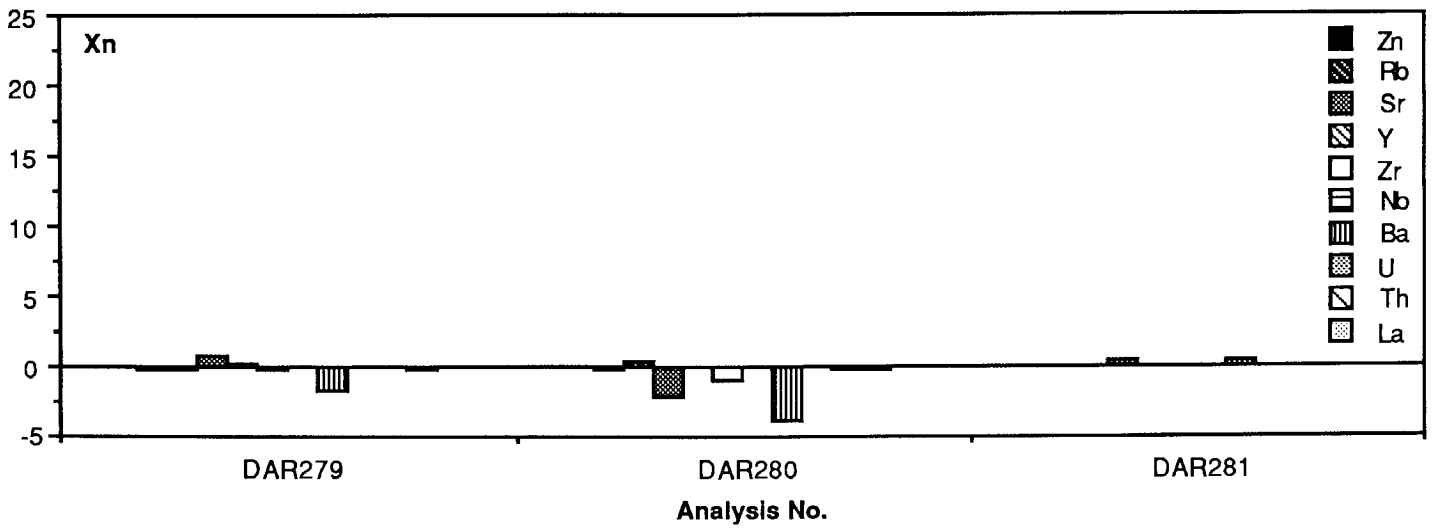
Xn
25
20
15
10
5
0
-5
Zn
Pb
Sr
Y
Zr
Nb
Ba
U
Th
La
DAR279
DAR280
DAR281
Analysis No.

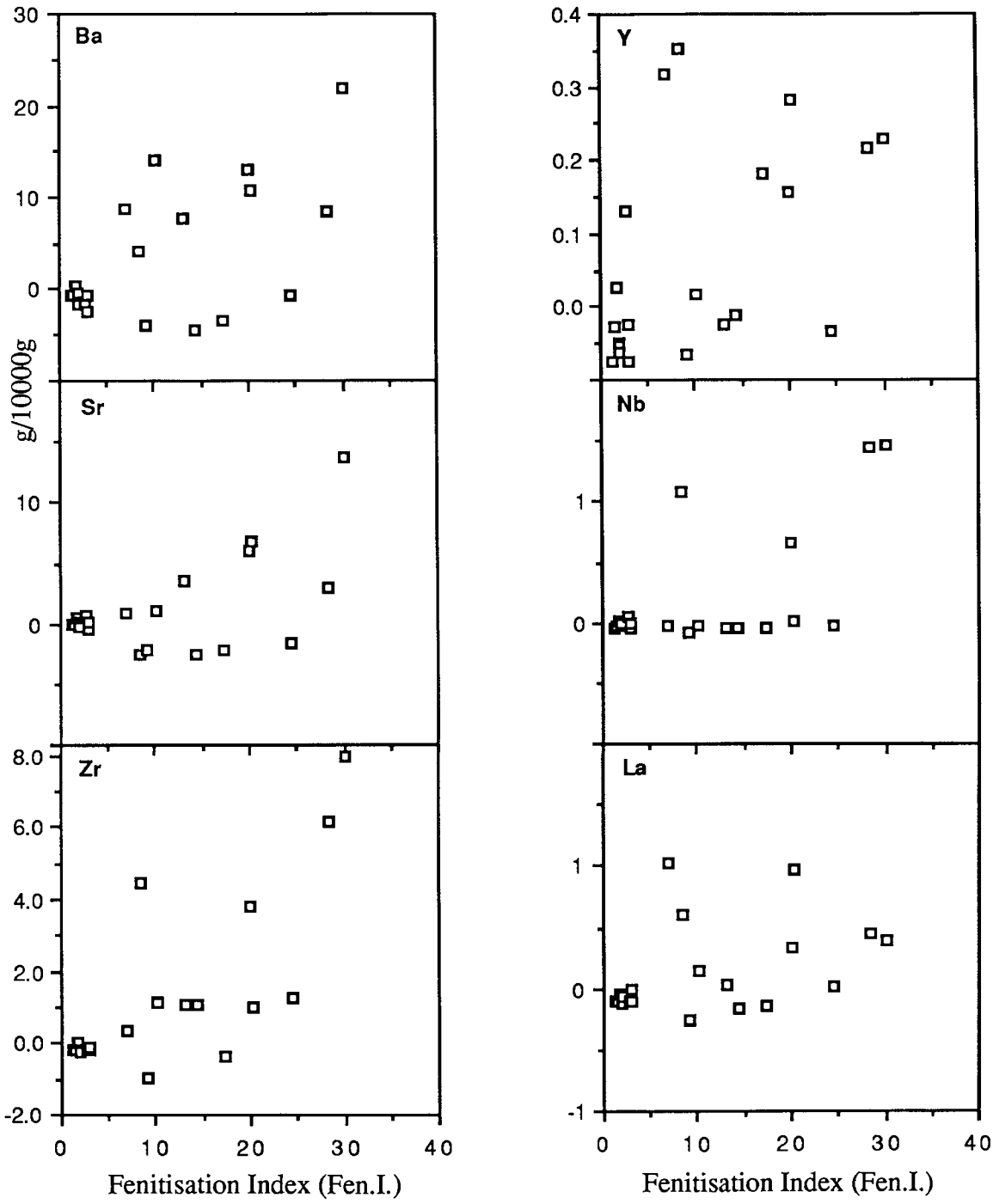

Figure 3.9 Trace element variation in the granite-gneiss.
Gains and losses (g/10000g) as calculated from Gresens' equation plotted against the fenitisation index in order to identify trends with increasing fenitisation.

units SN4B and SN1A of the syenite centre.

3.4 Chemistry of the quartzite

Only a limited number of fenitised quartzite samples were suitable for whole-rock chemical analysis due to the heterogeneous nature of the alteration and so cation plots can yield only a limited amount of information. Eight metasomatised samples are plotted along with one unaltered sample against the baseline of Na-Si (Figure 3.10). The irregular nature of the metasomatism in the quartzite, as described in chapter 2, results in a lack of clearly defined trends. The most regular variation is in Si but this is, of course, because it is plotted in part against itself. The important feature to note in the Si plot is that, despite the lack of samples, the trend is clearly back to the unaltered quartzite close to pure SiO_2. If the quartzite originally contained significant detrital feldspar then extrapolation of the trend would not approach 50 cations Si per 100 oxygens and so this graph indicates that the original quartzite was very pure. The most regular increases with increasing Na-Si are in Ti, Fe, Mn, Na and P. The highly irregular variation in Al is due to the patchy albitisation occuring while quartz is still present. The large amounts of P are a reflection of the presence of abundant apatite.

The use of Gresens' equation in the quartzite is very problematic due to the pure nature of the starting material making it difficult to assess the value of Fv. Because all elements are added except Si the histogram of volume factors for zero mass change shows one large peak near Fv=0 which is of course impossible. This is emphasised by calculating the volume factors for zero mass change for Si and Al. For Si to be constant, volume increases of up to 85% are needed and for constant Al, volume decreases of 95% are required, figures that are ridiculous.

The total rock lines (Figure 3.11) simply balance gains and losses and so produce volume factors in relation to the measured density difference. While the values of Fv produced are feasible (up to 13% volume decrease) there is no quantitative supporting evidence. There is abundant field and petrographic evidence for volume

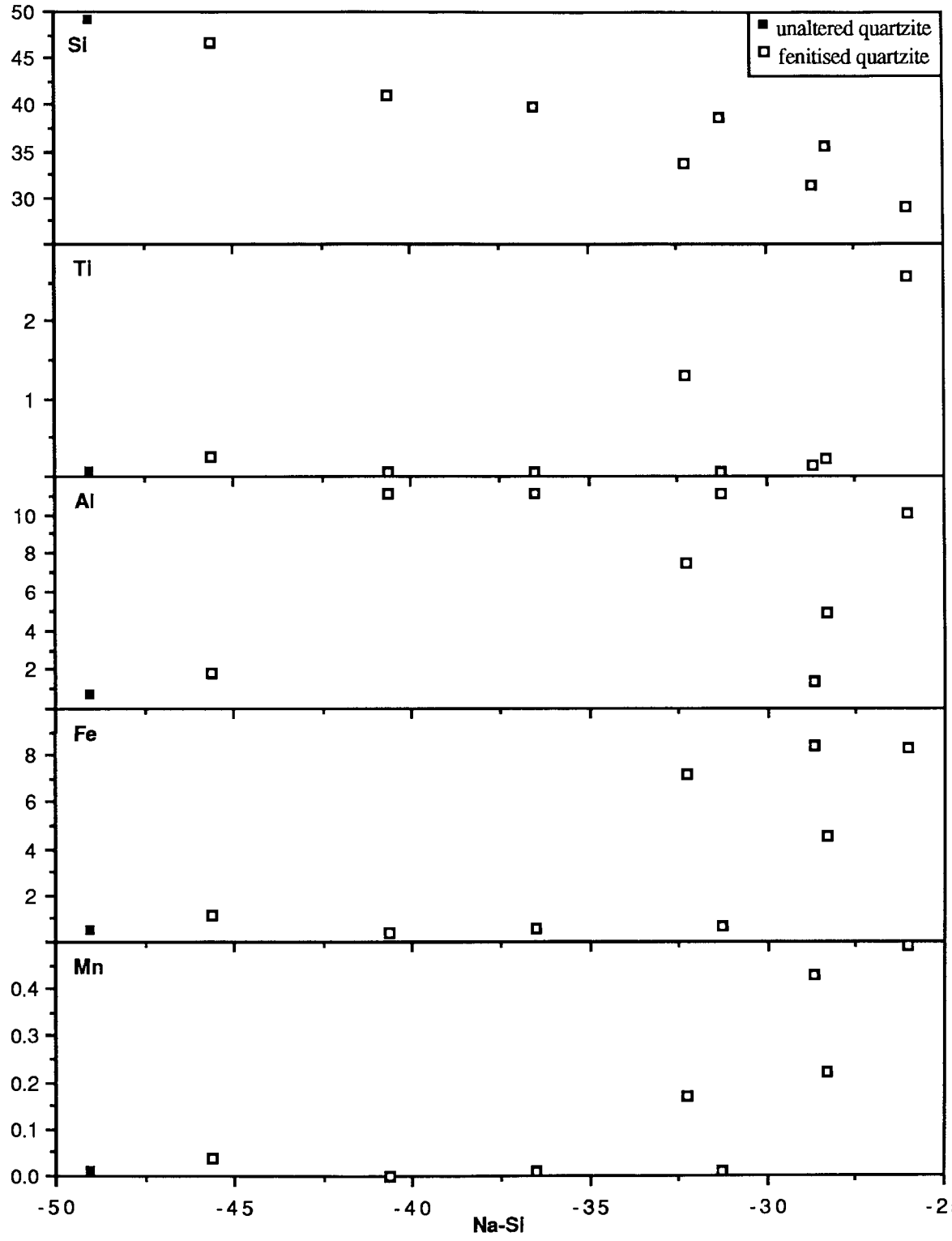

Figure 3.10 (two pages) Whole-rock chemical variation in the quartzite raft in terms of cations per 100 oxygens plotted versus the baseline of Na-Si in which increasing numerical value corresponds to increasing fenitisation.

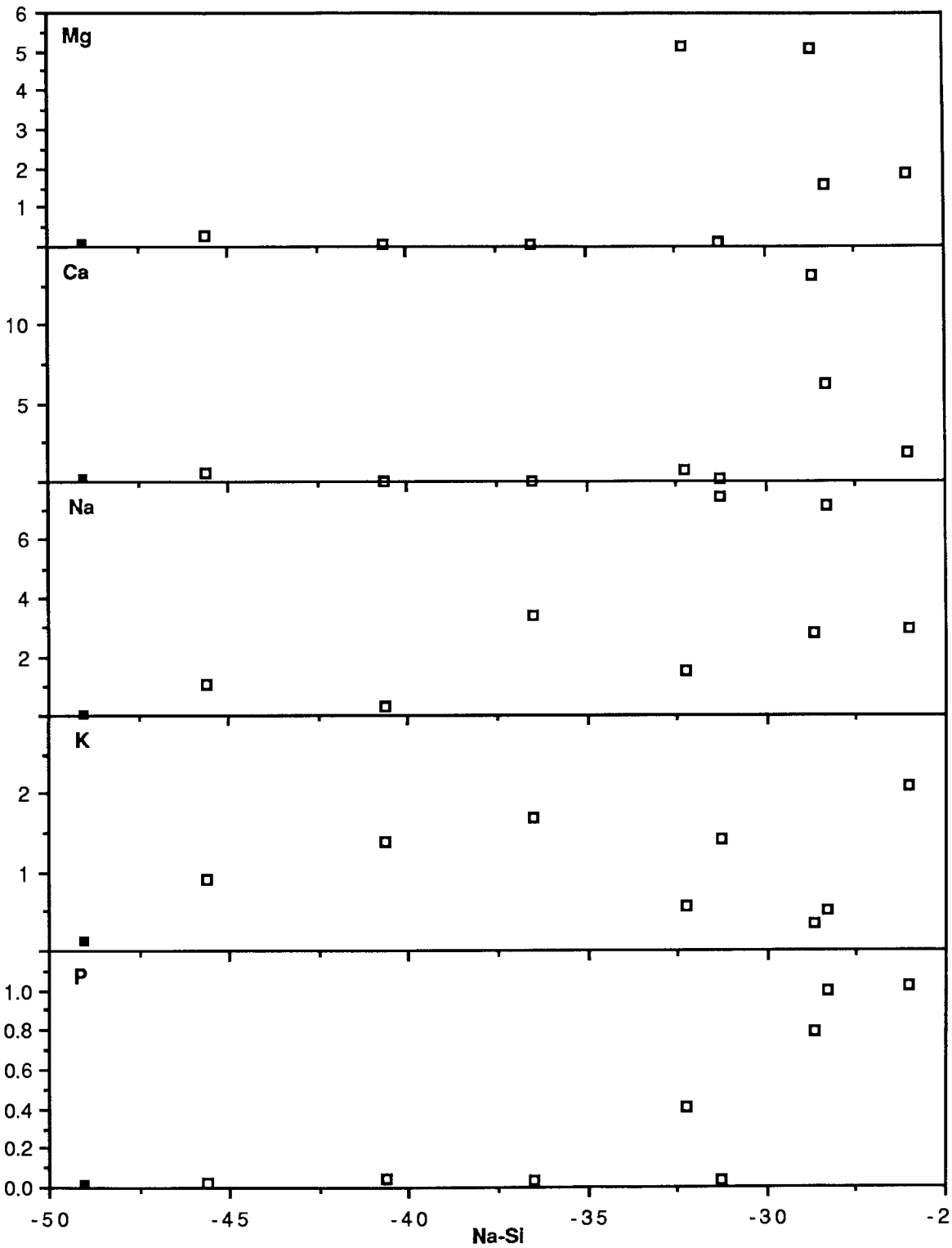
Mg
Ca
Na
K
P
Na-Si
-50
-45
-40
-35
-30
-25

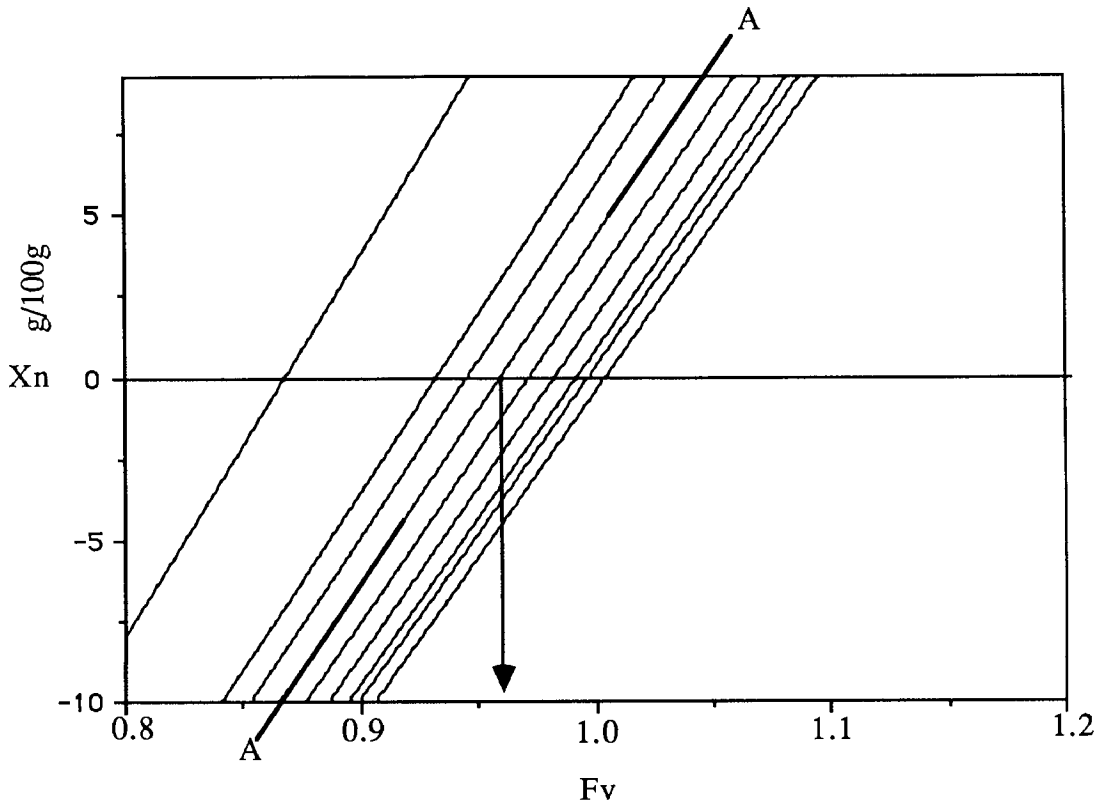

Figure 3.11 Total rock lines for the quartzite plotted on an Xn-Fv graph. The individual component gains and losses are summed to produce the totoal rock gains and losses and these are plotted on the above graph with the lines showing all possibilities. As in Figure 3.5, line A-A represents the average value and the arrowed line shows the value of Fv that would be deduced from this. Note that in this case there is a considerable spread in the Fv values that would be deduced from the individual samples and so the average value is not applicable.

change in the rock in the form of veins and pods of new material that appear to fill cracks, but this is of course only qualitative information. As it is impossible to tie down the value of Fv, the gains and losses cannot be calculated with any reliability. If the volume factors deduced from the total rock lines are used then Si is lost and all other elements are added to balance mass (Figure 3.12) but if the process was dominantly Si loss then greater volume decreases would be indicated and less material would be added. It can be said that no element was immobile as any such assumption would produce unrealistic volume factors and, despite the difficulties in quantifying mass balance, it seems certain that the dominant process was one of desilicification combined with the addition of the other major elements. Plots against the fenitisation index are subject to all the same difficulties and only show the same features as the cation plots, namely Si loss and variable increases in the other elements.

The trace elements are almost always added relative to the parent rock chosen (Figure 3.13) with the most regular and largest increases in Ba, Sr and Zr. La, and by analogy the other rare earth elements, shows large increases in the samples containing significant apatite, a feature that will be discussed in chapter 6. Ni is the only element to show a consistent loss in all but two samples.

3.5 Chemistry of Unit SN4B

Although unit SN4B displays an initial compositional variation, this is well defined and more limited than the variation in unit SN1A. Hence while the unit demonstrates one of the major problems in the study of fenite chemistry, that of parent rock variation, this is sufficiently limited for solutions to be discussed meaningfully.

All elements are recalculated into cations per 100 oxygens and plotted against the baseline of Na-Si. Several clear differences between unaltered and metasomatic rocks can be seen (Figure 3.14). There are decreases in Si, Ti, Mg and Ca and increases in Al and Na, while Fe, Mn and K show no clear trend. One important difference between these plots and the oxide wt% values is in the behaviour of silica.

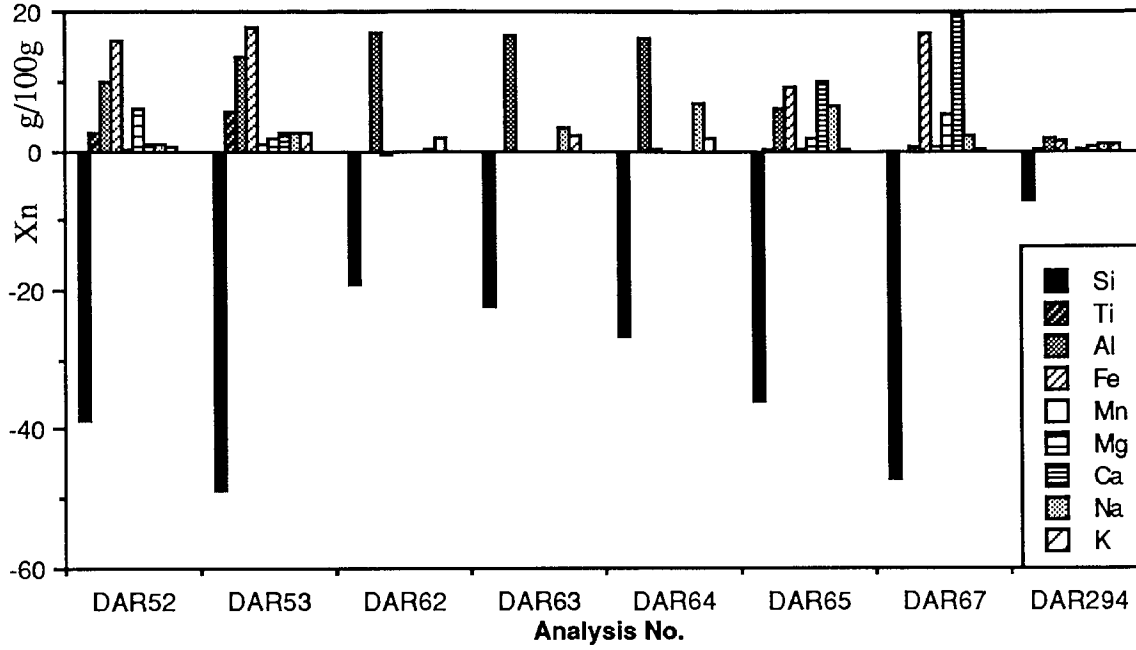

Figure 3.12 Major element variation in the quartzite presented on a barchart of gains and losses calculated from Gresens' equation.

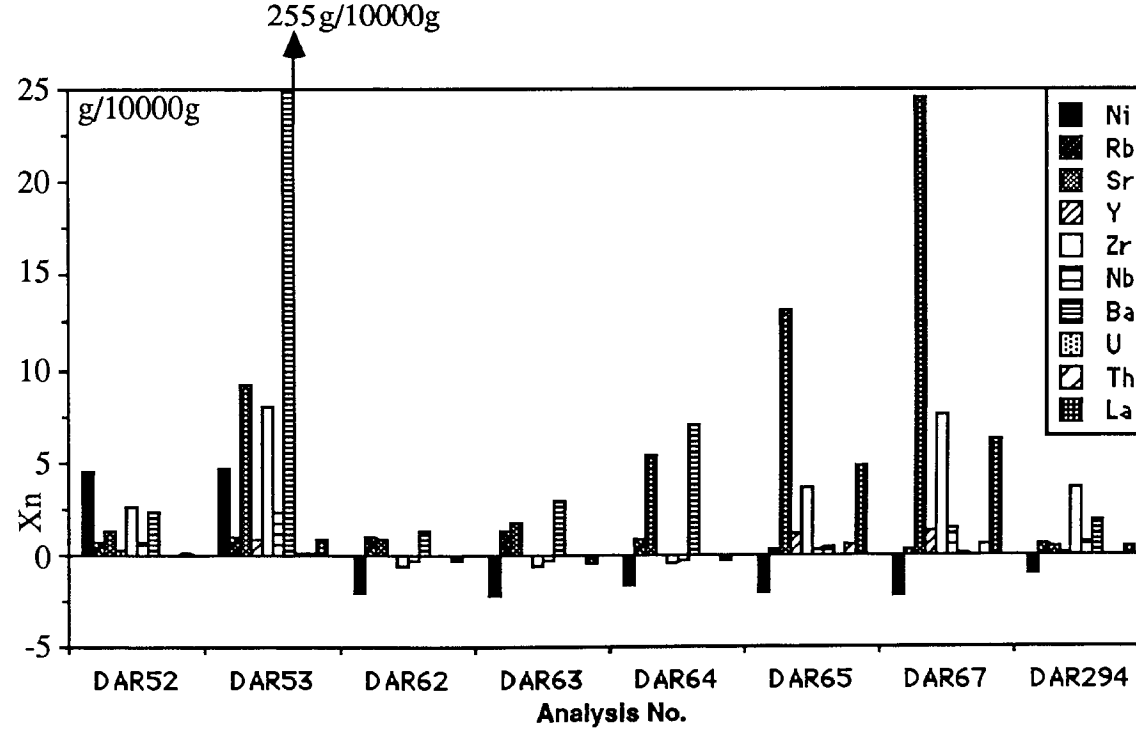

Figure 3.13 Trace element variation in terms of g/10000g calculated from Gresens' equation.

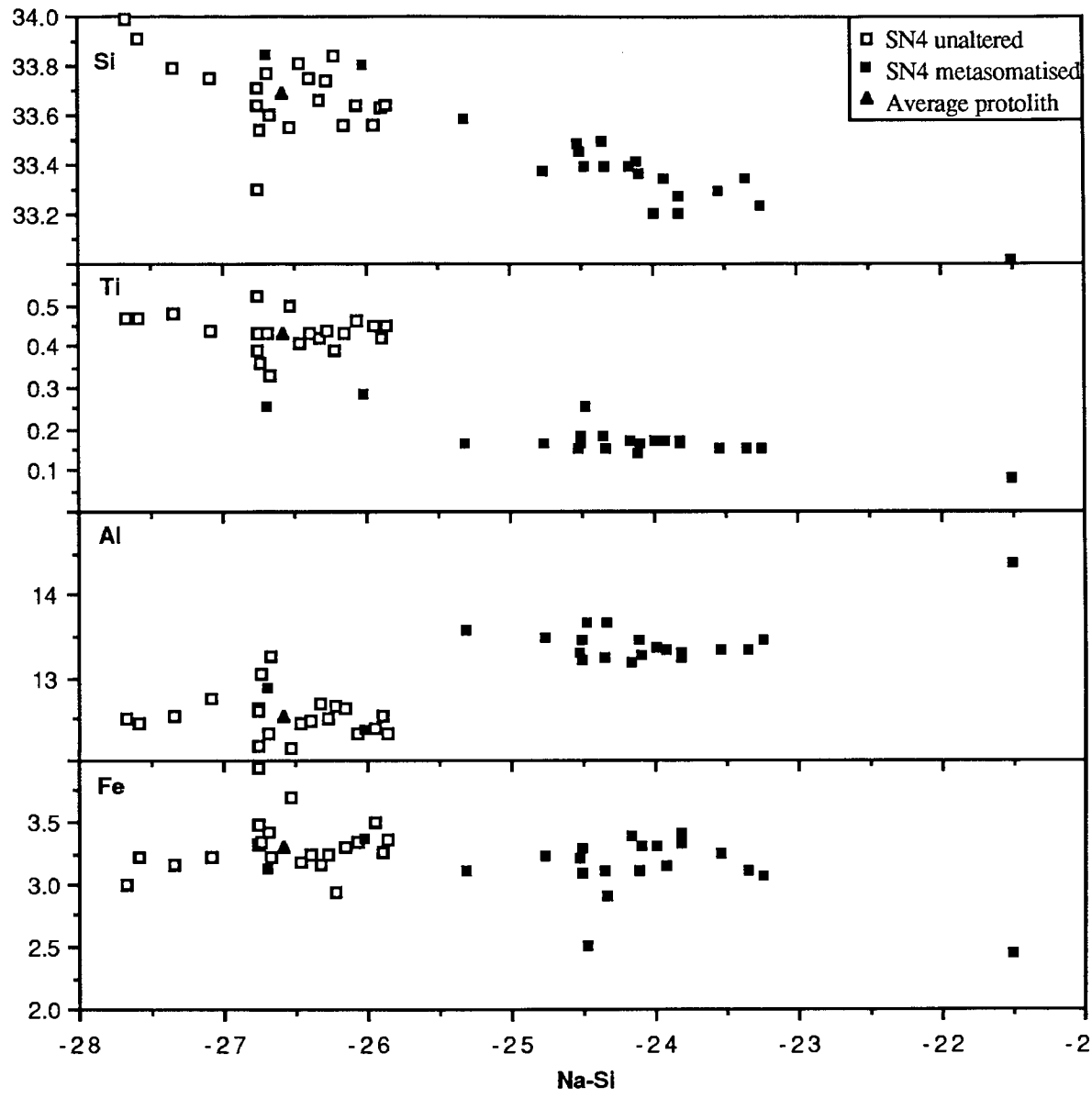

Figure 3.14 (two pages) Whole-rock chemical variation in unit SN4B of the syenite centre plotted in terms of cations per 100 oxygens versus the baseline of Na-Si. Symbols are the same for all plots.

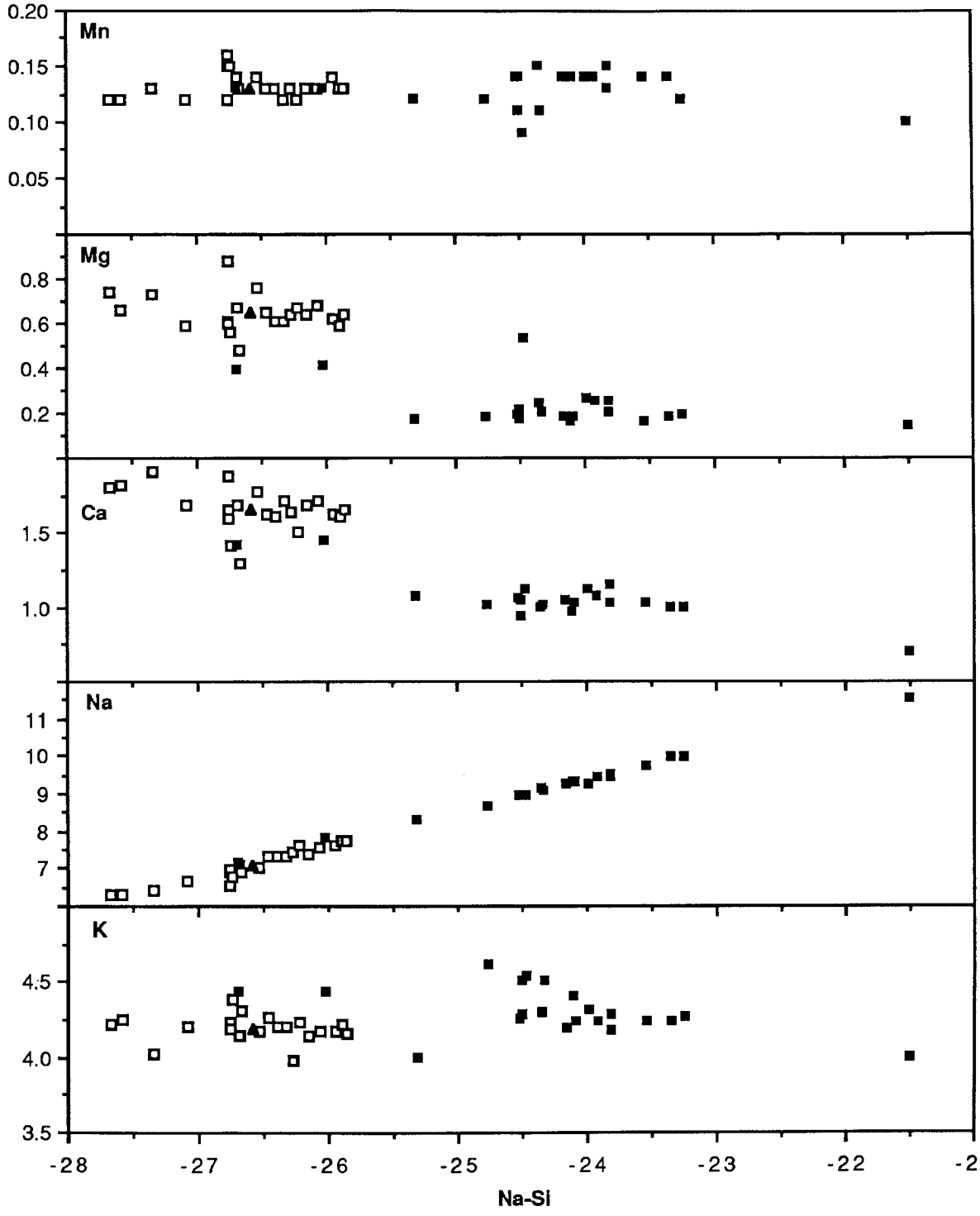
Mn
0.20
0.15
0.10
0.05
Mg
0.8
0.6
0.4
0.2
Ca
1.5
1.0
Na
11
10
9
8
7
K
4.5
4.0
3.5
-28
-27
-26
-25
-24
-23
-22
-21
Na-Si

There is considerable overlap in the SiO_2 content of the unaltered and metasomatic rocks but a clear distinction exists in the Si-cations content. Eighteen out of twenty-one metasomite analyses have less than 33.5 Si cations per 100 oxygens and twenty out of twenty-one protolith analyses have more than 33.5 Si cations. This distinction, coupled with the clear difference in the Na contents, results in the good separation produced by the Na-Si baseline. While these plots only provide a qualitative indication of element gains and losses some important differences are highlighted. A significant increase in Al is indicated on both oxide wt% and cation plots and if this is to be regarded as a real increase in Al then a source and means of transport must be found. Aluminium, though, could be regarded as constant and the gains and losses of the other elements adjusted accordingly. This can be examined using Gresens' equation.

The first thing that must be decided is the composition of parent rock (protolith) to be used in the calculations. Unit SN4B is of limited aerial extent and also has a limited initial compositional range, the analyses of unaltered rocks tending to form clusters rather than any clear trend. The samples of metasomatic material cannot be tied down geographically or petrographically to one part of the unit and so no one analysis can be thought of as more representative of the parent rock than any other. The average of the unaltered samples has been chosen and will be used in all the subsequent calculations as the parent material.

On histograms for zero mass change Si, Al, Fe, Mn and K all show large peaks near constant volume though, as Kresten (1988) noted, the apparent immobility of Si and Al may be due in part to the large initial abundances of those elements. The equation is calculated such that the weight fraction component in the metasomite is multiplied by the volume factor prior to the subtraction of the weight fraction component in the protolith and so elements present in large amounts will produce steeper lines on a C-V diagram and hence a tighter grouping across the gain-loss zero line. In other words a change of 1g Si per 100g rock will have a much smaller relative effect than 1g Mg per 100g rock and so Si appears relatively immobile. The grouping of Fe, Mn and K is

possibly more significant as these elements showed no clear loss or addition in terms of cations per 100 oxygens. As in the granite-gneiss the spread shown by the other elements, Ti, Mg, Ca and Na suggests that they were mobile during the metasomatic process. The histogram for all the elements in all the samples shows one large peak centred on a volume factor of 1 or constant volume (Figure 3.15). Detailed examination of the region between 0.9 and 1.1 shows the top of this peak to be at just greater than constant volume and the volume factor that would be deduced from this plot is 1.01. The range of possible volume factors deduced from the mass balance for the total rock is limited, from a minimum of 0.99 up to a maximum of 1.03, and the average value for the whole unit is once again 1.01 (Figure 3.16). The range of volume factors deduced from constant oxygen is again limited and once more the average value is close to 1.01. There is no field or petrographic evidence in unit SN4B for a significant volume change (the felsic groundmass recrystallises to a fine grained matrix and mafic minerals become poikilitic) and so Fv can be set at close to constant volume with some confidence.

The gains and losses of each element are calculated at the value of Fv deduced from the total rock line of each sample and the results are presented as barcharts (Figure 3.17). The patterns produced are naturally similar to the cation plots but some minor differences are found. Only two samples have a Si increase over the average parent material on the cation plot whereas three samples show an increase on the barcharts. This can either be interpreted as a better representation of the mass changes by the Xn-Fv method or an example of its limitations when using a single parent to represent a range of rocks with initial variation. As the mass balance lines for Si on the Xn-Fv diagrams are very steep and cross the gain-loss zero line near constant volume only very small changes in the value of Fv can make the difference between subtraction and addition of material. The gains shown in Si are minor and would become losses with only slight adjustments of Fv. Even if they are real with respect to the average parent they would be losses with respect to a less evolved and perhaps more appropriate starting material. There is no petrographic evidence for silicification in the three samples and it is therefore suggested that this apparent increase only highlights the limitations

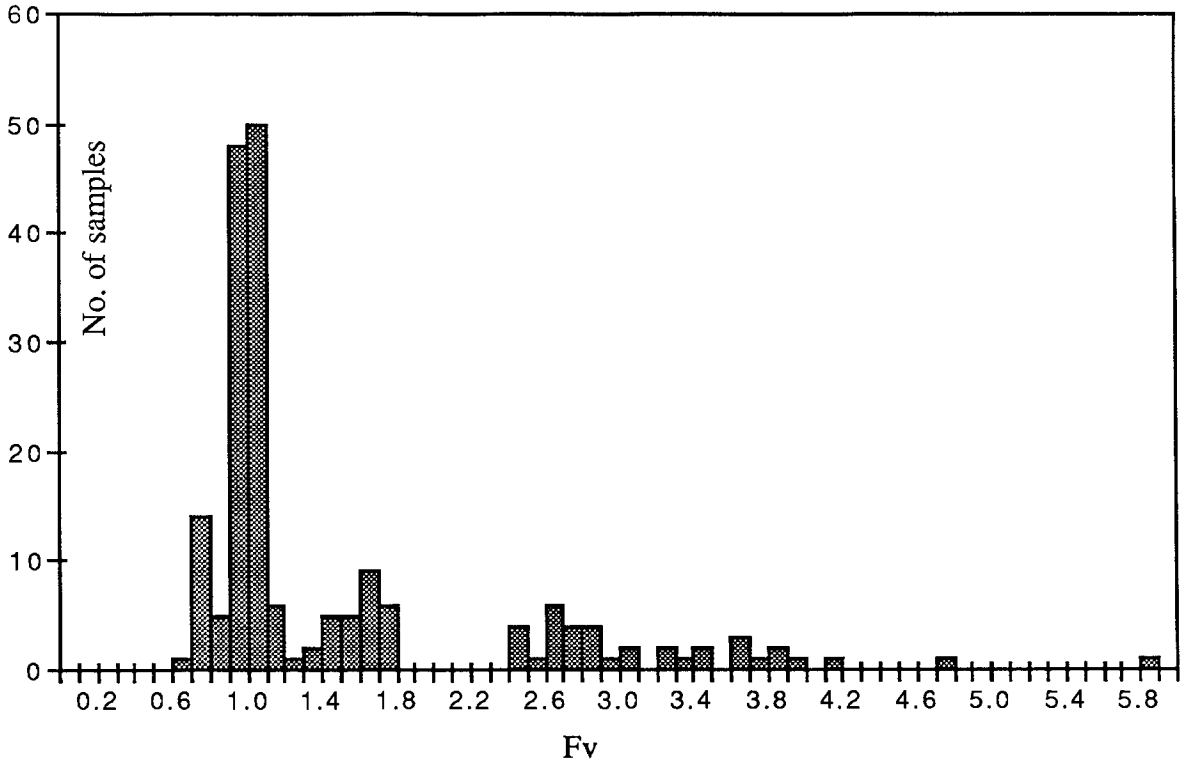

Figure 3.15 Combined histogram of Fv values for zero mass change for all elements in all samples, unit SN4B. Graph produced in the same way as for the granite-gneiss (see Figure 3.4).

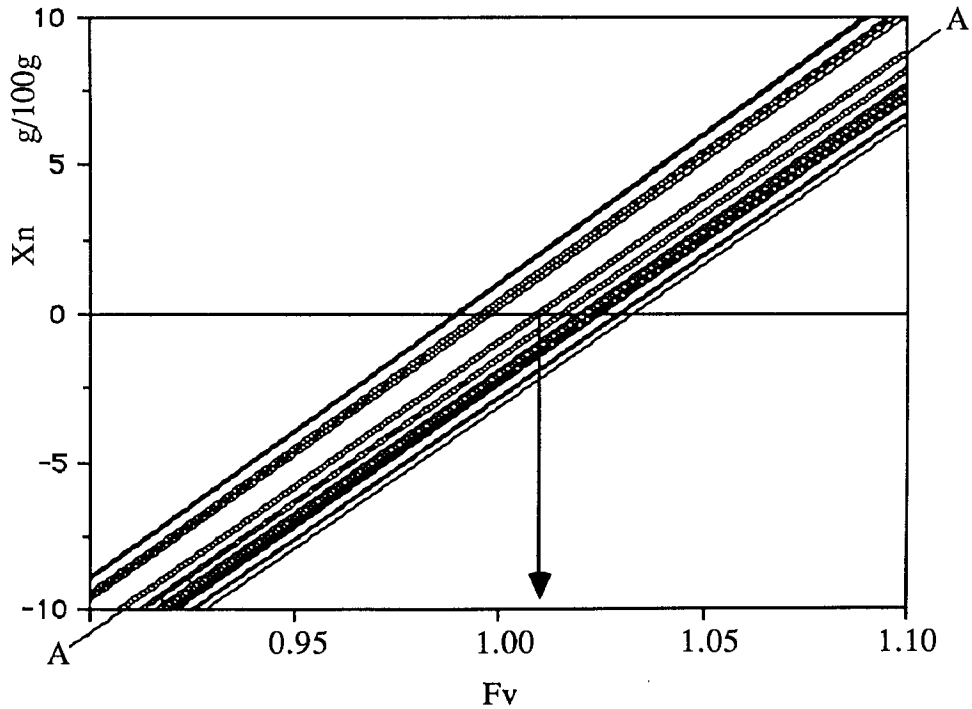

Figure 3.16 Total rock lines for unit SN4B plotted on an Xn-Fv graph. Line A-A represents the average value for the unit and the arrowed line indicates the Fv value deduced from this line. Graph produced in the same way as for the gneiss (see Fig. 3.5).

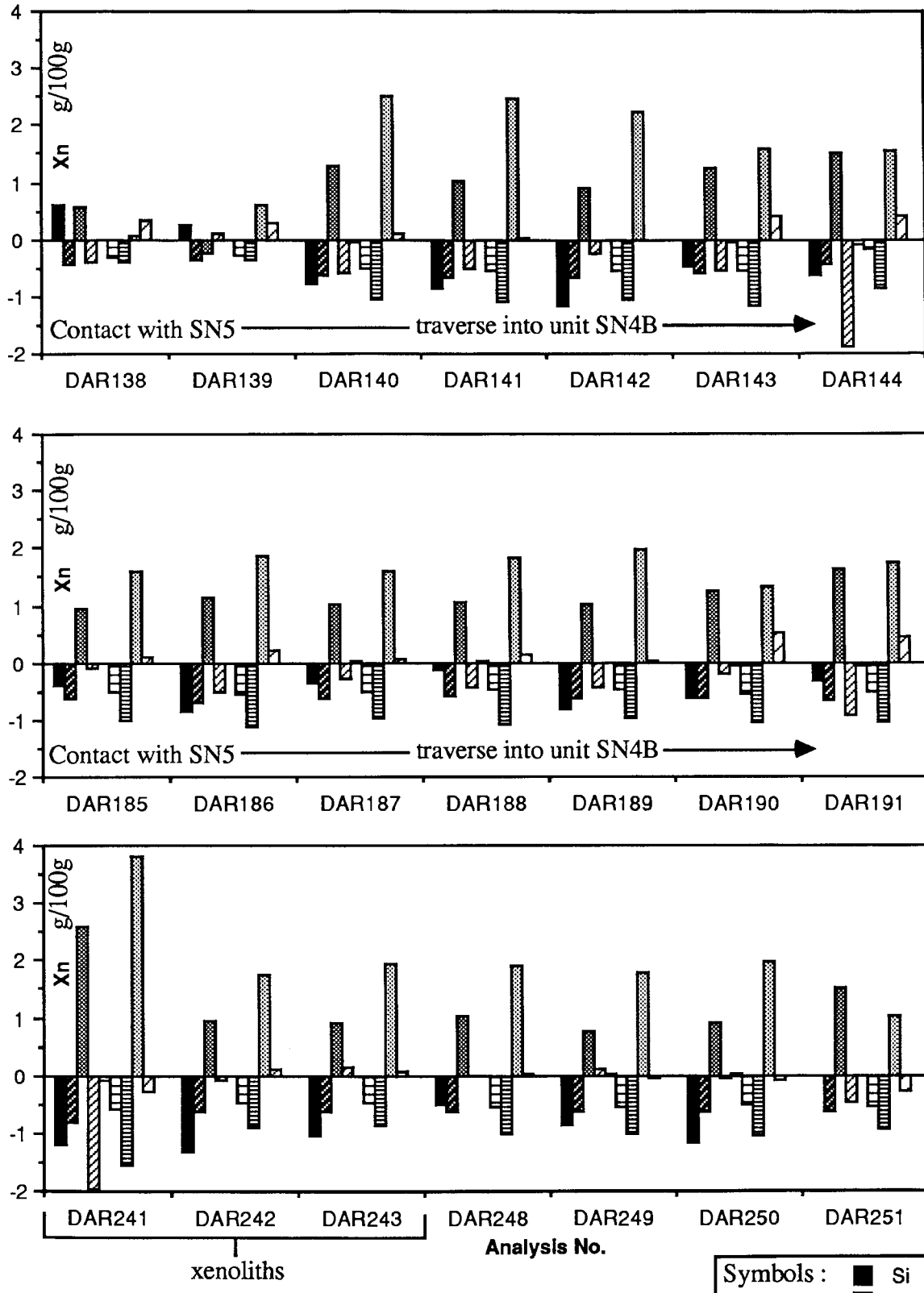

Figure 3.17 Major element variation in unit SN4B presented on barcharts of gains and losses calculated from Gresens' equation. Arrowed lines indicate traverses from the contact with unit SN5.

introduced when there is a compositional range in the starting material.

Kresten (1988), working on the Fen region, found a range of 0.94-1.05 in the Fv deduced from the total rock lines of each sample and, apart from the extreme ends of the range, assumed Fv=1 for all samples. As stated above, the range in unit SN4B is less than half this but it was found that if the average value of 1.01 was used then important differences were produced. Seven samples showed a Si increase, more samples showed increases in FeT and K and other elements changed from subtraction to addition. This is because the Fv values for zero mass change of these elements overlap the Fv values for zero mass change of the total rock. An average value of Fv, as employed by Kresten, is therefore not applicable, especially for Si which has steep mass balance lines.

The other elements that unequivocally decrease on both cation and Xn-Fv plots are Ti, Mg and Ca, results that are in agreement with the petrographic changes to more alkaline minerals such as aegerine-augite and alkali amphibole. Relative to the parent rock chosen, FeT shows a general decrease but it is probable that despite this there is an increase in Fe^{3+}. Mn and K show only minor changes though K is generally gained and is probably controlled by the presence or absence of biotite. The only two elements that show consistent and significant increases are Na and Al. If Al was assumed to be constant then all Si gains would become losses, more Ti, FeT, Mg and Ca would be lost and less Na would be gained. Na would become the only element added to the rock and a slight volume decrease would be indicated. While all this is perfectly feasible it contradicts all the other three lines of evidence for a slight volume increase or at least constant volume. The increase in Al is consistent from the oxide wt% through the cation plots to the Xn-Fv relations and for the mass balance arguments to be consistent an increase in Al must be envisaged. The increases in Na and Al are very consistent and for all but 2 samples the increase in Na is larger than that of Al while the relative decreases tend to be more variable.

As stated in section 3.2 the fenitisation index (total mass exchange) is applicable to rocks with a limited initial compositional variation, such as the

granite-gneiss, but is less appropriate when dealing with the syenites where there is primary magmatic variation. The unaltered samples of the syenites show a range in fenitisation index values due solely to crystal fractionation processes and so no attempt will be made to relate chemical variation in the syenites to this index.

The trace element variations are represented on barcharts (Figure 3.18) and the most obvious feature of these graphs is the universal and consistent loss in Ba and Sr. Zr shows the largest increases and there is a concomitant rise in Y, Nb and La, though some samples show depletions in Zr (+Y, Nb and La). Rb shows increases in every sample. The other trace elements show only minor and irregular changes in comparison to these elements. The consistency of the Ba and Sr depletions and Rb additions probably indicates that these elements are controlled by alterations to the major mineralogy of the rock eg. feldspar breakdown and biotite alteration. The more irregular nature of the Zr, Y, Nb and La variations shows that these elements' abundances are controlled by the minor phases such as apatite and 'rinkite'. The distribution of these minerals is patchy, even on the thin section scale. Chambers (1976), in preliminary studies on the metasomatism in the North Qoroq syenites, implied the presence of a 'zone of depletion' at the contacts between units. He suggested that highly active fluids at the contacts scoured the rocks of trace elements such as Zr, Y, Nb and La, present in microscopic mineral grains along grain boundaries, only to re-deposit them further out as the fluid changed composition or as temperature dropped. The apparently irregular gains and losses of these elements lend some support to this theory. Samples DAR191-185 and DAR144-138 form two traverses away from the contact with unit SN5 and it can be seen that in both cases the samples nearest the contact are depleted in Zr, Y, Nb and La whereas the rest are enriched in these elements. Samples 241-243 are from a xenolith from within unit SN5 and 248-251 are miscellaneous samples from SN4B. Again the xenolith samples appear less enriched than the others. Certainly the contact samples show a predominant leaching of the rock in trace elements whereas the mass balance is more even in the others.

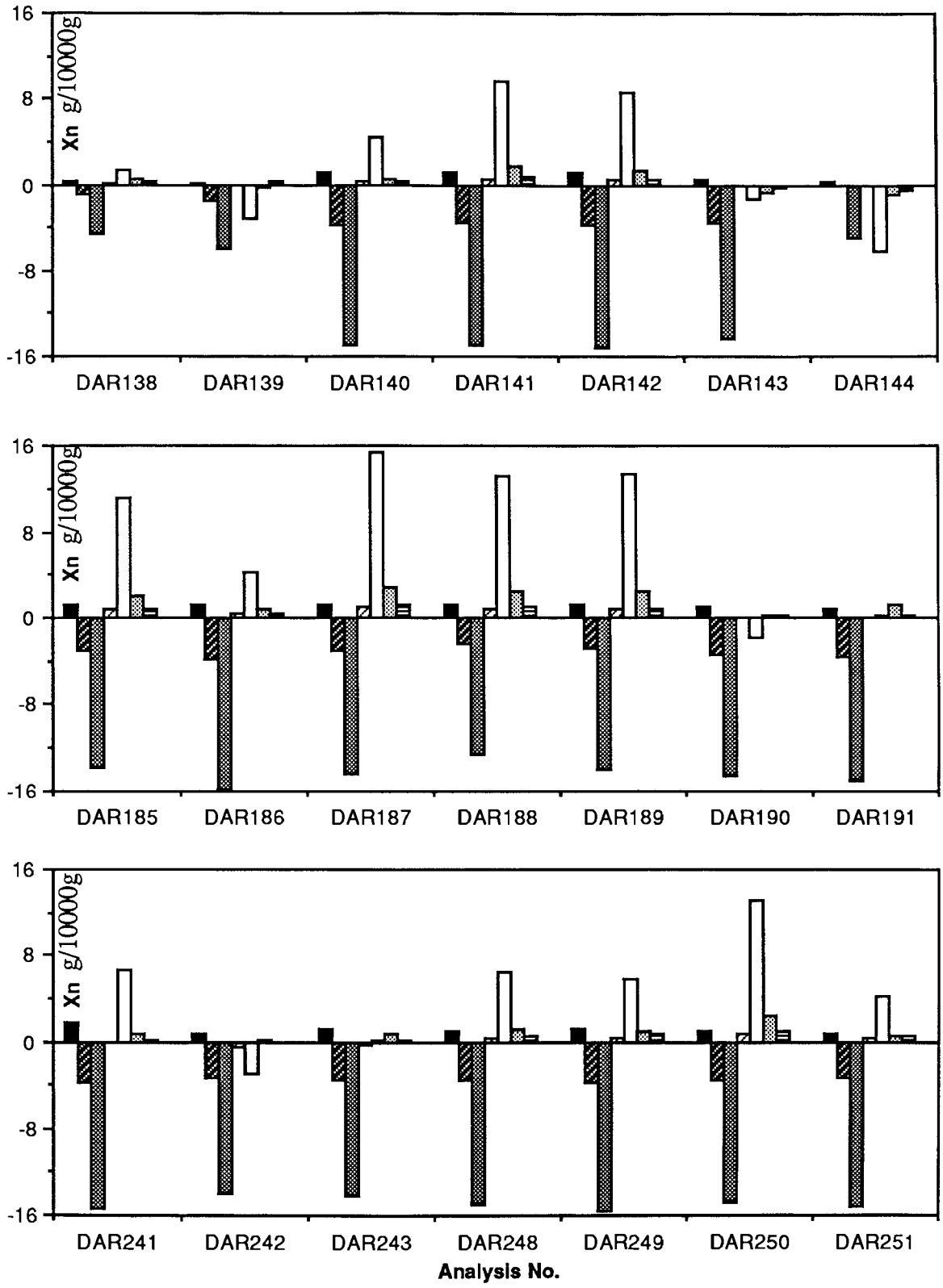

Figure 3.18 Selected trace element variations in unit SN4B in terms of g/10000g calculated from Gresens' equation. Traverses are the same as those shown on Figure 3.17.

Symbols : Rb, Sr, Ba, Y, Zr, Nb, La

3.6 Chemistry of unit SN1A

The plots of cations per 100 oxygens against the baseline of Na-Si immediately highlight the major problem in the study of SN1A (Figure 3.19). The initial compositional range in the unit is very large, going from an augite syenite rim to a highly peralkaline interior. The metasomatised samples always overlap with the more evolved end of the unaltered data ie. at the higher values of Na-Si and, in contrast to unit SN4B, this overlap is complete so any metasomatic change could be envisaged depending on the starting material chosen. For instance, if the parent material was considered to be an augite syenite then a large increase in Al would be implied but if a more evolved starting material was used then Al would decrease. In SN4B an Al increase is produced regardless of which sample is used as the parent rock. Only a very limited amount of information is gained from these plots and so the Gresens equation will now be employed.

Obviously the choice of starting material is of crucial importance. Chambers (1976) subdivided unit SN1A into three petrographic and petrologic zones, A, B and C. The outer rim of augite syenite forms zone A, the highly fractionated interior zone C and the intermediate areas zone B. The boundaries between zones are somewhat arbitary and gradational but it is clear that zone A is very restricted to the margins of the unit and zone C is found only in the north-west quadrant. The intermediate zone B forms the largest geographical area and this is explained by topographic effects which mean that most of the unit is exposed only just below the roof zone. It is clear that taking an average analysis of the unit would be meaningless, unlike in the compositionally more restricted unit SN4B. The parent rock will therefore be picked on petrographic and geographic criteria such that it represents appropriate parent material to the metasomatised syenites.

Most of the metasomatic samples were taken from the contact zone between SN1A and SN1B, though a few came from near to the South Qoroq centre. This places them in zone B of the unit and so both ends of the compositional range are excluded as possible parents. Samples were sought that were taken from close to the SN1A/1B contact and only two petrographically fresh unaltered samples were found to have come

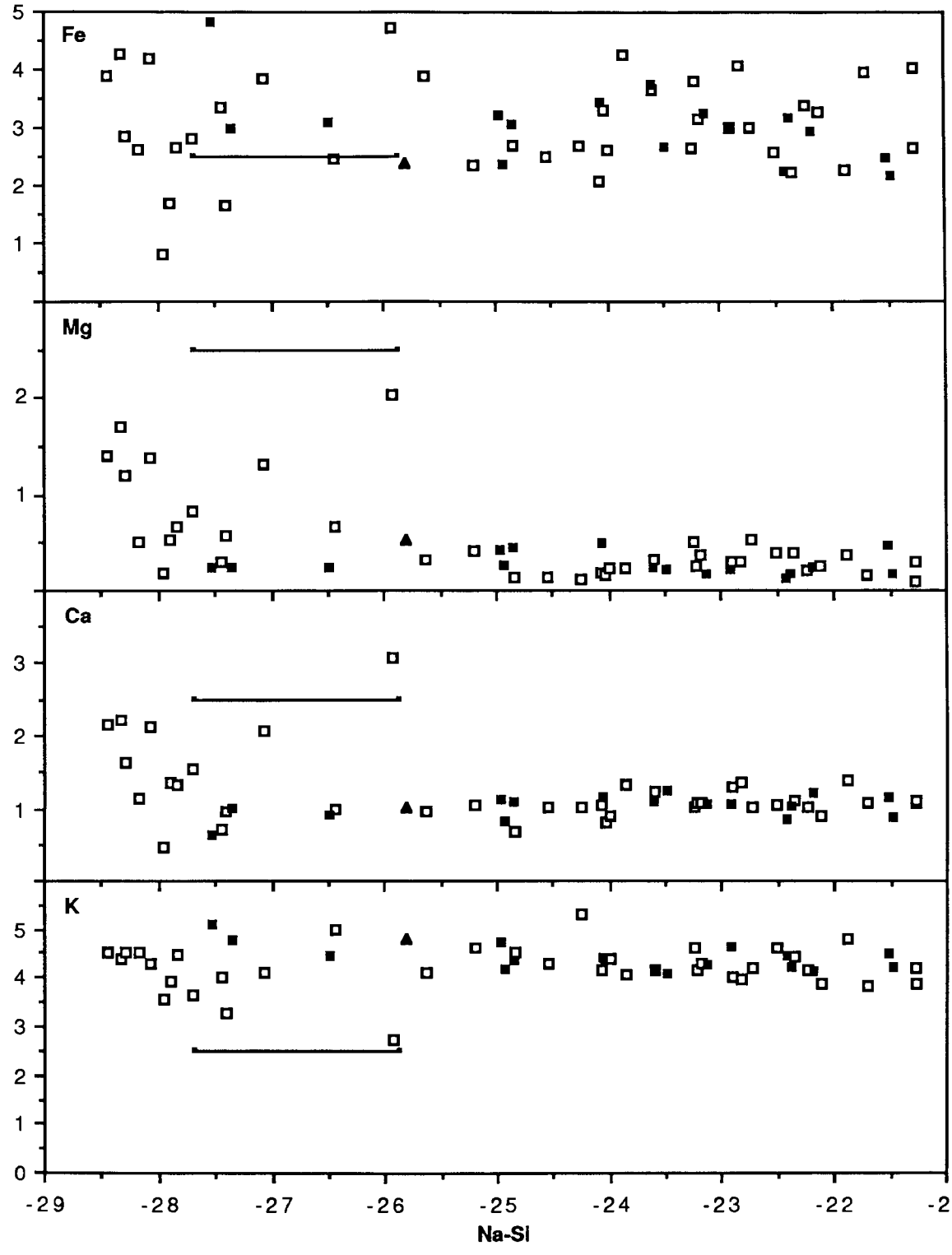

Figure 3.19 Selected plots of cations per 100 oxygens versus Na-Si for unit SN1A showing the large initial range in the unit. The heights of the bars for SN4B do not represent the Fe, Mg, Ca and K conents of the unit.

from this area. These two analyses were averaged and the average values used to calculate the gains and losses. While this may appear a somewhat limited selection it is thought to be the best estimate possible of the starting material.

The volume factor is estimated in the same way as before. The histogram of all elements in all samples shows a good peak near constant volume (Figure 3.20a), though this is not as tightly defined as for SN4B. Detailed examination of the region from 0.9 to 1.1 shows the peak to be just above 1 with the best estimate being 1.04. The total rock lines again show a tight grouping near constant volume with a range from 1.00 up to 1.04 and an average of 1.02 (Figure 3.20b). An assumption of constant oxygen would yield a volume factor of 1.02 and so once again there is excellent agreement between all three lines of evidence. There is no field or petrographic evidence for a volume change and so the gains and losses will be calculated at the individual values of Fv deduced from the total rock lines.

All the samples taken from the contact zone between SN1A and SN1B show very consistent gains and losses (Figure 3.21). Si, Ti, Mg and K always decrease and Na always increases. FeT is the other major gain in all but two samples. Al is more variable but is lost more often, and in greater amounts, than it is gained. Mn and Ca show only minor and variable changes. The five samples taken from near the South Qoroq centre have different patterns. Four out of five have Si increases and three out of five, Na decreases. FeT is the only major increase and all the other elements show minor changes. Given the variable nature of the unit it is most likely that this difference between the two areas is primarily due to unsuitable parent material. The samples from near South Qoroq show less evidence of metasomatic alteration both chemically and petrographically and so are more susceptible to the influence of an unrepresentative parent.

The most striking feature of the trace element barcharts (Figure 3.22) is that trace element leaching of the rocks is the dominant process. Zr is the only element that shows significant increases relative to the other elements and even this is lost as often as it is gained. This is probably a reflection of the scouring of the rocks by active fluids and

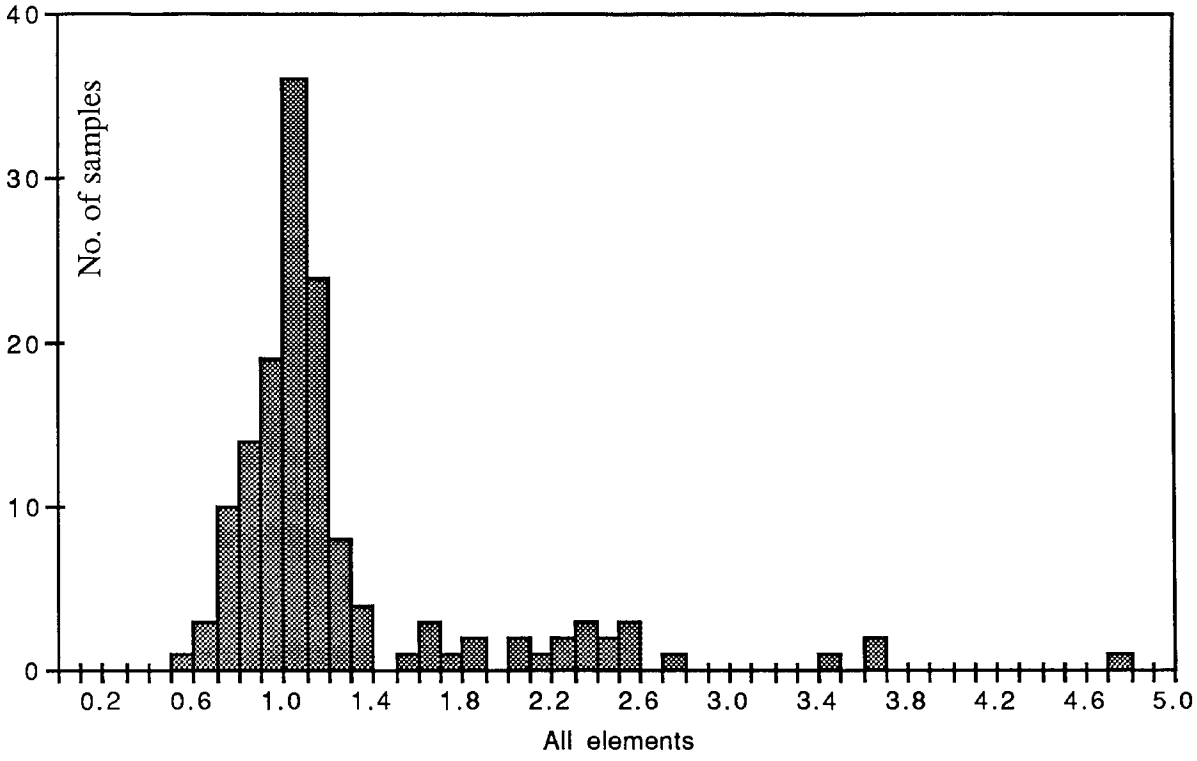

Figure 3.20a Combined histogram of Fv values for zero mass change for all elements in all samples, unit SN1A. Graph produced in the same way as Fig.3.4.

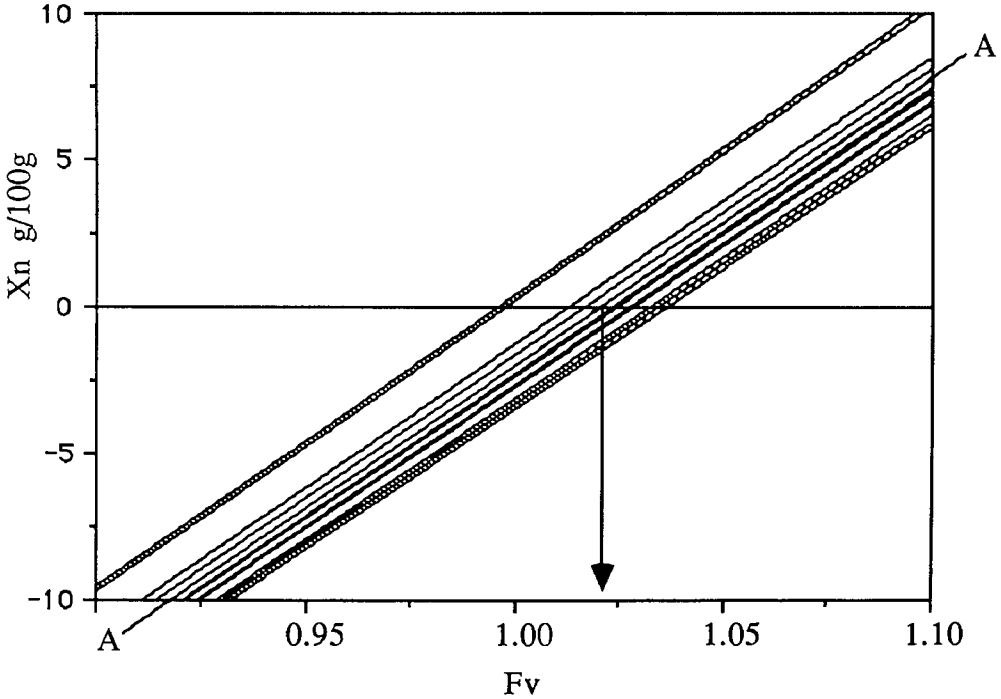

Figure 3.20b Total rock lines for unit SN1A plotted on an Xn-Fv graph. Line A-A represents the average value for the unit and the arrowed line indicates the Fv value deduced from this line. Graph produced in the same way as Figure 3.5.

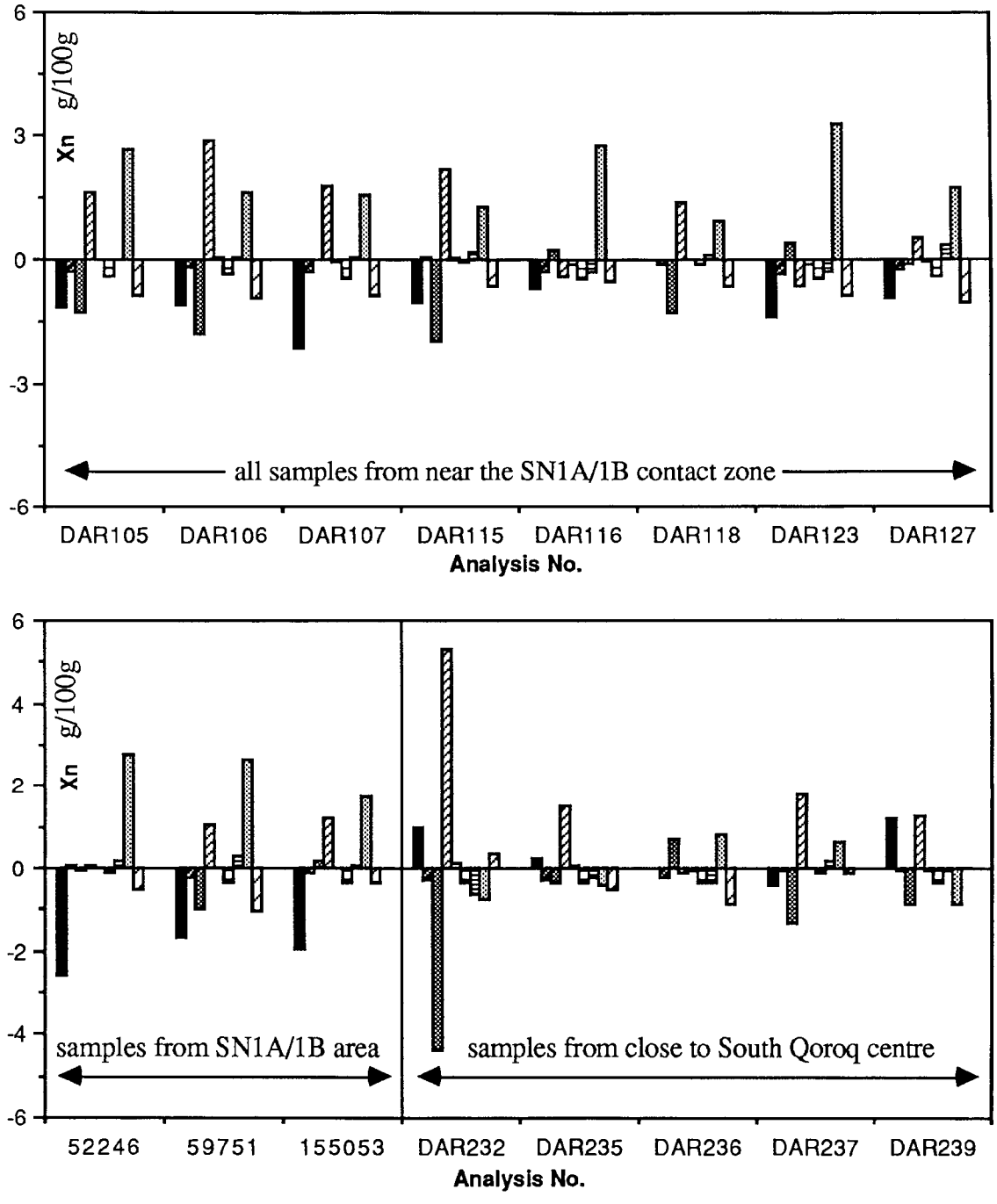

Figure 3.21 Major element variation in unit SN1A presented on barcharts of gains and losses calculated from Gresens' equation. Note the difference in the patterns between the samples from close to SN1B and those close to the South Qoroq centre.

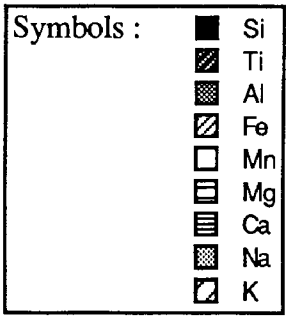

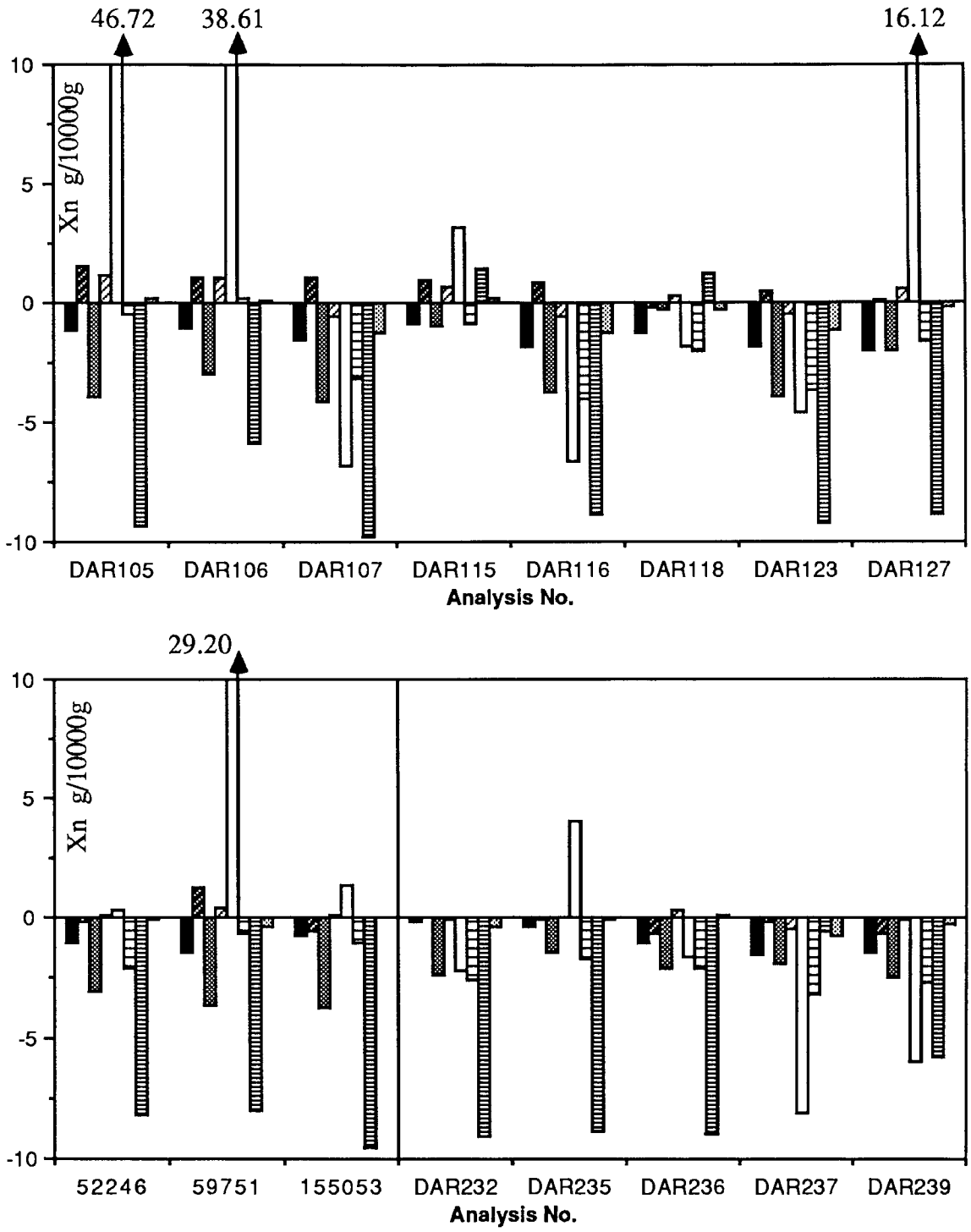

Figure 3.22 Selected trace element variations in unit SN1A in terms of g/10000g calculated from Gresens' equation. Sample number locations are given on Figure 3.21.

the localised precipitation of Zr bearing phases. Chambers (1976) first demonstrated a zone of depletion in unit SN1A adjacent to the younger intrusive units and the majority of the samples analysed come from close to the contact with SN1B. The shallow and irregular nature of this contact zone makes a correlation with distance from contact impossible. The most consistent losses are in Ba, Sr and Zn, with the magnitude of the losses also very consistent.

3.7 Discussion

The two syenite units studied, despite the problems of choosing appropriate parental material, both seem to show dominant losses in Si, Ti and Mg and consistent gains in Na. These are results that would be expected in the re-equilibration of a fluid evolving from an undersaturated, peralkaline syenitic magma with less evolved syenite. Mn appears relatively immobile in both units but there are differences in the behaviour of the other major elements. Total Fe is gained in unit SN1A but lost in SN4B although this depletion could mask a change in the oxidation state with increased Fe^{3+}. Robins and Tysseland (1983) and Robins (1984) demonstrated that Fe^{3+} can increase while total iron decreases during metasomatism due to the oxidation of the iron, an important process in the development of alkali mafic minerals such as aegerine. McKie (1966), Vartiainen and Woolley (1976) and Rock (1976) also show increases in the oxidation ratio of Fe during fenitisation.

Al and K are both gained during metasomatism of unit SN4B whereas in unit SN1A both these elements are lost. These differences, and those in the behaviour of Fe, may be partly due to the difficulties in selecting appropriate parent material and the most important observation to be made is that in both cases Al is not immobile, relative to the parent rock chosen. This is particularly important as immobile Al was a controlling condition favoured by Rubie (1982) and Rubie and Gunter (1983) in the fenitisation of granodioritic basement surrounding the Kisingiri nephelinite volcano. Hards (1976) showed that the distribution coefficients between a Cl-rich vapour phase and nepheline syenite melt are much lower for Al than for the alkalis and experiments on natural rocks

by Ermanovics *et al.* (1967) and Burnham (1967) showed that even the more mobile elements such as Fe, Ca and Mg require moderate to high concentration of Cl^- in solution before they will be liberated. It is apparent then that the fluids responsible for the metasomatism must have contained significant quantities of the halogens, Cl and F, and that complexing of Al by fluorine was important in the transport of this high-charge element. Robins and Tysseland (1983), Robins (1984), Appleyard and Woolley (1979) and Woolley *et al.* (1972) all invoke the transport of Al in metasomatic fluids derived from syenitic magmas and given the infiltrative rather than diffusive nature of the process the transport of Al-F complexes would not be a problem. This is supported by the trace element variations which show considerable depletions and enrichments of Zr, Y, Nb and La all of which require the presence of halide and/or carbonate complexes to be transported in solution (Mineyev 1963, Alderton *et al.* 1980). The highly irregular distributions of these elements reflects the localised precipitation and dissolution of accessory phases such as 'rinkite' and apatite. Much more regular are the depletions in Ba and Sr and the increases in Rb which are partly explicable in terms of the initial fractionation trends of the syenites. Crystal fractionation processes rapidly depleted the syenite magmas in Ba and Sr while Rb was progressively enriched and so late fluids migrating from the fractionated interior of the syenites would be in equilibrium with a syenite magma that was poor in Ba and Sr and relatively rich in Rb. The Ba and Sr are therefore leached from the syenites during the breakdown of perthite in the metasomatism while Rb could be added to the orthoclase produced and also to biotite. The very regular variations also reflect the dominant control that the major phases have on the concentrations of these elements.

The major process in all the country rock samples studied is desilicification. This is accompanied by the addition of most other major elements, maintaining near constant volume. The quartzite raft shows the strongest sodic and ferromagnesian alteration due to its location in the roof zone of unit SN1B where it will have acted as a sink for cations from the high temperature fluids emanating from the interior of the unit. The albitisation of the originally very pure quartzite also supports the idea of the

transport of significant quantities of Al. The granite gneiss shows potassic metasomatism in places but no correlation can be made with distance from contact due to the irregular nature of the metasomatism and the transport of fluids along fractures. Chambers (1976) suggested a diffusion of K to the cooler areas away from the syenite contact and diffusion of sodium towards the contact in accordance with the experimental results of Orville (1963) but, despite albite often being present in the immediate contact zone, heavily fenitised samples also close to the contact have gained as much K as samples further out. High K contents are associated with the formation of biotite which is stabilised in the granite-gneiss, but not in the quartzite, by the high initial Al content from the feldspars. It is documented, though, that potassic alteration is indicative of lower temperatures than sodic alteration (Siemiatkowska and Martin 1975, Jahns *et al.* 1969) and it is likely that the quartzite raft, enclosed in the syenite, suffered higher temperatures than the country rock gneiss. A combination of factors probably led to the differences in the fenitic alteration between the quartzite raft and the granite-gneiss, the most important of which were probably the original composition, temperature and the Na-rich nature of the fluid.There was probably extensive interaction between the metasomatic fluids, derived from the syenites, and meteoric solutions in the granite-gneiss and this may have affected Na/K ratios in the fluid and hence the fenitisation (Lagache and Weisbrod 1977). Trace elements are dominantly added to the country rocks, most notably Ba, Sr, Zr and La. These are the elements leached from the syenites and it seems likely that the metasomatic fluids have flushed these elements from the syenite centre and then redeposited them in the country rocks as temperature decreased.

3.8 Conclusions

1. The representation of chemical change in terms of a 100 oxygen cell gives only qualitative information except under very restricted geological conditions ie. constant oxygen and constant volume. The chemistry of metasomatism should, therefore, be considered using the composition-volume equation derived by Gresens (1967).

2. The most important problem in quantifying mass balance in this way is the assumption or constraint that the author feels best represents the process and so is used to define the volume factor for calculation. This assumption must be supported by as many lines of evidence as possible and must always be related to field and petrographic evidence.

3. It is suggested that the total rock mass balance lines derived by Kresten (1988) provide the best estimate of volume factor for near constant volume processes. If field and/or petrographic evidence suggests a large volume change ($>\pm 15\%$) then it is highly unlikely that the rock can have balanced mass by changing density and so the total rock lines will give a false estimate of Fv. The same restriction is true of oxygen mass balance.

4. The metasomatism in and around the North Qoroq centre took place at near consant volume and was dominated by desilicification coupled with addition of sodium. Ti and Mg were the other major losses from both syenite units while SN4B lost FeT and gained Al whereas SN1A gained FeT and lost Al relative to the parent rocks chosen. The trace elements are dominantly leached from the heavily metasomatised syenites and added to the country rock aureole.

5. A process of material transfer from the syenite centre outwards is proposed which occured in a continuous phase of fluid activity. A persodic, undersaturated fluid emanated from the syenite interior and re-equilibrated with the less evolved syenite. On reaching the country rocks the same fluid cycle began to react once again, though probably at lower temperatures and with a less sodic fluid composition. There was probably interaction with meteoric fluids in the country rocks.

References

Alderton, D.H.M., Pearce, J.A. & Potts, P.J. 1980. Rare earth element mobility during granite alteration ; evidence from southwest England. EARTH PLANET SCI LETT **49**, 149-65.

Appleyard, E.C. 1980. Mass balance computations in metasomatism: Metagabbro/nepheline syenite pegmatite interaction in northern Norway. CONTRIB MINERAL PETROL **73**, 131-44.

Appleyard, E.C. & Woolley, A.R. 1979. Fenitisation: an example of the problems of characterising mass transfer and volume changes. CHEM GEOL **26**, 1-15.

Babcock, R.S. 1973. Computational methods of metasomatic processes. LITHOS **6**, 279-90.

Barth, T.F.W. 1948. Oxygen in rocks: a basis for petrographic calculation. J GEOL **56**, 50-60.

Bottinga, Y. & Weill, D.F. 1970. Densities of liquid silicate systems calculated from partial molar volumes of oxide components. AM J SCI **269**, 169-82.

Burnham, C.W. 1967. Hydrothermal fluids at the magmatic stage. *In* Barnes, H.L. (ed) *Geochemistry of hydrothermal ore deposits*, 34-76. Holt, Rinehart & Winston.

Chambers, A.D. 1976. The petrology and geochemistry of the North Qoroq centre, Igaliko Complex, South Greenland. UNPUBL PhD THESIS, UNIV OF DURHAM.

Cox, K.G., Bell, J.D. & Pankhurst, R.J. 1979. *The Interpretation of Igneous Rocks.* Allen & Unwin : London.

Ermanovics, I.F., Edgar, A.D. & Currie, K.L. 1967. Evidence bearing on the origin of the Belleoram stock, southern Newfoundland. CAN J EARTH SCI **4**, 413-31.

Gresens, R.L. 1967. Composition-volume relationships of metasomatism. CHEM GEOL **2**, 47-65.

Hards, N. 1976. Distribution of elements between the fluid phase and silicate melt phase of granites and nepheline syenites. NERC Pub Series D **6**, 88-90.

Hoeve, J. 1978. Composition and volume changes accompanying soda metasomatic alterations, Vastervik Area, SE Sweden. GEOL RUNDSCHAU **Bd 67**, 920-942.

Jahns, R.H., Martin, R.F. & Tuttle, O.F. 1969. Origin of granophyre in dykes and sills of tholeiitic diabase. AM GEOPHYS UNION TRANS **50**, 337.

Kresten, P. 1988. The chemistry of fenitisation: examples from Fen, Norway. CHEM GEOL **68**, 329-351.

Lagache, M. & Weisbrod, A. 1977. The system: Two alkali feldspars-KCl-NaCl-H_2O at moderate to high temperatures and low pressures. CONTRIB MINERAL PETROL **62**, 77-101.

McKie, D. 1966. Fenitisation. *In* Tuttle, O.F. & Gittins, J. (eds) *Carbonatites*, 261-94. New York: Wiley-Interscience.

Mineyev, D.A. 1963. Geochemical differentiation of the rare earths. GEOCHEMISTRY **12**, 1129-149.

Orville, P.M. 1963. Alkali ion exchange between vapor and feldspar phases. AM J SCI **261**, 201-37.

Rae, D.A. & Chambers, A.D. 1988. Metasomatism in the North Qoroq Centre, South Greenland: cathodoluminescence and mineral chemistry of alkali feldspars. TRANS R SOC EDINBURGH **79**, 1-12.

Robins, B. 1984. Petrography and petrogenesis of nephelinized metagabbros from Finnmark, Northern Norway. CONTRIB MINERAL PETROL **86**, 170-77.

Robins, B. & Tysseland, M. 1983. The geology, geochemistry and origin of ultrabasic fenites associated with the Pollen carbonatite (Finnmark, Norway). CHEM GEOL **40**, 65-95.

Rock, N.M.S. 1976. Fenitisation around the Monchique alkaline complex, Portugal. LITHOS **9**, 263-79.

Rubie, D.C. 1982. Mass transfer and volume change during alkali metasomatism at Kisingiri, Western Kenya. LITHOS **15**, 99-109.

Rubie, D.C. & Gunter, W.D. 1983. The role of speciation in alkaline igneous fluids during fenite metasomatism. CONTRIB MINERAL PETROL **82**, 165-75.

Siemiatkowska, K.M. & Martin, R.F. 1975. Fenitization of Mississagi Quartzite, Sudbury area, Ontario. GEOL SOC AM BULL **86**, 1109-122.

Taylor, H.P. 1971. Oxygen isotope evidence for large-scale interaction between meteoric ground waters and Tertiary granodiorite intrusions, western Cascade Range, Oregon. J GEOPHYS RES **76**, 7855-74.

Vartiainen, H. & Woolley, A.R. 1976. The petrography, mineralogy and chemistry of the fenites of the Sokli carbonatite intrusion, Finland. GEOL SURV FINL BULL **280**, 87pp.

Woolley, A.R., Symes, R.F. & Elliot, C.J. 1972. Metasomatised (fenitised) quartzites from the Borrolan Complex, Scotland. MINERAL MAG **38**, 819-36.

CHAPTER 4

Cathodoluminescence and Mineral Chemistry of Alkali Feldspars

4.1 Introduction

The majority of studies on metasomatism have followed the format set by either McKie (1966) or Gresens (1967) and looked at whole-rock chemical changes. This approach was examined in Chapter 3 and from this point the effects of metasomatism in the North Qoroq Centre will be discussed from a dominantly mineralogical viewpoint. This chapter will concentrate on the outer syenite unit (SN1A) and deal principally with the reactions between felsic mineralogy and fluid phase, concentrating on the cathodoluminescence effects produced in the alkali feldspars.

It has been clearly demonstrated that hot aqueous fluids can react with feldspars in alkaline intrusions. Parsons (1978) reviewed the important role of hydrothermal fluids in controlling structural state variation in alkali feldspars. The same author demonstrated the value of exsolution textures as a guide to water-rock interactions in the Klokken intrusion, South Greenland (Parsons 1980). In addition to structural changes hot aqueous fluids have been shown to react with feldspars producing pronounced chemical changes (eg Orville 1963).

A combination of mineral chemistry and cathodoluminescence forms the basis of this study. From the observed compositional and textural changes shown by the feldspars it has been possible to gain information on the behaviour of the fluid phase. Cathodoluminescence is a well-established technique but until recently was used only occasionally outside the field of sedimentology. To the best of the author's knowledge, only Mariano (1976,1979) has previously used it to characterise alkali metasomatic processes. The results presented here challenge some of his conclusions and raise important questions about the occurence and interpretation of luminescence in feldspars.

4.2 Petrography

A brief description will be given of only the petrographic textures developed in the felsic phases in response to the actions of the metasomatising fluids. A more general petrography of the North Qoroq Centre is given in 2.3. A common feature of metasomatically formed minerals is the development of a markedly poikilitic texture. This characteristic is displayed by nepheline and sodalite which have both grown in some quantity. Petrographic evidence suggests that this growth has been at the expense of feldspar, with small rounded crystals of feldspar enclosed within the poikilitic feldspathoids. Sodalite can also be seen to replace nepheline, which at times is heavily embayed. Less commonly, analcite,cancrinite, natrolite and fluorite are present in the altered syenites. The formation of these abundant sodium-rich felsic phases implies metasomatism and this is confirmed by bulk-rock chemical investigation (see 4.4 and Ch.3).

The feldspars show a number of textural features developed in response to the activity of a fluid phase. Furthest from the contact with the younger unit the aqueous fluid has merely promoted unmixing of the feldspars. Initially, this is seen as a coarsening of the perthites into patch perthites, with the Na-phase showing Albite twinning and the K-phase commonly being turbid (Plate 4.1a). As the contact with a younger unit is approached the aqueous phase caused irregular areas of albite to form along feldspar-feldspar grain boundaries and eventually the virtually continuous development of albite rims (Plate 4.1b). These take the form of double layers with the twin lamellae in each layer in optical continuity with those in the opposite, adjacent feldspar. These 'swapped rims' are a result of enhanced exsolution in the two feldspars (Ramberg 1962). In a number of samples fluid/rock interaction has resulted in the complete breakdown of the feldspar, with the formation of distinct crystals of the sodic and potassic phases (Plate 4.1c). Immediately adjacent to the contact with younger units original feldspars show corroded outlines against sodalite or nepheline and frequently quite extensive clear rims of albite. The remainder of the feldspar in the rock occurs as part of a fine-grained mosaic involving albite, altered K-feldspar, nepheline and sodalite

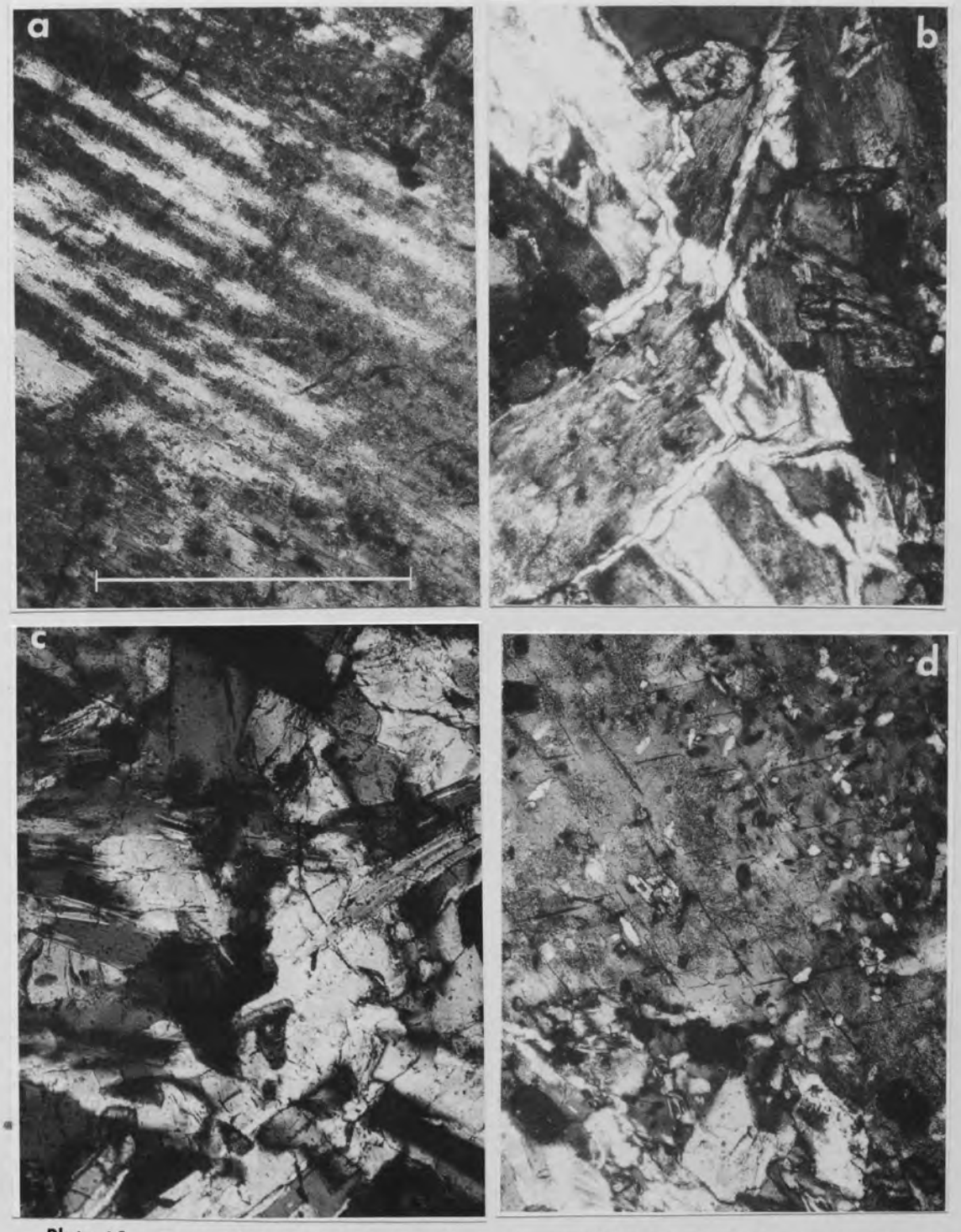

Plate 4.1 Textural features shown by the feldspars from unit SN1A of the North Qôroq centre; all crossed nicols (scale bar 1 mm applies to all four figures):

(a) very coarse perthite with broad Ab and Or lamellae; the K-phase is turbid and the Na-phase shows albite twinning;

(b) swapped albite rim between feldspar grains;

(c) assemblage of albite and K-feldspar formed from the complete breakdown of original perthite; nepheline is also present;

(d) mosaic of albite, nepheline and sodalite with remnant crystal of K-feldspar in a strongly metasomatised syenite.

(Plate 4.1d) and, less frequently, cancrinite, analcite and fluorite.

Textural relationships in these altered syenites are difficult to interpret using a standard petrological microscope and are best studied using cathodoluminescence.

4.3 Cathodoluminescence Petrography of the Feldspars

The details of luminescence will not be discussed here but a review of luminescence in minerals is given by Walker (1985) and a practical guide to cathodoluminescence petrography and its uses by Miller (1985).

Plates 4.2(a-d) show the same textural features described in Plates 4.1(a-d). Both were taken with the same microscope of the same field of view and illustrate the greatly enhanced detail available using cathodoluminescence.

The patch perthites illustrated in Plate 4.1a consist of broad albite and K-feldspar lamellae both luminescing blue but, in addition in Plate 4.2a, secondary fine cross-cutting bands can be seen showing red luminescence. This later albite forms along perthite lamellar boundaries and cross-cuts the original albite lamellae at intervals, giving the appearance of red and blue striping. In this way, red luminescing albite indicative of the action of a late-stage fluid phase can be easily distinguished from the primary albite phase of the perthite. The significance of the red albite in relation to the nature and role of the fluid phase is discussed later (see 4.4 and 4.7.2).

Similarly, for the swapped rims texture illustrated in Plate 4.1b, the contrast between the red luminescent albite rims and the blue luminescent remnants of the original feldspar (Plate 4.2b) allows a better interpretation to be made of the exact form and true extent of the rims. The lobate margins represent an irregular front of exsolution (of the Na-phase of one feldspar into the adjacent feldspar) and the more regular lines through the centres of the rims represent the original grain boundaries.

Where the perthites have completely broken down into discrete crystals of albite and K-feldspar, twinning in the albite is absent, or only poorly developed, making it difficult to distinguish from the potassic phase. Using cathodoluminescence the red albite crystals (Plate 4.2c) are dramatically revealed. In addition, red luminescent albite

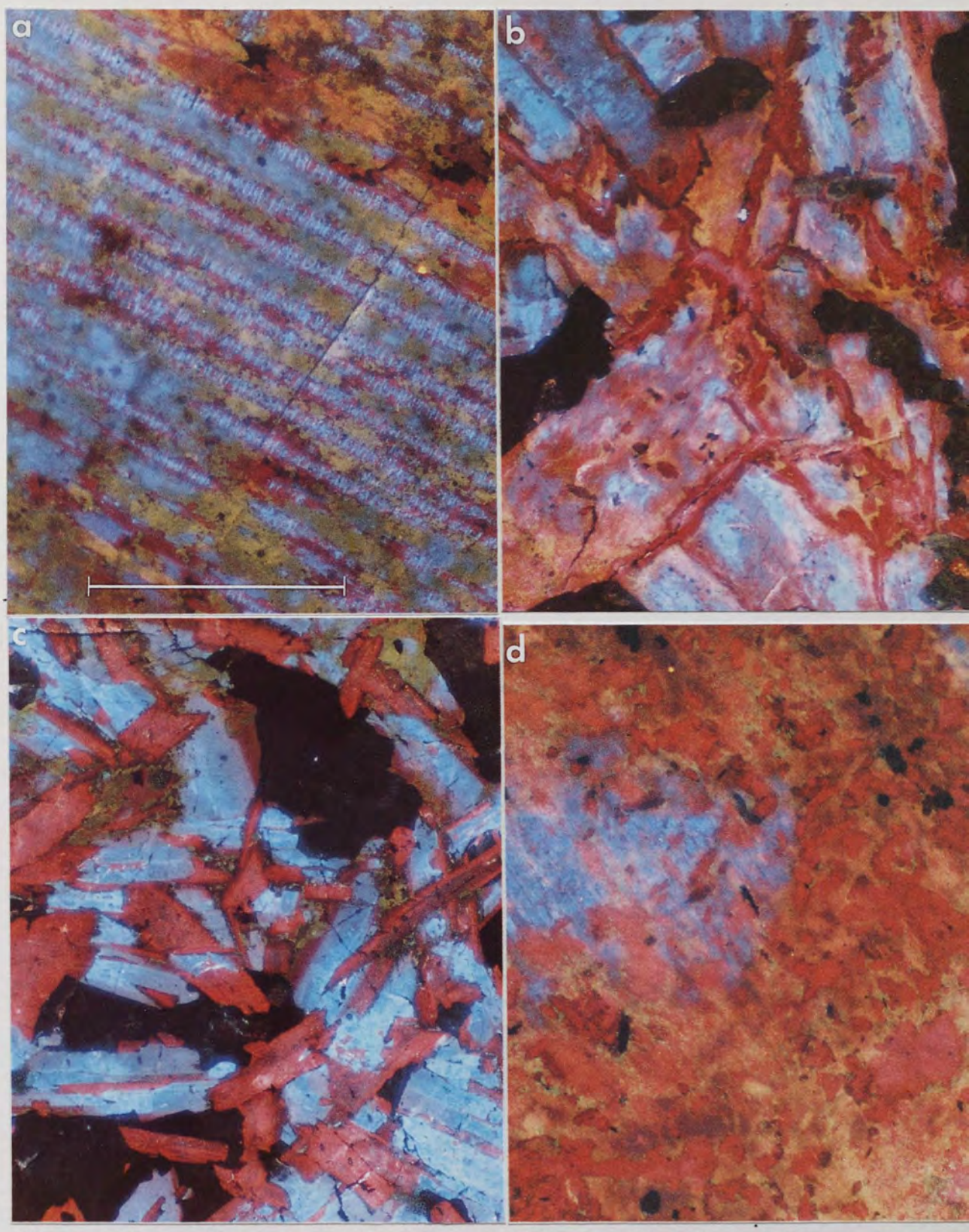

Plate 4.2 Metasomatic textures in feldspars from unit SN1A of the North Qoroq centre seen using cathodoluminescence (scale bar 1mm). The fields of view shown here correspond to those in Plate 4.1(a)-(d).
(a) Late stage, red luminescent albite can now be seen cross-cutting the earlier Ab and Or lamellae, both of which luminesce blue.
(b) The red luminescence of the albite rims contrasts with the blue luminescent K-feldspar giving a clearer idea of the extent of the rims.
(c) The contrast between the red luminescent albite, blue luminescent K-feldspar and almost non-luminescent nepheline quickly resolves the phases present and clarifies the intricate relationships shown in Plate 4.1(c).
(d) The complex matrix in the strongly metasomatised syenite shown in Plate 4.1(d) is an intergrowth of red luminescent albite, dull nepheline and orange luminescent sodalite with remnants of blue luminescent K-feldspar.

occurs along cleavages and twin planes in the blue luminescent K-feldspar and forms rims as a stage in the development of new discrete albite crystals. The two feldspars are present in roughly equal proportions and non-luminescent alkali-amphibole, aenigmatite and nepheline are the other major phases.

In syenites closest to the contact with a younger unit and most affected by the action of the fluid phase it is usually difficult using a normal optical microscope to make any quantitative assessment of the proportions of remnant feldspar, albite and associated feldspathoids because of the fine grained nature of the resulting mosaic. Cathodoluminescence produces dramatic colour contrasts which highlight the major textural features of the rock. In Plate 4.2d the original feldspars (blue) can be clearly seen to have been pervasively corroded by fluid and replaced by a mosaic involving anhedral crystals of red luminescing albite associated with anhedral nepheline, sodalite, analcite and fluorite.

The obvious textural and mineralogical adjustments outlined above and so clearly seen using cathodoluminescence raise the question as to the role of the fluid involved in these changes. Was it an active metasomatising fluid, responsible for the introduction and removal of elements in solution, or merely a pervasive, passive phase promoting localised chemical readjustments? An investigation of bulk-chemical changes answers the question and allows textural and mineralogical changes to be placed in context.

4.4 Whole rock chemistry

A detailed discussion of whole-rock chemical changes during metasomatism is given in Chapter 3 but a typical composition-volume diagram for unit SN1A, constructed using the average SN1A parent, chosen in Chapter 3 on petrographic and petrologic criteria, and the samples used in the study of feldspar mineralogy, is reproduced here (Fig. 4.1) and brief comment is given on the gains and losses shown with regard to the felsic mineralogy.

Examination of Fig. 4.1 shows a number of elements crossing the gain-loss

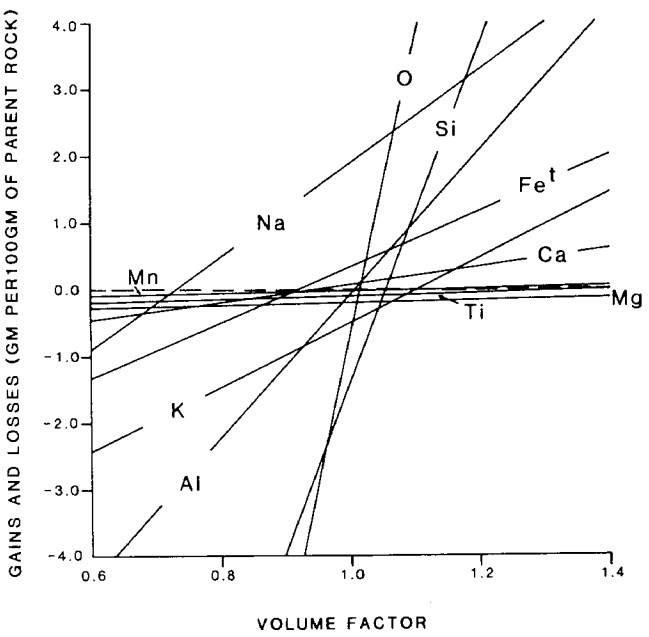

Figure 4.1 Composition-volume diagram (after Gresens 1967) of the bulk rock chemical changes produced by metasomatism of unit SN1A of the North Qoroq centre, calculated using the samples studied for feldspar chemistry. A volume factor (Fv) = 1 represents constant volume.

zero line at a similar point. This suggests that they may have been immobile during metasomatism and, as the point at which they cross the gain-loss zero line is close to constant volume (~1.02), that little volume change occured. Using the assumption of constant volume metasomatism, or other parameters frequently used such as constant oxygen or constant Al and despite variability in the parent material, it is clear that certain elements have been added or removed during the metasomatic process. A marked increase in Na and decrease in Si are the dominant changes, together with a smaller but still significant decrease in K and a possible increase in total Fe. The implications of these metasomatic changes on the felsic mineralogy of SN1A is discussed in 4.7.2. A gradation exists, both texturally and chemically, from rocks showing clear metasomatic alteration to those, further from the contacts with younger units, where textures of enhanced unmixing of the feldspars are dominant (Plate 4.2a). Here bulk-rock chemical changes are less apparent or absent and it may be that the chemical effects of the fluid phase on the syenites were limited and localised.

4.5 Feldspar Chemistry

4.5.1 Analytical Techniques

Wavelength dispersive electron microprobe analyses were carried out using a Cameca camebax instrument. For the analyses of bulk compositions of perthites the beam was either defocussed or rastered over an area of ~20μm diameter. When analysing individual exsolved phases the beam was rastered for analysis of the alkalis and then moved up to 5 m away before analysing the other elements with a fully focussed beam. This assumes homogeneity over a small area but minimises Na loss and results in good totals and stoichiometry. The elements Si, Al, Ti, Fe, Mn, Mg, Ca, Na, K and Ba were analysed for and all analyses totalled 98-101%. Representative analyses are listed in Table 4.1.

Table 4.1 Representative microprobe analyses of alkali-feldspars from unit SN1A of the North Qôroq centre; analyses 1–3 are bulk compositions of unaltered perthites, analyses 4 and 5 are K-feldspar produced by the breakdown of the perthites and analyses 6–8 are albites formed during interaction of the rock with a fluid phase; N.D. = below detection limits; all analyses are by wavelength dispersive technique; total Fe expressed as Fe_2O_3

	1	2	3	4	5	6	7	8
SiO_2	66·64	67·05	67·12	64·03	63·94	67·48	68·00	67·49
TiO_2	0·03	N.D.	0·03	N.D.	0·03	N.D.	N.D.	0·02
Al_2O_3	19·60	19·36	19·31	18·30	18·53	19·17	19·81	18·96
Fe_2O_3	0·11	0·32	0·21	0·27	0·15	0·14	0·19	0·43
MnO	N.D.	N.D.	0·05	0·02	0·02	N.D.	0·04	N.D.
CaO	0·46	0·20	0·15	N.D.	N.D.	0·02	0·02	N.D.
BaO	0·41	0·28	0·31	0·05	0·04	N.D.	N.D.	N.D.
Na_2O	6·39	7·40	6·15	0·89	0·93	11·78	11·36	11·92
K_2O	6·21	5·47	6·73	15·48	15·36	0·14	0·24	0·14
Total	99·85	100·08	100·06	99·04	99·00	98·73	99·03	98·96
Ab	59·57	66·61	57·70	8·05	8·46	99·12	98·55	99·21
Or	38·06	32·39	41·52	91·95	91·54	0·79	1·36	0·74
An	2·37	1·00	0·78	0·00	0·00	0·09	0·09	0·05

4.5.2 Major Element Variation

Bulk composition analyses of perthites from rocks unaffected by the fluid phase form a cluster, centred on $Ab_{59}Or_{40}An_1$, close to the thermal minimum of the Ab-Or-An system at 1kb pH_2O (Tuttle & Bowen 1958, Parsons & Brown 1984). The anorthite content is low and probably had little effect on properties of the feldspar such as exsolution and coarsening rates. There is a small scatter in the Ab:Or ratio which may be the result of unrepresentative sampling of the bulk composition but it is more likely to be a real feature of the feldspars. Brown *et al* .(1983) found real variations of the order of 10% Or in perthites from the Klokken syenites of the Gardar Province. For the purpose of this study such minor variations are unimportant compared to the compositional adjustments resulting from fluid activity. The sequence of increasing unmixing and breakdown of the feldspars, culminating in the formation of separate crystals of albite and K-feldspar, is the result of exsolution of nearly pure end-member albite (>Ab_{98}), leaving a residual bulk composition in the range Or_{90}-Or_{96}, with the rims commonly more potassic than the cores. The An content of the metasomatic albite is always less than An_1 and is often below detection limits (<100ppm).

4.5.3 Minor Element Variation

Ba, Fe,Ti and rarely Mn were found in the feldspars. Fe was present in significant quantities whereas Ba and Ti were frequently below detection limits.

Barium was not found in the albites affected by the metasomatism but is present in the rest of the feldspars, both primary magmatic and where fluids have enhanced and aided exsolution, and in both potassic and sodic phases. Mason (1982) showed a definite partitioning of Ba into the K-phase of perthites from pegmatites and this is probably the cause of the lack of Ba in the albite. The same pattern is not as well developed in the North Qoroq perthites and although there is a tendency for the K-phase to contain more Ba than the Na-phase, there is considerable overlap in values.

Iron concentrations in the feldspars (Fig. 4.2), ranged from a minimum of

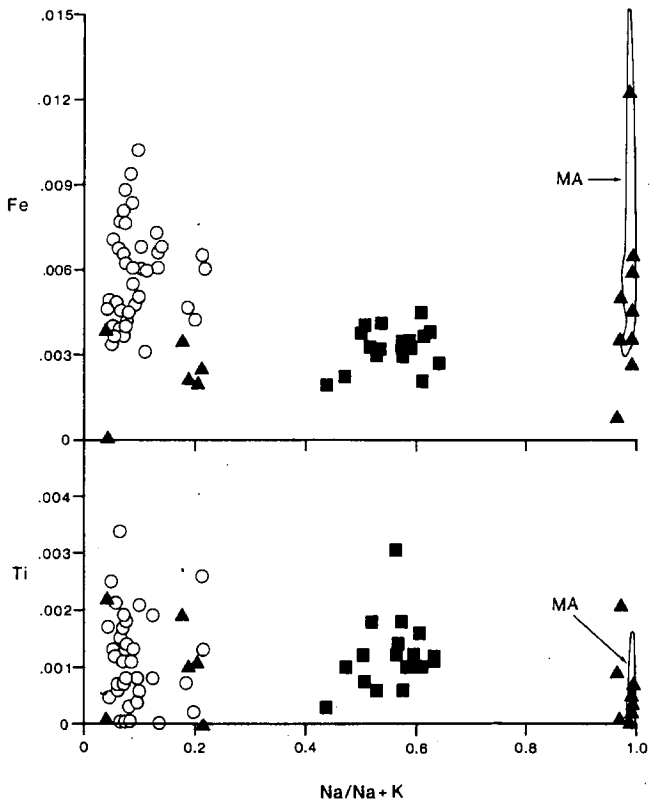

Figure 4.2 Microprobe analyses of the North Qôroq alkali feldspars; atomic proportions of Na/Na + K are plotted against atomic proportions of Fe and Ti expressed on the basis of 8 oxygens; solid squares—bulk compositions of unaltered perthites; solid triangles—the individual sodic and potassic phases of the perthites; open circles—K-feldspar produced by the breakdown of original perthite in the metasomatised syenites; the outlined field (MA) represents fifty-seven analyses of metasomatic albite which show red luminescence; all the other groups, including albitic compositions, show blue luminescence.

~200ppm in the perthites to a maximum of ~3500ppm in the metasomatic albites. No obvious partitioning of Fe into either of the perthite phases was observed but there are significant differences between the apparently unaltered perthites and the feldspars affected by fluids, both albite and coarse perthites. Irrespective of bulk composition, the latter contain more Fe than the unaltered feldspars. This cannot be explained by partitioning of Fe already present and indicates addition to the feldspars. This could be interpreted as minor metasomatic alteration or could be the result of local re-adjustments involving Fe-rich mafic or opaque phases. Bulk-rock chemistry indicates a slight increase in total Fe in the metasomatised rocks and the higher Fe content of all the red luminescing feldspars, probably as Fe^{3+} (see 4.6), may indicate that the addition applies even in less altered rocks with no obvious gross chemical changes. Whole rock increases in Fe^{3+} have commonly been described (Robins 1984, Wooley *et al.* 1972) in standard cell studies of metasomatised rocks and Mason *et al.* (1985) have demonstrated convincingly that various trace elements in Klokken feldspars are affected by deuteric alteration.

Titanium is present in much smaller quantities than Fe and ranges from below detection limits to a maximum of ~580ppm in an unaltered perthite. As Ti is only in concentrations close to detection limits, values plotted in Fig. 4.2 should be treated with caution. As with Fe, there is no obvious partitioning of Ti into either phase of the perthite. In the majority of the red-luminescing albites Ti is undetectable but that is the only systematic depletion or enrichment observed. This feature was clarified with high precision ion probe analyses (see 4.6.2).

4.6 Luminescence Related to Chemistry

4.6.1 Introduction

Although cathodoluminescence proves to be a very useful petrographic tool, its application to the metasomatic alteration of feldspars by fluids would be greatly enhanced by an understanding of the causes of the luminescence. The red luminescence

of plagioclase is established as being the result of an impurity centre caused by Fe^{3+} substituting for Al^{3+} in the $(Al,Si)O_4$ tetrahedra (Geake *et al.* 1977). The predominant blue luminescence, however, is more problematic. Mariano *et al.* (1973) favoured the view that it is caused directly by the Ti^{4+} ion substituting into the tetrahedra, whereas Marfunin (1979) argued that it is due to an oxygen defect centre resulting from the substitution of a 4+ ion in place of a 3+ ion (in this case Ti^{4+} for Al^{3+}). G. Walker (pers. comm.) believes that the blue luminescence is the result of an oxygen defect centre, but is unrelated to the trace element concentrations.

One aim of the present study was to confirm that Fe^{3+} activates the red luminescence in North Qoroq albites and to examine any possible relationships between blue luminescence and Ti-content of the feldspars. Results show no simple, clear cut relationship between luminescence colour and trace element concentrations. All red luminescent albites show significant but variable Fe concentrations (500-3000ppm). Blue luminescent feldspars, however, of similar albitic composition contain similar amounts (see Fig. 4.2). Ti tends to occur in higher concentrations in blue luminescent feldspars but this is simply a reflection of the relative absence of Ti in albites. Ti in blue luminescent feldspars is also frequently below detection limits. It is apparent that if Fe^{3+} and Ti^{4+} do play a role in activating the luminescence a simple model based solely on their relative concentrations is not acceptable.

Although probe data can show relationships between trace element concentrations and luminescence, these may be coincidental and misleading. To enable more definite relationships to be established emission and excitation spectra of the luminescence have been recorded.

4.6.2 Luminescence Spectra

Emission spectra are caused by the electron transitions, to lower energy levels, that produce the luminescence. Excitation spectra relate to the transitions to higher energy levels, the excited states, that precede and make possible the emissions.

Four samples were selected for detailed spectral examination. One sample (46297) was of unmetasomatised perthitic feldspar and exhibited a pale blue luminescence colour. Two samples (59751 and 59755) were of strongly metasomatised syenites, with albite showing bright red luminescence, and the fourth (77-22) was of a granular syenite showing strong blue luminescence from the Klokken intrusion (Parsons 1980, Mason *et al.* 1985). This last sample was chosen for comparison as Parsons has demonstrated that the Klokken granular syenites have suffered minimal water-rock interaction, in marked contrast to the North Qoroq specimens.

The emission spectra of all four specimens are given in Fig. 4.3. In each case the red peak intensity (mostly in the infra-red 650-800nm) is indicated on the diagram and in two cases (a and c) the spectrum in the blue area (~450nm) has been exaggerated to make any blue peak more obvious.

The most noticeable feature of the spectrum of the Klokken syenite (Fig. 4.3a) is that, although the red peak is more pronounced the luminescence seen is a strong blue colour. This is because the red emission is in the near infra-red thus making it very difficult for the human eye to detect (the human eye picks up little above 650nm and is at its' most sensitive in the blue-green region of the spectrum). The important conclusion is that only a small blue emission peak is required for the visible luminescence to be blue, irrespective of the infra-red peak intensity. The Klokken syenite does have the strongest blue peak of the four measured.

The spectrum of the unaltered perthite from North Qoroq (Fig. 4.3b) is much less intense and the weak blue peak is very broad, forming a more or less continuous emission across the visible spectrum. The luminescence seen is correspondingly paler and once again the infra-red peak, although strong, cannot be detected by the human eye.

The third and fourth spectra (Fig. 4.3c,d) are of syenites from the contact zone between syenite units (SN1A and SN1B) in which the albite shows strong red luminescence. The main feature of these spectra is that the blue emission peak has now virtually disappeared. The infra-red peak has increased in intensity, with the tail reaching

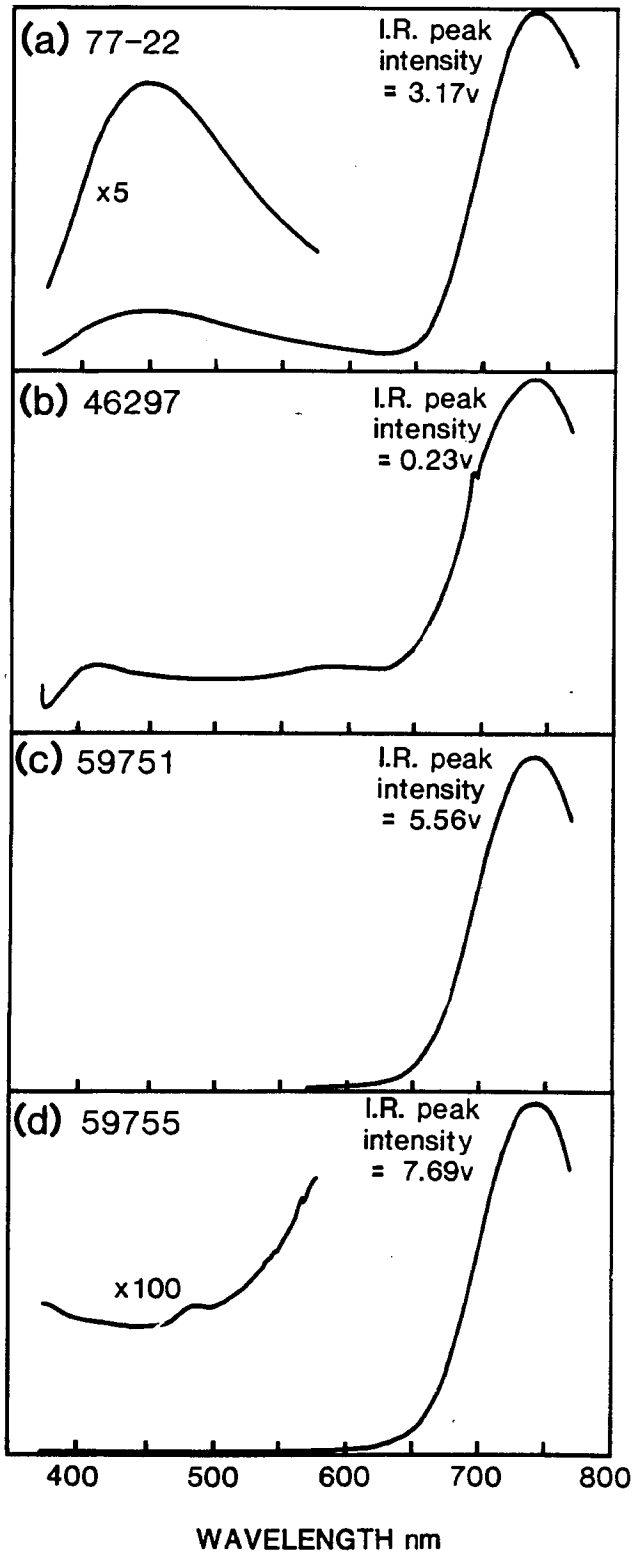

Figure 4.3 Luminescence emission spectra with the intensities of the infra-red peaks shown:

(a) 77–22 granular syenite from the Klokken intrusion, South Greenland;

(b) 46297 unaltered perthite from unit SN1A of the North Qôroq centre;

(c) 59751 strongly metasomatised syenite from the contact between units SN1A and SN1B of the North Qôroq centre;

(d) 59755 as (c).

into the visible spectrum, but it is because the blue peak is so weak or absent that the eye is able to detect the red luminescence. Hence, the metasomatic albites appear bright red.

It is clear that , although the size of the infra-red peak is important, and needs to be of at least a minimum intensity for the tail to show in the visible spectrum, the major control on the visible luminescence of the alkali feldspars is the intensity of the blue peak and only in its absence will the feldspar luminesce red.

The probe analyses have shown that all the red luminescent albites have significant Fe contents. Studies of the emission spectra show that there is also a possible correlation between the infra-red peak intensities and Fe content (Fig. 4.4). From this it would appear that the red luminescence is the result of electronic transitions in the Fe^{3+} ion present as an impurity in the feldspar. Final confirmation is found in the excitation spectra (Fig. 4.5) which are characteristic of Fe^{3+} in tetrahedral coordination. Telfer and Walker (1978) demonstrated this for plagioclase feldspars and the work on North Qoroq simply confirms the same in metasomatic albites.

It was shown that in many of the feldspars analysed, Ti was below the detection limits of the electron microprobe so in order to compare Ti contents to blue emission peak intensities, a total of 38 ion probe analyses were obtained using the Cambridge University instrument. The analytical procedure used in these analyses is detailed in Mason *et al.* (1985). The statistical errors are small, ranging from $\pm$0.2ppm at 3ppm Ti to $\pm$3ppm at 400ppm Ti.

Values ranged from 3 to 389ppm but no correlation was found between Ti content and the blue peak intensities and each individual sample shows a large range in Ti values, results confirming those obtained from electron probe analysis. The indication is that blue luminescence in alkali feldspars is not activated by a Ti^{4+} substitution. Indeed, no correlation could be found between the blue peak intensity and any element analysed suggesting that the blue luminescence may be the result of a defect centre, completely unrelated to minor element concentrations. The ubiquitous nature of the blue luminescence in feldspars, from a great variety of geological environments, supports the

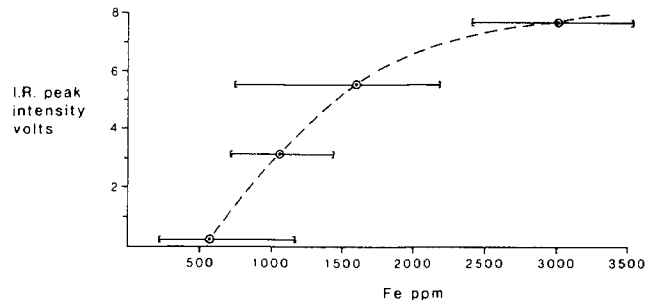

Figure 4.4 Intensity of the red luminescence peak versus Fe content of the feldspars from the four samples shown in figure 4.3. The bars represent the range in values for each sample and the circles the means of the analyses.

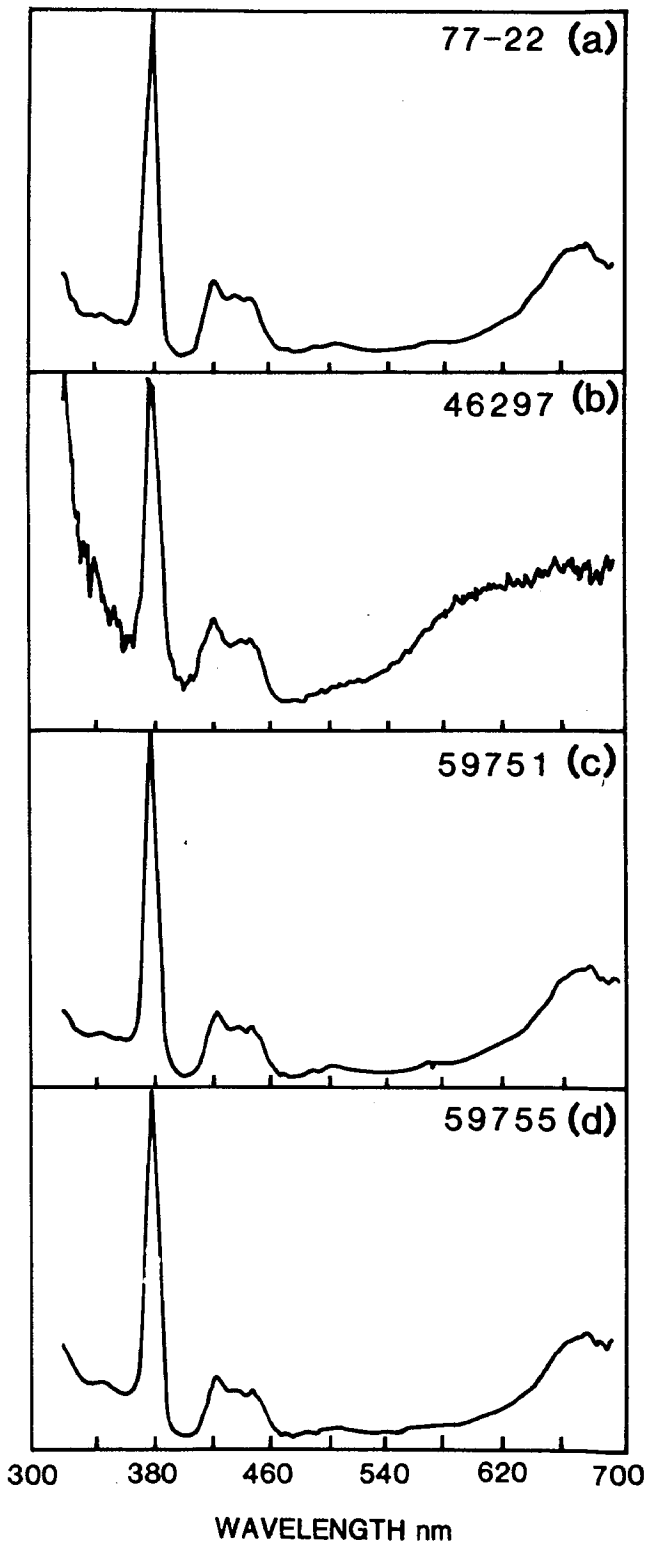

Figure 4.5 Luminescence excitation spectra of the four samples used in figures 4.3 & 4.4, showing peaks characteristic of Fe^{3+} in tetrahedral coordination (Telfer & Walker 1978).

idea of a defect centre being the cause. To invoke similar trace element concentrations for so many different situations would be unrealistic.

4.7 Discussion

4.7.1 Feldspar Luminescence

Of the North Qoroq feldspar compositions only end-member albites display red luminescence. The only record of any other feldspar composition luminescing red is that documented by Smith and Stenstrom (1965) and relates to end-member microcline. Obviously the presence of Fe^{3+} in the feldspar structure is a prerequisite for red luminescence and it is interesting to note that authigenic albites, which are relatively pure and contain little Fe^{3+} do not luminesce. Patch perthites from North Qoroq contain albite with similar iron contents to the metasomatic albites but these luminesce blue. This phenomenon of varying luminescence was noted by Mariano (1976, 1979) for fenitic feldspars associated with a carbonatite intrusion. He concluded that Ti^{4+} activated the blue luminescence and that the addition of Fe^{3+} in the fenitising fluid produced the change to red luminescence. It is shown here that any relationship between luminescence and Ti^{4+} is coincidental, caused by the partitioning of Ti out of the albite-phase and that the most important requirement for the albite to luminesce red is not the addition of Fe (numerous feldspars have similar Fe contents to the metasomatic albites) but the complete lack of blue emission. It appears that an effect of the metasomatism is to destroy the proposed defect centre thought responsible for causing the blue luminescence in end-member alkali feldspars. The nature of this defect is uncertain, but Parsons and Brown (1983) examined crypto-perthites showing blue luminescence using TEM and found them to have an extremely regular coherent phase and twin structure. This indicates that the defect is on a finer scale than the TEM can detect and points to the possibility of an oxygen defect centre. Hofmeister and Rossman (1985) demonstrated that the incorporation of structurally bound water into a feldspar inhibits the formation of smoky colour centres, which are caused by an electron hole defect between two

non-bonding oxygens. Perhaps the fluid processes operative in North Qoroq result in structurally bound water being incorporated into the albites so suppressing the blue luminescence. In a sample from one of the inner units of the North Qoroq centre, which has been recrystallised by the intrusion of a younger relatively dry syenite unit but has not apparently reacted with a fluid phase, the feldspars luminesce pale purple, but rarely red, indicating the continued presence of a blue emission peak. Structurally bound water might also explain the lack of blue luminescence in authigenic feldspars.

4.7.2 Metasomatism in the North Qoroq Centre

A study of the behaviour of alkali feldspars during metasomatism in the North Qoroq centre allows only tentative comments to be made concerning the metasomatic processes and resulting gross mineralogical and chemical variation. The nature of the fluid phase itself is uncertain although fluid inclusion studies on similar rocks (Sobolev *et al.* 1974, Roedder 1984) suggest it is highly saline. The peralkaline condition and the presence of Cl and F markedly increases the solubility of water in silicate melts, inhibits secondary boiling and may well result in a progressive change from hydrosilicate melt to hydrosaline fluids. It is also feasible that, for the sodalite rich rocks, the fluid responsible for metasomatism is a NaCl-rich immiscible liquid consistent with those observed in experimental studies (Koster van Groos & Wyllie 1969). Despite the uncertainties it is appropriate to make some comments on the behaviour of the fluid phase and the metasomatic processes.

Cathodoluminescence petrography (see 4.3) suggests that the replacement of K-feldspar by albite is one of the processes occuring during metasomatism. Orville (1963), working on alkali ion exchange between vapour and feldspar phases demonstrated that, in the presence of an alkali-bearing vapour phase, metasomatism is the natural response to P,T or compositional gradients. To achieve albitisation of a normal syenitic feldspar composition, depending on the P/T conditions, a relatively Na-rich chloride vapour would be required. Such a composition would be likely for fluids emanating from the highly peralkaline, Na-rich, late stage North Qoroq magmas.

Increase in Na and decrease in K in the bulk-rock as demonstrated in the composition-volume diagram (Fig. 4.1) would be a consequence of this process. Petrographic observation shows, however, that although albite is plentiful, its modal proportions are not significantly greater in the metasomatised syenite when compared to coarsely-perthitic syenites unaffected by metasomatism. Although albite is obviously in equilibrium with the metasomatic fluid, it would appear that its proportions are not greatly increased during metasomatism and that the bulk of the albite can be explained as a result of enhanced unmixing of alkali feldspar. It is worth noting that this is in marked contrast to the outer margins of the North Qoroq centre where both the country rock 2-feldspar granite-gneiss and the contact syenite at the immediate contact can show marked albitisation with up to 85% modal albite.

The composition-volume diagram (Fig. 4.1) also shows a marked decrease in Si, entirely consistent with the petrographic evidence showing replacement of K-feldspar by nepheline and sodalite during metasomatism. The development of nepheline at the expense of both plagioclase and alkali feldspar has been described by a number of workers (Robins 1984, Rao & Murthy 1974) and demonstrated experimentally (Currie, 1968) and the replacement of nepheline by sodalite demonstrated experimentally by Wellman (1970).

At a late stage in the evolution of the North Qoroq magmas a fluid evolved, in equilibrium with highly peralkaline undersaturated magma, and migrated to areas of earlier formed, less evolved syenite, with which it was out of equilibrium. As a consequence of this, metasomatic reaction occurred resulting in the formation of feldspathoids, particularly sodalite and nepheline and producing the red luminescent albite from pre-existing feldspar, as well as altering the mafic mineral assemblage. The chemical expression of this was a large gain in Na, loss in Si and small loss in K to the fluid with some K being found in micas and amphibole. As the fluid attained equilibrium with the less-evolved syenite active reaction was restricted to equilibration of fluid and solid phases as temperature decreased (Orville 1963, Wellman 1970). The major role of the fluid was to act as a passive medium facilitating the incoherent exsolution and

unmixing of the feldspars, a process involving only localised solution and reprecipitation. The addition of Fe^{3+} to many of the feldspars may be a further consequence of localised chemical transport and reaction.

4.8 Conclusions

Metasomatism has played a significant role in the chemical, mineralogical and textural development of the North Qoroq syenites. Perthitic alkali feldspar or separate K-feldspar and albite are the dominant phases in all the rocks studied. Cathodoluminescence allows the often subtle textural changes occuring during metasomatism of the feldspars to be identified more easily and in much greater detail and proves itself an important qualitative analytical technique.

From the cathodoluminescence spectral studies and mineral chemistry studies the following conclusions can be drawn :-

1. Red luminescence is restricted to albite and is indicative of reaction with late-stage aqueous fluids. All feldspars affected by the fluid phase show average iron (Fe^{3+}) values higher than those shown by feldspars apparently unaffected by the action of a fluid phase. The view of earlier workers that the red luminescence is due to electronic transitions in the Fe^{3+} ions, present as an impurity in the feldspars, is confirmed. Numerous feldspars, including albites, with similar iron contents do however show no red luminescence. Emission spectra demonstrate that a further requirement for red luminescence is the suppression of the blue emission peak which, if present, will always mask the red luminescence irrespective of the intensity of the red emission peak.

2. Blue luminescence shows no correlation with Ti or any other trace element measured. The exact cause of the luminescence remains uncertain but suggestions that it is due to an oxygen defect centre are not contradicted by the observations on the North Qoroq feldspars. Whatever the exact nature of the defect it would appear to be destroyed in albite by metasomatic processes involving a magmatic aqueous fluid phase. Structurally-bound water incorporated into the albite during the process may be the

reason for the suppression of the blue luminescence.

A number of conclusions can also be drawn concerning the metasomatic process:-

1. Adjacent to younger units, where reaction with the metasomatising fluid was most intense the felsic mineralogy shows the development of feldspathoids, particularly nepheline and sodalite. Both form at the expense of K-feldspar and sodalite at the expense of nepheline. Albite remains in the rock and occurs in a granular mosaic with the feldspathoids.

2. Further from the contact the fluid, now closer to equilibrium with the syenitic rocks, behaved largely as a passive medium. Reactions in the felsic mineralogy were restricted to the re-equilibration of feldspar, feldspathoids and fluid with falling temperature and the principle role of the fluid was to aid the extensive unmixing seen in the alkali feldspars.

References

Brown, W.L., Becker, S.M. & Parsons, I. 1983. Cryptoperthites and cooling rate in a layered syenite pluton : a chemical and TEM study. CONTRIB MINERAL PETROL **82**, 13-25.

Currie, K.L. 1968. On the solubility of albite in supercritical water in the range of 400° to 600°c and 750 to 3500 bars. AM J SCI **266**, 321-41.

Geake, J.E., Walker, G., Telfer, D.J. & Mills, A.A. 1977. The cause and significance of luminescence in lunar plagioclase. PHIL TRANS R SOC LOND **A285**, 403-8.

Gresens, R.L. 1967. Composition-volume relationships of metasomatism. CHEM GEOL **2**, 47-65.

Hofmeister, A.M. & Rossman, G.R. 1985. A model for the irradiative colouration of smoky feldspar and the inhibiting influence of water. PHYS CHEM MINERALS **12**, 324-32.

Koster van Gross, A.F. & Wyllie, P.J. 1969. Melting relationships in the system $NaAlSi_3O_8$-NaCl-H_2O at one kilobar pressure, with petrological applications. J GEOL **77**, 581-605.

Marfunin, A.S. 1979. *Spectroscopy, luminescence and radiation centers in minerals.* Berlin : Springer-Verlag.

Mariano, A.N. 1976. The application of cathodoluminescence for carbonatite exploration and characterisation. *In* : Simposio Internacional de Carbonatitos, 1. Pocos de Caldas.

Mariano, A.N. 1979. Enhancement and classification of fenitisation by cathode luminescence. GEOL ASS CAN-MIN ASS CAN, Jt. Ann. Meet., Program Abstr. **No.4**, 65.

Mariano, A.N., Ito, J. & Ring, P.J. 1973. Cathodoluminescence of plagioclase feldspars [abstr]. GEOL SOC AM ABSTR **5**,726.

Mason, R.A. 1982. Trace element distributions between the perthite phases of alkali feldspars from pegmatites. MINERAL MAG **45**, 101-6.

Mason, R.A., Parsons, I. & Long, J.V.P. 1985. Trace and minor element chemistry of alkali feldspar in the Klokken layered syenite series. J PETROL **26**, 952-70.

McKie, D. 1966. Fenitisation. *In* Tuttle, O.F. & Gittins, J. (eds) *Carbonatites*, 261-94. New York : Wiley-Interscience.

Miller, J. 1985. Introduction to cathodoluminescence microscopy. WORKSHOP NOTES, UNIV OF EDINBURGH.

Orville, P.M. 1963. Alkali ion exchange between vapor and feldspar phases. AM J SCI **261**, 201-37.

Parsons, I. 1978. Feldspars and fluids in cooling plutons. MINERAL MAG **42**, 1-17.

Parsons, I. 1980. Alkali-feldspar and Fe-Ti oxide exsolution textures as indicators of the distribution and subsolidus effects of magmatic 'water' in the Klokken layered syenite intrusion, South Greenland. TRANS R SOC EDINBURGH **71**, 1-12.

Parsons, I. & Brown, W.L. 1983. A TEM and microprobe study of a two perthite alkali gabbro : implications for the ternary feldspar system. CONTRIB MINERAL PETROL **82**, 1-12.

Parsons, I. & Brown, W.L. 1984. Feldspars and the thermal history of igneous rocks. *In* Brown, W.L. (ed) *Feldspars and feldspathoids*, 317-71. Dordrecht : Reidel.

Ramberg, H. 1962. Intergranular precipitation of albite formed by unmixing of alkali feldspar. NEUES JAHRB MINERAL ABH **98**, 14-34.

Rao, Y.J. & Murthy, I.S.N. 1974. Nepheline as a metasomatic product. AM MINERAL **59**, 690-93.

Robins, B. 1984. Petrography and petrogenesis of nephelinized metagabbros from Finnmark, Northern Norway. CONTRIB MINERAL PETROL **86**, 170-77.

Roedder, E. 1984. Fluid Inclusions. *Miner Soc Amer Reviews in Mineralogy* **12.**

Smith, J.V. & Stenstrom, R.C. 1965. Electron excited luminescence as a petrologic tool. J GEOL **73**, 627-35.

Sobolev, V.S., Bazarova, T.Y. & Kostyuk, V.P. 1974. Inclusions in the minerals of some types of alkaline rocks. *In* Sorenson, H. (ed) *The Alkaline Rocks*, 389-401. New York : Wiley-Interscience.

Telfer, D.J. & Walker, G. 1978. Ligand field bands of Mn^{2+} and Fe^{3+} luminescence centres and their site occupancy in plagioclase feldspars. MOD GEOL **6**, 199-210.

Tuttle, O.F. & Bowen, N.L. 1958. Origin of granite in the light of experimental studies in the system $NaAlSi_3O_8$-$KAlSi_3O_8$-SiO_2-H_2O. MEM GEOL SOC AM **74**.

Walker, G. 1985. Mineralogical applications of luminescence techniques. *In* Berry, F.J. & Vaughan, D.J. (eds) *Chemical bonding and spectroscopy in mineral chemistry,* 103-40. London : Chapman & Hall.

Wellman, T.R. 1970. The stability of sodalite in a synthetic syenite plus aqueous chloride fluid system. J PETROL **11**, 49-71.

Woolley, A.R., Symes, R.F. & Elliott, C.J. 1972. Metasomatised (fenitised) quartzites from the Borralan Complex, Scotland. MINERAL MAG **38**, 819-36.

CHAPTER 5

Modification of mafic silicate compositions

5.1 Introduction

5.1.1 Previous investigations

There have been several studies of mafic mineral chemistry associated with alkali metasomatism or fenitisation. Sutherland (1969) documented the growth of magnesio-arfvedsonite and aegerine during fenitisation around the carbonatite complexes of eastern Uganda and Kenya while Currie and Ferguson (1971) and Woolley *et al.* (1972) noted similar compositions developed in country rocks around alkaline centres in Canada and Scotland. The fenitisation at the Fen Complex, southern Norway is characterised by the development of magnesio-arfvedsonite, riebeckite and aegerine-hedenbergite (Kresten and Morogan 1986). Other studies highlighting changes in mafic mineral chemistry include those of Rock (1976), Robins and Tysseland (1983) and Morogan and Martin (1985).

There have been many investigations of the compositions of the mafic phases in the Gardar central complexes but most have been concerned with quantifying the P-T conditions of crystallisation, thermodynamic parameters such as fO_2 or pH_2O and the activities of chemical components in the magma (eg. Parsons 1981, Stephenson and Upton 1982 and Larsen 1976). Studies of postmagmatic fluid alteration have been relatively neglected though Parsons (1980) examined textural changes in the Fe-Ti oxides and Parsons and Becker (1986) documented compositional variations in the pyroxenes in the Klokken intrusion, which they related to the action of deuteric fluids.

The metasomatism within the North Qoroq centre and the fenitisation of the country rocks produced marked textural changes (see chapter 2) in the mafic silicates. Indeed, it is the spotted growth of poikilitic mafic phases that enables recognition of metasomatism in hand specimen. These petrographic changes are accompanied by distinct chemical alteration and it is the purpose of this chapter to detail the chemistry of

the major phases, pyroxene, amphibole and biotite.

5.1.2 Analytical Techniques

All analyses of mafic silicates were carried out at the University of Edinburgh with the Cameca Camebax electron microprobe using a wavelength dispersive system. The accelerating voltage used was 20kV and the specimen current was 20nA in all cases. Standards used were pure metals, oxides and simple minerals and ZAF correction procedures were used. Details of analytical procedures are given in Appendix 1. Representative analyses of all the mafic phases are listed in Table 5.1 and full data tables are given in Appendix 1.

5.2 Pyroxenes

5.2.1 Crystal chemistry

All pyroxenes analysed in the North Qoroq area can be represented in the diopside-hedenbergite-acmite ternary diagram and so it is important to determine the ferrous/ferric iron ratio before looking at site occupancy and molecular end-member proportions. Two methods of recalculating the Fe^{3+} content have been commonly used. Firstly it can be assumed that in the Di-Hd-Ac system the major substitution involving Fe^{3+} is the coupled substitution $Na^{+}Fe^{3+}$ <> $(Mg,Fe)^{2+}Ca^{2+}$ in which case equal amounts of Fe are allocated to Na as Fe^{3+} (Nash et al. 1969, Stephenson 1972). The drawback of this is the assumption that all the Na combines with Fe in the acmite molecule, effectively concealing the presence of other substitutions. In North Qoroq there is often excess Na in the pyroxenes in the more aegerine-rich compositions indicating that Na does indeed combine with other elements in significant amounts. Larsen (1976) found the same in the pyroxenes of the Ilimaussaq intrusion and proposed that the ferric iron should be recalculated by normalising the analyses to 4.00 cations and 6.00 anions. This gives an independent estimate of Fe^{3+} but assumes a good, complete analysis and also that there are no vacancies in the lattice. Cawthorn and Collerson

Table 5.1 Representative electron microprobe analyses of mafic silicates.
Column 1 - unit SN4B amphibole ; column 2 - unit SN1A amphibole ; column 3 - granite-gneiss amphibole ; column 4 - quartzite amphibole ; column 5 - unit SN4B pyroxene ; column 6 - unit SN1A pyroxene ; column 7 - quartzite pyroxene ; column 8 - unit SN1A biotite ; column 9 - granite-gneiss biotite.

	Column 1	Column 2	Column 3	Column 4	Column 5	Column 6	Column 7	Column 8	Column 9
Sample No.	DAR 140	DAR123	DAR165	DAR65	DAR186	DAR123	DAR65	DAR128	DAR163
SiO2	44.32	45.65	50.53	53.29	50.665	51.801	51.053	35.716	36.8710
Al2O3	4.80	4.34	1.30	0.12	0.890	0.800	0.167	10.998	12.904
TiO2	1.08	1.10	0.70	0.85	0.235	0.262	0.840	3.287	2.440
ZrO2		0.351	0.024		0.665	0.956	0.073		
Fe2O3					16.4885	22.8228	5.4698		
FeO	30.50	29.51	25.59	21.98	9.6859	4.9890	17.2230	31.383	22.356
MnO	1.44	1.43	0.81	0.95	1.241	0.588	1.019	3.560	0.599
MgO	1.43	2.09	5.49	7.74	1.147	0.639	3.027	1.963	9.754
CaO	5.82	3.47	6.36	2.93	11.817	7.996	18.447	0.050	0.000
Na2O	6.02	7.78	4.93	8.35	7.159	9.908	3.153	0.180	0.308
K2O	1.65	1.69	1.30	1.70				8.630	9.821
F	0.800	0.489	0.588	1.088				0.217	0.617
Cl								0.015	0.108
Total	97.06	97.06	97.01	97.91	99.9934	100.7618	100.4718	95.999	95.778
Si	7.23	7.36	7.90	8.11	1.9872	1.9934	2.0091	5.8749	5.7718
Al	0.92	0.83	0.24	0.02	0.0411	0.0362	0.0077	2.1321	2.3808
Ti	0.13	0.13	0.08	0.10	0.0069	0.0076	0.0248	0.4066	0.2873
Zr		0.0277	0.0018		0.0146	0.0206	0.0016		
Fe3+	0.06	0.20	0.00	0.00	0.4850	0.6586	0.1614		
Fe2+	4.10	3.78	3.35	2.80	0.3166	0.1600	0.5648	4.3172	2.9268
Mn	0.20	0.20	0.11	0.12	0.0411	0.0191	0.0339	0.4960	0.0794
Mg	0.35	0.50	1.28	1.76	0.0675	0.0369	0.1787	0.4813	2.2758
Ca	1.02	0.60	1.06	0.48	0.4966	0.3297	0.7778	0.0087	0.0000
Na	1.91	2.43	1.49	2.46	0.5435	0.7380	0.2402	0.0573	0.0934
K	0.34	0.35	0.26	0.33				1.8109	1.9611
F	0.4133	0.2499	0.2906	0.5235				0.1129	0.3056
Cl								0.0043	0.0287

(1974) demonstrated that low pressure igneous pyroxenes approximate to a stoichiometry of four cations very closely and also that only in the presence of significant jadeite component (~>20%) do site deficiencies become pronounced. All pyroxenes in North Qoroq have therefore been recalculated after the method detailed by Larsen (1976).

Element variations are plotted against the baseline of Na-Mg (Figure 5.1) used by Stephenson (1972) and Larsen (1976) to represent the full sodic pyroxene variation and nomenclature is the same as that of Larsen (1976). Before examining chemical differences between magmatic and metasomatic pyroxenes some general observations can be made on site occupancies and substitution schemes. All analyses are plotted on Figure 5.1, both magmatic and metasomatic syenite pyroxenes and all country rock pyroxenes. Similarly to Ilimaussaq, there is a steady increase in Si to aegerine in the syenite pyroxenes but, in contrast, the quartzite pyroxenes show high Si at ferrosalite to hedenbergite followed by a steady gradual decrease towards aegerine. Al shows a rapid decrease to hedenbergite, levels off and then shows some scatter to higher values at aegerine-rich compositions. In the great majority of analyses Si+Al>2, leaving some Al in octahedral coordination but a few do show a deficiency in the tetrahedral position, implying the presence of another element in this site. Ti varies in a similar way to Al, decreasing to hedenbergite and then scattering to higher values towards aegerine. Zr is present in the unaltered ferrosalites of the syenites in only minor amounts but shows strong enrichments in the aegerine-hedenbergites and aegerines, a feature that was also noted by Gomes *et al.* (1970), Jones and Peckett (1980) and Duggan (1988). Fe^{3+} shows a gentle increase from ferrosalite to hedenbergite before rising along a slope with a gradient of ~1 to aegerine. The approximation of this slope to unity implies that, although other 'molecules' are present, most of the Fe^{3+} and Na are present in the acmite molecule. Fe^{2+} and Mn both increase to hedenbergite before tailing down to zero at aegerine. In comparison to Ilimaussaq and South Qoroq the Fe^{2+} trend shows a larger scatter in the hedenbergites and aegerine-hedenbergites partly reflecting the more variable

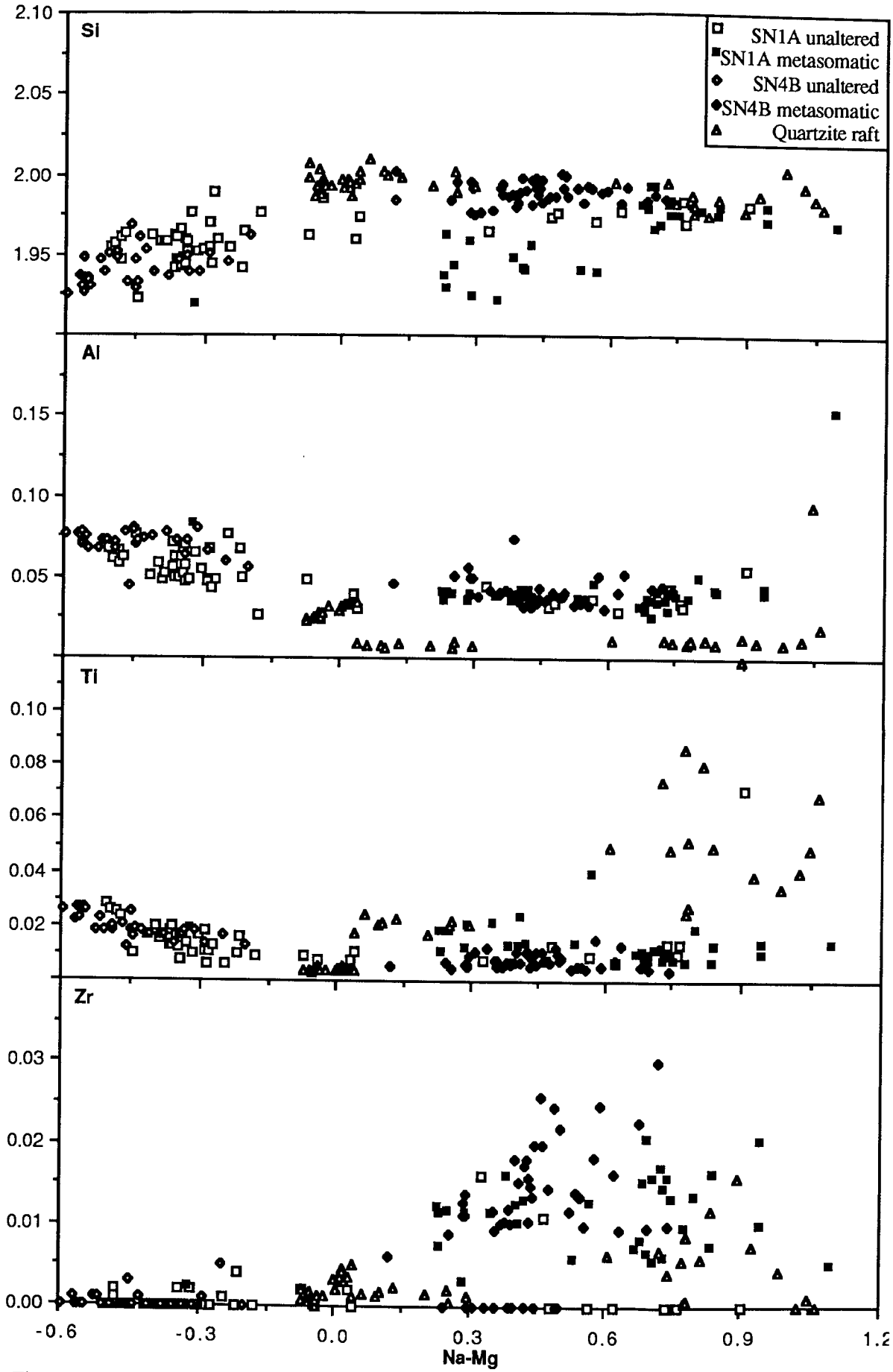

Figure 5.1 (two pages) Element variation in North Qoroq pyroxenes against the baseline of Na-Mg. All unit in atoms in the structural formula on the basis of 6 oxygens. Pyroxene nomenclature overleaf.

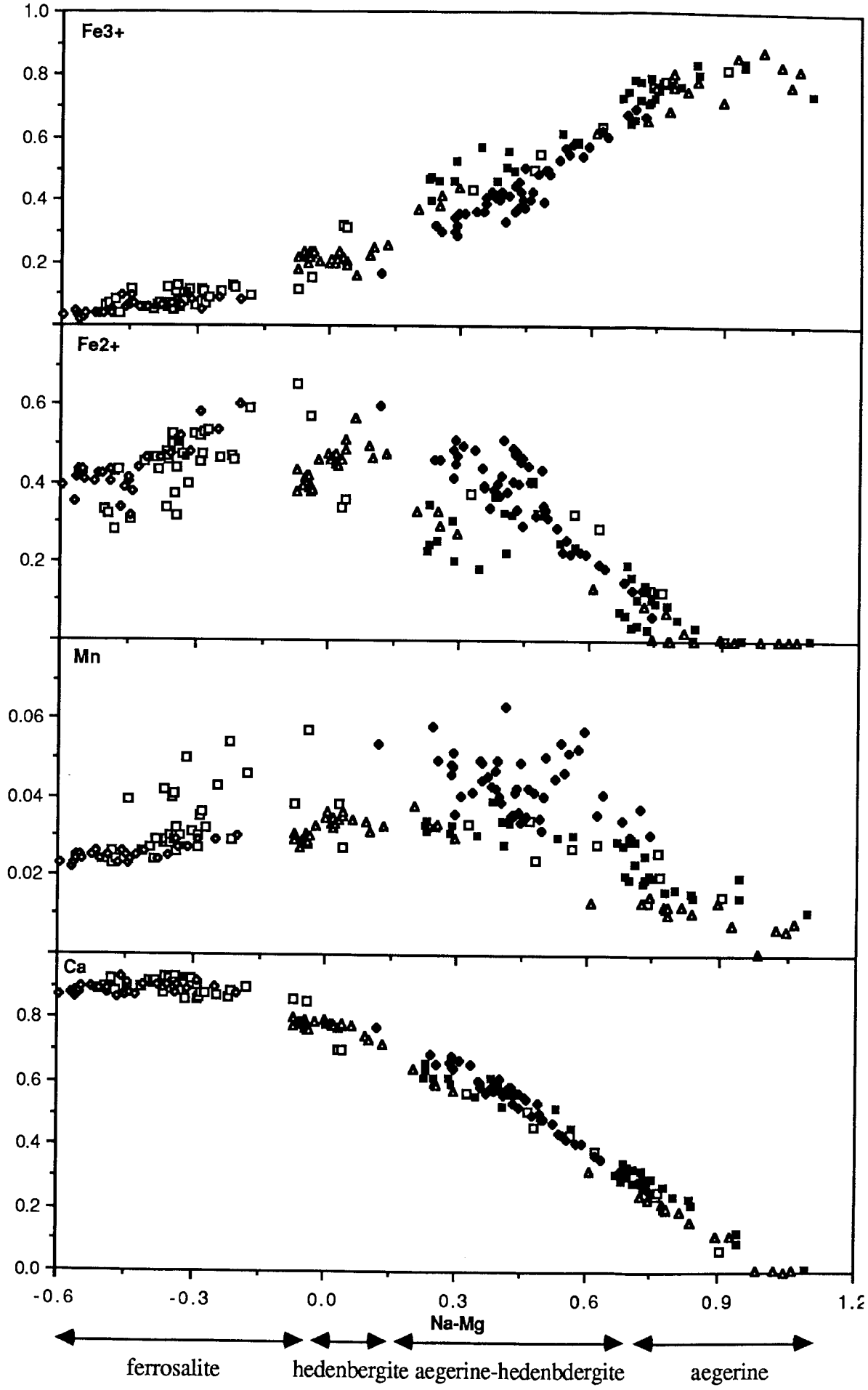
Fe3+
Fe2+
Mn
Ca
1.0
0.8
0.6
0.4
0.2
0.06
0.04
0.02
0.0
-0.6
-0.3
0.0
0.3
0.6
0.9
1.2
Na-Mg
ferrosalite
hedenbergite
aegerine-hedenbdergite
aegerine

trends to acmite enrichment produced during the metasomatic alteration of the North Qoroq rocks. Ca shows little variation to hedenbergite before dropping down to zero at aegerine.

Where Si+Al<2 the question arises of which element fills the remaining tetrahedral positions. Verhoogen (1962) and Hartman (1969) state that the Ti^{4+} ion is too large to substitute into this site and so the same will be true of the Zr^{4+} ion. It is highly unlikely that in the presence of significant Fe^{3+} either of these ions would be in the trivalent state and so they must be confined to the octahedral positions. A plot of Fe^{3+}-Na versus Si+Al (Figure 5.2) shows that large deficiencies in Si+Al are generally coupled with an excess of Fe^{3+} over Na, particularly when the fenitic pyroxenes in the quartzite are excluded. It is suggested that this excess is in the tetrahedral sites in the form of a ferri-Tschermak's component $CaFe^{3+}{}_{VI}Fe^{3+}{}_{IV}SiO_6$ (Larsen 1976). The Ilimaussaq pyroxenes have very similar features though they show a much better correlation between the two axes. The analyses of magmatic pyroxenes from the syenites were taken from Chambers (1976) and were recalculated assuming Fe^{3+}=Na and so are not plotted on this diagram.

Figure 5.2 shows that, where there is excess Na and Al, no more than half the excess Na, and often significantly less, is required to combine with the excess Al in a jadeite component ($NaAlSi_2O_6$) and so combinations of Na with Ti and Zr in components analogous to those proposed for the Ilimaussaq pyroxenes must also exist in North Qoroq. Figure 5.3, a triangular plot of Al-([Ti+Zr]*10)-Na, shows that in the Na-poor pyroxenes there is an excess of Al over that required for a $CaTiAl_2O_6$ molecule (Ca-Ti-Tschermak's component) indicating the presence of $CaAl_2SiO_6$ (Ca-Tschermak's component). The likelihood of these components is confirmed by a plot of Ca versus $Mg+Fe^{2+}$+Mn which shows an excess of Ca over that required for the diopside and hedenbergite molecules. As the pyroxenes become more sodic, Ti+Zr becomes equal to Al indicating the presence of components such as $Na(Ti,Zr)AlSiO_6$ (Hollister and

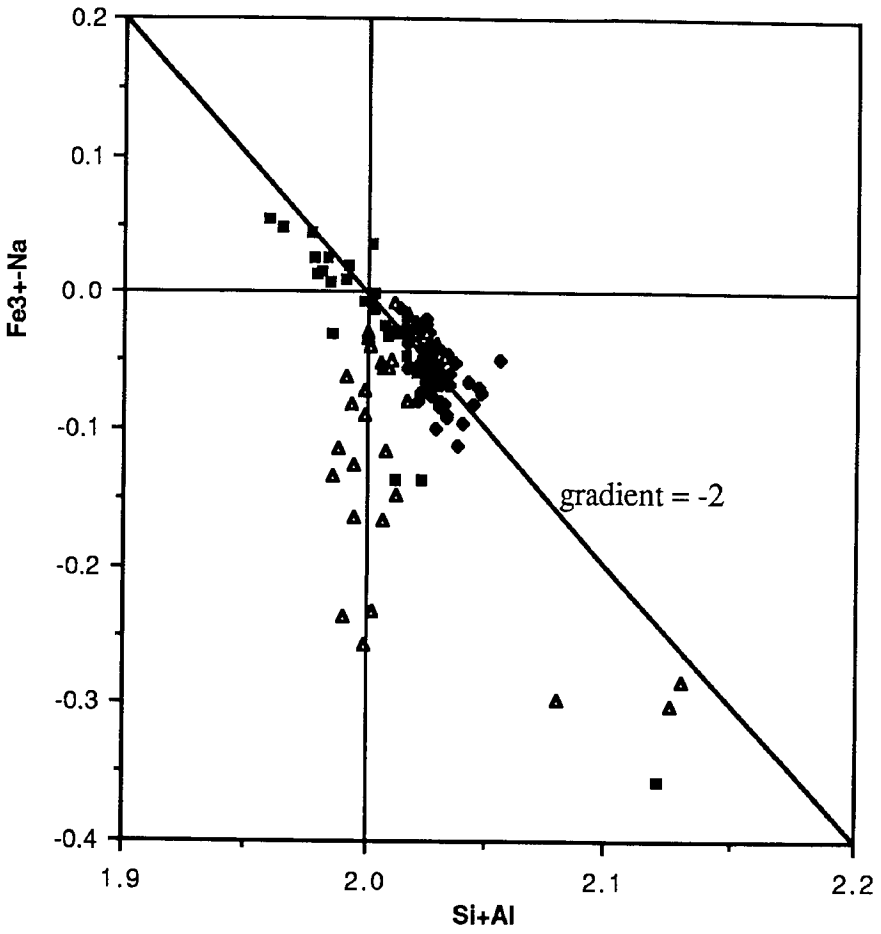

Figure 5.2 Relationship between excess Na and excess Al in North Qoroq pyroxenes. Scales are in atoms in the structural formula and symbols are the same as those on Figure 5.1.

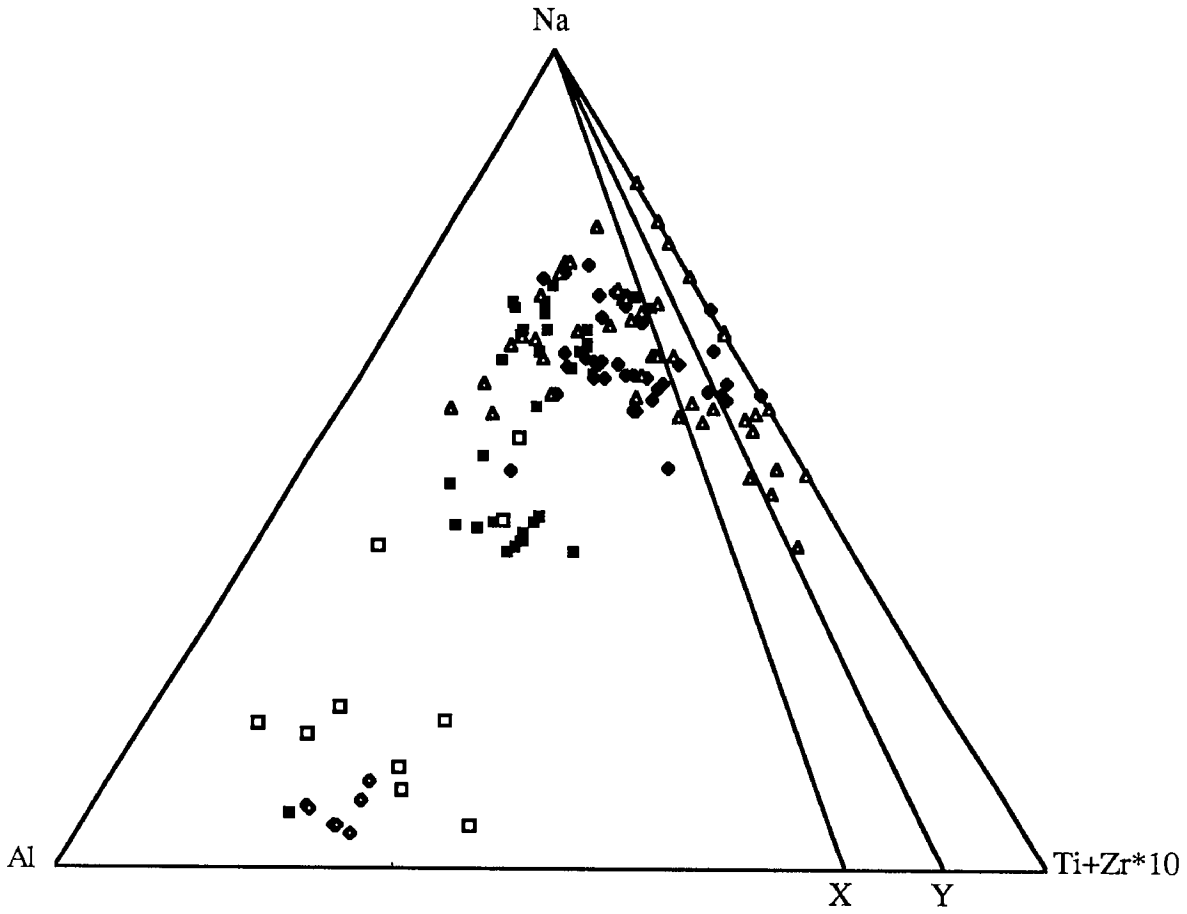

Figure 5.3 Relationship between Na, Al, Ti and Zr in North Qoroq pyroxenes.
Symbols are the same as those in Figure 5.1
Line Na-X represents an Al:(Ti+Zr) ratio of 2:1
Line Na-Y represents an Al:(Ti+Zr) ratio of 1:1

Gancarz 1971, Flower 1974, Grapes *et al.* 1979 and Nielsen 1979) and, in the most sodic compositions, Ti+Zr exceeds Al suggesting the presence of Zr and Ti end-members such as FM-NAZ ($Na[Fe^{2+}Mg]_{0.5}Zr_{0.5}Si_2O_6$) proposed by Jones and Peckett (1980) and Duggan (1988), and titan-aegerine (Flower 1974).

In summary, the predominant components in the ferrosalites and hedenbergites are diopside and hedenbergite with minor amounts of acmite and ferri-, Ca- and Ca-Ti-Tschermak's molecules. As the pyroxene compositions move to aegerine these give way to predominant acmite with minor NATAL, NAZAL ($Na(Ti,Zr)AlSiO_6$) and aegerine analogues such as FM-NAZ. The presence or amount of the jadeite component does not appear to correlate with position in the Di-Hd-Ac system.

5.2.2 Metasomatic variation

5.2.2.1 The syenites

Plots of compositional variation in the Di-Hd-Ac triangle (Figure 5.4) highlight the major effects of the metasomatism on the pyroxenes. The unaltered pyroxenes of unit SN1A are predominantly ferrosalites but trend to 70%Hd before moving to the acmite corner, always staying close to the Hd-Ac side. The metasomatic pyroxenes produce a much larger scatter away from the Hd-Ac join to apparently more Mg-rich portions of the triangle. In view of the consistent decrease in Mg in the whole-rock during metasomatism (see chapter 3) it seems unlikely that the pyroxenes show an increase in Mg and it is most likely that the scatter is produced by the conversion of Fe^{2+} to Fe^{3+} for a range of original pyroxene compositions. Chambers (1976) noted this feature in preliminary studies on the metasomatism in North Qoroq and Stephenson (1972) showed the same in the South Qoroq centre. The unaltered pyroxenes of SN4B are all ferrosalites with no progression to acmite, though this may reflect the available exposure of the unit, the presumably more fractionated interior of which was cored out by the intrusion of SN5. The metasomatic pyroxenes range from hedenbergite to acmitic compositions but in contrast to SN1A there is no scatter into the

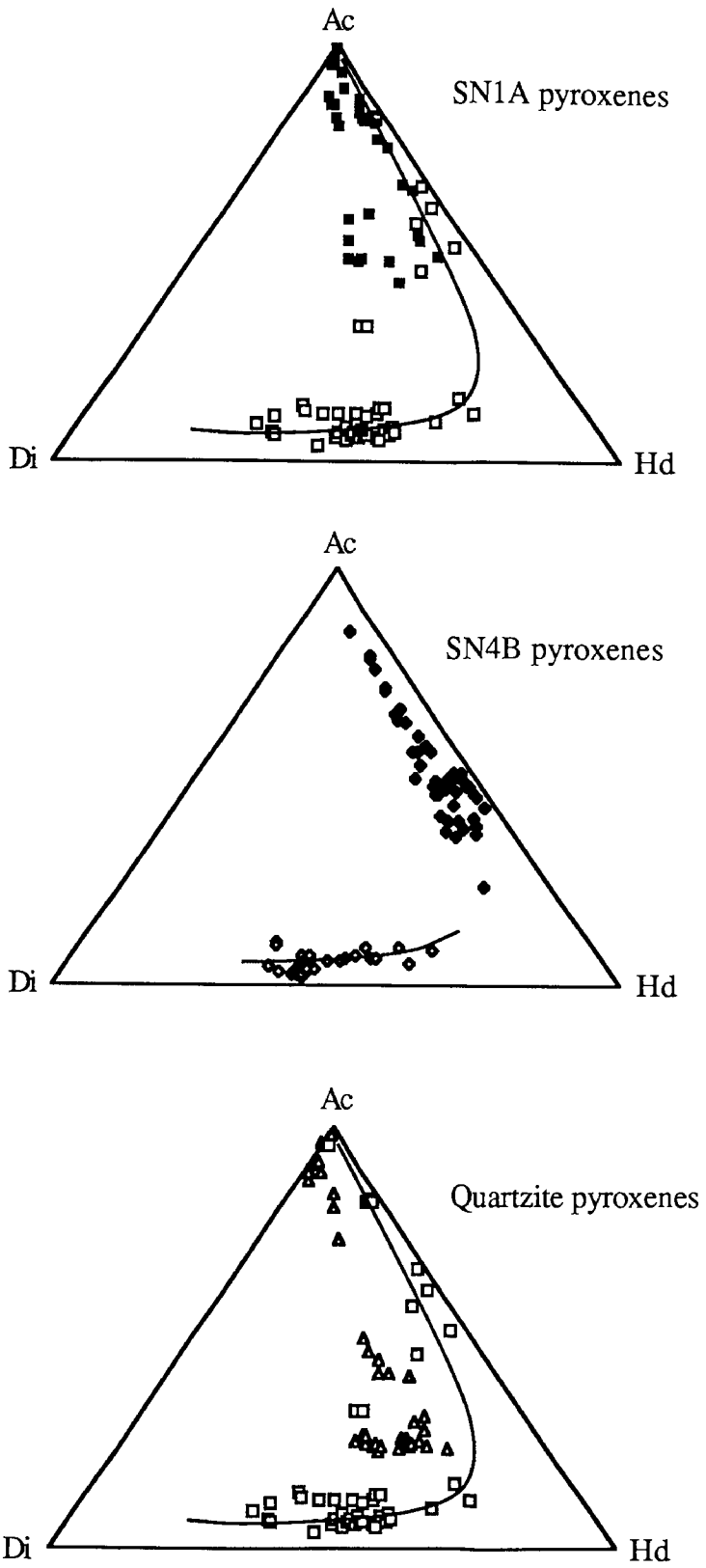

Figure 5.4 Pyroxene analyses plotted in the triangular diagram Mg-(Fe2+Mn)-Na [Di-Hd-Ac].
Symbols are the same as those used in Figure 5.1

central portions of the triangle and more Hd-rich compositions are formed. The examination of chemical differences between metasomatic and magmatic mafic minerals is subject to the same limitations detailed for whole-rock variation (Chapter 3) with regard to uncertainty in the original composition. As a large proportion of SN4B was lost by the intrusion of SN5 it is possible that the lack of scatter in the metasomatic pyroxenes is due to an originally more Fe-rich starting composition.

Apart from the more extensive trend shown by SN1A, both syenite units show similar magmatic trends in pyroxene compositions and these can be contrasted with the elemental abundances in the metasomatic pyroxenes. Detailed examination of Figure 5.1 also reveals differences in elemental abundances in the metasomatic pyroxenes between rock types. The aegerine-hedenbergites of SN1A contain less Si than those in the other rock types but do not contain noticeably more Al. The same compositions, though, contain more Fe^{3+} than the other samples supporting the idea of tetrahedral Fe^{3+} compensating the Si deficiency. In general the hedenbergites and aegerine-hedenbergites of SN1A contain more Fe^{3+} and less Fe^{2+}+Mn than those of SN4B confirming the early acmite enrichment in SN1A shown on Figure 5.4. Ti is generally lower in the metasomatic pyroxenes of SN4B than in those of the other rock types and the highest Zr contents are found in these pyroxenes, though there is a considerable scatter.

In general, the metasomatic pyroxenes of the syenites show low Ti, Al, Fe^{2+}, Mg and Ca and high Zr, Fe^{3+} and Na.

5.2.2.2 The country rocks

Pyroxene is absent from the granite-gneiss and so this section is concerned solely with the quartzite raft. There is a large compositional range in the pyroxenes of the quarztite raft and, in comparison to the unaltered samples of unit SN1A (Figure 5.4), the analyses show less Hd enrichment with an earlier tendency to Ac enrichment. This is very similar to the field of the metasomatic pyroxenes of unit SN1A though in the

quartzite it is extended to more Na-poor compositions. The most notable feature of the quartzite pyroxenes is that Si is higher and Al lower than in all other similar pyroxenes. The Al contents divide the quartzite pyroxenes into two groups. The ferrosalite to hedenbergite compositions display a trend of increasing Al whereas from hedenbergite to aegerine the pyroxenes remain very Al-poor. Whereas the metasomatic pyroxenes of the syenite units tend to contain less Ti than their igneous counterparts, those in the quartzite show strong Ti enrichment at more Na-rich compositions. Zr enrichments are found in the more sodic compositions.

In general the quartzite pyroxenes show high Ti, Zr, Fe^{3+} and Na and low Fe^{2+}, Mn, Ca and Mg.

5.3 Amphiboles

5.3.1 Crystal chemistry

All the amphibole analyses were recalculated for Fe^{3+} and assigned names using the method of Leake (1978) and all discussion of site occupancy or substitutions is based on the generalised amphibole formula of $AX_2Y_5Z_8O_{22}(OH,F)_2$. The compositional range in all the analyses, both magmatic and metasomatic syenite amphiboles and all country rock amphiboles, is displayed on Figure 5.5, a plot of Ca versus Al_Z, from which it can be seen that the syenite amphiboles range from hastingsitic compositions through katophorite towards arfvedsonite. This variation is characteristic of undersaturated alkaline centres, both in the Gardar (Stephenson and Upton 1982, Larsen 1976) and elsewhere (Giret *et al.* 1980) and results predominantly from the coupled substitution $Ca_XAl_Z <> Na_XSi_Z$. Figure 5.5 shows that the quartzite and granite-gneiss amphiboles do not follow the hastingsite-katophorite-arfvedsonite trend found in the syenites. Instead, they vary from katophorite to the more calcic richterite and ferro-actinolite compositions with the most Na-rich compositions being arfvedsonite and in some cases riebeckite. Also, not properly represented on this diagram, is the presence of the ferromagnesian amphibole, cummingtonite, which is found in the least

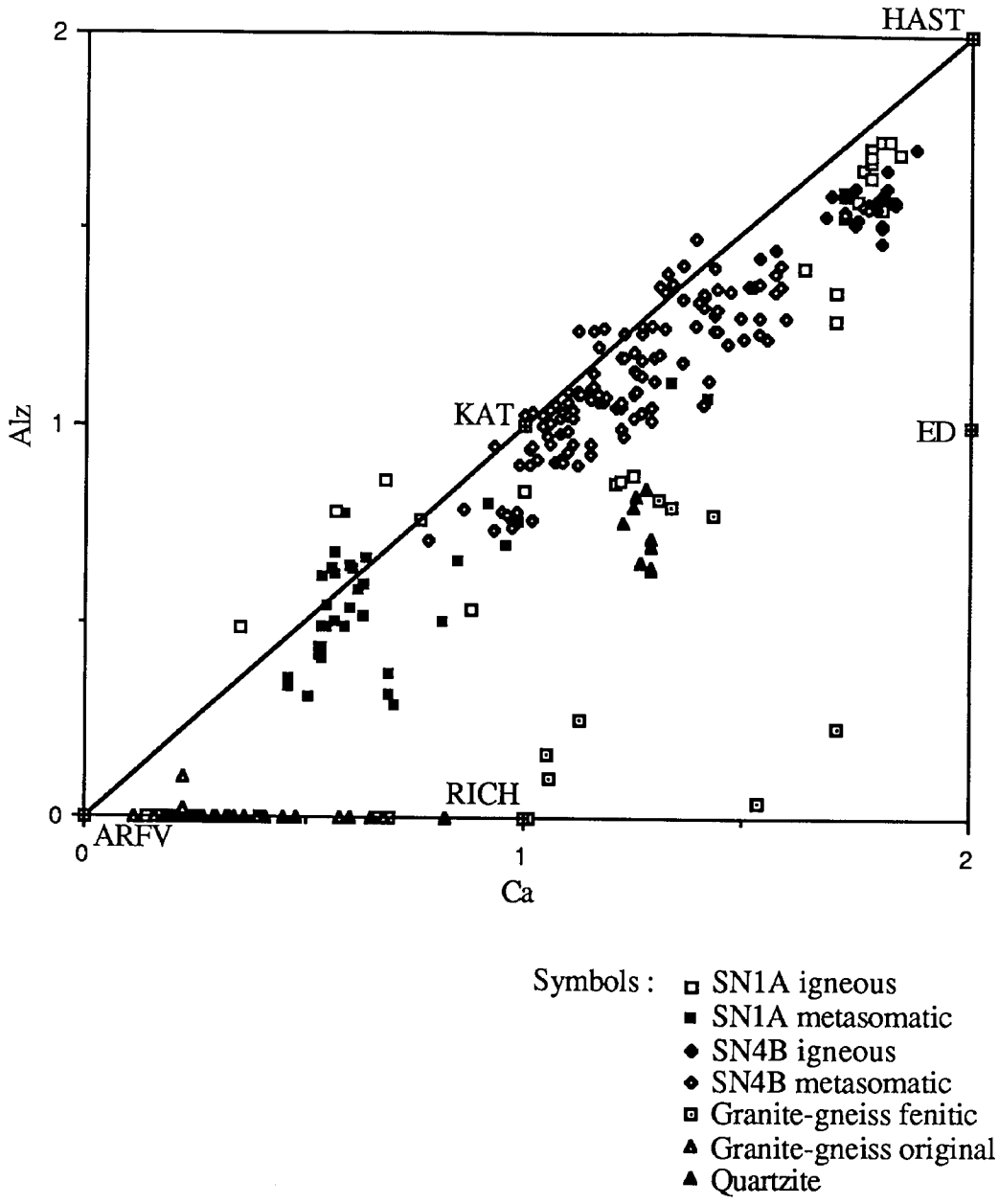

Figure 5.5 North Qoroq amphiboles plotted in terms of Ca against Alz. Scales are atoms per formula unit and abbreviations for amphibole names are as follows :

HAST = Hastingsite ; KAT = Katophorite ; ARFV = arfvedsonite ; RICH = Richterite ; ED = Edenite

petrographically altered sample of the granite gneiss. In thin section it is seen to breakdown with the formation of biotite and it probably represents the original regional metamorphic amphibole of the gneiss (Deer *et al.* 1966). Figure 5.6 shows their limited compositional range and Figure 5.7 (a plot of Si+Na+K versus Al_Z+Ca) displays the variation in the fenitic amphiboles of the country rocks. The major variation from katophorite to richterite is a substitution of Si_Z for Al_Z but, obviously, this requires some form of coupled substitution to compensate the charge balance. Stephenson and Upton (1982), in a study of mafic silicate variations in Gardar centres, concluded that the scheme $(Na,K)_A+Al_Z <> \square_A+Si_Z$ was the major control on the variation and this suggestion is supported in the North Qoroq country rock amphiboles by an increasing deficiency in the A-site, from close to zero at katophorite up to 0.9 at richterite. Two substitution schemes are commonly proposed to account for the change from richterite to arfvedsonite and from arfvedsonite to riebeckite. $Ca_X+(Mg,Fe^{2+})_Y <> Na_X+Fe^{3+}{}_Y$ produces the change to arfvedsonite and $Na_A+Fe^{2+}{}_Y <> \square_A +Fe^{3+}{}_Y$ the change to riebeckite (eg. Stephenson and Upton 1982, Neumann 1976 and Giret *et al.* 1980), and support is found for the occurence of these substitutions in the chemical variations shown by the country rock amphiboles associated with North Qoroq (see section 5.3.2.2).

5.3.2 Metasomatic variation

5.3.2.1 The syenites

The unaltered amphiboles in SN4B and much of SN1A are dominantly ferroan- and ferro-pargasites with a few hastingsites indicating some substitution of Al^{3+} for Fe^{3+} while the variation from ferroan to ferro-pargasite implies a substitution of $Fe^{2+}{}_y$ for $Mg^{2+}{}_y$. In a similar way to the whole-rock chemistry and the pyroxenes, SN1A contains more evolved compositions than SN4B, with the igneous crystallisation trend extending to magnesio-arfvedsonite. The metasomatic amphiboles of SN4B are

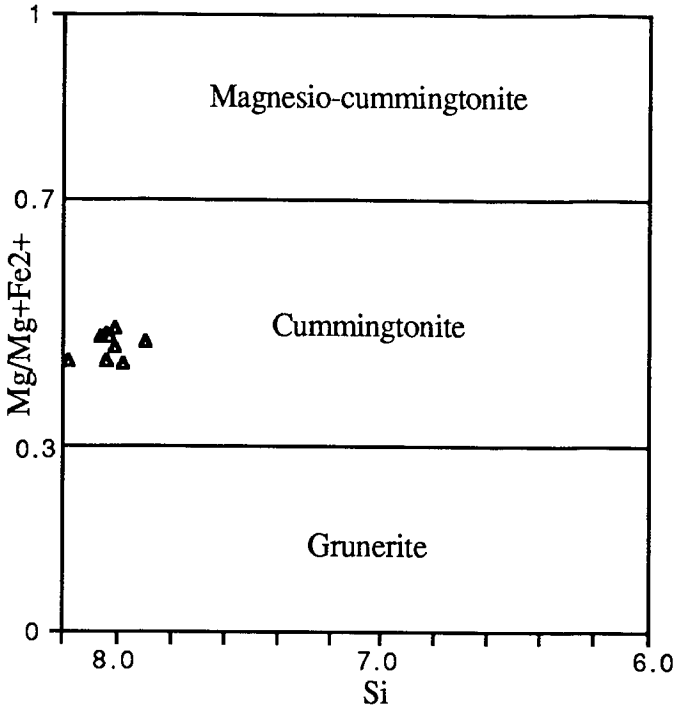

Figure 5.6 Classification of original metamorphic amphiboles in the granite-gneiss.

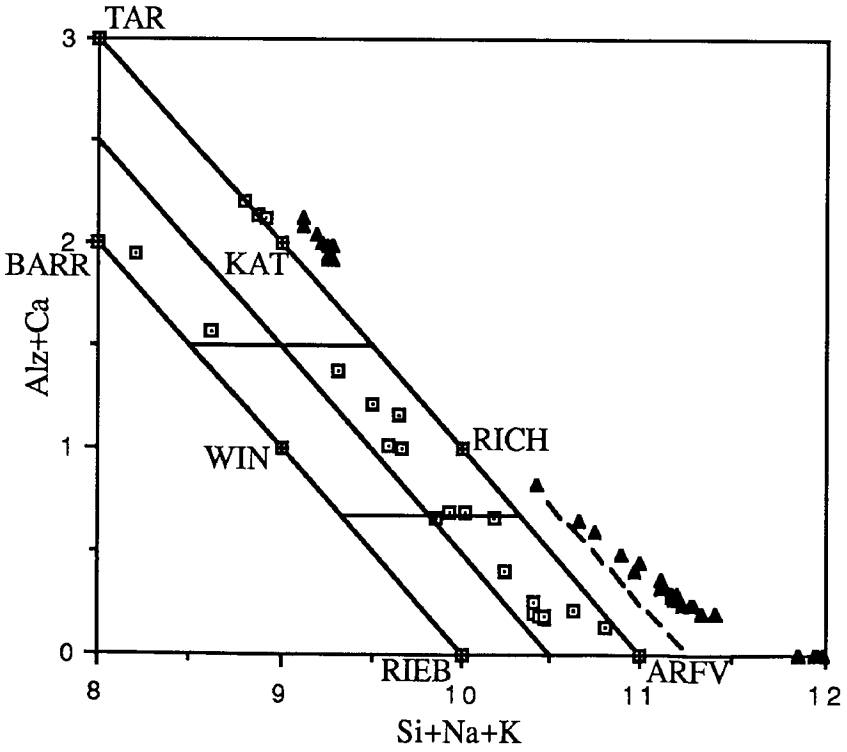

Figure 5.7 Amphiboles from the granite-gneiss and the quartzite raft plotted in terms of (Alz+Ca) against (Si+Na+K).
All symbols are the same as those used in Figure 5.5 and abbreviations not used before are as follows :
TAR = Taramite ; BARR = Barroisite ; WIN = Winchite ; RIEB = Riebeckite.

almost exclusively potassian-manganoan- or potassian-katophorites but there is some spread to more edenitic compositions. In SN1A the metasomatic amphiboles overlap and extend the evolved, Na-rich end of the igneous trend and are classed as magnesio-arfvedsonites and ferro-eckermannites, though some katophorites are found. Chambers (1976) used a baseline of Na_X-Al_Z against which to represent the chemical variation in the North Qoroq amphiboles and the same parameter will be used here to show changes with metasomatism (Figure 5.8). The steadily increasing Si and decreasing Ca, with little deviation, confirm that the major control on the syenite amphibole variation is the coupled substitution Ca_XAl_Z <> Na_XSi_Z. The unaltered pargasites and hastingsites are relatively Ti-rich though they show a rapid depletion with little increase in Na_X-Al_Z. Fe^{3+} increases in the pargasites by approximately twice the Ti depletion and a plot of Ti versus Fe^{3+} gives a good negative correlation along a slope of ~-2, suggesting a substitution of the type Fe^{2+}+Ti^{4+} <> $2Fe^{3+}$ proposed by Larsen (1976) for the Ilimaussaq amphiboles. The metasomatic amphiboles, while containing significant Fe^{3+}, display no correlation with increasing Na_X-Al_Z, though this may be partly due to the presence of fluorine in the hydroxyl site which affects the recalculation of the structural formula. The increases in Fe^{2+} and Mn in the metasomatic amphiboles, when compared to equivalent magmatic amphiboles, are compensated for by the decrease in Mg, confirming the substitution Mg^{2+} <> Fe^{2+}. Mn contents are highest in the metasomatic amphiboles of unit SN4B and, in general, these are more (Fe^{2+}+Mn)-rich than the metasomatic amphiboles in SN1A (Figure 5.9) . K shows a slight but definite increase in the alkali amphiboles during metasomatism but no pattern could be discerned for Zr which is generally no more than half that found in the pyroxenes.

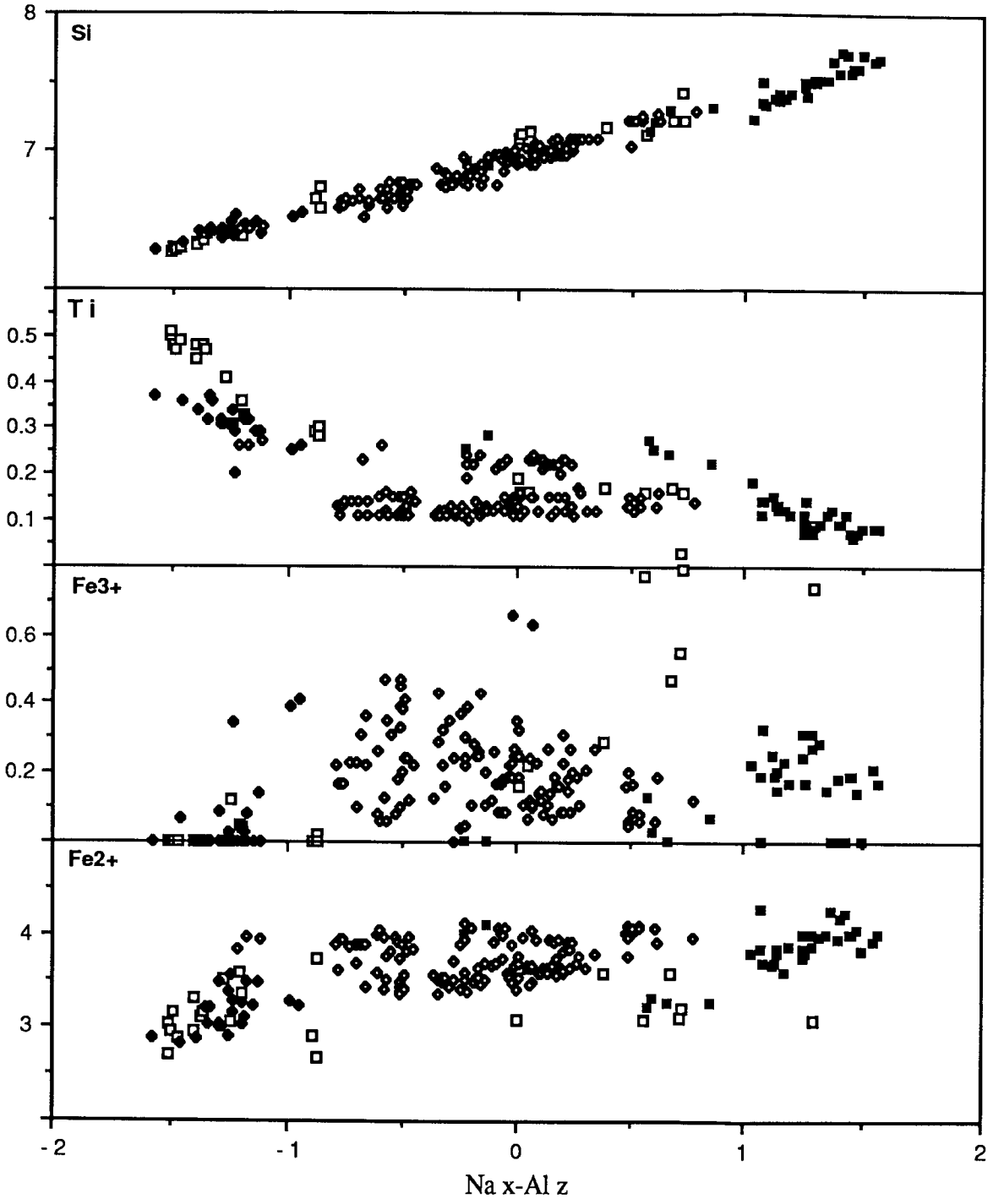

Figure 5.8 (two pages) Element variation in North Qoroq amphiboles.
All figures are in atoms per formula unit and all symbols are the same as those used in Figure 5.5.

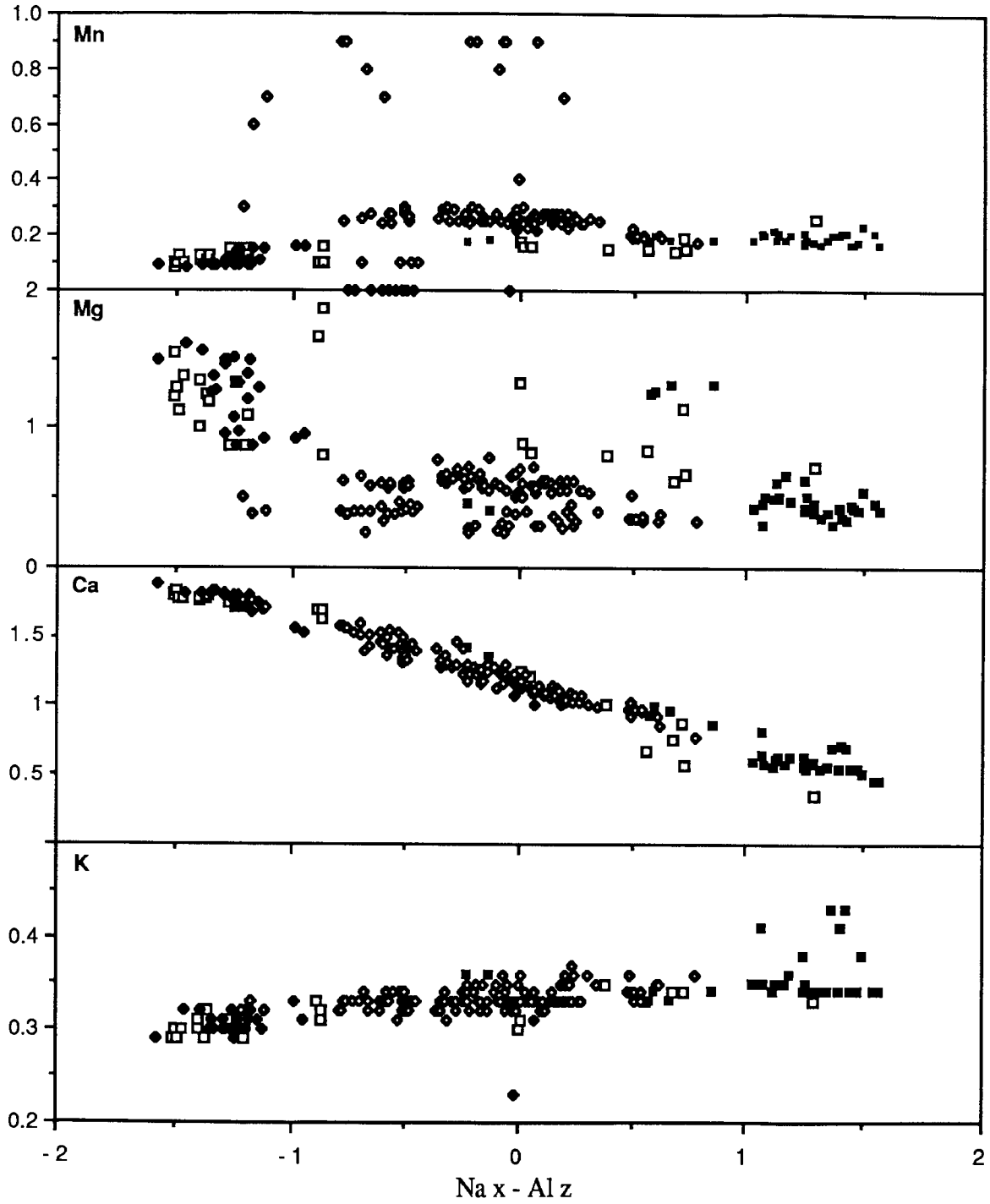
Mn
Mg
Ca
K
1.0
0.8
0.6
0.4
0.2
2
1
0
1.5
0.5
0.4
0.3
0.2
-2
-1
0
1
2
Na x - Al z

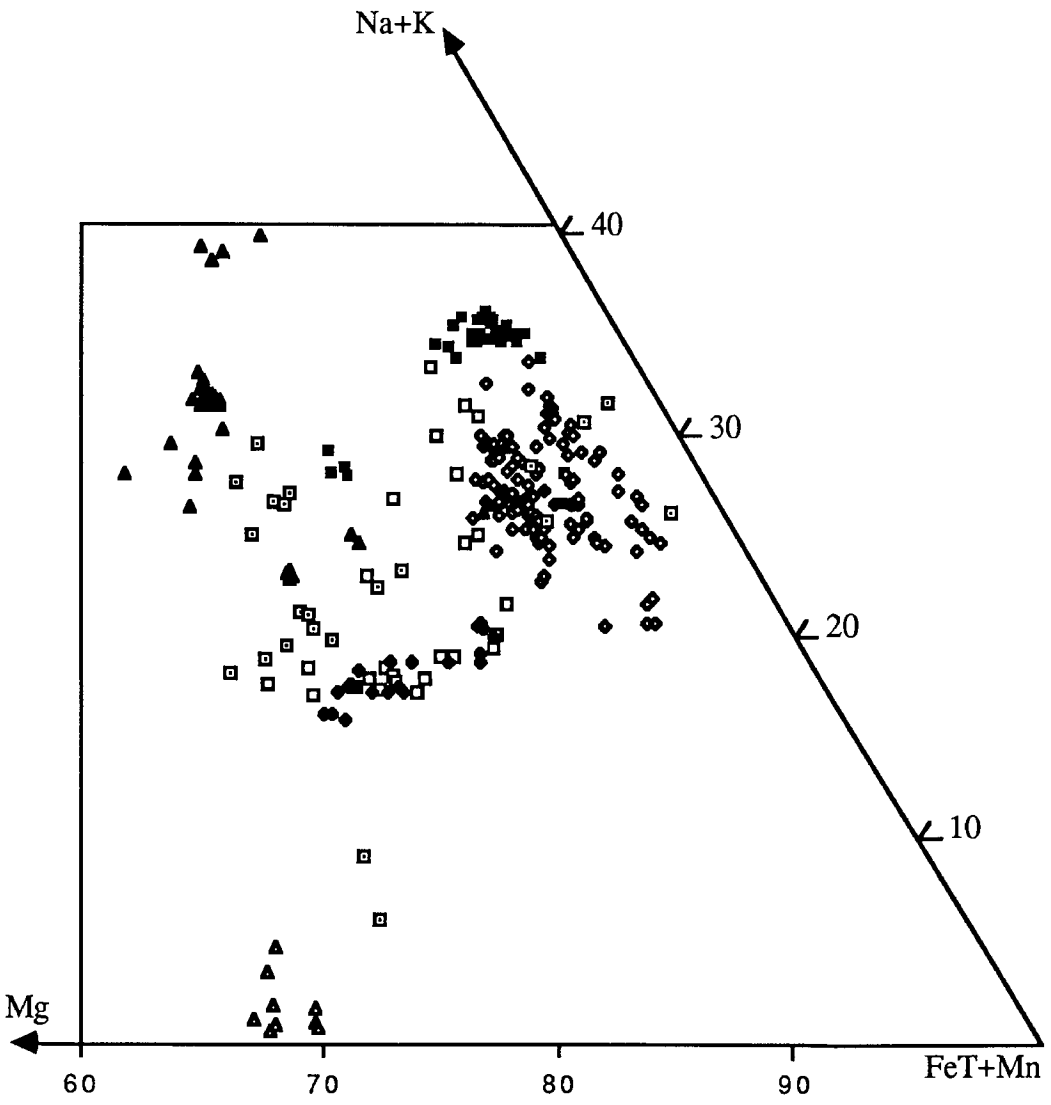

Figure 5.9 North Qoroq amphiboles plotted in the triangle Mg-(FeT+Mn)-Na. FeT = total iron. All symbols are the same as those used in Figure 5.5.

5.3.2.2 The country rocks

From Figure 5.7 it can be seen that the analyses from the quartzite define a considerably more (Si+Na+K)-rich trend than those from the granite gneiss. In fact, the quartzite amphiboles contain considerable excess Si+Na+K, especially at (Al_Z+Ca)-poor compositions where Si+Na+K=12. Siemiatkowska and Martin (1975) found excess Na in riebeckites formed in the fenitisation of the Mississagi quartzite, Ontario, with Na values distinctly greater than in riebeckite from other fenites. The computer programme used to recalculate the amphiboles (Rock 1987) assigns Fe^{3+} by assuming a stoichiometry of 13 in the Z+Y sites, and so if vacancies exist in the Y-sites all the Fe is left as Fe^{2+}. This is the case for the four amphiboles with Si+Na+K=12 in which the recalculated Si values are high (~8.5), a feature also noted in the fenitised quartzites at Borrolan by Woolley *et al.* (1972). They demonstrated that by recalculating the analyses with all the iron in the ferric state both the Si value and the Y-site total are reduced, creating a vacancy in Y. Full wet chemical analyses showed that more than half the iron was present as Fe^{3+}. Deer *et al.* (1966) state that members of the eckermannite-arfvedsonite series rarely correspond to the ideal formula ($Na_3(Mg,Fe^{2+})_4Al(Si_8O_{22})(OH,F)_2$) and substitutions involving Al, Ca and Fe^{3+} are all possible. If the four North Qoroq analyses in question are recalculated assuming that all the iron is in the ferric state then the Si value is reduced to ~8, the Y-site total to ~4 and Si+Na+K to ~11.3. It is therefore proposed that much of the iron is indeed present as Fe^{3+} (ie. the amphiboles are not stoichiometric) and the quartzite analyses more realistically plot along the dashed line in Figure 5.7.

The chemical variations from katophorite to richterite to arfvedsonite can be represented against a baseline of Al_Z+Ca (Figure 5.10). It can be seen that from katophorite to richterite there is a decrease in Al and an increase in Si supporting the suggestion of a $(Na,K)_A+Al_Z <> \square_A+Si_Z$ substitution. This scheme would lead to a decrease in (Na+K) but in fact they remain relatively constant or, in the case of Na, even

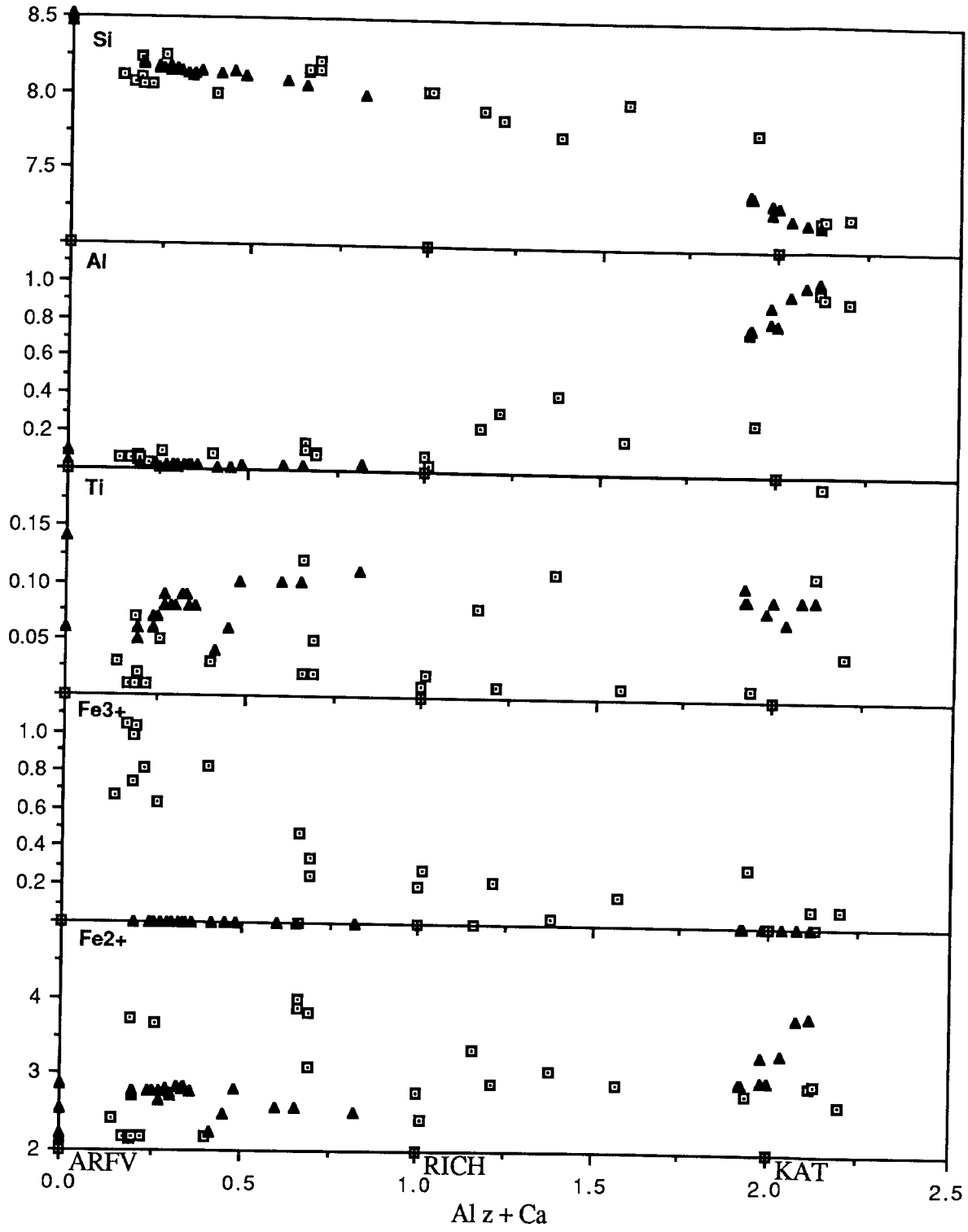

Figure 5.10 (two pages) Element variation in amphiboles from the country rocks surrounding the North Qoroq centre. All figures are in atoms per formula unit and symbols are the same as those used in Figure 5.5. Amphibole name abbreviations are given in Figure 5.5.

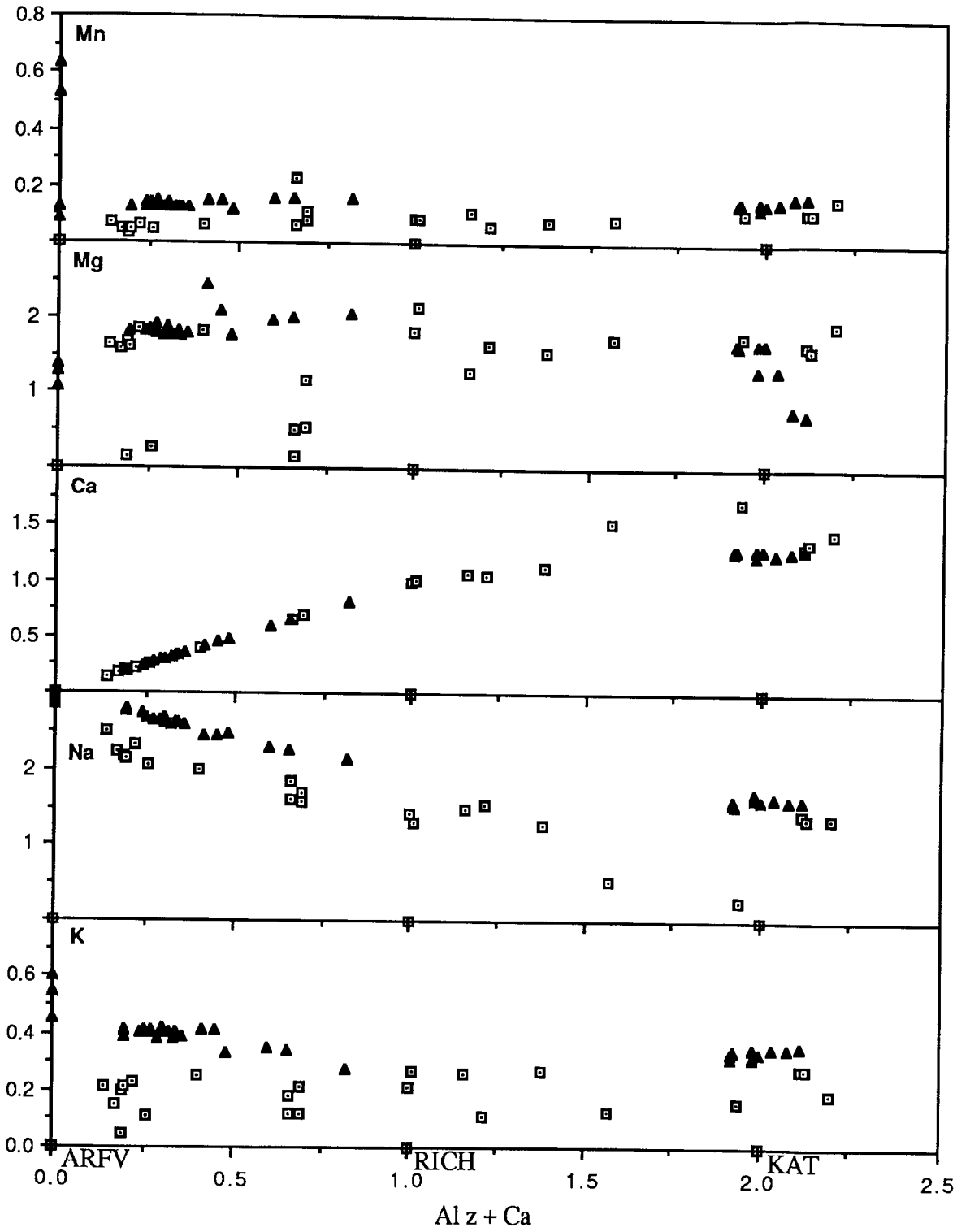
Mn
Mg
Ca
Na
K
ARFV
RICH
KAT
0.0
0.5
1.0
1.5
2.0
2.5
Al z + Ca

increase slightly and it is proposed that some Al is also lost in the coupled substitution seen in the syenites, $Ca_XAl_Z <> Na_XSi_Z$. The slight decrease in Ca, matching the increase in Na, supports this suggestion. From richterite to arfvedsonite there is little change in Si and Al but in the granite-gneiss there is a large increase in Fe^{3+} which, as argued above, probably also exists in the quartzite amphiboles but, due to vacancies in the Y-site, is not calculated by the computer programme. Ca decreases sharply and Na increases supporting the substitution schemes outlined in section 5.3.1. Figure 5.10 also shows that the quartzite amphiboles are noticeably richer in K and Mn than those in the granite gneiss, the former element also partly accounting for any excess Si+Na+K in the quartzite amphiboles.

5.4 Biotites

5.4.1 Crystal chemistry

The iron in all the biotite analyses has been left as in the original electron probe analysis and no attempt has been made to recalculate the Fe^{3+} content. The same approach was adopted by Parsons (1979), Stephenson and Upton (1982), Platt and Woolley (1986) and Woolley and Platt (1988). Stephenson and Upton (1982) suggested that, in the Kungnat biotites, a significant amount of Fe is present as Fe^{3+} and Parsons (1979) pointed out that discussions of site occupancy are limited by the lack of this data. Stephenson and Upton do, however, show that with total Fe as FeO the biotites appear stoichiometric with (Na+K)~2, (Fe+Mn+Mg)~5 and (Si+Al)~8 and Upton and Thomas (1980) found a very similar range in compositions in the Tugtutoq Younger Giant Dyke Complex. This might suggest that Fe^{3+} is in fact minor and Platt and Woolley (1986) failed to detect Fe^{3+} in a wet chemical analysis of biotite from the Mulanje complex, Malawi. The North Qoroq biotites are mostly stoichiometric and so treating all Fe as FeO will probably not have a significant effect on the representation of the chemical variation in the biotites, but no attempt will be made to discuss site occupancies.

5.4.2 Metasomatic variation

5.4.2.1 The syenites

The variation in the biotites is represented against a baseline of Fe+Mn/Fe+Mn+Mg (Figure 5.11) in which increasing numerical value corresponds to increasing annite content. All analyses are plotted on this figure, including those from the country rock granite-gneiss. The unaltered syenites contain biotites in the range $annite_{71}$-$annite_{82}$ with those of SN1A slightly more Mg-rich than SN4B. The metasomatic biotites in SN1A range from $annite_{71}$ up to $annite_{97}$ and the range for SN4B is from $annite_{85}$ up to $annite_{98}$. The metasomatism of the syenites, therefore, results in increasing (Fe+Mn) content ultimately leading to the formation of almost pure annite.

There is an increase in Si from the unaltered to the metasomatic biotites in the syenites whereas both Ti and Al show a decrease when compared to magmatic biotites. There is a significant increase in Mn contents in the biotites of the metasomatised syenites and those of SN1A are notably richer in Mn than those of SN4B. This feature of high Mn contents at high Fe/Mg ratios in biotites of alkaline intrusions is not unusual and has been recorded by Nash and Wilkinson (1970), Woolley and Platt (1988), Stephenson and Upton (1982) and Mitchell and Platt (1982) amongst others. Total alkalis (K+Na) in the biotites of the unaltered syenites are fairly constant and stoichiometric with (K+Na)~2 but the metasomatic biotites have a (K+Na) deficiency with values as low as 1.66. Although, as stated in section 5.4.1, the Fe^{3+} content has not been recalculated it is proposed that this deficiency is the result of the introduction of Fe^{3+} into the biotite via the substitution scheme $(K,Na)_X+(Mg,Fe^{2+})_Y <> \square_X+Fe^{3+}_Y$. This is analogous to the arfvedsonite to riebeckite substitution in the amphibole and may occur at a similar late stage. An introduction of Fe^{3+} into the biotite would correspond well with the same process occuring in the feldspars, pyroxenes and amphiboles.

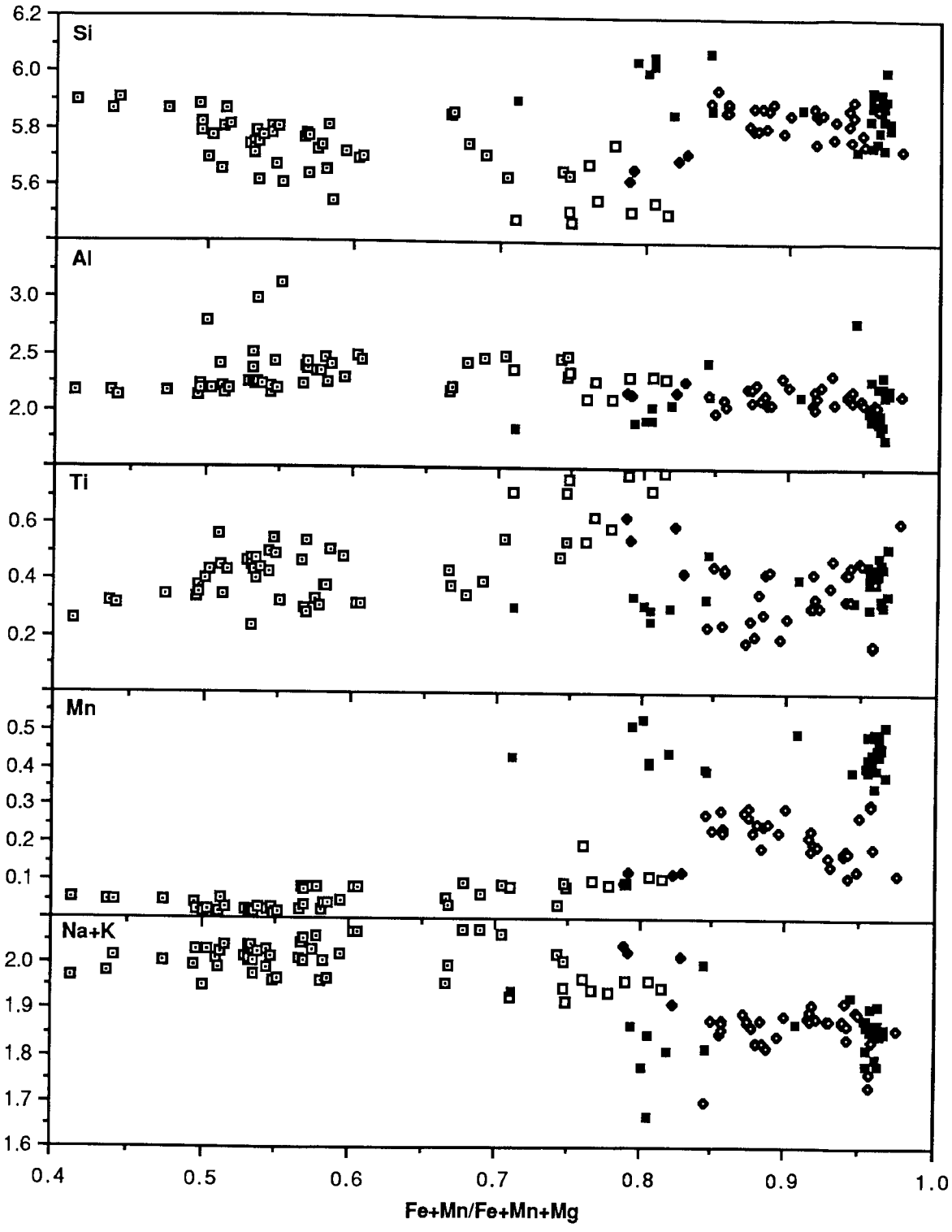

Figure 5.11 Element variation in biotites from the North Qoroq centre. All figures are in atoms per formula unit and all symbols are the same as those used on Figure 5.5, except that no distinction is made between original metamorphic and fenitic biotites in the granite-gneiss.

5.4.2.2 The country rocks

Biotite is absent from the quartzite raft and so this section is concerned solely with the granite-gneiss. In contrast to the syenites, the granite-gneiss biotites are considerably more Mg-rich and vary from $annite_{41}$-$annite_{75}$, which also represents a greater range in composition than that found in the syenite centre.

In the granite gneiss there is a variation to decreasing Si with increasing annite content and it is noticeable that the annite-rich compositions have silica values and annite contents very similar to those of the biotites in the unaltered syenites. The same feature is true of Ti, Al and Mn, though these elements all show increases with increasing annite content. It is possible that this is a reflection of the initial fluid composition affecting the granite-gneiss and may indicate that the fluid had substantially re-equilibrated with the less evolved syenite before reaching the country rock aureole. Total alkalis (K+Na) remain fairly constant in the granite-gneiss biotites with a range from 1.95 up to 2.08 indicating their good stoichiometry.

5.5 Halogen contents of amphiboles and biotites

Fluorine and chlorine were both analysed for in the biotites and fluorine was analysed in the amphiboles, and the results are presented on Figure 5.12 and 5.13. Analyses of magmatic biotites and amphiboles were taken from Chambers (1976) in which F and Cl were not analysed and so these are omitted from the figures. It can be seen that there is a general agreement with the Fe^{2+}-F avoidance rule in the biotites (Munoz and Ludington 1974, Rosenberg and Foit 1977), the more magnesian biotites containing more fluorine. The highest levels of fluorine are therefore found in the granite-gneiss biotites which also contain more chlorine, an element that was not detected in significant quantities in any biotite from within the syenite centre. For a given value of Fe it can be seen that the biotites in unit SN1A are richer in fluorine than those in SN4B and separate sub-parallel trends of Fe^{2+}-F avoidance could be drawn for the granite gneiss, SN1A and SN4B. This is clearer in the amphiboles for which fluorine

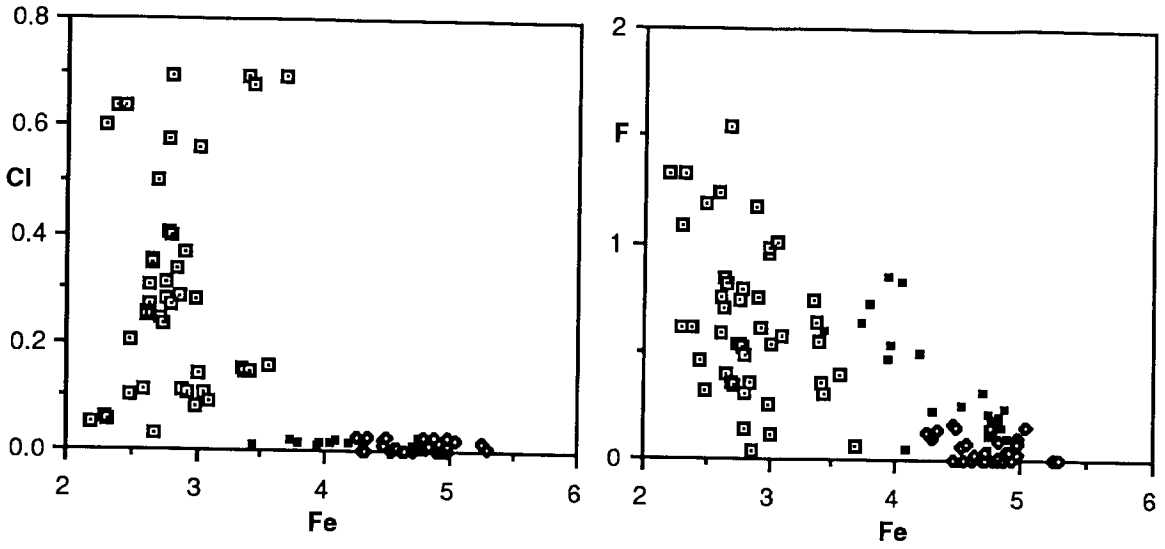

Figure 5.12 Halogen contents of North Qoroq biotites plotted against Fe.
Cl and F are in element wt% values, symbols as in Figure 5.5.

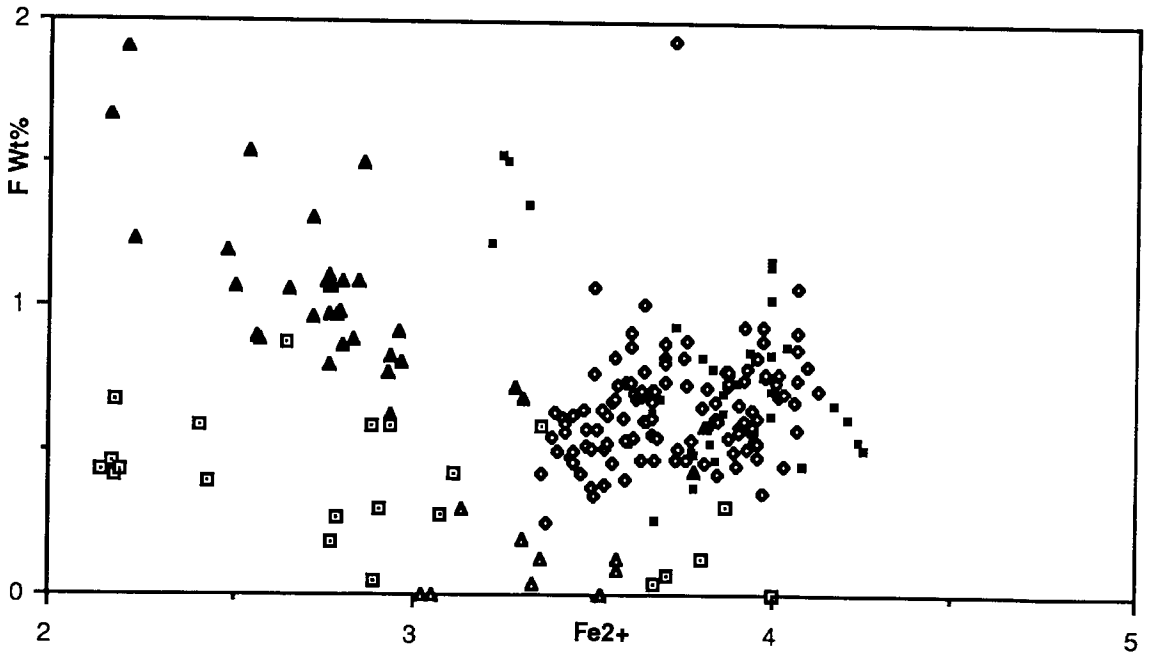

Figure 5.13 Relationship between Fe and F in North Qoroq amphiboles.
Fe2+ in atoms per formula unit, F in element wt%.
All symbols as in Figure 5.5.

was analysed (Figure 5.13). The analyses for unit SN4B have a relatively restricted range of Fe contents and show no correlation with F, which is generally low, but the amphiboles of SN1A, the quartzite and the gneiss all define separate sub-parallel trends. Ferguson (1978) stated that since the F content of an amphibole depends on both the availability of F and Fe^{2+} then, at similar values of Fe^{2+}, the F content of the amphibole will reflect differences in the availability of F in the fluid. On this basis both the biotite and amphibole data indicate an order of F availability during the metasomatism of SN1A>SN4B~quartzite>granite gneiss. The anion contents of the metasomatic fluids will be discussed in the study of apatite chemistry in the following chapter.

5.6 Discussion

The metasomatism associated with the North Qoroq centre is reflected in both textural (see chapter 2) and chemical changes in the mafic silicates. The chemical alteration agrees well with the whole-rock variations detailed in chapter 3. In general, the metasomatic mafic minerals of the syenite units, SN1A and SN4B, show low values of Al, Ti, Mg and Ca and high contents of FeT, Zr, Mn, Na and K, but some significant differences are found between the units. Both the metasomatic pyroxenes and amphiboles of unit SN4B are more (Fe^{2+}+Mn)-rich than those of SN1A (Figure 5.4 and Figure 5.9). The metasomatic biotites show more overlap in composition but, in contrast to the other mafic phases, those of SN1A are more Mn-rich. The apparently high Si contents of the metasomatic biotites may appear to contradict the whole-rock depletions but it must be remembered that the major control on the Si variation in the rock is the alteration of the felsic phases, which as described in chapter 4, recrystallise to a feldspathoidal matrix. The high Fe contents of the metasomatic mafic phases analysed in SN4B in no way contradicts the general Fe depletion in the whole-rock as most of the Fe will originally have been present in the Fe-Ti oxides.

The mafic mineral assemblages produced during the metasomatism of the syenite units are broadly similar though, in detail, there are some compositional differences. There are also differences in assemblages on the thin section scale within a

unit. This feature was noted in Chapter 2 where it was shown that local variations can produce sections where alkali amphibole and aenigmatite are the dominant mafic phases or where alkali pyroxene, biotite and opaques are the dominant phases. Aenigmatite is often closely associated with both amphibole and pyroxene, and acmitic pyroxene is seen rimming alkali amphibole and aegerine-hedenbergite. These often complicated relationships may reflect initial variations in the syenite that is being metasomatised and/or the development of local variations in the metasomatic fluid as reaction occurs. Although the syenites of SN1A and SN4B show similar variations in original mineralogy (perthite, ferrosalite, ferro-pargasite) and the similar trends in whole-rock chemistry (Chambers 1976) they evolved to different stages by crystal fractionation processes and so differences in the metasomatic mafic silicates within and between units must be interpreted in terms of both changing fluid composition and original mineralogy.

It is possible to reach some conclusions on the nature of the fluid phase from an appraisal of the physico-chemical conditions under which the mineral assemblages that are formed are stable. The alkali amphiboles produced (magnesio-arfvedsonite or ferro-eckermannite in SN1A and katophorite in SN4B) can be compared with the experimental studies of riebeckite-arfvedsonite solid solutions by Ernst (1962). He found that increasing temperature favoured the formation of arfvedsonite over riebeckite and also that arfvedsonite is only stable at magmatic temperatures if the oxygen fugacity (fO_2) is low and pH_20 is >=1000bars. This suggests that the arfvedsonite-bearing assemblages will have crystallised under conditions of low fO_2 and relatively high temperature. It should be noted, though, that the incorporation of fluorine into the amphibole greatly increases the amphibole stability field (Ernst 1962) and so, in these volatile (F and Cl)-rich systems, no quantitative estimates can be made of fO_2 from amphibole stabilities. Aoki (1964) and Yagi (1966) both demonstrated that hedenbergite and aegerine-hedenbergite are stable at high temperatures and low fO_2 similar to that of arfvedsonite and as all these minerals represent the highest grade metasomatic mafic assemblages it seems reasonable to conclude that the highest

temperature fluids were also characterised by relatively low oxygen fugacity. The fO_2-T^{oc} stability field of annite, which is commonly associated with the metasomatic pyroxene, has also been shown to overlap that of the alkali amphiboles (Eugster and Wones 1962, Wones and Eugster 1965).

It seems clear that the formation of a pyroxene-dominated assemblage over an amphibole-dominated assemblage or vice-versa cannot be attributed solely to variations in fluid composition. As stated in chapter 2, Chambers (1976) found local variations in the relative abundances of amphibole and pyroxene in the unaltered syenites, which he attributed to local fluctuations in pH_2O in the magma during crystallisation. The presence of a compositional gap in magmatic pyroxene trends, in which amphibole is stable, has also been noted by Stephenson (1972), Larsen (1976) and Ferguson (1978) who related the stability of amphibole over pyroxene primarily to an increase in $P_{volatiles}$ (fHF, pH_2O). Comparison of Figures 5.4 and 5.9 shows that the metasomatic amphiboles fill a gap between the compositions of the unaltered ferrosalites and the metasomatic pyroxenes and this may indicate that the metasomatic assemblage is closely related to the original magmatic assemblage. It is possible that metasomatic amphibole forms from magmatic amphibole and metasomatic pyroxene from magmatic pyroxene. Differences in the magmatic mineral assemblages may affect the metasomatic assemblages in two ways. Firstly, different elements may be available for conversion to metasomatic phases and secondly, different mineral assemblages may react and subtely change parameters such as fO_2 on a local scale, so stabilising one or another metasomatic mineral. Much of the metasomatic variation is probably controlled by reaction within small, limited micro- environments and it may be that, on this local scale, the depletion of F and Cl by the crystallisation of amphibole, sodalite and fluorite sufficiently restricts the alkali amphibole stability field so that pyroxene becomes the stable phase.

The presence of aenigmatite is generally taken to indicate low oxygen fugacities (eg. Grapes *et al.* 1979) and Marsh (1975) proposed the existence of a

'no-oxide' field in alkaline undersaturated liquids, in which aenigmatite is stable, lying well below the QFM buffer. Marsh, though, failed to convincingly demonstrate the 'no-oxide' field and Larsen (1977) concluded that the use of aenigmatite equilibria as a quantitative fO_2 barometer is not possible. Nicholls and Caermichael (1969) indicated that a more important control on aenigmatite stability is the peralkalinity (a.$Na_2Si_2O_5$), with increasing a.$Na_2Si_2O_5$ stabilising aenigmatite at higher fO_2. It is probable that during the metasomatism in North Qoroq, the formation of aenigmatite is related to both the high Na content of the fluid and the presence of original Fe-Ti oxides. It is likely that under the influence of a peralkaline metasomatising fluid original Fe-Ti oxides will react to form aenigmatite and so the continued presence of the former in the metasomatic rocks may reflect a less abundant fluid phase, again emphasising the patchy nature of the metasomatism. Local variations in fO_2 caused by local reactions in micro-environments may also be partly responsible for producing the different assemblages with Fe-Ti oxides+pyroxene representing high fO_2 and aenigmatite+ amphibole low fO_2.

It seems clear that, while overall observations can be made regarding generally low oxygen fugacities, the initial high temperature metasomatism is controlled largely by a fluid moving and reacting patchily on an already variable magmatic framework with the net result being a patchy variation.

The high temperature assemblages of alkali amphibole and aegerine-hedenbergite are both rimmed by almost pure acmitic pyroxene and this later variation may well reflect a change in fluid composition as temperature decreases. Aoki (1964) and Yagi (1966) suggested that the trend to acmite enrichment in sodic pyroxenes is controlled by increasing fO_2 and decreasing temperature. Acmite is unstable at low fO_2, eg. equivalent to wustite-magnetite or iron-wustite buffers, and is replaced by arfvedsonitic amphibole (Bailey 1969). Bailey demonstrated, though, that acmite is stable over a range of fO_2 down to that of the QFM buffer but will only crystallise from

liquids containing excess $Na_2Si_2O_5$. Mitchell and Platt (1978) showed that increasing acmite content can be combined with decreasing fO_2 and also concluded that alkalinity is the most important control on acmite enrichment. To invoke a real and significant increase in $a.Na_2Si_2O_5$ in the metasomatic fluid in North Qoroq, as the fluid progressively re-equilibrates with less evolved syenite, is unrealistic though, and it is suggested that in this case the formation of acmite is controlled by increasing fO_2 with decreasing temperature. While this increase in fO_2 may be real and significant, it is possible that, as the metasomatism represents, on a large scale, an open system, fO_2 ceases to be internally defined and so simply remains relatively constant with further decrease in temperature. At the same time, mineral reaction in micro-environments, acting effectively as small closed systems (eg. the conversion of Fe-Ti oxides to aenigmatite), could locally define fO_2.

The formation of the most Na-rich mafic mineral (acmite) as the low grade, low temperature assemblage, produced after the high grade, relatively Na-poor aegerine-hedenbergites and alkali amphiboles has to be explained. It might be expected that the highest grade, earliest formed metasomatic minerals would be the most Na-rich as the fluid is obviously strongly peralkaline but the clear petrographic association of acmite rimming both amphibole and pyroxene contradicts this (see Plate 2.2). It is suggested that initial reaction between fluid and rock leads to the breakdown of the original mafic minerals and Ti, Mg and Ca are released into the fluid while the Fe is used in the formation of the Fe-rich aegerine-hedenbergites and arfvedsonites. This process leads to the relatively rapid re-equilibration of these elements between fluid and rock and although the fluid is continually losing Na to the rock this takes longer, due to the initial high sodic content of the fluid. As temperature falls the fluid becomes increasingly dilute, oxygen fugacity rises and acmite is produced from a relatively low temperature sodic brine.

The mafic mineralogy of the granite gneiss and the quartzite contrasts

strongly with that of the syenites and also with each other. The mafic assemblage in the quartzite is pyroxene+amphibole with no biotite whereas in the gneiss it is amphibole+biotite with no pyroxene.

In contrast to the syenites the pyroxenes of the quartzite show little Hd-enrichment and an early tendency to acmite. The aegerines are also significantly more Ti-rich, to the point where they could be termed titan-aegerine (>0.1 atoms Ti per formula unit, Flower 1974). The Al contents split the pyroxenes into two groups, one of aegerine-augite composition with increasing Al and the more sodic pyroxenes with negligible Al (Figure 5.1). The pyroxenes were analysed in three samples which have different petrographies. The aegerine-augites containing Al occur in a rock that has been completely made over to pyroxene+amphibole+minor apatite, calcite and fluorite whereas the more sodic pyroxenes occur in rocks that still contain some quartz, are strongly albitised and have relatively abundant calcite and fluorite. These differences in Al content can be explained in terms of the $a.SiO_2$. Popp and Gilbert (1972) demonstrated that the jadeite component is much less soluble in acmitic pyroxenes from silica saturated environments than silica undersaturated ones. In the samples composed almost entirely of pyroxene and amphibole the $a.SiO_2$ will be lower than in those with free quartz still present and so the pyroxenes will incorporate greater amounts of Al. This is supported by the fact that all the quartzite pyroxenes have lower Al than the pyroxenes in the syenite where $a.SiO_2$ would be lower and defined by feldspathoid/feldspar assemblages. The presence of albite will also reduce the Al content of the pyroxene by acting as a sink for the Al available.

The amphiboles in the quartzite are generally more Mg- and alkali-rich than in the syenites. The granite gneiss amphiboles are also more Mg-rich than the syenites and in comparison to the quartzite there is a greater substitution to riebeckite. The biotites in the granite gneiss are generally more Mg-rich than those in the syenites although the more annite-rich compositions are very similar to the compositions of the unaltered syenite biotites.

All these features are explicable in terms of varying fluid compositions and P,T conditions combined with the very different initial country rock compositions. The metasomatism of the quartzite raft is of a very sodic nature as evidenced by the whole-rock chemistry (see chapter 3) and the mafic silicate compositions. This contrasts with the more potassic nature of the granite-gneiss alteration and may indicate that the temperature was higher in the quartzite raft (Jahns et al. 1969, Siemiatkowska and Martin 1975). It should be noted that the granite-gneiss is often albitised very close to the syenite contact and this may also reflect higher temperatures. The difference in amphibole compositions also supports the idea of higher temperatures in the quartzite as Ernst (1962) showed that arfvedsonite is stable to higher temperatures than riebeckite and the presence of aegerine-augite is considered to represent a high temperature environment (Sutherland 1969). These differences could also be partly explained in terms of the oxygen fugacity. Riebeckite is stable only under very oxidising conditions (Ernst 1962) and it could be that the cooler fluids affecting the granite gneiss and which had already reacted with less evolved syenite had a higher fO_2 than those in the quartzite. Both higher temperature and lower fO_2 may be expected in a raft enclosed within the syenites in comparison to the country rock aureole, as in the country rock there is likely to have been greater interaction with more dilute circulating solutions, possibly meteoric in origin, which would dilute the fenitising fluids, hence raising fO_2 and lowering temperature. Such dilute solutions may also be associated with the intrusion of unit SN1A but will simply be referred to as 'meteoric' in the following discussions.

The metasomatism of both the granite-gneiss and the quartzite is considered to have occured at higher values of fO_2 than in the syenite. Aenigmatite is never developed in the quartzite despite the peralkaline nature of the fluid that affected it (though this may simply reflect the lack of original Fe-Ti oxides) and haematite coatings on quartz grains are common. Flower (1974) demonstrated experimentally that high Ti content in acmite is indicative of high fO_2 and is also favoured by high temperature. The considerably more magnesian compositions of the mafic phases in the country rocks also imply higher oxygen fugacities (Platt and Woolley 1986). One reason for the higher fO_2

may be the lack of any significant quantity of original mafic phases in the country rocks which means that there is no method of internally buffering fO_2 in the same way as in the syenites, and so fO_2 is relatively uncontrolled and able to rise significantly.

It is likely that in the syenites, re-equilibration of fluid and rock raised the fO_2 to that equivalent to the QFM buffer, before the fluid reached the country rock aureole, as that is the conditions under which the marginal syenites crystallised. By the time the metasomatic fluid reached the country rock aureole, therefore, the fO_2 would be approximately equivalent to QFM conditions and the Na content would be significantly reduced. The formation of ferro-richterite and biotite as the early formed high temperature mafic phases in the granite-gneiss supports this suggestion. Charles (1975) studied the phase equilibria of ferro-richterite, which is formed in the granite gneiss, and found that completely ferrous ferro-richterite was stable at only very low fO_2, but at lower temperatures and with substitution of some Fe^{3+} stability was achieved up to 525^{oc} under fO_2 defined by the QFM buffer. It was noted that the most annite-rich biotites are compositionally very similar to the biotites in the unaltered syenites and this also suggests that the fluid had extensively re-equilibrated with the syenite before reaching the granite-gneiss. As the fenitisation of the granite-gneiss progressed the fenitising fluid mixed with circulating meteoric waters and as temperature decreased, fO_2 increased. This is reflected in the increasingly Mg-rich compositions of the biotites and in the formation of riebeckitic amphibole at a similar late stage to the development of acmite in the syenites (see Plate 2.7).

It is clear from the sodic nature of the fenitisation in the quartzite raft that not only was temperature higher than in the granite-gneiss but the fluid was still very Na-rich. The quartzite raft is enclosed in the roof zone of unit SN1B and so is subject to Na-rich fluids emanating directly from the fractionated interior of the unit. In a similar location to the quartzite, several small (~1m across) lujavritic bodies were found. A limited number of these were analysed by XRF and were found to be very peralkaline

and it is suggested that they indicate the close proximity of significantly more evolved syenite within unit SN1B. A similar mode of migration for the metasomatic fluids would help explain the still peralkaline nature of the fluid affecting the quarzite raft. The progressive fenitisation of the quartzite follows a similar course to that of the granite-gneiss with falling temperature and increasing fO_2 leading to the growth of almost pure acmite and more riebeckitic amphibole in the lowest grade of fenitisation. The presence of haematite indicates that fO_2 rose significantly during the fenitisation of the quartzite.

The formation of Na-rich minerals (acmite and riebeckite) as the low grade assemblages in the country rocks is again attributed to the evolution of the fluid to a low temperature sodic brine.

5.7 Conclusions

1. Modification of mafic silicate compositions indicates that metasomatism in the North Qoroq syenites was initially under the influence of volatile-rich, Na-rich fluids at relatively high temperature and low oxygen fugacity. Much of the metasomatic variation produced is controlled by a combination of the initial differences in magmatic assemblages and localised reactions in limited micro-environments. This gave rise to a patchy and variable metasomatism.

2. As metasomatism progressed and fluid and rock increasingly re-equilibrated there was a relative rise in fO_2 with decreasing temperature. The fluid became increasingly dilute and acmite formed at a late stage under conditions of higher fO_2 and lower temperature and as a result of the excess Na in the metasomatic fluid.

3. The mafic mineralogy developed in the country rocks shows that higher oxygen fugacities than those operating in the syenites prevailed. The alteration of the quartzite was initially at higher temperatures and lower fO_2 than the granite gneiss while the abundance of fluorite, calcite and F-rich arfvedsonite in the quartzite also suggests a

higher initial fHF and fHCl in the quartzite. In both rock types the final low grade assemblages are characterised by acmite and riebeckite formed at low temperature and under conditions of high fO_2.

References

Aoki, K. 1964. Clinopyroxenes from alkaline rocks of Japan. AM MINERAL **49**, 1199-223.

Bailey, D.K. 1969. The stability of acmite in the presence of H_2O. AM J SCI **267-A**, 1-16.

Cawthorn, R.G. & Collerson, K.D. 1974. The recalculation of pyroxene end-member parameters and the estimation of ferrous and ferric iron content from electron microprobe analyses. AM MINERAL **59**, 1203-08.

Chambers, A.D. 1976. The petrology and geochemistry of the North Qoroq centre, Igaliko Complex, South Greenland. UNPUBL PhD THESIS, UNIV OF DURHAM.

Charles, R.W. 1975. The phase equilibria of richterite and ferrorichterite. AM MINERAL **60**, 367-74.

Currie, K.L. & Ferguson, J. 1971. A study of fenitisation around the alkaline carbonatite complex at Callander Bay, Ontario, Canada. CAN J EARTH SCI **8**, 498-517.

Deer, W.A., Howie, R.A. & Zussman, J. 1966. *An introduction to the rock forming minerals*. London: Longman.

Duggan, M.B. 1988. Zirconium-rich sodic pyroxenes in felsic volcanics from the Warrumbungle Volcano, Central New South Wales, Australia. MINERAL MAG **52**, 491-96.

Ernst, W.G. 1962. Synthesis, stability relations and occurence of riebeckite and riebeckite-arfvedsonite solid solutions. J GEOL **70**, 689-736.

Eugster, H.P. & Wones, D.R. 1962. Stability relations of the ferruginous biotite, annite. J PETROL **3**, 82-125.

Ferguson, A.K. 1978. The crystallisation of pyroxenes and amphiboles in some alkaline rocks and the presence of a pyroxene compositional gap. CONTRIB MINERAL PETROL **67**, 11-15.

Flower, M.F.J. 1974. Phase relations of titan-acmite in the system Na_2O-Fe_2O_3-Al_2O_3-TiO_2-SiO_2 at 1000 bars total water pressure. AM MINERAL **59**, 536-48.

Giret, A., Bonin, B. & Leger, J. 1980. Amphibole compositional trends in oversaturated and undersaturated alkaline plutonic ring-complexes. CAN MINERAL **18**, 481-95.

Gomes, C. de B., Moro, S.L. & Dutra, C.V. 1970. Pyroxenes from the alkaline rocks of Itapirapua, Sao Paulo, Brazil. AM MINERAL **55**, 224-30.

Grapes, R., Yagi, K. & Okumura, K. 1979. Aenigmatite, sodic pyroxene, arfvedsonite and associated minerals in syenites from Morotu, Sakhalin. CONTRIB MINERAL PETROL **69**, 97-103.

Hartman, P. 1969. Can Ti^{4+} replace Si^{4+} in silicates. MINERAL MAG **37**, 366-69.

Hollister, L.S. & Gancarz, A.J. 1971. Compositional sector zoning in clinopyroxene from the Nacre area, Italy. AM MINERAL **56**, 959-79.

Jahns, R.H., Martin, R.F. & Tuttle, O.F. 1969. Origin of granophyre in dikes and sills of tholeiitic diabase. AM GEOPHYS UNION TRANS **50**, 337.

Jones, A.P. & Peckett, A. 1980. Zirconium-bearing aegerines from Motzfeldt, South Greenland. CONTRIB MINERAL PETROL **75**, 251-55.

Kresten, P. & Morogan, V. 1986. Fenitization at the Fen complex, southern Norway. LITHOS **19**, 27-42.

Larsen, L.M. 1976. Clinopyroxenes and co-existing mafic minerals from the alkaline Ilimaussaq intrusion, South Greenland. J PETROL **17**, 258-90.

Larsen, L.M. 1977. Aenigmatites from the Ilimaussaq intrusion, south Greenland: chemistry and petrological implications. LITHOS **10**, 257-70.

Leake, B.E. 1978. Nomenclature of amphiboles. MINERAL MAG **42**, 533-63.

Marsh, J.S. 1975. Aenigmatite stability in silica-undersaturated rocks. CONTRIB MINERAL PETROL **50**, 135-44.

Mitchell, R.H. & Platt, R.G. 1978. Mafic mineralogy of ferroaugite syenite from the Coldwell alkaline complex, Ontario, Canada. J PETROL **19**, 627-51.

Mitchell, R.H. & Platt, R.G. 1982. Mineralogy and petrology of nepheline syenites from the Coldwell Alkaline Complex, Ontario, Canada. J PETROL **23**, 186-214.

Morogan, V. & Martin, R.F. 1985. Mineralogy and partial melting of fenitised crustal xenoliths in the Oldoinyo Lengai carbonatitic volcano, Tanzania. AM MINERAL **70**, 1114-26.

Munoz, J.L. & Ludington, S.D. 1974. Fluoride-hydroxyl exchange in biotite. AM J SCI **274**, 396-413.

Nash, W.P. & Wilkinson, J.F.G. 1970. Shonkin Sag Laccolith, Montana I. Mafic minerals and estimates of temperature, pressure, oxygen fugacity and silica activity. CONTRIB MINERAL PETROL **25**, 241-69.

Nash, W.P., Carmichael, I.S.E. & Johnson, R.W. 1969. The mineralogy and petrology of Mount Suswa, Kenya. J PETROL **10**, 409-39.

Nicholls, J. & Carmichael, I.S.E. 1969. Peralkaline acid liquids: a petrological study. CONTRIB MINERAL PETROL **20**, 268-94.

Neumann, E. 1976. Compositional relations among pyroxenes, amphiboles and other mafic phases in the Oslo Region plutonic rocks. LITHOS **9**, 85-109.

Nielsen, T.F.D. 1979. The occurence and formation of Ti-aegerines in peralkaline syenites. CONTRIB MINERAL PETROL **69**, 235-44.

Parsons, I. 1979. The Klokken gabbro-syenite complex, south Greenland: cryptic variation and origin of inversely graded layering. J PETROL **20**, 653-94.

Parsons, I. 1980. Alkali-feldspars and Fe-Ti oxide exsolution textures as indicators of the distribution and subsolidus effects of magmatic 'water' in the Klokken layered syenite intrusion, South Greenland. TRANS R SOC EDINBURGH **71**, 1-12.

Parsons, I. 1981. The Klokken Gabbro-Syenite Complex, South Greenland: quantitative interpretation of mineral chemistry. J PETROL **22**, 233-60.

Parsons, I. & Becker, S.M. 1986. High temperature fluid-rock interactions in a layered syenite pluton. NATURE **321**, 764-69.

Platt, R.G. & Woolley, A.R. 1986. The mafic mineralogy of the peralkaline syenites and granites of the Mulanje complex, Malawi. MINERAL MAG **50**, 85-99.

Popp, R.K. & Gilbert, M.C. 1972. Stability of acmite-jadeite pyroxenes at low pressure. AM MINERAL **57**, 1210-31.

Powell, M. 1978. The crystallisation history of the Igdlerfigssalik nepheline syenite intrusion, Greenland. LITHOS **11**, 99-120.

Robins, B. & Tysseland, M. 1983. The geology, geochemistry and origin of ultrabasic fenites associated with the pollen carbonatite (Finnmark, Norway).CHEM GEOL **40**, 65-95.

Rock, N.M.S. 1976. Fenitisation around the Monchique alkaline complex, Portugal. LITHOS **9**, 263-79.

Rock, N.M.S. 1987. A FORTRAN programme for tabulating and naming amphibole analyses according to the International Mineralogical Association scheme. MINERALOGY AND PETROLOGY **37**, 79-88.

Rosenberg, P.E. & Foit, F.F. 1977. Fe^{2+}-F avoidance in silicates. GEOCHIM COSMOCHIM ACTA **41**, 345-46.

Siemiatkowska, K.M. & Martin, R.F. 1975. Fenitization of Mississagi Quartzite, Sudbury Area, Ontario. GEOL SOC AM BULL **86**, 1109-22.

Stephenson, D. 1972. Alkali clinopyroxenes from nepheline syenites of the South Qoroq Centre, South Greenland. LITHOS **5**, 187-201.

Stephenson, D. & Upton, B.G.J. 1982. Ferromagnesian silicates in a differentiated alkaline complex: Kungnat Fjeld, South Greenland. MINERAL MAG **46**, 283-300.

Sutherland, D.S. 1969. Sodic amphiboles and pyroxenes from fenites in East Africa. CONTRIB MINERAL PETROL **24**, 114-35.

Upton, B.G.J. & Thomas, J.E. 1980. The Tugtutoq younger giant dyke complex, South Greenland: fractional crystallisation of transitional olivine basalt magma. J PETROL **21**, 167-98.

Verhoogen, J. 1962. Distribution of titanium between silicates and oxides in igneous rocks. AM J SCI **260**, 211-20.

Wones, D.R. & Eugster, H.P. 1965. Stability of biotite: experiment, theory, and application. AM MINERAL **50**, 1228-72.

Woolley, A.R. & Platt, R.G. 1988. The peralkaline nepheline syenites of the Junguni intrusion, Chilwa province, Malawi. MINERAL MAG **52**, 425-33.

Woolley, A.R., Symes, R.F. & Elliott, C.J. 1972. Metasomatized (fenitised) quartzites from the Borrolan Complex, Scotland. MINERAL MAG **38**, 819-36.

Yagi, K. 1966. The system acmite-diopside and its bearing on the stability relations of natural pyroxenes of the acmite-hedenbergite-diopside series. AM MINERAL **51**, 976-1000.

CHAPTER 6

Apatite Chemistry, Rare Earth Element Transport and Fluid Inclusion Studies

6.1 Introduction

Apatite [$Ca_5(PO_4)_3(OH,F,Cl)$] can be found in a wide variety of igneous rock types and is a common accessory in numerous other environments (McConnell 1973). Although apatite is almost pure calcium phosphate with a hydroxyl-halogen member, it does constitute an important repository for certain trace elements. Together with phases such as monazite and allanite, the presence of apatite controls the distribution of the rare earth elements (REE) in igneous processes (Watson and Capobianco, 1981, Green and Watson, 1982). The REE contents of apatites, therefore, are critical to any model dealing with the behaviour of these elements.

The halogen chemistry of apatites has been used by several authors (eg Sisson 1987, Yardley 1985) as an indicator of the relative proportions of halides in igneous and metamorphic fluids, on the basis that the extent of substitution of F and Cl for OH depends on the relative fugacities of HF, HCl and H_2O in the fluid. This provides an alternative approach to fluid inclusion studies in which the inherent problem is that chloride is assumed to be the dominant anion in the aqueous phase and so little information is gained on the fluorine content of these fluids.

This chapter describes the REE and halogen chemistry of apatites associated with the metasomatism (fenitisation) of the basement gneiss and supracrustal rocks surrounding the North Qoroq centre. This information will be combined with a study of whole rock REE contents and fluid inclusion studies and the implications for the nature of the fluid phase will be discussed. The three lines of evidence provide information on anion contents, complexing in the fluid and salinities of the fluids.

6.2 General Geology and Petrography

The general setting of the North Qoroq centre is described in Chapter 2 where appropriate references are also listed. Only field and petrographic observations of direct relevance to this chapter will be emphasised here. The samples of Julianehab Granite examined form a traverse in the area west of the long lake where the syenite is exposed near its roof zone and the samples of supracrustal rocks are all taken from the quartzite raft stoped into unit SN1B of the syenite centre.

As stated in Chapter 2, the metasomatism of the quartzite produces areas of completely albitised rock (see Plate 2.9b) and other areas that are completely made over to alkali mafic minerals. The apatite in the quartzite occurs exclusively in association with the alkali mafic minerals and forms rims between the mafic pods and the albitised matrix (see Plate 2.11). In the granite gneiss the apatite also tends to occur in association with new mafic minerals (see Plate 2.8). Standard optical microscopy does not reveal any detail in the apatites which are all small equant crystals that appear to be internally homogeneous.

Cathodoluminescence microscopy (C.L.), previously used in the study of alkali feldspar in the North Qoroq centre (Rae and Chambers 1988), also proved to be a useful petrographic aid in the study of apatites. The luminescence shows distinct zonation in most of the crystals. The apatites in the quartzite usually show a circular zone in the middle of the crystal luminescing a different shade to both the core and the outer rim (Plate 6.1), whereas in the granite-gneiss the apatites commonly have only a simple outer rim (Plate 6.2) which is comparable to the outer rim of the apatites in the quartzite. Mariano and Ring (1975) attributed the cathodoluminescence (C.L.) of apatites to europium activation with minor effects produced by other rare earth elements such as samarium and dysprosium. He stated that Eu^{2+} produced a blue luminescence that was common to apatites of carbonatites and fenites. The apatites in North Qoroq do not luminesce blue but in shades of purple and brown, suggesting the presence of other activators. The details of variations in apatite C.L. are probably very complex and it is only the basic hypothesis that variations in luminescent colour are caused by variations

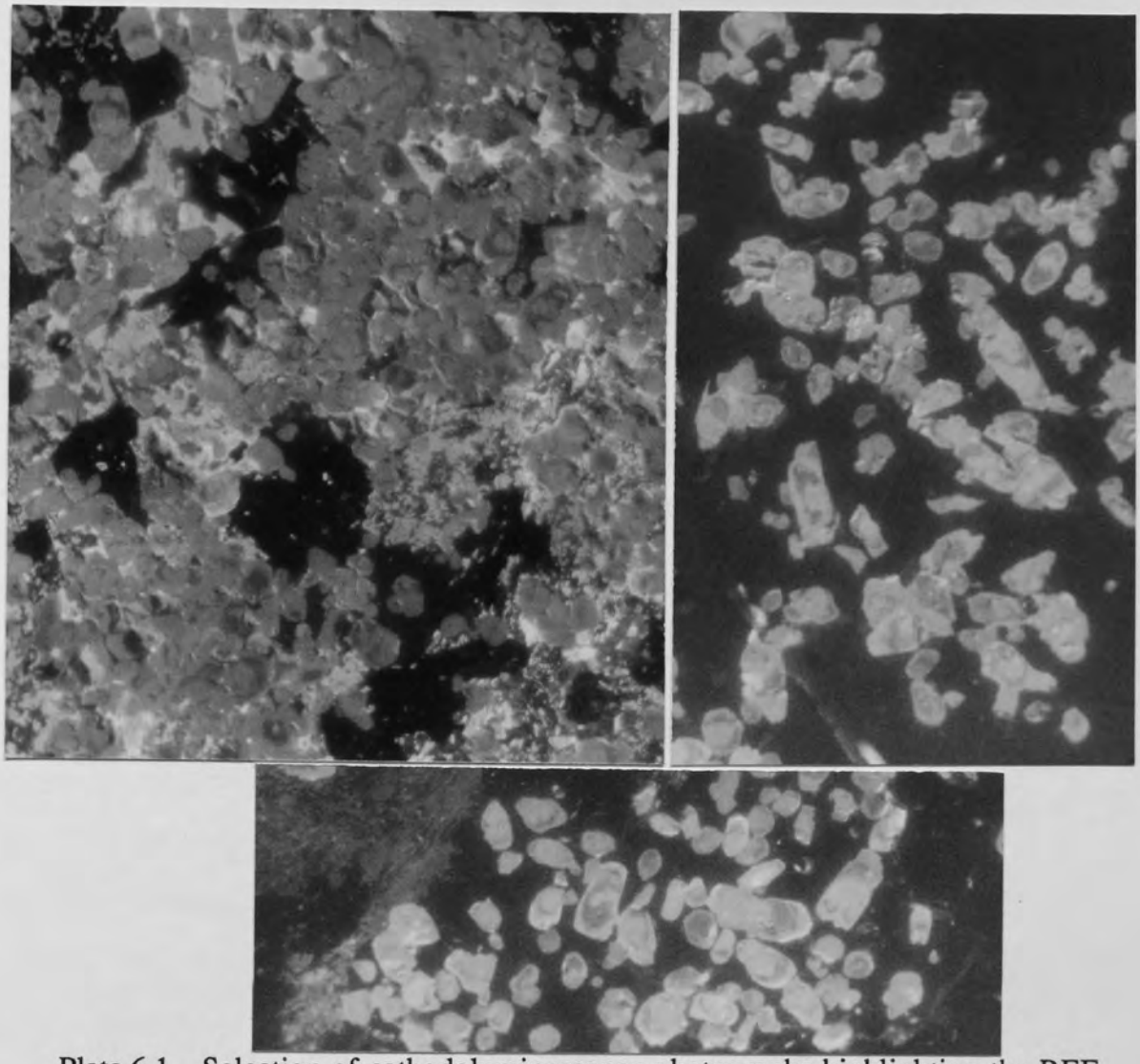

Plate 6.1 Selection of cathodoluminescence photographs highlighting the REE zonation in the apatites of the fenitised quartzite raft.
Width of field of view = 0.4mm

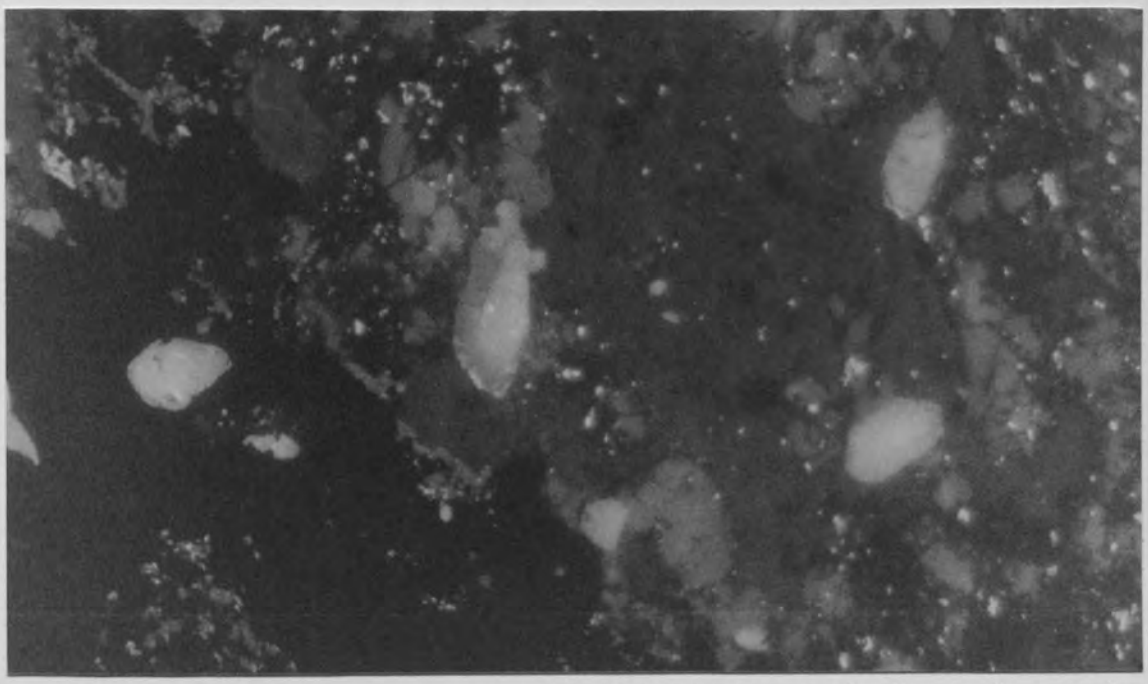

Plate 6.2 Cathodoluminescence photograph of the much simpler apatite zonation in the fenitised granite-gneiss. Width of field of view = 0.4mm

in REE contents that is of prime importance. This hypothesis is supported by the detailed electron microprobe study carried out.

6.3 Apatite Chemistry

6.3.1 Analytical Techniques

Wavelength dispersive electron microprobe analyses were carried out using a Cameca Camebax. The accelerating voltage was 20kv and the beam current was 25nA. Synthetic silicate glasses made at Edinburgh University were used as standards for the REE. The glasses are doped with between 15-20wt% of the appropriate REE oxide, making them significantly richer in rare earths than the standards of Drake and Weill (1972), usually used. The measured composition is not more than $\pm$0.2wt% away from the theoretical composition, a deviation no more significant than one of $\pm$0.02wt% at a theoretical composition of 2wt% (a concentration similar to that of the Drake and Weill standards). Details of analytical procedures are given in Appendix 1. The elements Ca, P, Si, Sr, Fe, Mn, Mg, La, Ce, Pr, Nd, Sm, F and Cl were analysed for and representative analyses are listed in Table 6.1. Eu and Dy were not analysed for as they were below the detection limits of the electron microprobe.

6.3.2 Element Variation

As apatites are essentially calcium phosphate the main interest is the variations in the minor element concentrations (Figure 6.1). The calcium content varies from the ideal of close to 55wt% CaO down to 46.35wt% in the quartzite and 50.38wt% in the basement gneiss. The P content also drops from the ideal of 42wt% to 35.02wt% in the quartzite and 37.71wt% in the gneiss. It is clear that there are extensive substitutions occuring in the apatites, with the quartzite apatites displaying a greater range in values. The major substitutions are for REE and Si. Ce_2O_3 values range from 0.24wt% to 4.96wt% in the quartzite and from 0.02wt% to 3.19wt% in the gneiss. Total REE range up to 10.36wt% and 6.77wt% in the quartzite and gneiss respectively. Si values co-vary with the REE and range from 0.13wt% to 4.08wt% SiO_2 in the

Table 6.1 Representative electron microprobe analyses of apatites.
Sample nos. DAR67, DAR65 - quartzite apatites ; nos. DAR164, DAR163 granite-gneiss apatites.

Sample No.	DAR67	DAR67	DAR67	DAR67	DAR67	DAR65	DAR164	DAR163	DAR163
CaO	52.845	52.996	50.743	51.836	47.984	46.345	54.914	50.381	53.694
P2O5	41.964	42.007	39.881	40.859	36.298	35.024	41.293	37.713	40.571
SiO2	0.144	0.290	1.433	0.815	3.213	4.076	1.818	2.766	1.004
FeO	0.215	0.310	0.313	0.321	0.411	0.074	0.103	0.259	0.039
MnO	0.028	0.000	0.000	0.000	0.000	0.000	0.062	0.000	0.031
MgO	0.001	0.000	0.014	0.001	0.000	0.000	0.020	0.000	0.000
SrO	3.091	3.065	2.740	2.694	1.043	1.316	0.053	0.084	0.025
La2O3	0.260	0.277	1.240	0.846	2.799	2.902	0.060	1.438	0.570
Ce2O3	0.254	0.365	1.759	1.044	4.220	4.959	0.140	3.185	1.288
Pr2O3	0.013	0.058	0.159	0.033	0.273	0.421	0.056	0.444	0.166
Nd2O3	0.089	0.128	0.557	0.254	1.433	1.750	0.121	1.416	0.541
Sm2O3	0.019	0.035	0.084	0.099	0.250	0.324	0.078	0.291	0.090
Cl	0.001	0.000	0.001	0.005	0.003	0.016	0.278	0.029	0.003
F	4.441	3.698	3.405	3.444	3.982	4.718	4.755	5.751	4.125
O=F	1.870	1.557	1.434	1.450	1.676	1.986	2.002	2.421	1.737
Total	101.494	101.670	100.861	100.802	100.233	99.937	101.749	101.336	100.409

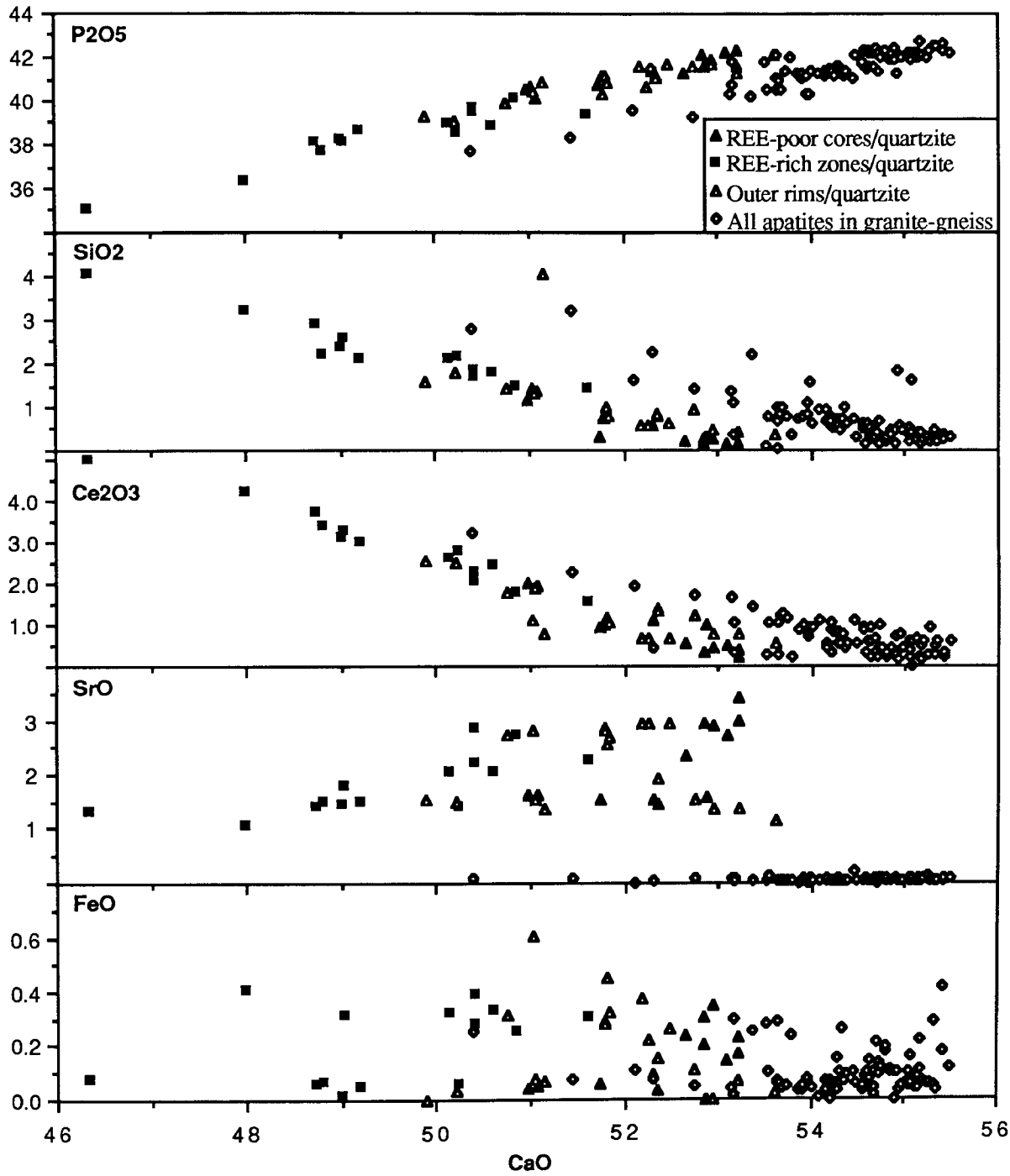

Figure 6.1 Selected element variations in the North Qoroq apatites plotted against CaO Symbols are the same for all plots and all scales are in oxide wt% values.

quartzite and 0.07wt% to 3.23wt% in the basement gneiss.

Of the other four elements analysed (excluding F and Cl) only iron and strontium were present in significant amounts with manganese and magnesium usually below detection limits. Strontium is present in the apatites from the quartzite in quantities ranging from 1.05wt% to 3.40wt% SrO but is present in only trace amounts or is below detection limits in apatites from the basement gneiss. Iron is present in quantities of less than 1wt% FeO (total iron is expressed as FeO in the probe analyses) in both rock types.

The strong REE enrichment observed in the apatites raises the question of the nature of the substitutions taking place. Several authors have noted significant REE substitution in apatites (eg Henderson 1980, Wass *et al.* 1980) and, from comparison of ionic radii, stated that they occupy the Ca^{2+} site. Nash (1972) and Watson and Green (1981) emphasised the fact that the substitution of $RE^{3+} <> Ca^{2+}$ upsets the charge balance and in order to maintain this there has to be a coupled substitution involving a 4+ ion entering the P^{5+} site. The co-variation of Si with the REE indicates that Si^{4+} is substituting for P^{5+} and the good 1:1 correlation shown in Figure 6.2 between $RE^{3+} + Si^{4+}$ and $Ca^{2+} + P^{5+}$ confirms that this is the major substitution occuring in the apatites. Variations from the line in Figure 6.2 are caused by the presence of minor elements such as Sr and Fe. Strontium shows a general decrease as the REE content increases and so is also present in the Ca^{2+} site. Fe may be present in the ferric or ferrous state but in either case will enter the Ca^{2+} site, though there is no systematic variation with either Ca or P. The apatites not only show an increase in abundance of REE in the middle zones and rims of the crystals but a chondrite normalised plot of REE abundances shows a steepening of the slope, implying a relative increase of the light REE over the middle REE (Figure 6.3).

6.3.3 Electron Imaging and Apatite Zonation

Nash (1972) identified the REE mineral britholite in the most evolved rocks of the Shonkin Sag Laccolith and noted that this mineral could be readily obtained from

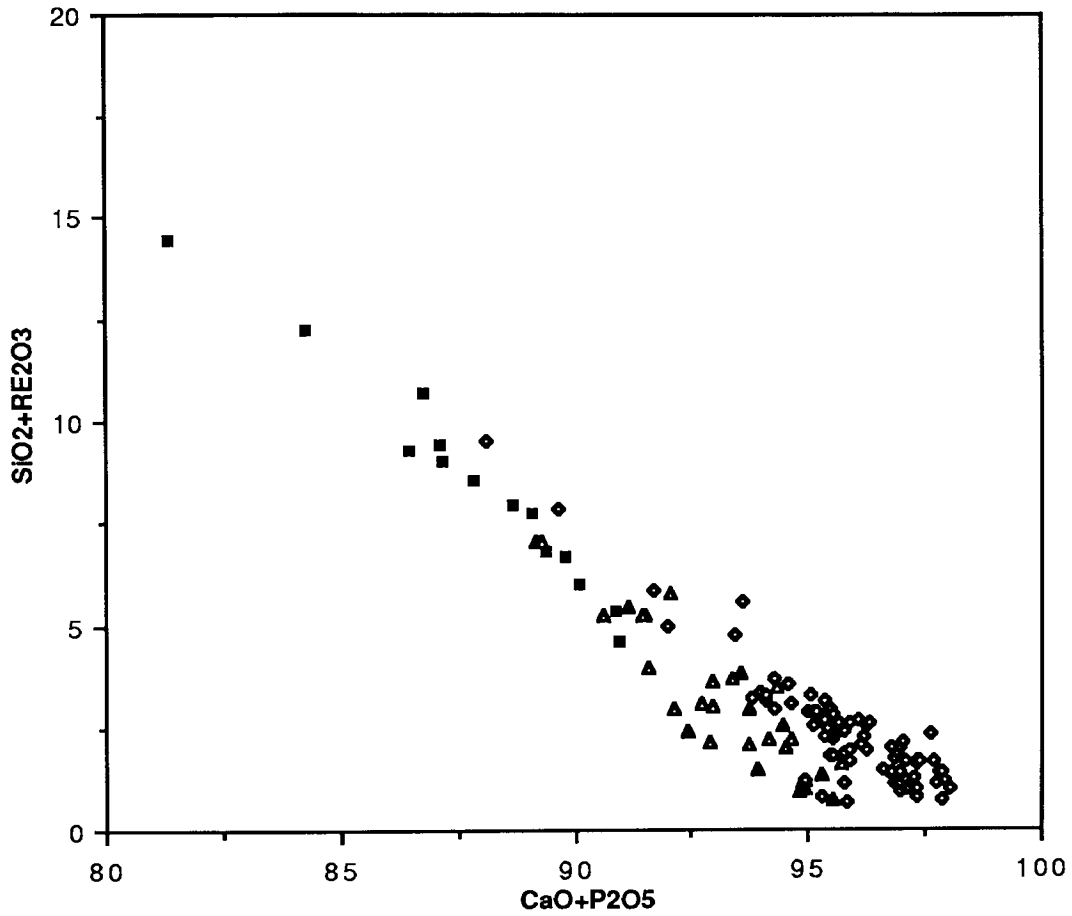

Figure 6.2 Rare earth element substitution in North Qoroq apatites.
RE2O3 = the sum of the rare earth element oxide wt% values
Both axes are in oxide wt% and all symbols are the same as those in Figure 6.1.

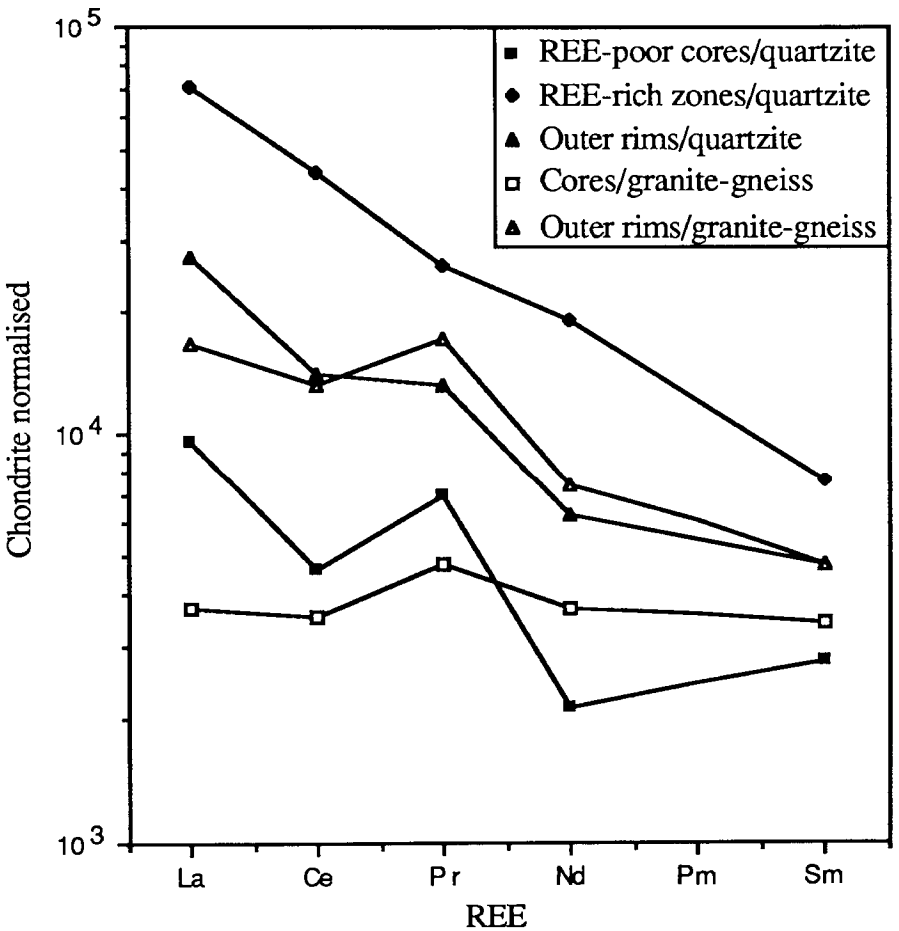

Figure 6.3 Rare earth element patterns in North Qoroq apatites.

apatite by the substitution $RE^{3+}/Si^{4+} <> Ca^{2+}/P^{5+}$. Rare earth minerals were identified in the quartzite in North Qoroq associated with the apatites, by means of back scattered electron imaging. The degree of backscattering is related to atomic number with high atomic number elements producing more backscattering of electrons and hence a brighter image. The presence of the heavy elements, such as the REE, can therefore be easily detected by this method. There are two REE minerals present - the phosphate, monazite and a fluor-carbonate mineral from the bastnaesite family, probably synchysite. While Nash (1972) could not resolve whether the britholite was formed directly from the magmatic residuum or from hydrothermal recrystallisation of apatite, Hogarth (1985), in studying fenites associated with carbonatites, attributed the presence of parisite and synchysite to the breakdown of apatite. It is uncertain in the North Qoroq quartzite whether apatite has dissociated into a Ca-REE phase (synchysite) and a PO_4-REE phase (monazite) or if the two minerals crystallised directly from late REE-rich fluids.

The zonation in the apatites, first observed using C.L., is very clearly seen on a backscattered electron image. A typical backscattered electron image of the apatites in the quartzite shows a dark core with an irregular, sharp contact against a bright zone which is rimmed by further zones of intermediate shades (Plate 6.3). Each zone in the crystal appears to be internally homogeneous and there are sharp boundaries between zones. The probe analyses confirm that this zonation is due to variations in REE content with the cores being relatively REE-poor, the bright rims REE-rich and the outer zones having intermediate REE contents. This distinct pattern of zonation is characteristic of the quartzite but is less commonly developed in the basement gneiss where it is more usual for the apatites to have one simple REE-rich rim, which is comparable to the outer rim of the quartzite apatites. Step traverses across the apatite crystals, analysing every micron, confirm that each zone is extremely homogeneous not only in REE but in Si, Ca and Sr as well (Figure 6.4).

An extensive treatment of the apatite zonation will be deferred until section 6.6 when all the implications for the metasomatising fluids will be discussed.

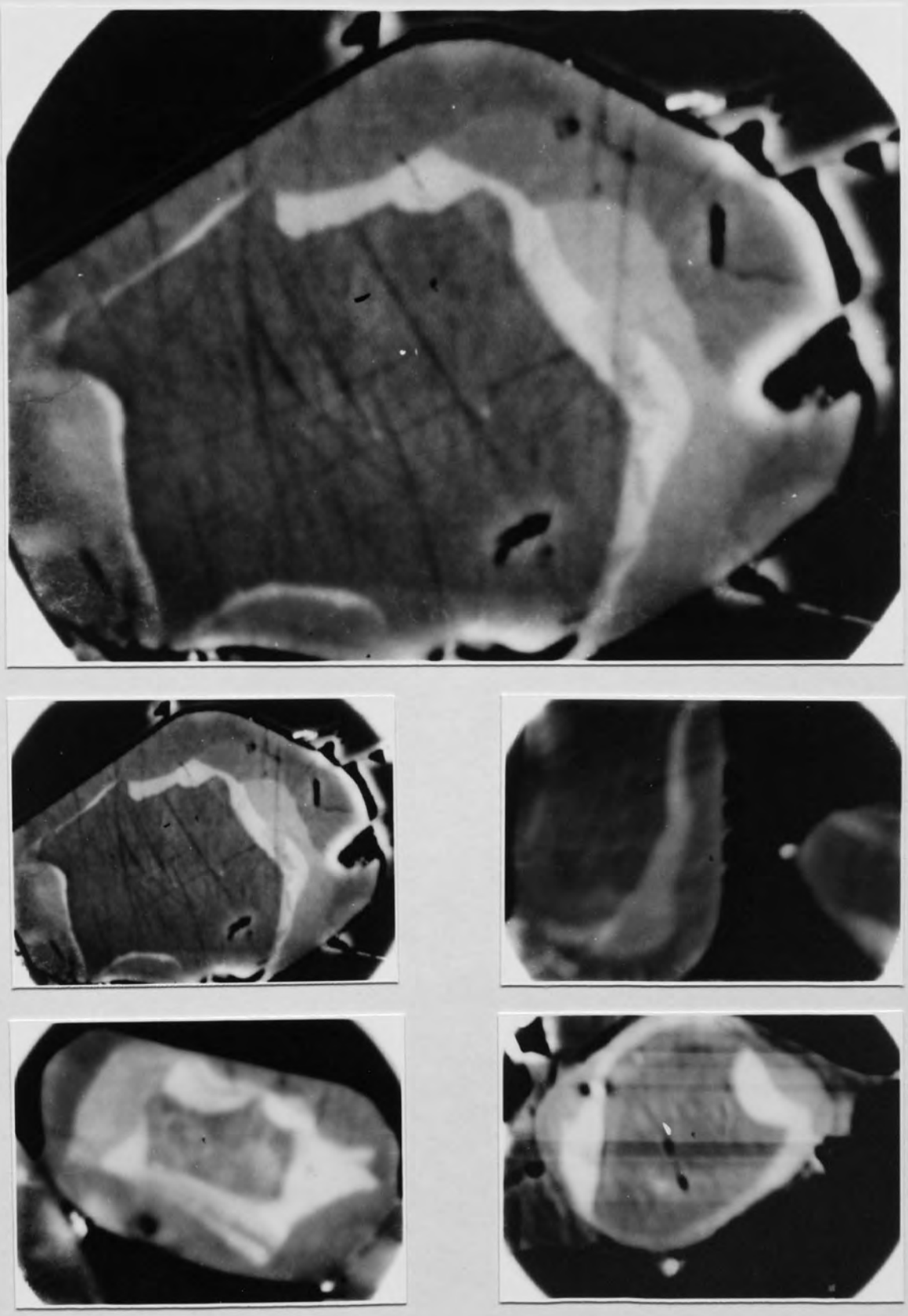

Plate 6.3 Selection of backscattered electron images showing the REE zonation in apatites from the fenitised quartzite raft. Width of field of view = 50um

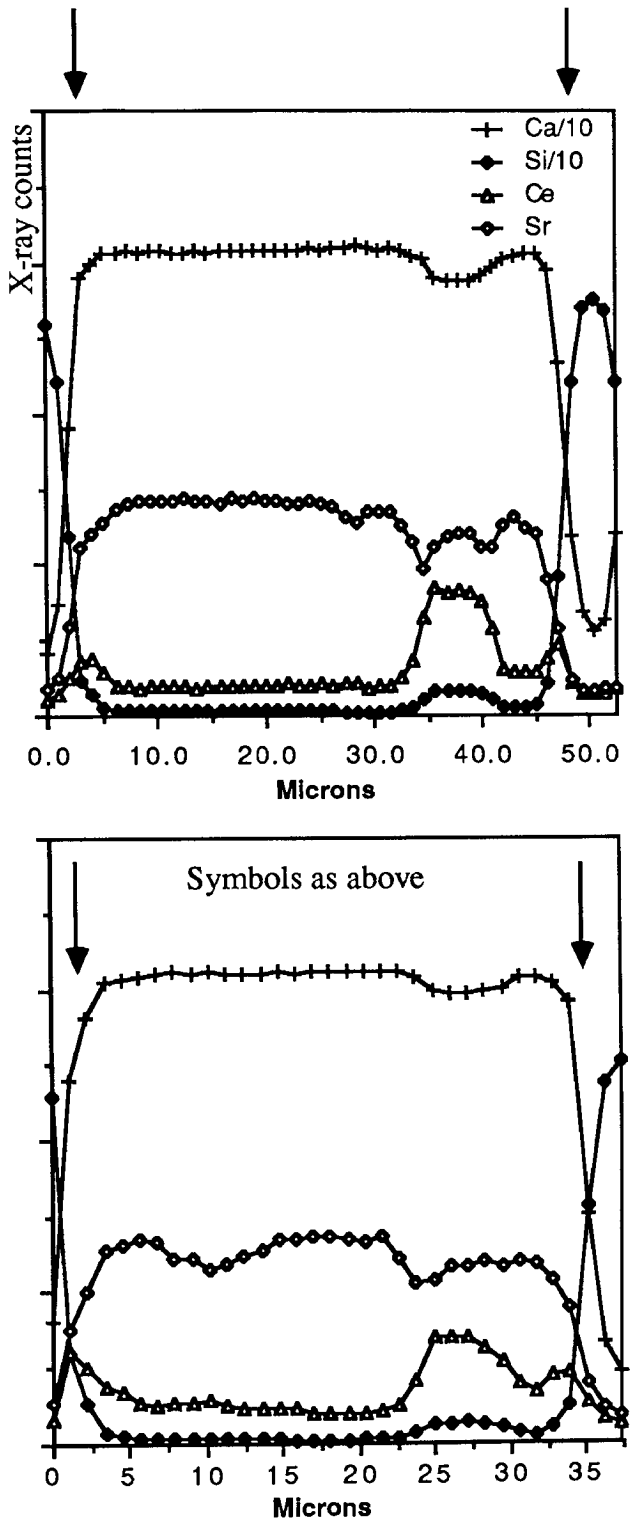

Figure 6.4 Selected step scan electron microprobe traverses across zoned apatite crystals from the quartzite raft enclosed in unit SN1B of the North Qoroq centre. Arrowed lines indicate crystal boundaries.

6.3.4 Halogen Chemistry

A large body of literature has been published on the use of F/Cl ratios in OH-bearing minerals in determining fHF and fHCl in igneous and metamorphic systems. Candela (1986) produced a thermodynamic model for the partitioning of F and Cl between apatite and a silicate melt and showed that F:Cl:OH ratios remained approximately constant until the system became vapour-saturated at which stage Cl partitions into the vapour phase, hence reducing the Cl/F ratio in the apatite. This change in chemistry could be used as an indicator of vapour evolution in felsic igneous systems. In North Qoroq the presence of sodalite in the most evolved syenites affects the partitioning of Cl and so this model may not be appropriate and it may be that a separate Cl-rich vapour phase does not separate from the North Qoroq syenites. Other studies have concentrated on the vapour phase. Stormer and Carmichael (1971), in attempting to define an apatite-biotite geothermometer, found that biotite is very susceptible to late exchange in the hydroxyl site with low temperature aqueous fluids. Apatite appeared more resistant to this process, a finding that received some support from Roegge *et al.* (1974).

Korzhinskiy (1981) provided expressions for the temperature and pressure dependence of F:Cl:OH ratios in apatites and equations for the calculation of fHF, fHCl and fH_2O in aqueous fluids. It was shown that at a constant pressure and fHF/fHCl in the fluid an increase in temperature increased the X_{Cl} in the apatite. Ekstrom (1972) and Latil and Maury (1977) also found that an increase in temperature favoured the incorporation of Cl into the apatite and also that an increase in pH favoured the hydroxyapatite phase. Yardley (1985) and Sisson (1987) use the equations derived by Korzhinskiy (1981) and the water fugacities of Burnham *et al.* (1969) in the calculation of fHF and fHCl in metamorphic fluids. There are three important assumptions inherent in this method. Firstly, that there is complete solid solution between hydroxy-, fluor- and chlorapatite, secondly that F+Cl+OH=1 in the structural formula and thirdly that the apatite attained equilibrium with the fluid. Most authors agree on the first point, though Hogarth (1988) suggests the existence of a miscibility gap between fluor- and chlorapatite. The latter two assumptions are open to considerable doubt and can be considered in relation to the

North Qoroq apatites.

In the majority of apatites F+Cl+OH will equal 1, though Hounslow and Chao (1970) report site deficiencies of up to 0.18 of the structural formula. Errors are introduced in analysis by electron microprobe. Both F and Cl are difficult elements to obtain reliable analyses for as both are subject to volatilisation problems. One of the elements will usually be present in only minor amounts but by increasing count times to improve precision the problem of beam damage is aggravated. These problems are important in the apatites in North Qoroq, nearly all of which are pure fluorapatite. The fluorine content varies from ~3 to ~5wt% with most analyses close to 4wt%. The chlorine content is low and often below detection limits except in one sample of basement gneiss which, on petrographic grounds, is relatively little altered. Here the chlorine content reaches a maximum of 0.39wt% although it is inevitable that these Cl values are open to considerable errors (Figure 6.5). Another major analytical problem with the North Qoroq apatites is the presence of large quantities of REE. The ZAF correction procedures will overestimate the amounts of light elements if there are significant quantities of heavy elements present. Therefore, fluorine is likely to be overestimated in the REE-rich North Qoroq apatites. This becomes clear when the end-members are calculated in the F-Cl-OH ternary, assuming OH by difference. Fluorine is always close to 1 and sometimes slightly greater, and so OH values become negative. It is clear that the apatites can only have limited use in the calculation of fHF, fHCl and fH_2O from the F:Cl:OH ratios in these essentially pure fluorapatites. Analyses of apatites from other Gardar intrusives show them to be pure fluorapatites containing negligible Cl (P. Hill, Edinburgh University, pers. comm.) and so they are also subject to the same problems.

The third assumption, that the apatite attained equilibrium with the late-stage hydrous fluids, is also open to question. Both Stormer and Carmichael (1971) and Ekstrom (1972) found fluorapatite to be very stable while biotite was easily hydrated.

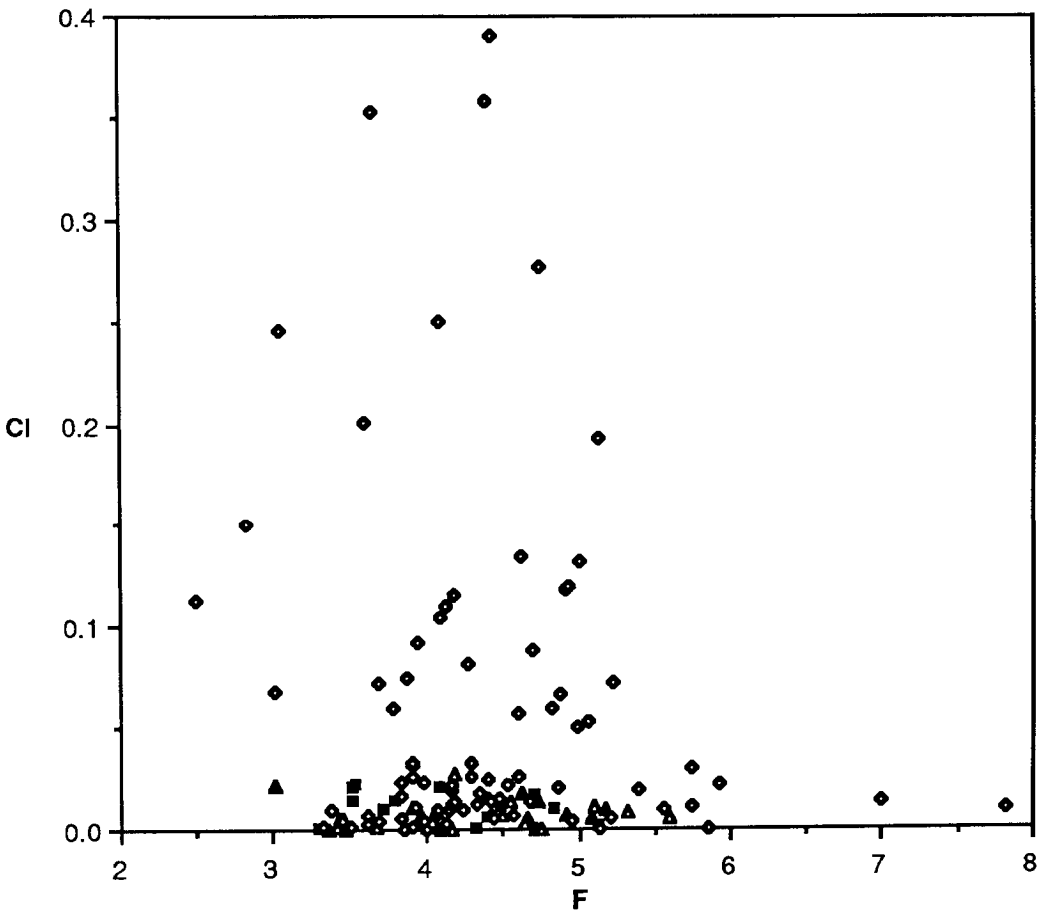

Figure 6.5 Fluorine and chlorine contents of North Qoroq apatites. Note that Cl is below detection limits in all apatites from the quartzite raft. Symbols are the same as those in Figure 6.1. Axes are in element wt%.

Ekstrom heated ground fluorapatite at 600°C for one week in the presence of $CaCl_2$ and found no exchange in the apatite. Roegge *et al.* (1974) also implied that apatite was more stable and Nash (1976) showed that while biotite was hydrated by meteoric circulation in the Skaergaard Intrusion, fluorapatite remained unaffected. In contrast, Gunow *et al.* (1980) in a study of the Henderson molybdenite deposit, Colorado implied that apatite composition was reset by later fluids while biotite reflected original fluid composition. Korzhinskiy (1981), in preparing pure hydroxyapatite for experimental purposes, exchanged natural fluorapatite with excess $Ca(OH)_2$ under hydrothermal conditions at 700°C and 2kb. While fluorapatite will hydrate under hydrothermal conditions it will not undergo any exchange to chlorapatite. To obtain $X_{Cl}/X_F=1$ in apatite at 600°C and 1kb the fHCl must be 170 times greater than fHF in the fluid (Korzhinskiy 1981).

The most important factors in the stability of apatite to fluid alteration are the original composition of the apatite and the nature of the exchange being attempted. A chlorapatite will readily exchange and reach equilibrium with a fluorine rich solution whereas a fluorapatite will not react with a chlorine rich solution. The fact that only the least altered sample of basement gneiss contains apatites with significant Cl contents suggests that the apatites in the gneiss were originally more chlorine rich. They have then exchanged, in most cases completely, with fluorine in the fenitising solution, though, as Korzhinskiy points out this in itself does not prove that there is a predominance of fluorine over chlorine in the fluid. Despite the problems outlined above (analytical uncertainties, low Cl contents and the possibility that the apatite did not reach equilibrium with the fenitising fluid) the fugacities of fluorine and chlorine in the fluids have been calculated for the apatite in the basement gneiss with the highest Cl content (Table 6.2), using the equations derived by Korzhinskiy (1981) and the water fugacities of Burnham *et al.* (1969). While the figures should be treated with caution, they provide an approximate upper limit for the fHCl and a lower limit for the fHF in the fenitising fluids in the granite gneiss. It is interesting to note that the fHCl is an order of magnitude greater than the fHF, though this may not apply in the syenites in which it is not possible

to calculate the fugacities.

Table 6.2 Calculation of fHCl and fHF

Pbars = 1000	Pbars = 1000
T^{oC} = 600	T^{oC} = 600
fH_2O = 631bars	fH_2O = 631bars
$\log K_e^{Cl/OH}$ = -3.5905	$\log K_e^{F/OH}$ = -5.8295
$X_{Cl\text{-}Ap}/X_{OH\text{-}Ap}$ = 2.1087	$X_{F\text{-}Ap}/X_{OH\text{-}Ap}$ = 40.3696
$K_e^{Cl/OH}$ = 2.5674 x 10-4	$K_e^{F/OH}$ = 1.4808 x 10-6
fHCl = 0.3416	fHF = 3.77 x 10-2

6.4 Whole Rock Rare Earth Elements

6.4.1 Introduction

An alternative approach to gaining information on the anion contents of the fluids is the more circumstantial evidence provided by the REE contents of the metasomatised rocks. The extreme REE enrichments in the apatites show that the metasomatic fluids carried significant quantities of the REE. These elements are transported in solution in the form of structurally intricate complexes (Kosterin 1959, Ganeyev 1962) and it is the nature of the complexes that gives a clue to the pH and anion content of the fluid. The REE are differentiated into the light rare earths and the heavy rare earths by the relative acidity of the mineralising solutions (Mineyev 1963, Mineyev *et al.* 1966), the light rare earths being more concentrated by more basic, higher pH solutions. It has also been shown, both empirically (McLenan and Taylor 1979, Kerrich and Fryer 1979, Taylor and Fryer 1980) and experimentally (Flynn and Burnham 1978), that the light REE are concentrated by Cl-bearing fluids whereas the heavy REE are concentrated by F and CO_3^{2-}-bearing fluids.

Apatites preferentially partition the light to middle REE over the heavy REE (Watson and Green 1981, Nagasawa 1970) and so may not be representative of the whole rock REE pattern if other REE-bearing phases are present. In order to complement the data on the apatites and to examine relative REE enrichments in the metasomatic rocks whole rock REE analyses have been carried out. The analyses were carried out by

inductively coupled plasma spectrometry (ICP) and the experimental methods are described in Appendix 3.

6.4.2 REE Concentrations

The samples from the quartzite raft show extreme enrichment with cerium, the most abundant REE, reaching 1013ppm and the total REE constituting 0.22wt% as oxide of the rock. The basement gneiss is not as enriched but cerium still reaches 251ppm and total REE 0.054wt%. The syenites in the contact zone between units SN1A and SN1B are also enriched in REE with cerium up to 427ppm and total REE 0.094wt% of the rock. Two different approaches were taken to examining the REE patterns in these rocks. Firstly, the patterns are represented normalised to the chondrite values of Nakamura (1974) and secondly normalised to representative unaltered samples (Figure 6.6).

The chondrite normalised patterns of the Julianehab Granite (Figure 6.6a,b) all show a break in slope at europium and the unaltered samples have a small negative Eu anomaly. The metasomatised samples show variable anomalies with some having little or no Eu anomaly and others a negative anomaly. The patterns indicate a slight relative increase in the light REE over the heavy REE in the most enriched samples with La 10^2 to 10^3 times chondrite. The patterns normalised to the unaltered samples show more clearly the relative enrichments of each REE over the original rock. In the most enriched sample there is a negative slope indicating enrichment in the light REE but the other patterns are flatter and appear to be slightly concave downwards, reaching a maximum relative increase at samarium. The Eu anomalies vary from positive to non-existent to negative. The light REE, La, Ce and Nd were analysed for by XRF and the results compare favourably with the ICP analyses. When these results from the Julianehab Granite are plotted against distance from the syenite contact no pattern emerges indicating that the metasomatism, at least with respect to the rare earth elements, is a very irregular process.

The chondrite normalised patterns of the unaltered quartzite (Figure 6.6c,d)

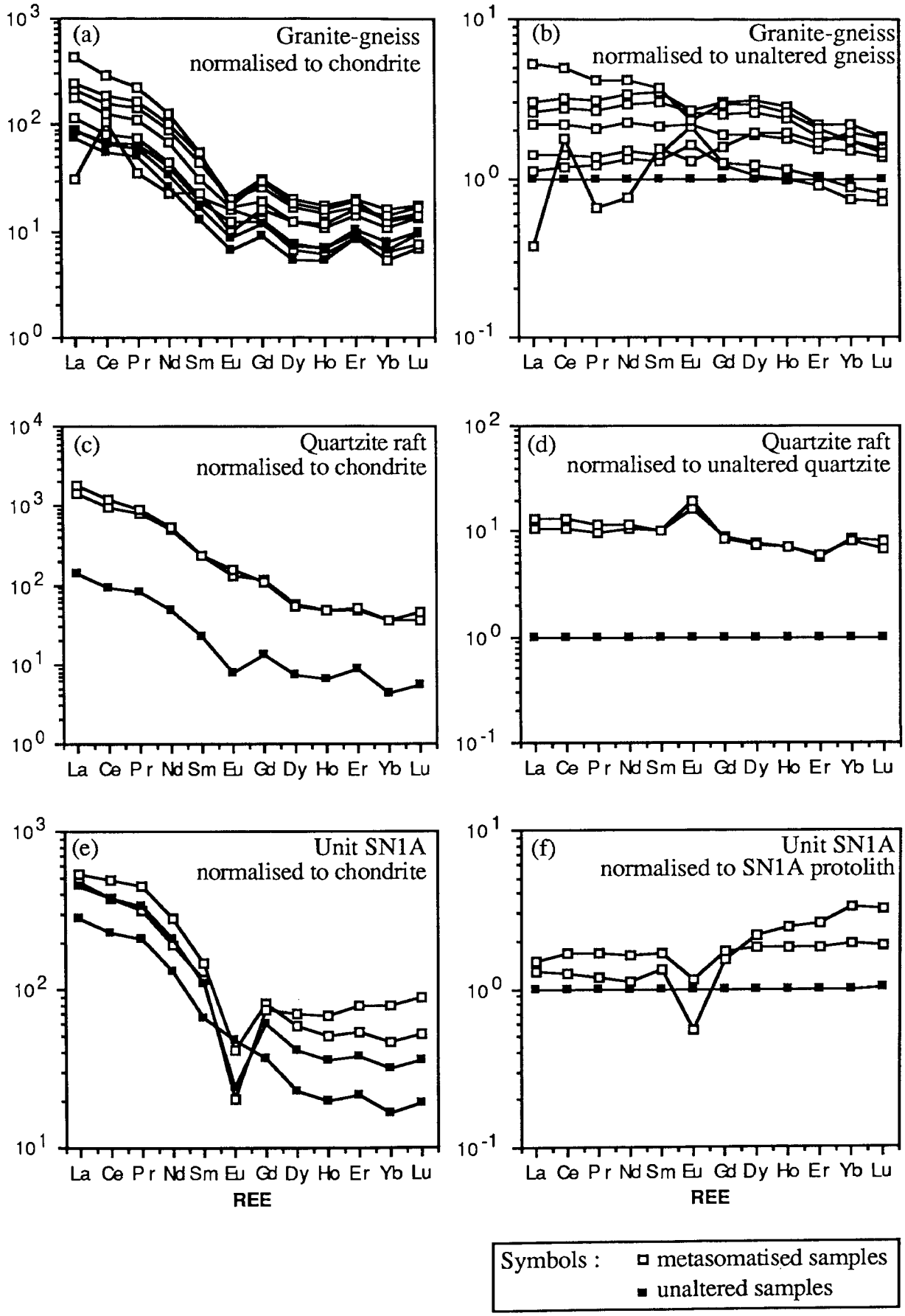

Figure 6.6 Whole-rock rare earth element patterns in the North Qoroq centre. SN1A protolith represents the average REE contents of the two samples chosen in Chapter 3 as suitable parent material for the unit.

are very similar both in abundance and shape to those of the unaltered basement gneiss. The effect of the metasomatism is to enrich light and heavy REE by similar amounts and to smooth the pattern with the negative Eu anomaly disappearing. Both La and Ce are $>10^3$ times chondrite values. The fairly uniform increase from La to Lu is reflected in the patterns normalised to unaltered quartzite, though the smoothing of the Eu anomaly is now seen as a distinct positive anomaly.

The patterns for the syenites show significant differences from those of the country rocks (Figure 6.6e,f). The chondrite normalised patterns show a break in slope at Eu and distinct negative Eu anomalies. The metasomatised rocks, while showing relatively little increase in the light REE relative to the unaltered samples, are distinctly enriched in the heavy REE with Lu $\sim10^2$ times chondrite. The light REE are $\sim10^2$-10^3 times chondrite. The patterns normalised to unaltered syenite emphasise these features with positive slopes indicating relative increases in the heavy REE.

6.4.3 Discussion of REE Patterns

The major discussion of REE variation in relation to apatite chemistry and fluid evolution will be given in section 6.6 but some comments specific to the whole rock REE can be made at this point.

The REE patterns of the basement gneiss, normalised to unaltered samples, reflect the complete control of apatite on the whole rock variations. The concave downwards rare earth partition coefficient patterns of apatite (Watson and Green 1981, Nagasawa 1970) are closely mirrored by the whole rock patterns in the gneiss. The variations in Eu anomalies, from positive to negative, are probably the result of a combination of several factors ; the degree of feldspar alteration, the amount of apatite formed and the oxidation state of europium. Watson and Green (1981) demonstrated a large negative Eu^{2+} anomaly in apatite which in the gneiss would produce a whole rock anomaly unless it was counterbalanced by the fixation of Eu^{2+} in feldspar. Alternatively, the europium could be in the trivalent state in which case there would be no anomaly in

the apatite or the whole-rock.

The REE variations of the quartzite are also likely to be dominated by apatite but the flatter nature of the patterns normalised to the unaltered quartzite indicates the influence of other REE-bearing phases, increasing the light and heavy REE as well. The presence of monazite and synchysite in the rock, associated with the apatite, testifies to this. The Eu anomaly in the quartzite is removed during the metasomatism implying that europium is incorporated into the apatite as readily as the other REE. Given the results of Watson and Green (1981) this suggests that europium is in the trivalent state, indicating an oxidising environment. Cullers and Medaris (1977) and Eby (1975) both note the same effect in fenites associated with carbonatites and they attribute this to the preferential addition of Eu relative to the other REE. The C.L. of the apatites might also give a clue to the oxidation state of europium. Eu^{2+} induces blue luminescence in apatites but Eu^{3+} produces luminescence at longer wavelengths (Mariano and Ring 1975). It is possible that the violet to brown C.L. colours of the apatites indicates that the Eu is in the oxidised state.

The heavy REE enrichment in the syenites indicates the predominance of fluorine in the fluid (eg. Flynn and Burnham 1978) and the strong influence of phases other than apatite on the patterns. The abundance of fluorite along the contact zone between units SN1A and SN1B and the presence of minerals from the rinkite-mosandrite series supports these conclusions.

In general, the REE patterns demonstrate the strong increase in the REE during the metasomatic activity and emphasise the presence of halide and carbonate complexes in the fluid. Differences in the REE patterns indicate variations in the types of complexes present and so suggest variations in the fluids as the metasomatism progresses, a proposal that will be discussed later (section 6.6).

6.5 Fluid Inclusion Study

6.5.1 Introduction

Previous studies on fluid inclusions in the Gardar province have concentrated on the igneous rocks of the Ilimaussaq intrusion (Petersilie and Sorensen 1970, Sobolev *et al.* 1970, Konnerup-Madsen *et al.* 1981 and Konnerup-Madsen and Rose-Hansen 1982), though Konnerup-Madsen (1984) extended this to seven of the Si-oversaturated complexes in the province. The aim of the present section is to examine the temperature and, where possible, the salinities of the metasomatic fluids associated with the North Qoroq nepheline syenites. Only a limited number of inclusion rich samples were selected. The following three areas were studied : 1) samples of fluorite, taken from veins and a plug associated with unit SN5 of the syenite centre, 2) inclusions in quartz in the quartzite raft 'soaked' in unit SN1B and 3) inclusions in quartz in samples of basement gneiss taken from the area west of the long lake. 2) and 3) are the same set of samples that were used in the study of apatite and biotite chemistry and whole rock REE.

6.5.2 Inclusion Type and Occurence

Konnerup-Madsen (1984) found three main types of inclusion within quartz from the other Gardar centres : 1) aqueous inclusions, 2) CO_2-CH_4 inclusions and 3) aqueous-CO_2-CH_4 inclusions. In contrast, only aqueous inclusions were found in the samples studied from North Qoroq. These have a clear appearance and are usually in the form of 2-phase liquid-vapour inclusions. Some inclusions were 1-phase liquid at room temperature but unlike the CO_2-CH_4 inclusions of Konnerup-Madsen (1984), which nucleated a vapour bubble on cooling, no trace of CO_2 was identified. These inclusions simply represent low temperature aqueous solutions. No daughter minerals were found in any inclusions, though a few contained trapped phases. The inclusions from the fluorite are generally larger than those from the quartz and show a variety of forms from very irregular to rounded or negative crystal shapes (Plate 6.4). The inclusions in quartz

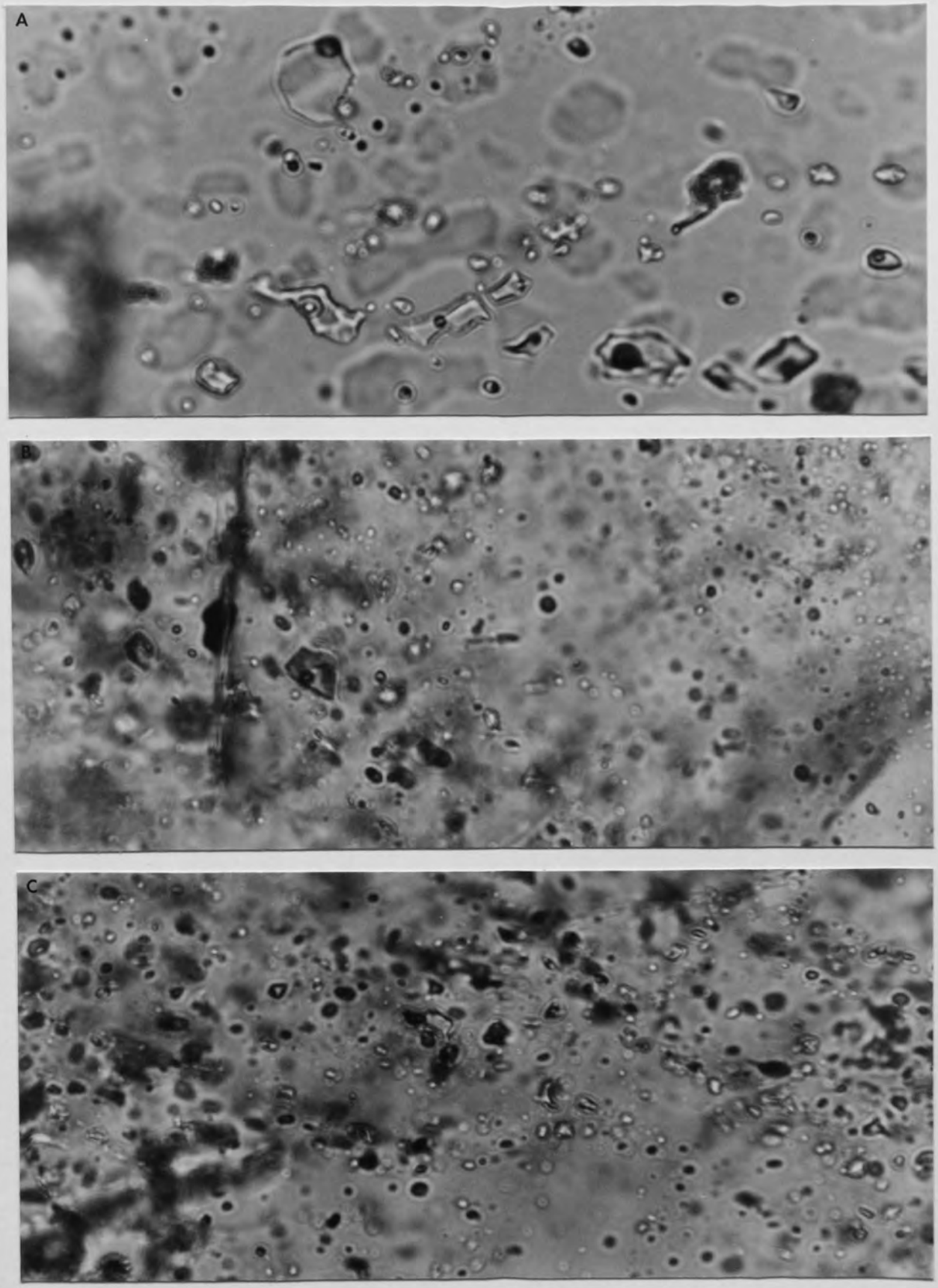

Plate 6.4 The type and occurence of analysed fluid inclusions from North Qoroq.
(a) inclusions in fluorite
(b) inclusions in the granite-gneiss
(c) inclusions in the quartzite
Width of field of view = 0.23mm

from both the quartzite and the gneiss are small and irregular or rounded in shape (Plate 6.4). The majority of inclusions from all three areas are liquid-rich. The origin of the inclusions and the different generations present are difficult to determine as both the fluorite and the quartz appear to have repeatedly fractured. There are numerous planes of inclusions extending to the crystal edges and also abundant inclusions isolated with no obvious relation to fractures.

6.5.3 Results of Microthermometry

The microthermometry was carried out on unmounted, doubly polished slices of about 200μm thickness. A Linkam 600 heating-freezing stage was used and the inclusions were studied from -100°C up to +500°C. The microthermometry results are presented in Figure 6.7. No systematic variation could be found between the isolated and planar occuring inclusions and so no distinction is made between them on the figures.

Salinities of the inclusions are deduced from the temperature of final melting of ice (Roedder 1984, Shepherd *et al.* 1985) formed during freezing of the inclusions. The measured freezing temperatures are interpreted in terms of the binary NaCl-H_2O system. There is little or no range in salinities in the inclusions in the fluorite which all have freezing temperatures in the range -3°C to +1°C with most very close to 0°C. They therefore have very low salinities with equivalent NaCl ranging from zero to a maximum of 4.922wt% (Potter *et al.* 1978). The inclusions in the quartzite raft display a greater range in freezing temperatures, from -8°C to 0°C. The majority have a final melting temperature in the range -5°C to -7°C, indicating that the fluids in the quartzite were of a generally higher salinity than those from the fluorite with equivalent NaCl~10wt%. No freezing experiments could be attempted on the basement gneiss due to the small size and irregular shape of the inclusions.

A relatively large spread in homogenisation temperatures (Th) is observed but no correlation can be made with the occurence of the inclusion. The Th for

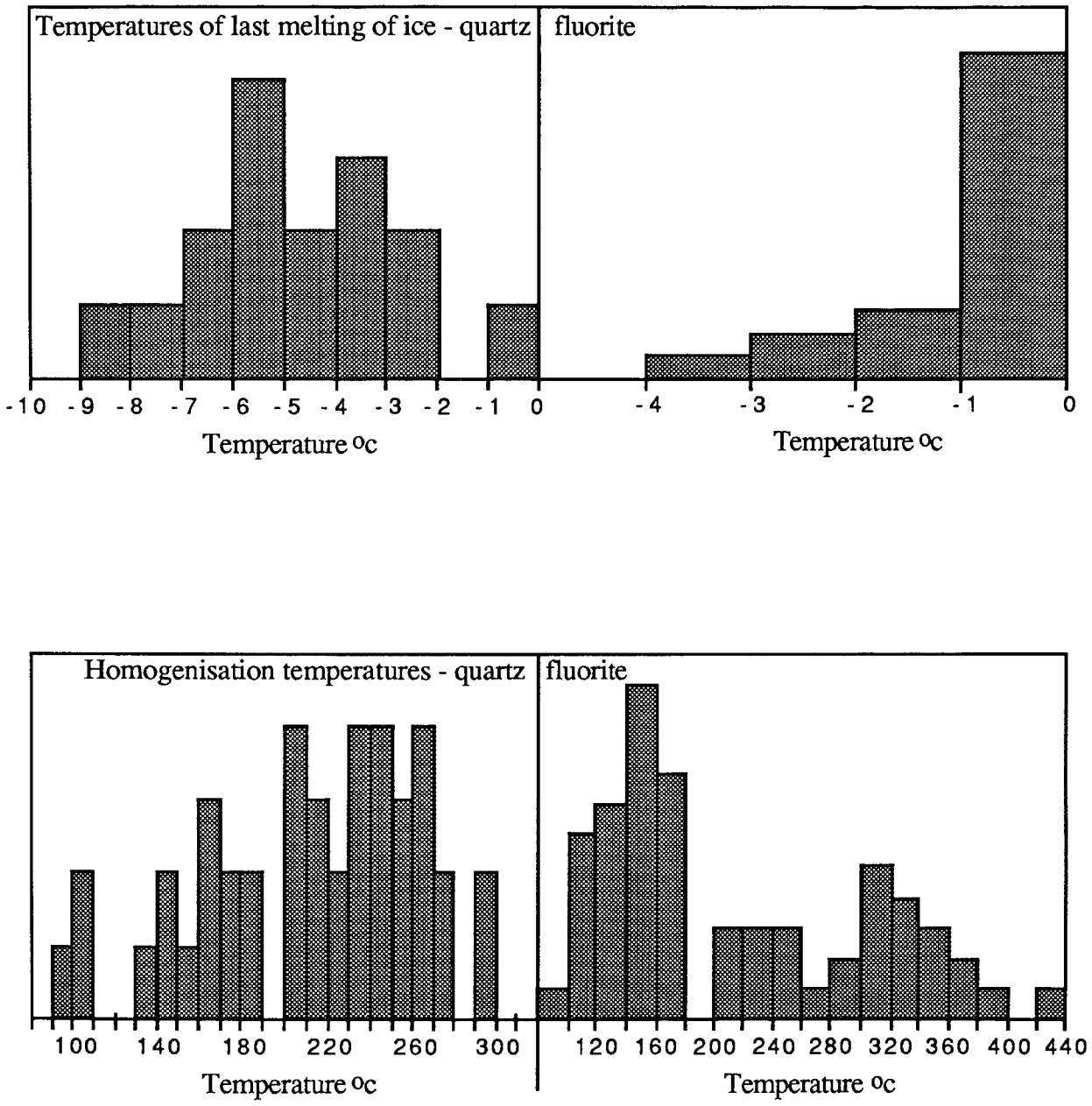

Figure 6.7 Freezing (last melting of ice) and homogenisation temperatures in fluid inclusions from North Qoroq.

'Quartz' represents inclusions occuring in quartz grains in the granite-gneiss and the quartzite raft.

'Fluorite' represents inclusions occuring in fluorite veins and plugs from within unit SN5 of the syenite centre.

NB 'Quartz' freezing temperatures are from the quartzite raft only

inclusions in the fluorite shows a distinctly bimodal distribution with concentrations of inclusions between 100°C-200°C, centred around 150°C, and also between 300°C-400°C, centred around 330°C. The inclusions in both the quartzite and the gneiss have a similar distribution of Th to each other and show a concentration of inclusions in the region of 250°C with values tailing down to 100°C. The strong similarity between the inclusions of the quartzite and the gneiss in Th, type and occurence suggests that the inclusions in the gneiss may also have similar salinities to those in the quartzite.

6.5.4 Interpretation of Fluid Inclusion Data

The abundance of planes of inclusions demonstrates how the rocks were thoroughly permeated by aqueous fluids. Although planes of inclusions are normally assumed to be later than isolated ones (Roedder 1984, Shepherd *et al.* 1985) this may not be true in the metasomatised rocks in North Qoroq. No correlation could be found between type of occurence (isolated or planar) and homogenisation temperature or salinity and the nature of the metasomatic process would have led to a repeated fracturing and veining of the rock. The bimodal distribution of the homogenisation temperatures implies that two fluids have affected the rocks, a lower temperature one (~150°C) and a higher temperature one (~300°C). The low temperature, low salinity fluid inclusions may be inclusions of heated circulating meteoric water, permeating through the rocks, whereas the higher temperature inclusions may represent the magmatic fluid evolved from the syenites. It is likely that both fluids were active at the same time and probably interacted. Homogenisation temperatures in the 300°C range are comparable with those found for similar inclusions in other Gardar centres (Konnerup-Madsen 1984) and also with the apatite-rich rocks in the Lovozero and Khibiny massifs of USSR (Kogarko and Romanchev 1977, Valyashko *et al.* 1968).

The major difference between the inclusions sampled in North Qoroq and those elsewhere in the Gardar is the complete lack of CO_2- and CH_4-rich inclusions, which are characteristic of the alkaline Gardar rocks (Konnerup-Madsen *et al.* 1981) and

alkaline igneous rocks in general (Konnerup-Madsen and Rose-Hansen 1982). The fact that only low salinity aqueous inclusions were found in North Qoroq is partly a result of the limited number of samples studied, possibly leading to an unrepresentative sampling of the inclusion population. The fluorite, occuring as late veins and plugs, is the latest activity in the syenite centre and so the contained inclusions probably do not represent the first fluids from the syenites. The higher salinity of the inclusions in the quartzite indicate that there are variations in fluid composition.

The metasomatic effects seen in and around the North Qoroq centre are in places very intense and would be hard to explain if the only fluids present had the very low salinities observed. The limited study carried out could easily have missed the presence of higher temperature, high salinity fluids and there is a need for a more detailed study, outside the scope of this thesis, looking at inclusions in nepheline and apatite as well as fluorite and quartz in a far greater variety of samples.

6.6 General Discussion

One of the most interesting features of the metasomatic quartzite and gneiss is the zonation in the apatites. REE zonation was noted in apatites from carbonatites and associated fenites near Gatineau, Quebec (Hogarth et al. 1985) and from regional skarns in the same area (Hogarth 1988). This zonation took the form of a simple Ce-rich rim, in contrast to the more complex patterns developed at North Qoroq. An important feature of the North Qoroq apatites is the Sr contents. The apatites from the basement gneiss and the syenites do not contain any Sr whereas those from the quartzite contain ~1 to ~3wt% SrO. This is important in determining the origin of the apatites and their zonation. Similar features were noted by Larsen *et al.* (1952) who found 11.6wt% SrO in apatites from veins in a syenite dyke in Montana, but no appreciable Sr in apatite separated from the syenite itself.

The zoning in the apatites from the quartzite could be explained in three ways : 1) the REE-poor core is detrital, weathered from the basement during the initial deposition of the sediment, and has been overgrown metasomatically by fluids that

became increasingly depleted in REE, 2) the whole crystal was formed in a single metasomatic process, governed by variations in the fluid and 3) the cores are formed during early circulation of meteoric waters and are then overgrown by later magmatic REE-rich fluids. The first solution is the simplest but the petrographic association of the apatite rules it out as the exclusive association of the apatite with alkali mafic minerals and the apatite rims on the mafic pods are incompatible with a detrital origin (see Plate 2.10). Also the difference in Sr contents between the apatites of the basement gneiss and those in the quartzite rule out the detrital origin. The second option is possible but if this is the case it has to be explained how a REE-poor core could develop from the metasomatic fluids before the influx of REE to the rock. It is most likely that the cores were formed from a dilute aqueous fluid, possibly meteoric, and the REE-rich zones reflect the influx of metasomatic fluids derived from unit SN1B. The homogeneity of the zones and the sharp boundaries between them indicates that there was either a time gap in the crystal growth and/or the zones were formed under the influence of very different fluid compositions. It is possible that the early alteration was due to fluids derived from SN1A which were relatively dilute due to the greater distance from their source. These fluids could have been responsible for some albitisation and the growth of the apatite cores while fluids derived from SN1B led to the development of the REE-rich rims. Whatever the source of the fluid that produced the apatite cores, it is clear that it contrasted strongly in composition with the later REE-rich fluid and so confirms the presence and interaction of more than one fluid in and around the North Qoroq centre.

The fluid inclusion results show that more than one fluid interacted with the rocks and also that there were salinity variations in the fluids. The contrasting whole rock REE patterns also point to fluid variations, possibly in the relative proportions of Cl and F complexing. The halogen chemistry of the apatites in the basement gneiss indicates an introduction of F into the hydroxyl site. Within the syenite centre there is abundant late fluorite and the metasomatised samples of unit SN1A contain significant sodalite (Rae and Chambers 1988), indicating the presence of both F and Cl in late-stage fluids. Humphris (1985) points out that similar rocks along the path of the fluid can be

exposed to fluids of very different composition as they are open systems with a continuous flow-through of a fluid phase during the alteration process.

There is abundant experimental and geological evidence concerning the transport and concentration of the REE in hydrothermal systems. Mineyev (1963) shows that the REE must be transported in the form of complexes because ionic compounds of the REE have very similar chemical properties and so transport in this form would not lead to the fractionation observed in nature. Kosterin (1959) and Ganeyev (1962) noted that high concentrations of the REE are associated with high concentrations of alkalis and volatiles and with complexing elements such as Al, Fe and Zr, indicating their simultaneous presence in solution. Alderton *et al.* (1980) showed that the presence of fluoride significantly increases the mobility of the REE while Balashov and Krigman (1975) showed that the stability constants of REE-chloride complexes are several orders of magnitude lower than those of fluorides, phosphates and carbonates of the alkalis. Kosterin (1959) favoured the transport of the REE by fluor-carbonate complexes in Na-rich and oxidising fluids. The close association of the apatite with calcite, fluorite, synchysite and alkaline minerals such as aegerine supports this theory and it is proposed that the bulk of the REE in North Qoroq were transported in such complexes. Taylor *et al.* (1981) favour a similar scheme for REE enrichment in the peralkaline granites of the Topsails complex, Newfoundland.

Burnham (1967) showed that chloride will partition into the vapour phase and fluoride into the melt in the late-stage crystallisation of a felsic magma and Flynn and Burnham (1978) demonstrated that the REE will partition into the melt rather than the vapour phase. The melt/vapour experiments of Wentlandt and Harrison (1979) also showed that REE do not partition favourably into aqueous vapour phases at low pressures. This implies that the REE will be concentrated into the final magmatic residuum with fluorine while a chloride-rich vapour phase could be present at an earlier stage due to the interaction of circulating meteoric waters and the cooling pluton.

A model of this nature could explain the metasomatic effects seen in the quartzite, including the apatite zonation. If the first fluids that affected the quartzite raft

were relatively chloride-rich and acidic, transporting only easily soluble cations such as Na and K, this could lead to the albitisation seen in the quartzite and in the contact zones with the basement gneiss. In an experimental study of the metasomatic replacement of calcite by apatite it was shown that apatite was stable in neutral and alkaline (high pH) media and unstable in acid medium regardless of temperature and pressure (Syromyatnikov 1968). Albitisation indicates acidic solutions (Mineyev 1963) and so this could explain the absence of apatite in the albitised areas. When the magmatic fluids evolved from the syenites they were considerably more alkaline and rich in fluor-carbonate complexes of the REE, Mg, Fe and Ca. The apatite developed REE-rich rims and the veins filled with the alkali mafic minerals and calcite and fluorite. Synchysite also probably precipitated at this stage.The outer rims on the apatites represent the last stages of the alteration and reflect the dilution of the magmatic fluids either simply by reaction with the quartzite and/or interaction with meteoric waters continuing to circulate in the intrusion.

6.7 Conclusions

1. Homogenisation temperatures indicate that there was more than one fluid phase active in and around the North Qoroq centre. There was probably an interaction between circulating meteoric waters and later magmatic fluids and meteoric circulation could have continued after the magmatic effects had stopped. There are variations in fluid salinity between the quartzite and late fluorite in the syenite indicating changes in fluid composition.

2. There was considerable transport of REE in the North Qoroq centre. This is most likely to have occured in the form of fluoride and carbonate complexes. Both F and Cl are present in significant quantities during the metasomatism, as evidenced by the presence of sodalite and fluorite.

3. The metasomatic effects seen in the quartzite are best explained in terms of the interaction of at least two different fluids. Initial alteration was under the influence of a low pH, Cl-rich fluid, possibly derived from the circulation of meteoric waters through

the cooling syenite. This gave way to a more alkaline, F-rich, oxidising hydromagmatic phase rich in the REE which was concentrated in the final residuum of the syenite magma.

4. The lack of intricate REE zonations in the apatites of the granite gneiss and the less REE-rich compositions developed, in comparison to the quartzite apatites, indicates that the fenitising fluids in the granite gneiss were more dilute and were less able to transport large complexes.

References

Alderton, D.H.M., Pearce, J.A. & Potts, P.J. 1980. Rare earth element mobility during granite alteration ; evidence from southwest England. EARTH PLANET SCI LETT **49**, 149-65.

Balashov, Y.A. & Krigman, L.D. 1975. The effects of alkalinity and volatiles on rare-earth separation in magmatic systems. GEOKHIMIYA **12**, 1885-890.

Burnham, C.W. 1967. Hydrothermal fluids at the magmatic stage. *In* Barnes, H.L. (ed) *Geochemistry of hydrothermal ore deposits*, 34-76. Holt, Rinehart & Winston.

Burnham, C.W., Holloway, J.R. & Davis, N.F. 1969. Thermodynamic properties of water to 1000^{oC} and 10000bars. GEOL SOC AM SPEC PAP **132**, 96.

Candela, P.A. 1986. Toward a thermodynamic model for the halogens in magmatic systems: an application to melt-vapor-apatite equilibria. CHEM GEOL **57**, 289-301.

Cullers, R.L. & Medaris, G. 1977. Rare earth elements in carbonatite and cogenetic alkaline rocks: examples from Seabrook Lake and Callander Bay, Ontario. CONTRIB MINERAL PETROL **65**, 143-53.

Drake, M.J. & Weill, D.F. 1972. New rare earth element standards for electron microprobe analysis. CHEM GEOL **10**, 179.

Eby, G.M. 1975. Abundance and distribution of the rare-earth elements and yttrium in the rocks and minerals of the Oka carbonatite complex, Quebec. GEOCHIM COSMOCHIM ACTA **39**, 597-620.

Ekstrom, T.K. 1973. Synthetic and natural chlorine-bearing apatite. CONTRIB MINERAL PETROL **38**, 329-38.

Flynn, R.T. & Burnham, C.W. 1978. An experimental determination of rare earth partition coefficients between a chloride containing vapour phase and silicate melts. GEOCHIM COSMOCHIM ACTA **42**, 685-701.

Ganeyev, I.G. 1962. On the possible transport of matter in the form of complicated complex compounds. GEOCHEMISTRY **10**, 1042-1049.

Green, T.H. & Watson, E.B. 1982. Crystallisation of apatite in natural magmas under high pressure, hydrous conditions, with particular reference to 'orogenic' rock series. CONTRIB MINERAL PETROL **79**, 96-105.

Gunow, A.J., Ludington, S. & Munoz, J.L. 1980. Fluorine in micas from the Henderson molybdenite deposit, Colorado. ECON GEOL **75**, 1127-137.

Henderson, P. 1980. Rare earth element partition between sphene, apatite and other coexisting minerals of the Kangerdlugssuaq, E. Greenland. CONTRIB MINERAL PETROL **72**, 81-85.

Hogarth, D.D. 1988. Chemical composition of fluorapatite and associated minerals from skarn near Gatineau, Quebec. MINERAL MAG **52**, 347-58.

Hogarth, D.D., Hartree, R., Loop, J. & Solberg, T.N. 1985. Rare-earth element minerals in four carbonatites near Gatineau, Quebec. AM MINERAL **70**, 1135-142.

Hounslow, A.W. & Chao, G.Y. 1970. Monoclinic chlorapatite from Ontario. CAN MINERAL **10**, 252-59.

Humphris, S.E. 1984. The mobility of the rare earth elements in the crust. *In* Henderson, P. (ed) *Rare earth element geochemistry*, 317-42. Elsevier.

Kerrich, R. & Fryer, B.J. 1979. Archean precious-metal hydrothermal systems, Dome mine. Abitibi greenstone belt II. REE and oxygen isotope relations. CAN J EARTH SCI **16**, 440-58.

Kogarko, L.N. & Romanchev, B.P. 1977. Temperature, pressure, redox conditions, and mineral equilibria in agpaitic nepheline syenites and apatite-nepheline rocks. GEOCHEM INT , 113-128.

Konnerup-Madsen, J. 1984. Compositions of fluid inclusions in granites and quartz syenites from the Gardar continental rift province (South Greenland). BULL MINERAL **107**, 327-40.

Konnerup-Madsen, J., Rose-Hansen, J. & Larsen, E. 1981. Hydrocarbon gases associated with alkaline igneous activity : evidence from compositions of fluid inclusions. RAPP GRONLANDS GEOL UNDERS **103**, 99-108.

Konnerup-Madsen, J. & Rose-Hansen, J. 1982. Volatiles associated with alkaline igneous rift activity : fluid inclusions in the Ilimaussaq intrusion and the Gardar granitic complexes South Greenland. CHEM GEOL **37**, 79-93.

Korzhinskiy, M.A. 1981. Apatite solid solutions as indicators of the fugacity of HCl^o and HF^o in hydrothermal fluids. GEOCHEM INT , 44-60.

Kosterin, A.V. 1959. The possible modes of transport of the rare earths by hydrothermal solutions. GEOCHEMISTRY **4**, 381-87.

Larsen, E.S., Fletcher, M.H. & Cisney, E.A. 1952. Strontian apatite. AM MINERAL **37**, 656-58.

Latil, C. & Maury, R. 1977. Contribution a l'etude des echanges d'ions OH^-, Cl^-, F^- et leur fixation dans les apatites hydrothermales. BULL SOC FR MINERAL CRISTALL **100**, 246-50.

Mariano, A.N. & Ring, P.J. 1975. Europium-activated cathodoluminescence in minerals. GEOCHIM COSMOCHIM ACTA **39**, 649-60.

McConnell, D. 1973. *Apatite : its crystal chemistry, utilization, and geologic and biologic occurences.* New York : Springer-Verlag.

McLenan, S.M. & Taylor, S.R. 1980. Rare earth elements in sedimentary rocks, granites and uranium deposits of the Pine Creek geosyncline. Proc Intl Uranium Symp on the Pinecreek Geosyncline, 175-190. I A E A Vienna.

Mineyev, D.A. 1963. Geochemical differentiation of the rare earths. GEOCHEMISTRY **12**, 1129-149.

Mineyev, D.A., Dikov, Y.P., Sobolev, B.P. & Borutskaya, V.L. 1966. Differentiation of rare-earth elements under supercritical conditions. GEOCHEM INT **2**, 357-59.

Nagasawa, H. 1970. Rare earth concentrations in zircons and apatites and their host dacites and granites. EARTH PLANET SCI LETT **9**, 359-64.

Nakamura, N. 1974. Determination of REE, Ba, Fe, Mg, Na and K in carbonaceous and ordinary chondrites. GEOCHIM COSMOCHIM ACTA **38**, 757.

Nash, W.P. 1972. Apatite chemistry and phosphorous fugacity in a differentiated igneous intrusion. AM MINERAL **57**, 877-86.

Nash, W.P. 1976. Fluorine, chlorine and OH-bearing minerals in the Skaergaard intrusion. AM J SCI **276**, 546-57.

Petersilie, I.A. & Sorensen, H. 1970. Hydrocarbon gases and bituminous substances in rocks from the Ilimaussaq alkaline intrusion, South Greenland. LITHOS **3**, 59-76.

Potter, R.W., Clynne, M.A. & Brown, D.L. 1978. Freezing point depression of aqueous sodium chloride solutions. ECON GEOL **73**, 284-85.

Rae, D.A. & Chambers, A.D. 1988. Metasomatism in the North Qoroq centre, South Greenland : cathodoluminescence and mineral chemistry of alkali feldspars. TRANS R SOC EDINBURGH **79**, 1-12.

Roedder, E. 1984. Fluid inclusions. *Min Soc Am Reviews in Mineralogy* **12**.

Roegge, J.S., Logsdon, M.J., Young, H.S., Barr, H.B., Borcsik, M. & Holland, H.D. 1974. Halogens in apatites from the Providencia area, Mexico. ECON GEOL **69**, 229-40.

Shepherd, T., Rankin, A.H. & Alderton, D.H.M. 1985. *A practical guide to fluid inclusion studies.* New York : Chapman & Hall.

Sisson, V.B. 1987. Halogen chemistry as an indicator of metamorphic fluid interaction with the Ponder pluton, Coast Plutonic Complex, British Columbia, Canada. CONTRIB MINERAL PETROL **95**, 123-31.

Sobolev, V.S., Bazarova, T.Y., Shugurova, N.A., Dolgov, Y.U. & Sorensen, H. A preliminary examination of fluid inclusions in nepheline, sorensenite, tugtupite and chkavolite from the Ilimaussaq intrusion, South Greenland. BULL GRONLANDS GEOL UNDERS **81**, 32.

Sourirajan, S. & Kennedy, G.C. 1962. The system H_2O-NaCl at elevated temperatures and pressures. AM J SCI **260**, 115-41.

Stormer, J.C. & Carmichael, I.S.E. 1971. Fluorine-Hydroxyl exchange in apatite and biotite : a potential igneous geothermometer. CONTRIB MINERAL PETROL **31**, 121-31.

Syromyatnikov, F.V. & Vorobev, I.M. Experimental study of the metasomatic replacement of calcite by apatite under endogenic conditions. CHEM ABSTRACTS **71**, 62921a.

Taylor, R.P. & Fryer, B.J. 1980. Multiple-stage hydrothermal alteration in porphyry copper systems in northern Turkey : the temporal interplay of potassic, propylitic and phyllic fluids. CAN J EARTH SCI **17**, 901-26.

Taylor, R.P., Strong, D.F. & Fryer, B.J. 1981. Volatile control of contrasting trace element distributions in peralkaline granitic and volcanic rocks. CONTRIB MINERAL PETROL **77**, 267-71.

Valyashko, V.M., Kogarko, L.N., Lider, V.V. & Roshanskii, V.N. 1969. Inclusions in Khibiny apatites. CHEM ABSTRACTS **71**, 41138k.

Wass, S.Y., Henderson, P. & Elliott, C.J. 1980. Chemical heterogeneity and metasomatism in the upper mantle : evidence from rare earth and other elements in apatite-rich xenoliths in basaltic rocks from eastern Australia. PHIL TRANS R SOC LONDON **A297**, 333-46.

Watson, E.B. & Capobianco, C.J. 1981. Phosphorous and the rare earth elements in felsic magmas : an assessment of the role of apatite. GEOCHIM COSMOCHIM ACTA **45**, 2349-358.

Watson, E.B. & Green, T.H. 1981. Apatite/liquid partition coefficients for the rare earth elements and strontium. EARTH PLANET SCI LETT **56**, 405-21.

Wentlandt, R.F. & Harrison, W.J. 1979. Rare earth partitioning between immiscible carbonate and silicate liquids and CO_2 vapor : results and implications for the formation of light rare earth-enriched rocks. CONTRIB MINERAL PETROL **69**, 409-19.

Yardley, BW.D. 1985. Apatite composition and the fugacities of HF and HCl in metamorphic fluids. MINERAL MAG **49**, 77-79.

CHAPTER 7

Discussion and conclusions

7.1 Introduction

In the preceding chapters a number of conclusions have been reached regarding the characteristics of the metasomatic processes that have affected the North Qoroq syenites and the surrounding country rocks. Each chapter has examined separate lines of evidence and the conclusions drawn have been specific to the topic discussed. It is the intention here to draw these conclusions together and summarise the evidence presented. The implications for the nature of the fluid phase are discussed with consideration being given to cation and anion contents and the role of complexing in the fluid. Properties of the metasomatic fluid such as alkalinity, oxidation state and temperature are considered. The nature of the early stages of the metasomatism has implications for the nature of the late stages of crystallisation of the syenitic magma and some speculation is made on the processes of fluid evolution in the highly fractionated North Qoroq syenites. Comparisons are drawn with other Gardar centres and also, in a global context, with documented areas of fenitisation such as Callander Bay, the Fen complex and Borrolan. Finally, a brief model is presented to summarise the metasomatic activity associated with the North Qoroq centre.

7.2 The nature of the metasomatic fluids

Field and petrographic evidence indicates that there are significant differences in the nature of the metasomatic process between rock types. The metasomatic activity in the syenites is characterised by the recrystallisation of the felsic phases into an anhedral fine-grained matrix consisting of albite and feldspathoids or more rarely a poikilitic texture, with the mafic phases developing a highly poikilitic texture. In contrast, in the granite-gneiss there is little recrystallisation and there are no poikilitic phases developed. The quartz and microcline react out with the formation of alkali amphibole and biotite and plagioclase becomes extensively sericitised and partly

replaced by calcite. The mafic minerals form large subhedral grains or granular aggregates. These differences can be explained in terms of proximity to the source of the fenitising fluids. The metasomatism at internal syenite unit contacts takes place closest to the source of the fluids and hence at the highest temperatures and with the most concentrated active fluids. Further from the contacts, rocks are subject to fluids that have at least in part equilibrated with less evolved syenites. The formation of feldspathoids (nepheline, sodalite), hydrous and fluor-hydrous mafic phases and accessory phases such as fluorite will have resulted in the fluids becoming less halide-rich and less concentrated. The granite-gneiss is furthest from the fluid source and so, in general, would be affected by the lowest temperature and most dilute fluids, especially if there is significant mixing with meteoric waters.

These features have implications for the classification of fenitic and metasomatic rocks by their petrographic grade (Le Bas 1977, Morogan and Martin 1985). Kresten and Morogan (1986) in a study of the Fen complex, Norway, showed that petrographically medium grade fenites from one area were not comparable with those from another area and concluded that the petrographic grade of fenitisation could only be used with reference to comparable protolith compositions and comparable fluids. Hence, classification of the petrographic grade of fenitised or metasomatised North Qoroq rocks is complicated by three factors. Firstly, the initial parental material is markedly contrasting from quartzitic sandstone through granite-gneiss to undersaturated syenites. Secondly, superimposed on this variation, is the action of a fluid progressively changing in composition and reacting at progressively lower temperatures. Thirdly, more than a single fluid phase could have been active at a particular point in or around the complex. In addition to the granite-gneiss suffering lower temperature alteration it may, despite its distance from the magmatic source, have suffered some high temperature metasomatism with the formation of albite. Such alteration may however have been due to changes promoted by and occuring within a meteoric fluid, contrasting strongly in composition to the magmatic fluids responsible for the other changes. Even considering fluids evolving from the syenites alone, multiple intrusion of syenitic

magmas will have resulted, to some extent, in fluids associated with these magmas overprinting and modifying the pre-existing changes. The conclusion of Kresten and Morogan that fenites from different complexes cannot be compared in terms of petrographic grade is therefore supported by this study.

It is also interesting to note that the chemical grade of fenitisation (the fenitisation index used in chapter 3) has the same limitations as the petrographic grade. The heavily metasomatised syenites have considerably lower values of Fen.I. than the fenitised granite-gneiss samples but it is obviously unreasonable to conclude that they have been less affected by a fluid phase. Comparisons of Fen.I. values are therefore also restricted to rocks of similar initial starting compositions that have been altered by similar fluid compositions.

The whole-rock chemistry allows conclusions to be drawn on the cation contents of the metasomatic fluids and also on the overall processes of the metasomatism. It is clear that within the syenite centre the dominant effect of the fluid is to add Na to and subtract Si from the rock. The other consistent losses from the rock are in Ti, Mg and Ca while Al, Fe and K show variable behaviour between SN4B and SN1A. Mn appears relatively immobile in all rock types, though this may partly reflect its low abundances in comparison to the other elements and it is likely that Mn will vary with Fe^{2+}. The country rocks show some differences with the dominant effect in both the quartzite and the granite-gneiss being desilicification with the addition of most of the other major elements. All the chemical evidence points to a near constant volume metasomatism in the North Qoroq rocks and there is no field or petrographic evidence to contradict this assumption.

These conclusions lead to a mass balance problem with excess Si. If the dominant chemical change in the basement gneiss and quartzite is desilicification then it follows that the silica released must be redeposited elsewhere. Many authors have proposed that it is simply transported further into the country rocks and cited the presence of quartz veining as evidence of this (eg. Hoeve 1978, Cathelineau 1986). In contrast, Rubie (1982) demonstrated the transport of Si inwards from the fenitised

country rock to the ijolitic magmas at the Kisingiri volcano, Kenya and used this process to explain the late-stage occurence of poikilitic orthoclase. Chambers (1976) invoked the influx of meteoric water into the North Qoroq centre to explain the development of marginal pegmatites in the syenites but did not suggest an influx of Si. Computer modelling of massive hydrothermal systems (L.M. Cathles, Cornell University, pers. comm.) has suggested that these convecting aqueous fluid systems rise with time above the solidifying and cooling pluton and may only start to precipitate elements such as silica much later when, for example, they intersect a rock-water interface where temperatures would drop rapidly. Such an explanation for North Qoroq rocks would mean that silica was deposited well above the top of the syenite units in country rocks now eroded and removed. The destination of the removed Si remains unclear and even further detailed studies of both the country rocks and the marginal syenites may not resolve the problem.

It seems clear that the cation content of the first fluids to emanate from the interior of the highly fractionated syenites was dominated by Na and it also follows that these fluids were very Si-poor in comparison to the less evolved syenites into which they migrated. Fe would appear to have been the only other major element initially transported by the fluids affecting SN1A whereas in SN4B it appears that significant quantities of Al accompanied the Na. During re-equilibration with the syenites, the fluid gained Mg, Ti and Ca which were then redeposited during fenitisation of the country rocks. The trace element variations show that significant quantities of Ba, Sr, Rb, Zr, Y, Nb and La (which by analogy indicates the REE as a whole) were transported in the metasomatic fluids.

Both the major and trace element transportation has implications for the anion content of the fluids. Burnham (1967) and Ermanovics *et al.* (1967) demonstrated experimentally that the transport of Fe, Mg and Ca in ionic form required the presence of Cl in solution while Hards (1976) showed that Al was not partitioned into a chloride-bearing vapour phase. The relative immobility of Al is well documented (eg. Carmichael 1969) and often used as the parameter to define volume changes in

calculating mass balance (eg. Rubie 1982). It is clear that Al will not be transported in simple ionic form and so complexes must be formed. The whole-rock chemistry indicates that Al is mobile in the North Qoroq centre, most notably in the metasomatism of the quartzite raft and in unit SN4B. It is possible that in the quartzite raft there was a patchy occurence of detrital clay minerals which have been converted into albite with only localised transport of Al, but even in the least altered samples there is no evidence for sufficient quantities of detrital minerals to explain the often extensive albitisation. The study of the quartzite raft also showed significant increases in the REE. It was also shown that, whether they are being enriched or depleted in any particular rock, Zr, Y and Nb are mobile in the syenite centre. All these elements require the presence of complexes to be transported in solution (Mineyev 1963). Kosterin (1959) proposed that the REE were dominantly transported in complexes of the form $[RE(CO_3)_3]^{3-}$ whereas Mineyev (1963) favoured fluorine complexes such as $NaYF_4$ and $Na_5Ce_3F_{14}$. It was concluded in chapter 6, from the formation of REE-rich apatite and fluor-carbonate REE-bearing phases and the close association of these minerals with calcite and fluorite, that complexes of this nature are the probable modes of transport of the REE in North Qoroq. It is likely that the 'residual' elements (Zr, Y, Nb) and Al are also transported in fluorine complexes. The abundance of fluorine during the metasomatism is evidenced by the common development of fluorite in the contact zone between units SN1A and SN1B, in the quartzite raft and also cutting the granite-gneiss. The development of sodalite in the felsic matrix of the heavily metasomatised syenites testifies to the presence of chlorine in solution. It is concluded from the evidence presented in chapters 3, 4 and 6 and summarised above that the metasomatic fluids were initially very Na-rich, Si-poor and halogen-rich.

The study of the mafic silicates allows conclusions to be drawn on the thermodynamic parameters that controlled or were controlled by the metasomatic processes. The differing mineral compositions and assemblages also indicate the importance of protolith composition on the evolution of the metasomatism.

Stephenson and Upton (1982) compared the pyroxene and amphibole compositional trends from several Gardar alkaline centres, both over- and undersaturated. They noted that the pyroxenes from the oversaturated centres showed, in general, a greater Hd-enrichment, before trending to acmite, than those from the undersaturated centres. The amphiboles from the oversaturated centres evolved from katophorite > richterite or actinolite > arfvedsonite-riebeckite whereas in the undersaturated centres the trend was hastingsite > katophorite > arfvedsonite. Giret *et al.* (1980) noted the same features in amphiboles from a number of alkaline centres around the world. It is interesting that in North Qoroq the amphiboles within the syenite centre, both magmatic and metasomatic, follow the undersaturated trend whereas the metasomatic amphiboles in the gneiss and the quartzite follow the oversaturated trend, despite being formed by the action of an alkaline, undersaturated fluid. It is proposed that this difference is due to the presence of free quartz in the country rocks, raising the a.SiO_2 in the fluid. Once again it emphasises the importance of protolith composition in determining the course of the metasomatism.

Stephenson and Upton concluded that the a.SiO_2 was probably not a direct control on the trends observed but some other chemical factor such as oxygen fugacity or peralkalinity, which exhibits an interdependence with Si saturation, was a more likely controlling factor. This concurred with the conclusions of Mitchell and Platt (1978) who studied trends in the Coldwell complex, Ontario. Nicholls and Carmichael (1969) and Chambers (1976) both showed that in fact higher a.SiO_2 favours the acmite molecule and so the greater degree of Hd-enrichment in the pyroxenes of the oversaturated centres must be explained by factors other than a.SiO_2. The rapid acmite enrichment in the quartzite pyroxenes is probably due to high oxygen fugacity, as proposed in Chapter 5. It is suggested that the lack of original mafic minerals in the quartzite means that there is no method of internally defining fO_2 and so interaction with meteoric solutions produces a significant rise in this parameter.

It was suggested in chapter 5 and emphasised above that several factors play an important and interactive role in determining the nature of the metasomatic alteration. It was shown in Chapter 5 that differing initial mineral assemblages and changing values of fHF, fO_2, a.SiO_2 and a.$Na_2Si_2O_5$ in the fluid combined to control the metasomatism. It was proposed that much of the reaction occured in limited micro-environments in which oxygen fugacity was locally defined by reactions such as the conversion of Fe-Ti oxides to aenigmatite, a process that would produce a local increase in fO_2. Conversely, the reaction of arfvedsonite to acmite would locally decrease fO_2. Superimposed on these variations is the large scale re-equilibration of the fluid with the less evolved syenite.

The initial metasomatic fluid that emanated from the fractionated interior of the syenites is likely to have had a low oxygen fugacity, as Chambers (1976) demonstrated that the final stages of crystallisation occured at oxygen fugacities defined by the reaction :

$$4Fe_3O_4 + 6Na_2Si_2O_5 + 12SiO_2 + O_2 <> 12NaFeSi_2O_6$$

magnetite liquid liquid acmite

which is the reaction used by Nicholls and Carmichael (1969) to define the lower boundary of the 'no-oxide' field in which aenigmatite is stable. The 'no-oxide' field lies well below the QFM buffer (Marsh 1975). On reaching less evolved syenite, the fluid will react with a new mineral assemblage and so fO_2 could be re-defined, possibly by an assemblage such as magnetite-sanidine-annite. Migration of the fluid through the marginal augite syenite, in which fayalitic olivine and magnetite are both present, could re-define the oxygen fugacity to that of QFM with the silica as a component in the fluid. This implies that the fluid entering the country rock aureole will have extensively re-equilibrated with the syenite and so both fO_2 and a.SiO_2 will be significantly higher than in the initial fluids. This process of defining fO_2 by reaction between pre-existing mafic mineral assemblages and the metasomatic fluid represents one of the major

differences between the metasomatism within the syenite centre and the fenitisation in the country rocks where fO_2 is likely to be uncontrolled, due to the lack of original mafic minerals. Indeed the dilution of the magmatic fluid by meteoric solutions, a process that is likely to occur in the granite-gneiss, could cause a marked increase in fO_2 (Ernst 1962).

One consistently important factor during the metasomatism is the temperature as a set value of fO_2 will correspond to different defining reactions at different temperatures. Some constraints can be placed on the upper temperature limits of the metasomatism by the upper thermal stability limits of the minerals produced. Ernst (1962) demonstrated experimentally that at low fO_2, defined by the iron-wustite buffer, arfvedsonite is stable up to 655^{oc} at 250bars P_{fluid} and to 712^{oc} at 2000bars P_{fluid}. He also demonstrated that an increase in oxygen fugacity lowers this upper limit. It was concluded by Chambers (1976) that pH_2O ranged from ~350bars up to a maximum of ~1600bars in the North Qoroq centre and so at a pH_2O of 1000bars and an fO_2 between that of the QFM and magnetite-wustite buffers, arfvedsonite is stable up to approximately 650^{oc} (Ernst 1962, Figures 8 and 9). This places an upper limit on the temperature of metasomatism in the syenites, and hence in the centre as a whole, as the poikilitic arfvedsonite is considered to represent the highest grade of alteration. Although the presence of fluorine extends the stability of arfvedsonite, this temperature agrees well with the temperatures of final crystallisation deduced by Chambers (1976) from the feldspar solvus. Bailey (1969) showed that acmite was stable up to 780^{oc} under QFM conditions but also demonstrated the dependence of this limit on fO_2 conditions. In this case an increase in fO_2 increases the upper limit. The fact that acmite is stable up to 780^{oc} does not, of course, mean that this was the temperature of metasomatism and the common relationship of acmite rimming arfvedsonite indicates that the acmite was formed at temperatures no higher than 650^{oc}. Flower (1974) found the upper thermal

stability limit of titan-acmite to be approximately 750-800^{oc} at 1000bars P_{H_2O} which again is significantly higher than the proposed upper limit for the metasomatism.

Popp and Gilbert (1972) demonstrated that the solubility of the jadeite molecule in acmite is temperature and pressure dependent and acmitic pyroxene co-existing with albite and quartz can be used as an indicator of P or T conditions. It was shown in chapter 5 that the jadeite substitution in the quartzite pyroxenes is very limited and, assuming a pressure of 1kb, a temperature range of 300-500^{oc} can be deduced from the pyroxene compositions (Popp and Gilbert (1972), Figure 4), though it should be noted that quantitative assessments of the jadeite component in the pyroxenes are open to considerable error. The occurence of riebeckite in the granite gneiss indicates temperatures below 500^{oc} as Ernst (1962) showed that at high oxygen fugacities riebeckite decomposes at 469^{oc} at 250bars P_{fluid} and 515^{oc} at 2000bars P_{fluid}. Charles (1975) stated that ferrorichterite is stable to only 525^{oc} at oxygen fugacities equivalent to the QFM buffer. The limited fluid inclusion study carried out on some of the North Qoroq rocks found homogenisation temperatures of ~300^{oc} and numerous low temperature inclusions homogenising at ~150^{oc}. As stated in chapter 6 the higher temperature inclusions probably represent the later stages of the metasomatism and the low temperature population is considered to reflect circulating meteoric waters.

In summary, it is proposed that the highest temperatures of metasomatism in the syenites were no greater than 650^{oc} and the occurence of aegerine-augite and arfvedsonite indicates similar temperatures in the quartzite. Maximum temperatures in the granite gneiss are considered to be no more than 500^{oc} and it is thought that fluids were circulating through the North Qoroq centre at temperatures as low as 100^{oc}.

7.3 Fluid evolution from the North Qoroq syenites

The extensive metasomatic alteration seen in and around the North Qoroq centre raises the question of how the fluid evolved and separated from the late-stage melts. Did a 'boiling-off' process occur or did the magmas fractionate continuously to a

hydromagmatic fluid?

Burnham and Jahns (1962) and Hamilton *et al.* (1964) showed that a solubility gap exists between water and felsic rock melts up to pressures of at least 10kbars. Burnham (1967) concluded that unless large quantities of volatile components were present, continuous solubility between felsic magmas and aqueous fluids was precluded. These results, though, are probably not directly applicable to the residual North Qoroq magmas and the effects of volatile components and peralkalinity need to be examined.

Chambers (1976) studied the occurence of sodalite and analcite in the highly fractionated syenites and concluded, on petrographic grounds, that both phases crystallised directly in some rocks from the late-stage melts. Analcite was the only hydrous phase crystallising as, by this stage, amphibole had been replaced by acmite. Experimental work by Ki-Tae Kim and Burley (1971) and Peters *et al.* (1966) on analcite stability in the nepheline-albite-H_2O system indicates that it will only crystallise from a melt over a very limited temperature range and only at pressures >5kb. Ki-Tae Kim and Burley state categorically that analcite cannot crystallise directly from a melt at less than 5kb but Peters *et al.* show that the incorporation of small amounts of potassium into the analcite reduces this pressure limit to ~2.3kb. The North Qoroq rocks have been shown to have formed at pressures of ~1kb (Chambers 1976) and so other factors must aid the stability of analcite if it is indeed a primary magmatic phase. Platt and Rose-Hansen (1975) in a study of the persodic portions of the system Na_2O-Al_2O_3-SiO_2-H_2O found that in the presence of persodic liquids and at pressures of 1kb analcite can co-exist with melt over a wide temperature range. The highly fractionated North Qoroq syenites containing analcite have acmite and occasionally sodium metasilicate ($NaSiO_3$) in the norm (Chambers 1976) and it is proposed that the strongly peralkaline nature of the residual magma enables the primary crystallisation of analcite. The primary crystallisation of analcite and sodalite has important implications for the conditions of late-stage crystallisation in the syenite.

Wellman (1970) in a study of sodalite stability suggested that the crystallisation of anhydrous phases from a hydrous melt would result in the separation of an aqueous phase unless either large quantities of analcite were formed or the initial melt was very dry. Koster van Groos and Wyllie (1968,1969) studied the systems $NaAlSi_3O_8$-NaF-H_2O and $NaAlSi_3O_8$-NaCl-H_2O and concluded that the presence of both fluorine and chlorine significantly lowers the solidus of a crystallising magma. They also showed that the solubility of H_2O in the melt is greatly increased by the presence of the halogens although on separation of a separate aqueous fluid Cl is shown to partition preferentially into this phase while F remains in the melt.

It is proposed that in the final stages of crystallisation of the most fractionated North Qoroq syenites and at relatively low temperatures, the presence of significant quantities of F and Cl and the high peralkalinity promoted the solubility of H_2O in the melt. The peralkalinity helped stabilise analcite as a primary phase, the crystallisation of which further inhibited the separation of an aqueous phase and led to a build up of Cl in the melt. This would have resulted in the formation of sodalite and the crystallisation of the two phases together prevents any 'boiling-off' of a Cl-rich vapour phase. Implicit in this process is the continued build up of F in the melt which also inhibits the release of a fluid. It is suggested, therefore, that the evolution of the metasomatic fluids represents the last process in the crystallisation history of the syenites and that there is no necessity to invoke the 'boiling-off' of a separate aqueous halide phase. Also, there is no evidence to support the formation of a NaCl-rich immiscible liquid, as mentioned in Chapter 4 and demonstrated experimentally by Koster van Groos and Wyllie (1969). Despite the occurence of sodalite in the feldspathoidal groundmass of the heavily metasomatised syenites, there are no large scale sodalite formations similar to those seen in Ilimaussaq. Therefore, the composition of the metasomatic fluid, evolving as it has from a peralkaline undersaturated magma, may well be dominantly that of a hydrous, halide-rich fluid. It will however have a significant cation content, dominated by sodium, and will be an aggressive corrosive agent of metasomatism.

This conclusion is supported by the metasomatic effects seen in the syenites. It has been shown throughout the thesis that the textures developed and the whole-rock and mineralogical chemical variations are best explained in terms of a single metasomatic process controlled both by protolith composition and evolving fluid composition as reaction occurs. The intimate association of sodalite and fluorite in the recrystallised matrix of the highly metasomatised syenites indicates the simultaneous presence in solution of Cl and F. Only in the quartzite raft is there evidence that a more dilute aqueous phase affected the rock before the influx of the REE- and F-rich metasomatic fluid. It was proposed in chapter 6 that this first fluid was that involved in meteoric circulation around the syenite centre and has affected the quartzite due to its position high in the roof zone of unit SN1B and close to the margins of the centre.

In studies of trace element distributions in the Ilimaussaq intrusion, Bailey *et al.* (1981) and Andersen *et al.* (1981) showed that there was significant post-magmatic metasomatism in the intrusion but made no definitive statement on the source or evolution of the fluids. Konnerup-Madsen and Rose-Hansen (1982), though, in a study of fluid inclusions from the complex suggested that retention of volatiles during crystallisation played an important part in the formation of hydrocarbon-rich inclusions. Konnerup-Madsen (1984) studied inclusions in the alkali granite of the complex and concluded that secondary boiling of aqueous fluids was not the mechanism responsible for the generation of high salinity fluids. While the Ilimaussaq intrusion contains rock types slightly more evolved than any exposed in the North Qoroq centre (eg. the lujavrites) it is worth noting that secondary boiling is also discounted as a significant process in this undersaturated, peralkaline centre. Upton and Emeleus (1987), in a review of the Gardar province, suggest that high concentration of F, Cl and CO_2 are a regional feature and that the volatile components of Gardar magmas in general are H_2O-poor and halogen-rich.

7.4 Metasomatism associated with Gardar centres

Metasomatism and hydrothermal alteration has been recorded at several Gardar centres but only at Ilimaussaq have detailed studies been carried. Within the Igaliko complex, metasomatic effects have been noted at all three of the other centres, South Qoroq, Igdlerfigssalik and Motzfledt.

Stephenson (1972) noted the hydrothermal alteration of rock of the South Qoroq centre, particularly in the vicinity of faults, shear zones and 'marginal areas'. He was unable to demonstrate any significant change in bulk rock chemistry but did show variations in pyroxene compositional trends. Pyroxenes from the metasomatised rocks had a much earlier trend to acmite enrichment than in the unaltered rocks and this was attributed to increased oxygen fugacity, though Stephenson maintained that this parameter remained internally buffered during the alteration. The same author (Stephenson 1976) described the alteration of rocks of the South Qoroq centre by aqueous solutions emanating from the later Igdlerfigssalik centre. Again, no metasomatic transfer of major elements was demonstrated but a clear zone of depletion of the 'residual' trace elements, similar to that described in the North Qoroq centre, was found at the contact with Igdlerfigssalik. Mineralogical changes include the coarse exsolution of perthite, the development of more sodic pyroxene and the occurence of biotite as the major hydrous mafic silicate. It was concluded that the recrystallisation took place under conditions of increased fO_2 and increased PH_2O. Stephenson also proposed that this fluid activity caused limited re-melting of some South Qoroq rocks but, assuming that temperatures of metasomatism are no higher than those deduced for the more intense alteration in North Qoroq, and given a solidus temperature of ~700^{oc} for a relatively unevolved syenite, it seems highly unlikely that this process could occur.

Jones and Larsen (1985) in a study of REE minerals in the Motzfeldt centre suggested possible metasomatic enrichments of these elements. They noted that the metasomatic rocks had geochemical signatures very similar to lujavrites occuring within the centre and implied a genetic relationship between the metasomatic fluids and the

lujavrites. Syenites elsewhere in the centre contained nepheline replaced by sodalite and cancrinite and albitic rims on perthites, features that were also attributed to metasomatic activity. Tukiainen *et al.* (1984) carried out radiometric mapping of the Motzfeldt centre and found strong Th-U-Zr-Nb-REE mineralisation. Th/U ratios were high and the altered rocks were notably enriched in fluorine. They concluded that there had been extensive metasomatic alteration within the Motzfeldt centre, due to the upward migration of a highly mobile alkali-rich volatile phase rich in incompatible elements, and compared the intrusion to the Ilimaussaq centre.

There was extensive metasomatism associated with the Ilimaussaq intrusion, which has been the subject of much detailed investigation eg. Anderson *et al.* (1981), Bailey *et al.* (1981) and Kunzendorf *et al.* (1982). Obviously only a few of the major features can be described here and the reader is also referred to the studies of Karup-Moller (1978), Nielsen (1981) and Mackovicky (1981). The major reason for the attention given to Ilimaussaq is the economic potential of the uranium deposits that have been formed by the action of metasomatic fluids. Kunzendorf *et al.* (1982) also described Nb mineralisation in some country rocks and concluded that Nb, REE and fluorine are sufficiently enriched to constitute potential by-products during any uranium mining. Major element variation is characterised by an increase in Na and decrease in Si, Ti, Mg, K and Fe. There is a lack of pneumatolytic contact alteration of the country rocks, a feature that Kunzendorf attributed to a lack of halides and water in a separate fluid phase and which were to a high degree retained and dissolved in the peralkaline magmas.

Other documented occurences of metasomatism in the Gardar are rare. MacDonald *et al.* (1973) recorded the K and F alteration of a gabbro adjacent to sheets of alkali granite at the oversaturated Kungnat complex. They concluded that a K- and F-bearing aqueous solution separated from the granite at a late stage in its crystallisation. It is interesting to note that the basalts around North Qoroq show strong K-metasomatism and it is likely that the original rock composition dictated the style of metasomatism more than the fluid composition. Parsons (1980) noted coarse exsolution

textures in feldspars and Fe-Ti oxides and also compositional variations in pyroxenes (Parsons and Becker 1986) in the Klokken intrusion and attributed these to the action of circulating deuteric solutions.

Of the undersaturated Gardar centres in which metasomatism has been documented, the Motzfeldt centre appears to most closely resemble North Qoroq. This centre is also the most closely associated geographically and chronologically. Metasomatism at Ilimaussaq appears to be of a more intense and evolved nature whereas South Qoroq and Igdlerfigssalik seem to have suffered less from fluid activity though this may only reflect differing levels of exposure. Some support is given to the conclusions reached in North Qoroq by similar processes operating in the other centres but it is clear that there is a great need for more detailed studies of metasomatism in the Gardar province, especially in the other Igaliko syenite centres. It would appear that intense metasomatic alteration is confined to the undersaturated plutons and it may be that the oversaturated plutons actually 'boil-off' separate fluids at a much earlier stage. These might be more dilute and so have less intense metasomatic changes associated with them.

7.5 Metasomatism associated with other alkaline igneous centres

There have been many investigations of alkali metasomatism and fenitisation and only a few notable occurences are described here.

Sutherland (1969) studied fenites associated with ijolite-carbonatite complexes in the East African rift province. Mineralogically, the fenitisation was characterised by the development of magnesio-arfvedsonite, aegerine-augite and aegerine. By comparison with the experimentally deduced stability fields of these minerals Sutherland concluded that oxygen fugacities were similar to those defined by the QFM buffer and that temperatures of fenitisation could theoretically have been as high as 800^{oc}, but there was no indication that crystallisation in fact took place near this upper limit. Aegerine-augite was considered to have formed at higher temperatures to aegerine and so the gradual change from one to the other represents crystallisation from

an increasingly alkaline fluid at gradually reducing temperatures.

Currie and Ferguson (1971) studied the fenitisation around the carbonatite complex of Callander Bay, Ontario. They noted features such as the formation of haematite veinlets, the conversion of plagioclase to albite+calcite, the increased ordering of K-feldspar towards maximum microcline and the increased abundance of acmitic pyroxenes. They concluded that the fenitising fluid was a NaCl brine with a high content of Fe, Mg and Ca and that oxygen fugacities were high, roughly equivalent to haematite-magnetite buffer conditions. Interestingly, they record fenitisation temperatures as high as 700^{oc} and state that the main fenitisation took place above 500^{oc} and in fact had ceased altogether by 450^{oc}. This seems like an unreasonably high temperature for the cessation of fluid activity and, in contrast, Siemiatkowska and Martin (1975), in a study of the fenitisation in the Sudbury area, Ontario place no lower limit on the temperature of alteration, pointing out that aegerine and riebeckite can crystallise together at normal surface temperatures. They show that the highest temperature in this area was no more than 500^{oc} and in fact cite the formation of maximum microcline as evidence of this.

The fenitisation of almost pure quartzite at the Borrolan complex, Scotland (Woolley *et al.* 1972, Martin *et al.* 1978) provides an interesting parallel with the quartzite raft in the North Qoroq centre. It was shown that early formed amphiboles were richteritic but these were replaced by more alkaline varieties with increasing grade of fenitisation. Whole-rock analyses showed expected increases in most major elements at the expense of Si but, unlike in the North Qoroq quartzite, the final product of fenitisation was a syenite lying close to the albite-orthoclase minimum. Martin *et al.* demonstrated the mobility of the REE in the fenitisation and their enrichment in the quartzite, but the maximum concentration of Ce (the most abundant REE) was only ~100ppm which is an order of magnitude less than that recorded in North Qoroq. These differences can be explained by the different sources of the fenitising fluids. Whereas in North Qoroq the fluids are evolved from a highly persodic and F-rich residue the

fenitisation at Borrolan is associated with potassic, psuedoleucite syenites.

The type locality for fenitisation is the Fen complex, Norway and it is surprising that, until recently, it had recieved little attention. Kresten and Morogan (1986) studied the mineralogy of the fenites while Kresten (1988) examined the whole-rock chemical changes. General conclusions were that significant differences in fenite parageneses between areas were due to differences in the source and hence composition of the fluids. Variations in XCO_2, fO_2, $a.SiO_2$, the activities of most of the major elements and temperature were shown to control the metasomatism of an originally very homogeneous granite gneiss. Upper temperature limits varied between areas but were of the order of 600-700^{oc} and, for one area, lower temperature limits were said to be as high as 500^{oc}. Again, it seems unreasonable to generate active fenitising fluids at 700^{oc} and imply that they cease to operate at 500^{oc}, a temperature at which the fluids would still be supercritical.

One feature that is common to most of these studies is the order of increasing fenitisation. It is always implied, and detailed by Kresten and Morogan, that the lowest grade assemblages are formed first and the highest grade assemblages at a later stage, after the activity and temperature of the fluid have increased, though this increase in temperature with time seems difficult to explain. The pyroxene trends shown by Kresten and Morogan (Figure 5) start at the acmite apex and move towards the Di-Hd join with increasing temperature and grade of fenitisation. While it is agreed that Hd-rich compositions represent the highest grade and Ac-rich compositions the lowest grade, it is proposed that the sequence is from Hd > Ac and not the other way around. It was shown in North Qoroq that the more $Na^{+}Fe^{3+}$-rich mineral compositions were formed after the higher temperature more Fe^{2+}-rich compositions eg. acmite rimming amphibole and acmite rims on aegerine-hedenbergite. It seems natural that the first fluids to be released from the source rock and to affect the surrounding rocks will be the highest temperature fluids and it is as the fenitisation is waning, as fluid and rock increasingly re-equilibrate, that the low grade assemblages are formed.

7.6 Future work

The work carried out on the North Qoroq centre has necessarily been of a general nature as it is the first detailed study of fluid activity in the centre. Numerous interesting areas of future research remain to be covered and some of these are outlined below.

It was shown in chapter 6 that there are significant variations in the compositions of the fluids circulating in the intrusion and there is a great need for thorough fluid inclusion studies similar to those carried out on the Ilimaussaq intrusion (eg. Konnerup-Madsen 1984). Also of interest are the strong enrichments of the REE and the 'residual' elements such as Zr, Y and Nb. These have been shown to be highly mobile in the metasomatic fluids and detailed studies of accessory phases, such as apatite and 'rinkite', in the North Qoroq centre may yield more information on the conditions of transport and deposition of these increasingly economically important elements. The transport of the REE also has profound implications for any genetic modelling of magma source regions as it is clear that the assumption that REE patterns are inherited in the source region and remain unchanged by later processes is doubtful in any pluton affected by fluid alteration. Much of the work in this thesis has concentrated on the syenite centre and there is scope for more detailed examination of fenitisation in the country rock aureole. In particular, the sequence of impure sediments and basalts adjacent to both the North and South Qoroq centres provides an ideal opportunity to examine the effects of varying protolith composition on metasomatic alteration.

In a more general way, studies of alkali metasomatism and fluid activity associated with other Gardar centres, both over- and undersaturated, should be initiated. It is interesting that, on the basis of the limited amount of work carried out so far, Motzfeldt is the most closely comparable centre to North Qoroq. The two centres were emplaced at very similar times and much earlier than South Qoroq or Igdlerfigssalik and it may be that the nature of final fluid activity at least in part reflects the original volatile content of the magma, inherited in the source region at that time and similar for both centres.

7.7 Conclusions

In order to summarise the results of the thesis a simplified model will be presented to explain the major effects of the metasomatic activity in and around the centre. It must be emphasised again that local variations will always exist to contradict any general rule and it is the intention here only to give an overall picture.

Fluid evolution from the highly fractionated North Qoroq syenites occured at approximately 600^{oc} and these fluids were very Na-rich, Si-poor and volatile-rich. Oxygen fugacities were relatively reducing, below those defined by the QFM buffer in agreement with the crystallisation history outlined for the centre by Chambers (1976). Initial alteration of the syenites produced the large poikilitic arfvedsonitic and katophoritic amphiboles and the aegerine-hedenbergites and also led to the complete recrystallisation of the felsic groundmass with the formation of feldspathoids such as nepheline, sodalite and analcite. Local variations were produced by reactions occuring within micro-environments on already variable magmatic mineral assemblages. As temperature decreased and fluid and rock progressively re-equilibrated there was an increase in fO_2 and a.SiO2 which initiated a trend to more acmitic pyroxene compositions. This formation of Na-rich minerals at a late stage in the metasomatic alteration is also due to the high Na content of the initial fluids which meant that re-equilibration for this element took longer than for the other elements. The high Na content combined with the presence of original Fe-Ti oxides controlled the formation of aenigmatite. As the fluid migrated through the syenite it progressively re-equilibrated with it and with falling temperature the principle role of the fluid became that of a passive medium, aiding the unmixing of the alkali feldspars.

On reaching the country rock aureole the fluid began to react once again with the new oversaturated assemblage but this time at lower temperatures and with oxygen fugacities initially equivalent to those defined by the QFM buffer, due to the equilibration of the fluid with the marginal syenite before entering the country rock aureole. The presence of free quartz in the protolith played an important role in

determining the trends seen in the mafic silicates and led to the development of richterite and biotite as the stable assemblage. Biotite compositions produced are very similar to the compositions of biotite from within the syenites. There was extensive mixing between metasomatic and meteoric fluids in the basement gneiss and this produces a significant increase in fO_2 (Ernst 1962) which, with further decrease in temperature, led to the formation of riebeckite in the low grade fenites.

The metasomatism of the quartzite raft is not directly comparable to that of the other rock types due to its originally very pure composition and its location in the roof zone of SN1B and within the syenite body. The quartzite was initially affected by dilute heated meteoric waters circulating within the country rock and chilled margins of the intrusion and some albitisation occured at an early stage. The large compositional difference between the quartzite and the syenite meant that the quartzite acted as a sink for cations from the Na- and F-rich fluids emanating from the interior of unit SN1B and so the influx of these fluids produced a very sodic, high temperature alteration with the development of aegerine-augite and arfvedsonite. Earlier formed apatite was partly resorbed and overgrown by very REE-rich rims. In a similar way to the basement gneiss, the presence of free quartz was important in determining the course of amphibole and pyroxene trends. Increased $a.SiO_2$, increasing fO_2 and falling temperature were the prime controls on the evolution of the mineral compositions with low grade assemblages of acmite, haematite and riebeckitic amphibole. The REE-rich rims on the apatites were resorbed and overgrown as the metasomatism waned or under the influence of meteoric waters that continued to circulate around the margins of the intrusion.

References

Andersen, S., Bailey, J.C. & Bohse, H. 1981. Zr-Y-U stratigraphy of the kakortokite-lujavrite sequence, southern Ilimuassaq intrusion. *In* Bailey, J.C., Larsen, L.M. & Sorensen, H. (eds) *The Ilimaussaq intrusion, South Greenland. A progress report on geology, mineralogy, geochemistry and economic geology*. RAPP GRONLANDS GEOL UNDERS **103**, 69-76.

Bailey, D.K. 1969. The stability of acmite in the presence of H_2O. AM J SCI **267-A**, 1-16.

Bailey, J.C., Rose-Hansen, J., Lovborg, L. & Sorensen, H. 1981. Evolution of Th and U whole-rock contents in the Ilimaussaq intrusion. *In* Bailey, J.C., Larsen, L.M. & Sorensen, H. (eds) *The Ilimaussaq intrusion, South Greenland. A progress report on geology, mineralogy, geochemistry and economic geology*, RAPP GRONLANDS GEOL UNDERS **103**, 87.98.

Burnham, C.W. 1967. Hydrothermal fluids at the magmatic stage. *In* Barnes, H.L. (ed) *Geochemistry of hydrothermal ore deposits*, 34-76. Holt, Rinehart & Winston.

Burnham, C.W. & Jahns, R.H. 1962. A method for determining the solubility of water in silicate melts. AM J SCI **260**, 721-45.

Carmichael, D.M. 1969. On the mechanism of prograde metamorphic reactions in quartz bearing pelitic rocks. CONTRIB MINERAL PETROL **20**, 244-67.

Cathelineau, M. 1986. The hydrothermal alkali metasomatism effects on granitic rocks: quartz dissolution and related subsolidus changes. J PETROL **27**, 945-65.

Chambers, A.D. 1976. The petrology and geochemistry of the North Qoroq centre, Igaliko Complex, South Greenland. UNPUBL PhD THESIS, UNIV OF DURHAM.

Charles, R.W. 1975. The phase equilibria of richterite and ferrorichterite. AM MINERAL **60**, 367-74.

Currie, K.L. & Ferguson, J. 1971. A study of fenitisation around the alkaline carbonatite complex at Callander Bay, Ontario, Canada. CAN J EARTH SCI **8**, 498-517.

Ermanovics, I.F., Edgar, A.D. & Currie, K.L. 1967. Evidence bearing on the origin of the Belleoram stock, southern Newfoundland. CAN J EARTH SCI **4**, 413-31.

Ernst, W.G. 1962. Synthesis, stability relations, and occurence of riebeckite and riebeckite-arfvedsonite solid solutions. J GEOL **70**, 689-736.

Flower, M.F.J. 1974. Phase relations of titan-acmite in the system Na_2O-Fe_2O_3-Al_2O_3-TiO_2-SiO_2 at 1000 bars total water pressure. AM MINERAL **59**, 536-48.

Giret, A., Bonin, B. & Leger, J. 1980. Amphibole compositional trends in oversaturated and undersaturated alkaline plutonic ring complexes. CAN MINERAL **18**, 481-95.

Hamilton, D.L., Burnham, C.W. & Osborn, E.F. 1964. The solubility of water and the effects of oxygen fugacity and water content on crystallisation in mafic magmas. J PETROL **5**, 21-39.

Hards, N. 1976. Distribution of elements between the fluid phase and silicate melt phase of granites and nepheline syenites. NERC Publ Series D **6**, 88-90.

Hoeve, J. 1978. Composition and volume changes accompanying soda metasomatic alterations, Vastervik area, SE Sweden. GEOL RUNDSCHAU **Bd 67**, 920-942.

Jones, A.P. & Larsen, L.M. 1985. Geochemistry and REE minerals of nepheline syenites from the Motzfeldt Centre, South Greenland. AM MINERAL **70**, 1087-100.

Karup-Moller, S. 1978. The ore minerals of the Ilimaussaq intrusion: their mode of occurence and their conditions of formation. BULL GRONLAND GEOL UNDERS **127**.

Ki-Tae Kim & Burley, B.J. 1971. Phase equilibria in the system $NaAlSi_3O_8$-$NaAlSiO_4$-H_2O with special emphasis on the stability of analcite. CAN J EARTH SCI **8**, 311-37.

Konnerup-Madsen, J. 1984. Compositions of fluid inclusions in granites and quartz syenites from the Gardar continental rift province (South Greenland). BULL MINERAL **107**, 327-40.

Konnerup-Madsen, J. & Rose-Hansen, J. 1982. Volatiles associated with alkaline igneous rift activity : fluid inclusions in the Ilimaussaq intrusion and the Gardar granitic complexes South Greenland. CHEM GEOL **37**, 79-93.

Kosterin, A.V. 1959. The possible modes of transport of the rare earths by hydrothermal solutions. GEOCHEMISTRY **4**, 381-87.

Koster van Groos, A.F. & Wyllie, P.J. 1968. Melting relationships in the system $NaAlSi_3O_8$-NaF-H_2O to 4 kilobars pressure. J GEOL **76**, 50-71.

Koster van Groos, A.F. & Wyllie, P.J. 1969. Melting relationships in the system $NaAlSi_3O_8$-NaCl-H_2O at one kilobar pressure, with petrological applications. J GEOL **77**, 581-606.

Kresten, P. 1988. The chemistry of fenitisation: examples from Fen, Norway. CHEM GEOL **68**, 329-351.

Kresten, P. & Morogan, V. 1986. Fenitisation at the Fen complex, Southern Norway. LITHOS **19**, 27-42.

Kunzendorf, H., Nyegaard, P. & Nielsen, B.L. 1982. Distribution of characteristic elements in the radioactive rocks of the northern part of Kvanefjeld, Ilimaussaq intrusion, South Greenland. RAPP GRONLANDS GEOL UNDERS **109**.

Le Bas, M.J. 1977. *Carbonatite-Nephelinite volcanism.* Wiley, New York, N.Y., 347pp.

MacDonald, R., Upton, B.G.J. & Thomas, J.E. 1973. Potassium- and fluorine-rich hydrous phase coexisting with peralkaline granite in South Greenland. EARTH PLANET SCI LETT **18**, 217-22.

Mackovicky, M. 1981. Preliminary results on the distribution of uranium in drill cores from Kvanefjeld, Ilimaussaq intrusion. *In* Bailey, J.C., Larsen, L.M. & Sorensen, H. (eds) *The Ilimaussaq intrusion, South Greenland. A progress report on geology, mineralogy, geochemistry and economic geology.* RAPP GRONLANDS GEOL UNDERS **103**, 109-12.

Martin, R.F., Whitley, J.E. & Woolley, A.R. An investigation of rare-earth element mobility: fenitised quartzites, Borrolan Complex, NW Scotland. CONTRIB MINERAL PETROL **66**, 69-73.

Mineyev, D.A. 1963. Geochemical differentiation of the rare earths. GEOCHEMISTRY **12**, 1129-49.

Mitchell, R.H. & Platt, R.G. 1978. Mafic mineralogy of ferroaugite syenite from the Coldwell Alkaline Complex, Ontario, Canada. J PETROL **19**, 627-51.

Morogan, V. & Martin, R.F. 1985. Mineralogy and partial melting of fenitised crustal xenoliths in the Oldoinyo Lengai carbonatitic volcano, Tanzania. AM MINERAL **70**, 1114-126.

Nicholls, J. & Carmichael, I.S.E. 1969. Peralkaline acid liquids: A petrological study. CONTRIB MINERAL PETROL **20**, 268-94.

Nielsen, B.L. 1981. Radioactive albitites bordering the Ilimaussaq complex: Agpat and Sondre Siorarsuit. *In* Bailey, J.C., Larsen, L.M. & Sorensen, H. (eds) *The Ilimaussaq intrusion, South Greenland. A progress report on geology, mineralogy, geochemistry and economic geology.* RAPP GRONLANDS GEOL UNDERS **103**, 119-23.

Parsons, I. 1980. Alkali-feldspar and Fe-Ti oxide exsolution textures as indicators of the distribution and subsolidus effects of magmatic 'water' in the Klokken layered syenite intrusion, South Greenland. TRANS R SOC EDINBURGH **71**, 1-12.

Parsons, I. & Becker, S.M. 1986. High-temperature fluid-rock interactions in a layered syenite pluton. NATURE **321**, 764-69.

Peters, T.J., Luth, W.C. & Tuttle, O.F. 1966. The melting of analcite solid solutions in the system $NaAlSiO_4$-$NaAlSi_3O_8$-H_2O. AM MINERAL **51**, 736-53.

Platt, R.G. & Rose-Hansen, J. 1975. The system ussingite-water and its bearing on crystallisation in persodic portions of the system Na2O-Al2O3-H2O at 1kb total pressure. J GEOL **83**, 763-72.

Popp, R.K. & Gilbert, M.C. 1972. Stability of acmite-jadeite pyroxenes at low pressure. AM MINERAL **57**, 1210-231.

Rubie, D.C. 1982. Mass transfer and volume change during alkali metasomatism at Kisingiri, Western Kenya. LITHOS **15**, 99-109.

Siemiatkowska, K.M. & Martin, R.F. 1975. Fenitisation of Mississagi quartzite, Sudbury area, Ontario. GEOL SOC AM BULL **86**, 1109-122.

Stephenson, D. 1972. Alkali clinopyroxenes from nepheline syenites of the South Qoroq Centre, South Greenland. LITHOS **5**, 187-201.

Stephenson, D. 1976. The South Qoroq Centre nepheline syenites, South Greenland: petrology, felsic mineralogy and petrogenesis. BULL GRONLANDS GEOL UNDERS **118**.

Stephenson, D. & Upton, B.G.J. 1982. Ferromagnesian silicates in a differentiated alkaline complex: Kungnat fjeld, South Greenland. MINERAL MAG **46**, 283-300.

Sutherland, D.S. 1969.Sodic amphiboles and pyroxenes from fenites in East Africa. CONTRIB MINERAL PETROL **24**, 114-35.

Tukiainen, T., Bradshaw, C. & Emeleus, C.H. 1984. Geological and radiometric mapping of the Motzfeldt Centre of the Igaliko Complex, South Greenland. RAPP GRONLANDS GEOL UNDERS **120**, 78-83.

Upton, B.G.J. & Emeleus, C.H. 1987. Mid-proterozoic alkaline magmatism in southern Greenland: the Gardar province. *In* Fitton, J.G. & Upton, B.G.J. (eds) *Alkaline Igneous Rocks*. GEOL SOC SPEC PUBL **No 30**, 449-71.

Wellman, T.R. 1970. The stability of sodalite in a synthetic syenite plus aqueous chloride fluid system. J PETROL **11**, 49-71.

Woolley, A.R., Symes, R.F. & Elliott, C.J. Metasomatized (fenitised) quartzites from the Borrolan Complex, Scotland. MINERAL MAG **38**, 819-36.

APPENDIX 1

Electron microprobe analysis

1.1 Analytical techniques

All the electron microprobe analyses reported in this thesis were carried out using a Cameca Camebax electron microprobe in the Grant Institute of Geology, University of Edinburgh. A summary of the operating conditions used for each mineral phase is given below :

Mineral	Acc. voltage	Faraday current	No. of oxygens (structural formula)
Feldspar	20kV	25nA	8
Pyroxene	20kV	20nA	6
Amphibole	20kV	20nA	23
Biotite	20kV	20nA	22
Apatite	20kV	25nA	25

Analytical details for each element are :

Element	Standard	Crystal	Count time (Pk-Bkgd)
Si	$CaSiO_3$	TAP	20-10
Al	Al_2O_3	TAP	20-10
Ti	TiO_2	PET	20-10
Zr	$ZrSiO_4$	TAP	30-15
Fe	Fe	LIF	20-10
Mn	Mn	LIF	20-10
Mg	MgO	TAP	20-10
Ca	$CaSiO_3$	PET	20-10
Ba	$BaSO_4$	PET	20-10
Na	$NaAlSi_2O_6$	TAP	20-10
K	$KAlSi_3O_8$	PET	20-10
F	MgF_2	TAP	40-20
Cl	NaCl	PET	40-20
La	see below	PET	60-30
Ce	see below	PET	60-30
Pr	see below	PET	60-30
Nd	see below	PET	60-30
Sm	see below	LIF	60-30

Data reduction was done using the ZAF correction software supplied by Cameca. The rare earth elements were analysed using synthetic silicate glass standards developed in the Grant Institute of Geology. The following table lists the standard compositions (Wt% oxide) :

Element	R.E. Oxide	SiO_2	CaO	Al_2O_3
La	16.60	55.80	17.07	10.52
Ce	19.71	53.72	16.44	10.13
Pr	16.27	56.02	17.14	10.56
Nd	16.89	55.59	17.02	10.49
Sm	20.20	48.55	19.44	11.81

1.2 Data tables

Full data tables of all the analyses carried out by the author and used in the thesis are given on the following pages. The analyses of magmatic mineral phases, used for comparison, were taken from Chambers (1976) [see Chapter 7 for reference] and are not listed here. A listing is given of sample numbers and corresponding rock units, that is applicable to all the appendices data tables.

Sample Numbers

Unit SN4B

DAR138
DAR139
DAR140
DAR141
DAR142
DAR143
DAR144
DAR185
DAR186
DAR187
DAR188
DAR189
DAR190
DAR191
DAR241
DAR242
DAR243
DAR248
DAR249
DAR250
DAR251

Unit SN1A

DAR105
DAR106
DAR107
DAR115
DAR116
DAR118
DAR123
DAR127
DAR232
DAR235
DAR236
DAR237
DAR239
52246
59751
155053

Granite-gneiss

DAR70
DAR71
DAR72
DAR73
DAR74
DAR76
DAR77
DAR79
DAR162
DAR163
DAR164
DAR165
DAR167
DAR168
DAR169

DAR172
DAR175
DAR178
DAR179
DAR279
DAR280
DAR281

Quartzite

DAR52
DAR53
DAR62
DAR63
DAR64
DAR65
DAR67
DAR291
DAR294

PYROXENES

Sample No.	DAR140 N:6	DAR140 N:9	DAR140 N:10	DAR185 N:14	DAR186 N:2	DAR186 N:9	DAR189 N:2	DAR189 N:3	DAR191 N:5
SiO2	50.275	49.770	50.581	50.816	50.316	50.655	50.580	50.063	49.796
Al2O3	0.761	1.063	0.824	0.934	1.598	0.823	0.843	0.866	0.893
TiO2	0.218	0.317	0.331	0.217	0.232	0.268	0.254	0.239	0.413
ZrO2	0.000	0.000	0.000	0.000	0.000	0.000	0.000	0.000	0.000
Fe2O3	14.1255	12.0300	16.9341	17.2311	13.9623	16.8032	13.9241	10.7651	12.1433
FeO	12.7092	14.2079	10.4179	8.9257	11.4071	10.0797	11.8035	13.9461	14.5568
MnO	1.207	1.068	0.957	1.489	1.271	1.202	1.470	1.738	1.224
MgO	0.835	1.346	0.770	1.306	1.264	0.870	1.413	1.684	0.800
CaO	14.014	15.150	11.857	12.558	13.600	11.483	14.214	16.128	15.391
Na2O	5.828	4.912	7.099	6.941	6.056	7.190	5.772	4.481	4.973
Total	99.9727	99.8638	99.7710	100.4177	99.7064	99.3739	100.2735	99.9102	100.1902
Si	1.9894	1.9754	1.9916	1.9822	1.9808	1.9989	1.9874	1.9846	1.9772
Al	0.0354	0.0496	0.0382	0.0429	0.0740	0.0382	0.0390	0.0404	0.0417
Ti	0.0065	0.0094	0.0098	0.0063	0.0068	0.0079	0.0075	0.0071	0.0123
Zr	0.0000	0.0000	0.0000	0.0000	0.0000	0.0000	0.0000	0.0000	0.0000
Fe3+	0.4191	0.3580	0.5000	0.5040	0.4122	0.4972	0.4103	0.3200	0.3616
Fe2+	0.4191	0.4699	0.3418	0.2901	0.3742	0.3315	0.3865	0.4607	0.4817
Mn	0.0404	0.0358	0.0318	0.0491	0.0423	0.0401	0.0488	0.0582	0.0411
Mg	0.0496	0.0801	0.0455	0.0764	0.0746	0.0515	0.0833	0.1001	0.0476
Ca	0.5942	0.6443	0.5002	0.5249	0.5736	0.4855	0.5984	0.6850	0.6548
Na	0.4464	0.3773	0.5410	0.5240	0.4614	0.5492	0.4390	0.3438	0.3822
Di	5.1877	8.3194	4.7365	8.1322	7.8356	5.2970	8.6973	10.3996	5.0020
Hd	48.0916	52.5060	38.9182	36.1001	43.7293	38.2176	45.4603	53.8938	54.8768
Ac	46.7206	39.1746	56.3454	55.7677	48.4405	56.4855	45.8424	35.7066	40.1212

Sample No.	DAR191 N:6	DAR191 N:13	DAR186 N:1	DAR186 N:2	DAR186 N:3	DAR186 N:4	DAR186 N:5	DAR186 N:6	DAR186 N:7
SiO2	49.614	50.168	50.366	49.921	50.649	50.081	50.665	50.753	50.165
Al2O3	0.804	0.803	1.075	0.842	0.889	0.828	0.890	0.818	1.218
TiO2	0.364	0.372	0.169	0.195	0.232	0.204	0.235	0.183	0.208
ZrO2	0.000	0.000	0.507	0.612	0.472	0.566	0.665	0.473	0.507
Fe2O3	11.8497	15.0962	10.7372	9.6308	13.8319	9.9999	16.4885	15.6016	11.5596
FeO	14.8621	12.2287	13.5791	15.3508	11.6654	14.6436	9.6859	10.1639	12.6252
MnO	1.202	1.033	1.439	1.529	1.290	1.440	1.241	1.244	1.380
MgO	0.907	0.767	1.605	1.038	1.382	1.337	1.147	1.325	1.671
CaO	15.666	13.490	15.308	15.857	13.802	15.576	11.817	12.678	15.674
Na2O	4.738	6.143	5.021	4.593	6.049	4.763	7.159	6.733	5.068
Total	100.0068	100.1009	99.8064	99.5686	100.2623	99.4385	99.9934	99.9726	100.0757
Si	1.9760	1.9816	1.9917	1.9940	1.9885	1.9961	1.9872	1.9915	1.9769
Al	0.0377	0.0373	0.0500	0.0396	0.0411	0.0388	0.0411	0.0378	0.0565
Ti	0.0109	0.0110	0.0050	0.0058	0.0068	0.0061	0.0069	0.0054	0.0061
Zr	0.0000	0.0000	0.0112	0.0137	0.0104	0.0127	0.0146	0.0104	0.0112
Fe3+	0.3539	0.4471	0.3184	0.2885	0.4072	0.2989	0.4850	0.4591	0.3416
Fe2+	0.4933	0.4025	0.4475	0.5110	0.3817	0.4864	0.3166	0.3323	0.4146
Mn	0.0405	0.0345	0.0481	0.0516	0.0428	0.0485	0.0411	0.0413	0.0460
Mg	0.0542	0.0454	0.0952	0.0622	0.0814	0.0799	0.0675	0.0780	0.0988
Ca	0.6685	0.5709	0.6486	0.6786	0.5806	0.6652	0.4966	0.5330	0.6618
Na	0.3652	0.4696	0.3843	0.3551	0.4596	0.3674	0.5435	0.5113	0.3866
Di	5.6849	4.7731	9.7637	6.3470	8.4295	8.1378	6.9664	8.0989	10.4426
Hd	55.9963	45.8998	50.8241	57.4146	43.9627	54.4548	36.9289	38.7982	48.6910
Ac	38.3188	49.3271	39.4121	36.2384	47.6078	37.4074	56.1046	53.1029	40.8664

Sample No.	DAR186 N:8	DAR186 N:9	DAR186 N:10	DAR186 N:11	DAR186 N:12	DAR186 N:13	DAR186 N:14	DAR188 N:39	DAR188 N:40
SiO2	49.899	50.514	50.361	50.399	50.319	50.794	49.674	50.590	51.312
Al2O3	0.814	0.920	0.808	1.101	0.726	0.877	0.970	0.697	0.738
TiO2	0.202	0.194	0.246	0.165	0.197	0.187	0.173	0.221	0.172
ZrO2	0.531	0.463	0.897	0.405	0.663	0.430	0.268	0.696	1.045
Fe2O3	13.4139	14.5263	14.4685	9.9760	14.4828	13.2082	5.4463	14.1186	23.2468
FeO	12.0165	10.2786	12.3025	13.8431	12.0267	12.0486	17.8081	11.5494	4.5864
MnO	1.394	1.370	1.266	1.476	1.270	1.332	1.570	1.897	1.051
MgO	1.070	1.740	0.545	1.889	0.742	1.528	1.936	1.083	0.828
CaO	13.927	13.469	12.936	15.514	13.344	13.883	17.823	13.294	7.734
Na2O	5.846	6.240	6.471	4.782	6.286	5.901	3.045	6.213	9.762
Total	99.1134	99.7149	100.3011	99.5501	100.0565	100.1888	98.7135	100.3590	100.4752
Si	1.9880	1.9861	1.9872	1.9956	1.9884	1.9945	2.0022	1.9903	1.9838
Al	0.0382	0.0426	0.0375	0.0513	0.0338	0.0405	0.0462	0.0323	0.0336
Ti	0.0060	0.0057	0.0073	0.0049	0.0058	0.0055	0.0052	0.0065	0.0050
Zr	0.0119	0.0102	0.0198	0.0090	0.0147	0.0095	0.0061	0.0154	0.0227
Fe3+	0.4008	0.4283	0.4281	0.2962	0.4292	0.3889	0.1646	0.4165	0.6740
Fe2+	0.3990	0.3368	0.4045	0.4568	0.3960	0.3943	0.5982	0.3786	0.1478
Mn	0.0469	0.0455	0.0422	0.0494	0.0424	0.0442	0.0535	0.0631	0.0343
Mg	0.0639	0.1026	0.0323	0.1122	0.0440	0.0900	0.1170	0.0639	0.0480
Ca	0.5945	0.5674	0.5469	0.6582	0.5650	0.5841	0.7697	0.5604	0.3204
Na	0.4508	0.4749	0.4942	0.3665	0.4808	0.4485	0.2375	0.4731	0.7305
Di	6.6565	10.6921	3.3146	11.3922	4.5662	9.2124	11.6326	6.5301	4.9987
Hd	46.4166	39.8319	45.9048	51.3956	45.5200	44.8810	64.7596	45.1321	18.9572
Ac	46.9269	49.4761	50.7806	37.2121	49.9138	45.9065	23.6078	48.3379	76.0441

Sample No.	DAR188 N:41	DAR188 N:42	DAR188 N:43	DAR188 N:44	DAR188 N:45	DAR189 N:46	DAR189 N:47	DAR189 N:48	DAR189 N:49
SiO2	50.600	51.937	51.225	51.364	51.070	51.160	51.163	50.251	50.517
Al2O3	0.878	0.941	0.674	0.968	1.106	0.886	0.742	0.855	0.867
TiO2	0.288	0.126	0.196	0.414	0.526	0.250	0.177	0.248	0.243
ZrO2	0.997	0.466	1.131	1.390	0.844	0.752	0.642	0.523	0.463
Fe2O3	16.3927	26.4937	19.6405	23.0017	18.5681	21.4648	19.5934	12.2602	14.4579
FeO	9.5671	1.9967	6.7026	3.9260	6.9856	5.9280	6.9819	13.2527	11.1871
MnO	1.518	0.945	1.745	1.141	1.602	1.095	1.653	1.474	1.486
MgO	0.879	0.882	0.888	0.760	1.002	0.923	1.177	1.218	1.225
CaO	11.566	6.442	9.715	6.947	9.778	8.963	10.580	14.179	13.765
Na2O	7.339	10.748	8.578	10.239	8.469	9.020	8.096	5.534	6.147
Total	100.0248	100.9774	100.4951	100.1507	99.9506	100.4418	100.8053	99.7949	100.3580
Si	1.9868	1.9831	1.9907	1.9855	1.9889	1.9826	1.9829	1.9911	1.9834
Al	0.0406	0.0423	0.0308	0.0440	0.0507	0.0404	0.0338	0.0399	0.0400
Ti	0.0085	0.0036	0.0057	0.0120	0.0154	0.0073	0.0051	0.0074	0.0072
Zr	0.0220	0.0100	0.0246	0.0301	0.0184	0.0163	0.0140	0.0116	0.0102
Fe3+	0.4827	0.7586	0.5723	0.6667	0.5423	0.6238	0.5694	0.3643	0.4257
Fe2+	0.3130	0.0635	0.2171	0.1265	0.2267	0.1914	0.2255	0.4376	0.3660
Mn	0.0504	0.0305	0.0573	0.0373	0.0527	0.0359	0.0541	0.0494	0.0493
Mg	0.0518	0.0505	0.0518	0.0441	0.0585	0.0537	0.0684	0.0724	0.0721
Ca	0.4866	0.2635	0.4045	0.2877	0.4080	0.3722	0.4393	0.6020	0.5790
Na	0.5577	0.7943	0.6452	0.7661	0.6384	0.6765	0.6073	0.4244	0.4671
Di	5.3212	5.3807	5.3291	4.5250	5.9953	5.6035	7.1622	7.3588	7.5576
Hd	37.3526	10.0150	28.2465	16.8135	28.6206	23.7387	29.2701	49.4997	43.5085
Ac	57.3262	84.6043	66.4244	78.6614	65.3841	70.6578	63.5677	43.1415	48.9339

Sample No.	DAR189 N:50	DAR189 N:52	DAR189 N:53	DAR189 N:54	DAR189 N:55	DAR191 N:66	DAR191 N:67	DAR191 N:68	DAR191 N:69
SiO2	51.274	50.808	51.217	51.667	51.887	50.075	50.207	50.215	50.145
Al2O3	0.728	0.707	0.796	1.138	0.969	0.713	0.762	0.688	0.792
TiO2	0.150	0.145	0.171	0.440	0.169	0.319	0.367	0.351	0.365
ZrO2	0.454	0.532	0.614	0.441	0.448	0.703	1.158	0.806	0.886
Fe2O3	19.8896	18.0303	18.8341	21.0106	24.1127	12.5385	13.5812	12.3114	12.6825
FeO	6.7094	8.7705	7.8712	5.6807	3.9513	14.3293	13.4730	14.3487	13.9457
MnO	1.574	1.356	1.411	1.247	0.924	1.063	1.046	1.067	1.000
MgO	1.156	0.853	1.012	0.941	0.725	0.386	0.367	0.409	0.372
CaO	10.086	11.243	10.396	8.695	7.896	13.441	13.104	13.789	13.301
Na2O	8.313	7.604	8.081	9.230	9.983	5.913	6.311	5.860	6.107
Total	100.3340	100.0488	100.4033	100.4903	101.0650	99.4808	100.3762	99.8450	99.5962
Si	1.9919	1.9912	1.9929	1.9926	1.9874	1.9987	1.9859	1.9974	1.9968
Al	0.0333	0.0326	0.0364	0.0516	0.0437	0.0335	0.0355	0.0322	0.0371
Ti	0.0044	0.0043	0.0050	0.0127	0.0049	0.0095	0.0109	0.0105	0.0109
Zr	0.0099	0.0117	0.0134	0.0095	0.0096	0.0157	0.0257	0.0180	0.0198
Fe3+	0.5794	0.5299	0.5496	0.6076	0.6926	0.3753	0.4028	0.3672	0.3787
Fe2+	0.2172	0.2864	0.2552	0.1826	0.1261	0.4766	0.4441	0.4756	0.4628
Mn	0.0517	0.0449	0.0464	0.0406	0.0299	0.0359	0.0350	0.0359	0.0337
Mg	0.0674	0.0501	0.0591	0.0544	0.0417	0.0231	0.0218	0.0244	0.0222
Ca	0.4198	0.4721	0.4334	0.3593	0.3240	0.5748	0.5553	0.5877	0.5675
Na	0.6251	0.5768	0.6086	0.6890	0.7401	0.4568	0.4831	0.4512	0.4707
Di	7.0075	5.2328	6.0939	5.6317	4.4419	2.3288	2.2129	2.4724	2.2460
Hd	27.9705	34.5771	31.1184	23.0919	16.6384	51.6407	48.6857	51.8205	50.1781
Ac	65.0220	60.1901	62.7878	71.2764	78.9197	46.0306	49.1014	45.7072	47.5759

Sample No.	DAR191 N:70	DAR191 N:71	DAR191 N:72	DAR191 N:73
SiO2	50.234	49.914	50.101	50.281
Al2O3	0.734	0.782	0.744	0.806
TiO2	0.322	0.351	0.359	0.421
ZrO2	0.610	0.800	0.769	1.094
Fe2O3	13.5531	11.1006	12.1703	13.3073
FeO	13.6533	15.3102	14.6846	13.0125
MnO	1.074	1.143	1.051	1.029
MgO	0.422	0.363	0.375	0.307
CaO	13.417	14.232	13.699	12.531
Na2O	6.077	5.453	5.796	6.616
Total	100.0964	99.4488	99.7489	99.4048
Si	1.9914	1.9977	1.9963	2.0004
Al	0.0342	0.0368	0.0349	0.0377
Ti	0.0096	0.0105	0.0107	0.0126
Zr	0.0136	0.0180	0.0172	0.0244
Fe3+	0.4029	0.3332	0.3636	0.3970
Fe2+	0.4511	0.5106	0.4876	0.4314
Mn	0.0360	0.0387	0.0354	0.0346
Mg	0.0251	0.0218	0.0224	0.0183
Ca	0.5699	0.6103	0.5848	0.5341
Na	0.4663	0.4224	0.4470	0.5094
Di	2.5648	2.1935	2.2585	1.8463
Hd	49.7779	55.2888	52.6997	46.8927
Ac	47.6573	42.5177	45.0418	51.2638

Sample No.	52246 N:21	52246 N:22	52246 N:23	52246 N:24	52246 N:25	52246 N:26	58270 N:31	58270 N:32	58270 N:1
SiO2	49.643	49.155	49.265	49.731	49.625	49.023	49.743	49.284	48.640
Al2O3	0.822	0.871	0.775	0.849	0.896	0.819	0.908	1.000	0.908
TiO2	0.811	0.705	0.616	0.630	0.622	0.718	0.458	1.360	0.424
ZrO2	0.463	0.524	0.518	0.539	0.559	0.522	0.590	0.577	0.556
Fe2O3	18.8028	17.7478	16.1459	15.6502	15.9343	19.3044	16.6446	19.7842	16.8952
FeO	6.6804	6.1467	7.3481	7.7232	6.9526	5.4480	9.6704	7.1833	9.6019
MnO	0.834	0.983	1.013	0.970	0.991	0.915	0.994	0.899	1.002
MgO	2.204	3.148	3.310	3.305	3.639	2.811	1.252	0.764	1.241
CaO	12.437	14.044	15.158	14.550	14.647	13.119	13.319	10.680	13.452
Na2O	7.132	6.266	5.640	5.865	5.844	6.786	6.554	8.084	6.238
Total	99.8292	99.5905	99.7891	99.8124	99.7099	99.4654	100.1330	99.6154	98.9581
Si	1.9414	1.9246	1.9294	1.9427	1.9366	1.9222	1.9565	1.9399	1.9416
Al	0.0378	0.0401	0.0357	0.0390	0.0411	0.0378	0.0420	0.0463	0.0426
Ti	0.0238	0.0207	0.0181	0.0185	0.0182	0.0211	0.0135	0.0401	0.0127
Zr	0.0102	0.0115	0.0114	0.0118	0.0122	0.0115	0.0130	0.0127	0.0124
Fe3+	0.5514	0.5211	0.4742	0.4584	0.4663	0.5676	0.4909	0.5840	0.5057
Fe2+	0.2177	0.2006	0.2398	0.2514	0.2261	0.1780	0.3170	0.2356	0.3194
Mn	0.0276	0.0325	0.0335	0.0320	0.0327	0.0303	0.0330	0.0299	0.0338
Mg	0.1293	0.1849	0.1944	0.1937	0.2130	0.1653	0.0739	0.0451	0.0743
Ca	0.5211	0.5892	0.6360	0.6090	0.6124	0.5511	0.5613	0.4504	0.5753
Na	0.5398	0.4748	0.4275	0.4434	0.4414	0.5150	0.4989	0.6159	0.4820
Di	14.1393	20.7081	21.7186	21.0377	23.3261	18.6044	8.0045	4.8687	8.1704
Hd	26.8235	26.1064	30.5306	30.7905	28.3380	23.4436	37.9283	28.6589	38.8368
Ac	59.0372	53.1856	47.7508	48.1718	48.3359	57.9519	54.0672	66.4725	52.9928

Sample No.	58270 N:4	58270 N:5	58270 N:6	58270 N:7	155053 N:20	DAR123 N:12	DAR123 N:13	DAR123 N:14	DAR123 N:15
SiO2	49.859	49.820	48.502	48.854	48.892	51.796	52.491	52.472	51.764
Al2O3	0.886	0.763	1.788	0.773	0.781	0.891	0.913	0.956	0.867
TiO2	0.353	0.415	0.649	0.446	0.469	0.319	0.448	0.250	0.360
ZrO2	0.331	0.137	0.108	0.719	0.261	0.682	0.775	0.355	0.742
Fe2O3	13.2987	15.5144	3.4641	15.3012	20.4841	24.8946	28.4390	29.6384	25.2981
FeO	10.4492	9.1514	14.0539	10.9372	7.4595	3.7687	0.9412	0.0000	3.1466
MnO	0.934	0.919	0.812	1.144	0.874	0.587	0.441	0.480	0.611
MgO	2.740	2.573	6.536	1.106	0.528	0.639	0.424	0.460	0.653
CaO	15.566	14.566	21.835	14.236	12.193	7.118	5.275	5.667	6.983
Na2O	5.173	5.771	0.892	5.838	7.383	10.384	11.836	11.830	10.553
Total	99.5899	99.6298	98.6399	99.3545	99.3245	101.0793	101.9833	102.1084	100.9777
Si	1.9625	1.9580	1.9195	1.9489	1.9407	1.9835	1.9805	1.9750	1.9821
Al	0.0410	0.0353	0.0832	0.0363	0.0365	0.0401	0.0405	0.0423	0.0391
Ti	0.0104	0.0122	0.0193	0.0133	0.0140	0.0092	0.0127	0.0071	0.0103
Zr	0.0073	0.0030	0.0024	0.0161	0.0058	0.0146	0.0164	0.0075	0.0159
Fe3+	0.3925	0.4572	0.1028	0.4577	0.6097	0.7149	0.8046	0.8365	0.7264
Fe2+	0.3428	0.2997	0.4635	0.3636	0.2467	0.1203	0.0296	0.0000	0.1004
Mn	0.0311	0.0305	0.0272	0.0386	0.0293	0.0190	0.0141	0.0153	0.0198
Mg	0.1618	0.1517	0.3880	0.0662	0.0314	0.0367	0.0240	0.0260	0.0375
Ca	0.6565	0.6134	0.9258	0.6085	0.5186	0.2921	0.2132	0.2285	0.2865
Na	0.3941	0.4390	0.0683	0.4508	0.5672	0.7696	0.8643	0.8618	0.7821
Di	17.4011	16.4711	40.9725	7.2007	3.5940	3.8816	2.5748	2.8759	3.9909
Hd	40.2087	35.8604	51.8123	43.7558	31.5605	14.7272	4.6840	1.6907	12.7876
Ac	42.3903	47.6685	7.2151	49.0435	64.8455	81.3911	92.7412	95.4334	83.2215

Sample No.	DAR123 N:16	DAR123 N:17	DAR123 N:18	DAR123 N:1	DAR123 N:2	DAR123 N:3	DAR123 N:4	DAR123 N:5	DAR123 N:6
SiO2	52.032	53.530	51.581	51.699	52.446	51.780	51.801	51.678	52.212
Al2O3	0.826	3.535	0.906	0.860	0.897	0.815	0.800	0.802	1.101
TiO2	0.240	0.485	0.402	0.270	0.484	0.289	0.262	0.261	0.683
ZrO2	0.461	0.245	0.735	0.615	0.973	0.711	0.956	0.792	0.637
Fe2O3	26.9457	26.7957	25.1642	26.2620	29.3639	22.3973	22.8228	24.5778	27.0003
FeO	2.6940	0.0000	3.2821	2.8453	0.0000	5.9478	4.9890	4.2817	1.6098
MnO	0.485	0.340	0.704	0.599	0.450	0.612	0.588	0.543	0.503
MgO	0.441	0.084	0.686	0.503	0.426	0.486	0.639	0.421	0.617
CaO	6.558	0.215	7.910	7.113	3.036	8.386	7.996	7.775	5.796
Na2O	10.883	15.403	10.194	10.590	13.270	9.612	9.908	10.160	11.413
Total	101.5657	100.6327	101.5643	101.3562	101.3459	101.0362	100.7618	101.2915	101.5722
Si	1.9811	1.9691	1.9688	1.9751	1.9719	1.9927	1.9934	1.9810	1.9774
Al	0.0370	0.1530	0.0407	0.0387	0.0397	0.0369	0.0362	0.0362	0.0491
Ti	0.0069	0.0134	0.0115	0.0077	0.0136	0.0083	0.0076	0.0075	0.0194
Zr	0.0098	0.0051	0.0157	0.0132	0.0205	0.0153	0.0206	0.0170	0.0135
Fe3+	0.7693	0.7391	0.7203	0.7524	0.8279	0.6463	0.6586	0.7065	0.7668
Fe2+	0.0855	0.0000	0.1044	0.0906	0.0000	0.1907	0.1600	0.1368	0.0508
Mn	0.0156	0.0106	0.0227	0.0193	0.0143	0.0199	0.0191	0.0176	0.0161
Mg	0.0252	0.0046	0.0393	0.0288	0.0240	0.0281	0.0369	0.0242	0.0351
Ca	0.2675	0.0085	0.3235	0.2912	0.1223	0.3458	0.3297	0.3193	0.2352
Na	0.8020	1.0967	0.7531	0.7831	0.9657	0.7159	0.7380	0.7538	0.8366
Di	2.7133	0.4169	4.2716	3.1270	2.3930	2.9387	3.8665	2.5963	3.7346
Hd	10.8893	0.9506	13.8236	11.9246	1.4241	22.0655	18.7755	16.5562	7.1286
Ac	86.3974	98.6325	81.9048	84.9483	96.1829	74.9957	77.3580	80.8474	89.1368

Sample No.	DAR128 N:7	DAR128 N:8	DAR128 N:9	DAR128 N:10	DAR128 N:11	DAR128 N:12
SiO2	52.145	51.964	51.487	51.523	51.820	52.610
Al2O3	0.647	0.641	0.558	0.762	0.700	0.970
TiO2	0.377	0.373	0.353	0.392	0.353	0.360
ZrO2	0.385	0.293	0.302	0.260	0.334	0.470
Fe2O3	26.1349	27.6846	27.4068	27.1402	25.3395	29.6884
FeO	1.9096	0.7651	0.9420	1.1790	2.2113	0.0000
MnO	0.861	0.785	0.880	0.885	0.883	0.610
MgO	1.447	1.219	1.318	1.222	1.459	0.589
CaO	7.106	6.591	7.245	6.923	7.408	2.196
Na2O	10.473	10.906	10.502	10.587	10.219	13.418
Total	101.4855	101.2217	100.9939	100.8732	100.7268	100.9114
Si	1.9794	1.9754	1.9666	1.9687	1.9818	1.9803
Al	0.0289	0.0287	0.0251	0.0343	0.0315	0.0430
Ti	0.0107	0.0106	0.0101	0.0112	0.0101	0.0102
Zr	0.0082	0.0062	0.0065	0.0056	0.0072	0.0099
Fe3+	0.7439	0.7892	0.7850	0.7777	0.7267	0.8380
Fe2+	0.0604	0.0242	0.0300	0.0375	0.0705	0.0000
Mn	0.0276	0.0252	0.0284	0.0286	0.0285	0.0194
Mg	0.0824	0.0695	0.0755	0.0700	0.0837	0.0333
Ca	0.2890	0.2685	0.2965	0.2834	0.3036	0.0886
Na	0.7694	0.8024	0.7764	0.7830	0.7564	0.9775
Di	8.7662	7.5440	8.2955	7.6203	8.9122	3.2281
Hd	9.3657	5.3676	6.4144	7.1935	10.5431	1.8835
Ac	81.8681	87.0884	85.2901	85.1862	80.5447	94.8885

Sample No.	DAR67 N:1	DAR67 N:2	DAR67 N:3	DAR67 N:4D	DAR67 N:5L	DAR67 N:6L	DAR67 N:7D	DAR67 N:8L	DAR67 N:9D
SiO2	51.447	51.412	51.600	51.191	50.952	50.839	51.181	50.878	51.399
Al2O3	0.544	0.566	0.621	0.622	0.756	0.713	0.558	0.645	0.563
TiO2	0.135	0.126	0.133	0.169	0.140	0.137	0.112	0.142	0.145
ZrO2	0.045	0.048	0.056	0.012	0.158	0.210	0.086	0.147	0.039
Fe2O3	8.0863	6.7996	8.1926	7.5090	7.4131	7.0745	7.4140	6.6534	8.0861
FeO	12.1776	12.8334	11.7979	12.9681	13.9983	14.5580	12.6715	14.4140	11.7228
MnO	0.831	0.906	0.928	0.928	1.028	1.045	0.886	1.038	0.870
MgO	5.215	5.008	5.199	4.828	3.861	3.843	4.991	3.988	5.162
CaO	19.016	18.822	18.400	19.064	18.453	18.650	18.959	18.875	18.516
Na2O	3.236	3.202	3.514	3.117	3.371	3.177	3.153	3.093	3.473
Total	100.7329	99.7230	100.4415	100.4080	100.1304	100.2465	100.0115	99.8734	99.9758
Si	1.9866	2.0037	1.9935	1.9884	1.9939	1.9915	1.9926	1.9973	1.9949
Al	0.0247	0.0260	0.0282	0.0284	0.0348	0.0329	0.0256	0.0298	0.0257
Ti	0.0039	0.0037	0.0039	0.0049	0.0041	0.0040	0.0033	0.0042	0.0042
Zr	0.0010	0.0010	0.0012	0.0003	0.0035	0.0046	0.0019	0.0032	0.0008
Fe3+	0.2341	0.1987	0.2373	0.2187	0.2175	0.2078	0.2165	0.1959	0.2353
Fe2+	0.3919	0.4168	0.3798	0.4198	0.4565	0.4752	0.4111	0.4715	0.3791
Mn	0.0271	0.0298	0.0303	0.0305	0.0340	0.0346	0.0292	0.0344	0.0285
Mg	0.3021	0.2928	0.3013	0.2813	0.2266	0.2258	0.2915	0.2348	0.3005
Ca	0.7867	0.7860	0.7616	0.7934	0.7737	0.7827	0.7909	0.7939	0.7700
Na	0.2419	0.2415	0.2628	0.2343	0.2553	0.2409	0.2376	0.2350	0.2609
Di	31.3703	29.8456	30.9273	29.1243	23.3058	23.1243	30.0694	24.0654	31.0103
Hd	43.5124	45.5318	42.1001	46.6139	50.4386	52.2089	45.4197	51.8513	42.0687
Ac	25.1172	24.6227	26.9726	24.2618	26.2556	24.6668	24.5109	24.0833	26.9210

Sample No.	DAR67 N:10L	DAR67 N:11D	DAR67 N:12L	DAR67 N:13D	DAR67 N:14L	DAR67 N:15D	DAR67 N:16L	DAR67 N:17D	DAR67 N:18L
SiO2	50.802	51.517	50.874	51.404	50.867	51.765	50.987	51.539	50.855
Al2O3	0.719	0.488	0.720	0.568	0.689	0.595	0.752	0.525	0.707
TiO2	0.184	0.134	0.144	0.158	0.165	0.178	0.137	0.141	0.141
ZrO2	0.161	0.095	0.201	0.030	0.090	0.000	0.232	0.023	0.190
Fe2O3	6.7683	6.1160	7.2042	8.0844	7.1863	7.8920	6.8802	7.5253	7.9699
FeO	14.2385	13.3256	13.7813	12.0423	14.0985	12.1424	14.8719	12.9073	13.5883
MnO	0.996	0.881	0.969	0.848	1.089	0.863	1.062	0.896	1.006
MgO	3.965	5.104	4.033	5.169	4.050	5.179	3.609	4.952	3.991
CaO	18.609	19.197	18.492	18.649	18.702	18.559	18.494	18.815	18.523
Na2O	3.213	2.996	3.340	3.372	3.167	3.461	3.281	3.244	3.367
Total	99.6559	99.8535	99.7585	100.3247	100.1037	100.6344	100.3061	100.5677	100.2892
Si	1.9969	2.0064	1.9956	1.9908	1.9918	1.9964	1.9969	1.9958	1.9871
Al	0.0332	0.0224	0.0332	0.0259	0.0317	0.0270	0.0346	0.0239	0.0325
Ti	0.0054	0.0039	0.0042	0.0046	0.0048	0.0051	0.0040	0.0041	0.0041
Zr	0.0035	0.0021	0.0044	0.0007	0.0020	0.0000	0.0051	0.0005	0.0031
Fe3+	0.1995	0.1786	0.2119	0.2348	0.2110	0.2282	0.2021	0.2185	0.2335
Fe2+	0.4664	0.4325	0.4505	0.3887	0.4600	0.3902	0.4854	0.4165	0.4425
Mn	0.0331	0.0290	0.0321	0.0278	0.0360	0.0281	0.0351	0.0293	0.0332
Mg	0.2338	0.2982	0.2373	0.3003	0.2379	0.2996	0.2120	0.2876	0.2339
Ca	0.7837	0.8011	0.7772	0.7738	0.7846	0.7669	0.7760	0.7806	0.7755
Na	0.2444	0.2258	0.2536	0.2528	0.2400	0.2583	0.2487	0.2431	0.2546
Di	23.9111	30.2563	24.3761	30.9746	24.4234	30.6872	21.6069	29.4528	24.2595
Hd	51.0874	46.8274	49.5755	42.9528	50.9334	42.8516	53.0471	45.6514	49.3322
Ac	25.0015	22.9163	26.0484	26.0726	24.6432	26.4613	25.3460	24.8957	26.4083

Sample No.	DAR67 N:19D	DAR67 N:20L	DAR65 N:22	DAR65 N:23	DAR65 N:24D	DAR65 N:25L	DAR65 N:26L	DAR65 N:27D	DAR65 N:28L
SiO2	51.862	51.072	52.168	51.164	51.732	51.113	51.290	51.996	51.370
Al2O3	0.530	0.700	0.145	0.196	0.162	0.166	0.187	0.176	0.150
TiO2	0.143	0.144	0.727	0.595	0.589	0.712	0.785	0.724	0.738
ZrO2	0.034	0.065	0.095	0.066	0.070	0.062	0.100	0.063	0.078
Fe2O3	7.5754	6.8671	13.3107	6.5831	12.8785	7.6778	8.6449	15.3749	8.4569
FeO	11.6933	14.1036	10.1404	15.6783	10.1833	15.0832	14.6599	8.3999	14.3201
MnO	0.934	0.994	1.008	1.090	1.159	1.009	0.994	0.916	0.940
MgO	5.597	4.365	3.259	3.460	3.435	3.230	3.028	3.202	3.391
CaO	18.770	18.929	14.641	18.716	15.644	17.823	17.274	13.912	17.569
Na2O	3.345	3.047	5.913	3.208	5.382	3.699	4.089	6.482	3.960
Total	100.4837	100.2868	101.4071	100.7563	101.2348	100.5750	101.0518	101.2458	100.9730
Si	1.9984	1.9929	2.0018	2.0015	1.9924	2.0014	1.9985	1.9933	1.9991
Al	0.0240	0.0321	0.0065	0.0090	0.0073	0.0076	0.0086	0.0079	0.0069
Ti	0.0041	0.0042	0.0209	0.0175	0.0170	0.0209	0.0229	0.0208	0.0215
Zr	0.0007	0.0014	0.0020	0.0014	0.0015	0.0014	0.0022	0.0014	0.0017
Fe3+	0.2189	0.2009	0.3830	0.1931	0.3719	0.2254	0.2526	0.4420	0.2468
Fe2+	0.3755	0.4586	0.3243	0.5111	0.3268	0.4922	0.4760	0.2684	0.4644
Mn	0.0304	0.0328	0.0327	0.0360	0.0377	0.0334	0.0327	0.0297	0.0309
Mg	0.3235	0.2555	0.1876	0.2030	0.1984	0.1897	0.1770	0.1841	0.1979
Ca	0.7749	0.7914	0.6019	0.7844	0.6456	0.7477	0.7211	0.5714	0.7325
Na	0.2495	0.2301	0.4392	0.2429	0.4012	0.2803	0.3084	0.4810	0.2983
Di	33.0487	26.1503	19.0695	20.4448	20.5814	19.0550	17.8028	19.1181	19.9637
Hd	41.4658	50.2958	36.2868	55.0961	37.8095	52.7877	51.1766	30.9440	49.9544
Ac	25.4855	23.5539	44.6437	24.4591	41.6092	28.1572	31.0205	49.9373	30.0819

Sample No.	DAR65 N:29D	DAR65 N:30L	DAR65 N:31G	DAR65 N:32G	DAR65 N:33G	DAR65 N:34G	DAR65 N:35G	DAR65 N:36G	DAR65 N:37G
SiO2	51.936	51.053	52.974	52.639	52.791	53.007	52.680	52.881	52.689
Al2O3	0.222	0.167	0.286	0.224	0.270	0.210	0.205	0.248	0.244
TiO2	0.761	0.840	4.257	0.974	1.749	1.781	3.065	2.875	1.726
ZrO2	0.027	0.073	0.750	0.037	0.298	0.557	0.271	0.275	0.196
Fe2O3	14.5131	5.4698	25.7833	28.7371	21.7147	27.9759	24.2891	26.7644	26.9780
FeO	9.0744	17.2230	0.1320	0.0000	4.2581	0.0000	2.2115	0.6871	0.1949
MnO	1.024	1.019	0.427	0.325	0.409	0.345	0.376	0.384	0.461
MgO	3.372	3.027	1.183	1.617	2.135	1.324	1.369	1.267	1.776
CaO	14.464	18.447	2.794	4.816	7.903	3.969	5.327	4.744	5.659
Na2O	6.081	3.153	13.265	11.980	9.999	12.584	11.679	12.222	11.577
Total	101.4745	100.4718	101.8513	101.3491	101.5268	101.7529	101.4726	102.3475	101.5009
Si	1.9895	2.0091	1.9772	1.9817	1.9961	1.9859	1.9858	1.9752	1.9827
Al	0.0100	0.0077	0.0126	0.0099	0.0120	0.0093	0.0091	0.0109	0.0108
Ti	0.0219	0.0248	0.1192	0.0275	0.0496	0.0500	0.0867	0.0805	0.0487
Zr	0.0006	0.0016	0.0157	0.0008	0.0063	0.0117	0.0057	0.0058	0.0041
Fe3+	0.4169	0.1614	0.7216	0.8113	0.6157	0.7860	0.6866	0.7497	0.7613
Fe2+	0.2897	0.5648	0.0041	0.0000	0.1342	0.0000	0.0695	0.0214	0.0061
Mn	0.0331	0.0339	0.0135	0.0103	0.0131	0.0109	0.0120	0.0121	0.0147
Mg	0.1938	0.1787	0.0662	0.0913	0.1211	0.0744	0.0774	0.0710	0.1002
Ca	0.5937	0.7778	0.1117	0.1943	0.3202	0.1593	0.2152	0.1899	0.2282
Na	0.4509	0.2402	0.9583	0.8729	0.7318	0.9125	0.8521	0.8836	0.8432
Di	20.0277	17.5602	6.3558	9.3695	12.1080	7.4567	7.6570	7.1844	10.3969
Hd	33.3691	58.8382	1.6865	1.0609	14.7226	1.0947	8.0566	3.3914	2.1543
Ac	46.6032	23.6015	91.9578	89.5696	73.1694	91.4486	84.2864	89.4242	87.4488

Sample No.	DAR65 N:38G	DAR65 N:39G	DAR65 N:40G	DAR66 N:41G	DAR66 N:43G	DAR66 N:1G	DAR66 N:3G	DAR66 N:5G	DAR66 N:6G
SiO2	52.673	53.037	52.791	52.591	53.156	53.315	53.808	52.951	52.554
Al2O3	0.266	0.263	0.237	0.236	0.440	0.250	0.346	0.339	0.197
TiO2	1.849	2.630	0.906	1.381	2.457	1.442	0.617	0.720	1.198
ZrO2	0.410	0.330	0.023	0.350	N.A.	0.475	0.057	0.530	0.202
Fe2O3	27.1168	23.1810	28.2970	30.3518	29.4306	29.7795	11.5111	10.5852	30.6430
FeO	0.0000	2.8407	0.0000	0.0000	0.0000	0.0000	18.1548	19.9829	0.0000
MnO	0.389	0.421	0.372	0.241	0.251	0.210	0.089	0.071	0.019
MgO	1.662	1.664	1.627	0.442	0.270	0.751	4.944	4.015	0.728
CaO	5.098	5.977	5.000	2.755	0.196	0.163	0.024	0.022	0.148
Na2O	12.093	11.256	11.938	12.979	14.936	14.745	8.178	8.016	13.892
Total	101.5568	101.5996	101.1910	101.3268	101.1636	100.6555	97.7289	97.2321	99.5810
Si	1.9760	1.9958	1.9884	1.9883	1.9802	1.9924	2.1139	2.1096	2.0034
Al	0.0117	0.0116	0.0105	0.0105	0.0193	0.0110	0.0160	0.0159	0.0088
Ti	0.0520	0.0742	0.0256	0.0392	0.0686	0.0404	0.0182	0.0215	0.0343
Zr	0.0086	0.0070	0.0005	0.0074	0.0000	0.0000	0.0013	0.0118	0.0043
Fe3+	0.7628	0.6541	0.7992	0.8605	0.8221	0.8345	0.3391	0.3162	0.8759
Fe2+	0.0000	0.0891	0.0000	0.0000	0.0000	0.0000	0.5944	0.6635	0.0000
Mn	0.0123	0.0134	0.0118	0.0077	0.0079	0.0066	0.0030	0.0024	0.0006
Mg	0.0935	0.0939	0.0919	0.0251	0.0151	0.0421	0.2913	0.2399	0.0416
Ca	0.2049	0.2410	0.2018	0.1116	0.0078	0.0065	0.0010	0.0009	0.0060
Na	0.8780	0.8198	0.8703	0.9497	1.0789	1.0665	0.6218	0.6181	1.0250
Di	9.5053	9.2428	9.4371	2.5512	1.3693	3.7748	19.2881	15.7452	3.9006
Hd	1.2534	10.0834	1.2156	0.7837	0.7171	0.5947	39.5443	43.6929	0.0574
Ac	89.2413	80.6738	89.3473	96.6651	97.9136	95.6305	41.1676	40.5619	96.0421

Sample No.	DAR66 N:7G
SiO2	53.345
Al2O3	2.149
TiO2	1.764
ZrO2	0.052
Fe2O3	27.6269
FeO	0.0000
MnO	0.197
MgO	0.411
CaO	0.051
Na2O	14.818
Total	100.4139
Si	1.9857
Al	0.0941
Ti	0.0492
Zr	0.0011
Fe3+	0.7711
Fe2+	0.0000
Mn	0.0062
Mg	0.0229
Ca	0.0020
Na	1.0676
Di	2.0925
Hd	0.5650
Ac	97.3425

AMPHIBOLES

Sample No.	DAR 140 1	DAR 140 2	DAR 140 3	DAR 140 4	DAR 140 5	DAR 140 6	DAR 140 7	DAR 140 8	DAR 140 9
SiO2	44.36	44.47	44.32	44.35	44.61	44.28	44.58	44.46	44.79
Al2O3	4.79	4.81	4.80	4.77	4.73	4.81	4.68	4.79	5.07
TiO2	1.08	1.16	1.08	1.07	1.02	1.08	1.24	1.26	1.13
FeOT	30.47	30.58	30.50	30.72	30.82	30.64	30.34	30.58	30.01
MnO	1.43	1.43	1.44	1.44	1.41	1.37	1.39	1.39	1.33
MgO	1.41	1.45	1.43	1.44	1.51	1.49	1.51	1.43	1.35
CaO	5.58	5.63	5.82	5.60	5.57	5.44	5.54	5.50	4.45
Na2O	6.18	6.14	6.02	6.09	6.17	6.13	6.15	6.27	6.74
K2O	1.62	1.66	1.65	1.62	1.61	1.62	1.64	1.61	1.73
F	N.A.	N.A.	0.800	0.772	0.744	0.929	1.064	0.917	0.485
Total	96.92	97.33	97.06	97.10	97.45	96.86	97.07	97.29	96.60
Si	7.24	7.23	7.23	7.22	7.23	7.22	7.26	7.23	7.29
Al	0.92	0.92	0.92	0.92	0.90	0.92	0.90	0.92	0.97
Ti	0.13	0.14	0.13	0.13	0.12	0.13	0.15	0.15	0.14
Fe3+	0.08	0.09	0.06	0.16	0.17	0.20	0.06	0.08	0.12
Fe2+	4.08	4.06	4.10	4.02	4.01	3.97	4.07	4.07	3.96
Mn	0.20	0.20	0.20	0.20	0.19	0.19	0.19	0.19	0.18
Mg	0.34	0.35	0.35	0.35	0.36	0.36	0.37	0.35	0.33
Ca	0.98	0.98	1.02	0.98	0.97	0.95	0.97	0.96	0.78
Na	1.96	1.94	1.91	1.92	1.94	1.94	1.94	1.98	2.13
K	0.34	0.34	0.34	0.34	0.33	0.34	0.34	0.33	0.36
F	N.A.	N.A.	0.4133	0.3991	0.3832	0.4807	0.5488	0.4723	0.2506

Sample No.	DAR 140 10	DAR 140 11	DAR 185 12	DAR 185 13	DAR 185 14	DAR 185 15	DAR 185 16	DAR 185 17	DAR 185 18
SiO2	44.69	44.53	41.86	42.90	41.59	42.27	43.89	41.61	41.74
Al2O3	4.87	4.82	7.11	6.64	7.30	7.16	5.86	7.35	7.37
TiO2	1.29	1.10	0.95	0.95	0.90	1.01	1.02	0.92	0.92
FeOT	30.45	30.27	28.69	28.57	27.24	27.68	28.41	28.05	28.36
MnO	1.41	1.42	1.84	1.83	1.84	1.83	1.93	2.06	2.02
MgO	1.63	1.40	2.39	2.52	2.75	2.93	2.26	2.45	2.36
CaO	4.99	5.33	6.72	6.55	8.36	7.54	5.80	8.89	8.60
Na2O	6.57	6.30	5.36	5.52	5.04	5.02	5.89	4.17	4.41
K2O	1.69	1.68	1.71	1.76	1.58	1.58	1.74	1.58	1.56
F	0.930	0.746	0.421	0.387	1.935	1.068	0.776	0.728	0.505
Total	97.59	96.85	96.63	97.24	96.60	97.02	96.80	97.08	97.34
Si	7.22	7.27	6.80	6.92	6.80	6.82	7.10	6.78	6.78
Al	0.93	0.93	1.36	1.26	1.41	1.36	1.12	1.41	1.41
Ti	0.16	0.13	0.12	0.11	0.11	0.12	0.12	0.11	0.11
Fe3+	0.19	0.06	0.43	0.32	0.00	0.24	0.21	0.06	0.10
Fe2+	3.92	4.07	3.46	3.53	3.72	3.50	3.64	3.76	3.74
Mn	0.19	0.20	0.25	0.25	0.25	0.25	0.26	0.28	0.28
Mg	0.39	0.34	0.58	0.61	0.67	0.70	0.54	0.59	0.57
Ca	0.86	0.93	1.17	1.13	1.46	1.30	1.01	1.55	1.50
Na	2.06	1.99	1.69	1.73	1.60	1.57	1.85	1.32	1.39
K	0.35	0.35	0.35	0.36	0.33	0.32	0.36	0.33	0.32
F	0.4773	0.3854	0.2179	0.1986	1.0001	0.5481	0.3990	0.3754	0.2599

Sample No.	DAR 185 19	DAR 185 20	DAR 185 21	DAR 185 22	DAR 185 23	DAR 185 24	DAR 185 25	DAR 185 26	DAR 185 27
SiO2	43.13	42.28	41.39	41.06	40.96	41.31	42.52	43.08	43.29
Al2O3	6.60	6.90	7.76	8.29	7.99	7.91	6.96	6.47	6.51
TiO2	0.96	0.95	0.91	0.88	0.87	0.89	1.57	1.10	1.18
FeOT	28.00	28.74	27.88	27.97	28.38	28.52	27.83	28.02	28.20
MnO	2.01	1.92	1.86	1.84	1.77	1.76	1.77	1.82	1.77
MgO	2.49	2.43	2.68	2.62	2.51	2.55	3.03	2.95	2.81
CaO	7.31	7.35	9.15	9.14	8.47	8.13	7.30	6.49	6.85
Na2O	5.05	5.12	3.97	4.01	4.48	4.56	5.27	5.55	5.51
K2O	1.64	1.61	1.59	1.56	1.56	1.59	1.60	1.73	1.57
F	0.711	0.611	0.547	0.699	0.407	0.347	0.771	0.566	0.671
Total	97.19	97.30	97.19	97.37	96.99	97.22	97.85	97.21	97.69
Si	6.97	6.84	6.72	6.64	6.66	6.68	6.81	6.92	6.94
Al	1.26	1.32	1.48	1.58	1.53	1.51	1.31	1.23	1.23
Ti	0.12	0.12	0.11	0.11	0.11	0.11	0.19	0.13	0.14
Fe3+	0.12	0.30	0.10	0.17	0.26	0.35	0.22	0.35	0.22
Fe2+	3.66	3.58	3.68	3.61	3.59	3.50	3.50	3.42	3.55
Mn	0.28	0.26	0.26	0.25	0.24	0.24	0.24	0.25	0.24
Mg	0.60	0.59	0.65	0.63	0.61	0.61	0.72	0.71	0.67
Ca	1.27	1.27	1.59	1.58	1.47	1.41	1.25	1.12	1.18
Na	1.58	1.61	1.25	1.26	1.41	1.43	1.64	1.73	1.71
K	0.34	0.33	0.33	0.32	0.32	0.33	0.33	0.35	0.32
F	0.3643	0.3144	0.2814	0.3590	0.2101	0.1788	0.3922	0.2895	0.3416

Sample No.	DAR 185 28	DAR 185 29	DAR 185 30	DAR 185 31	DAR 185 32	DAR 185 33	DAR 185 34	DAR 185 35	DAR 186 36
SiO2	43.77	43.31	41.55	42.71	42.78	43.26	42.47	42.51	43.44
Al2O3	6.31	6.30	7.88	6.84	6.81	6.59	7.00	7.88	5.71
TiO2	1.25	1.20	1.02	0.97	0.91	1.00	0.91	0.92	1.05
FeOT	27.79	28.20	28.24	28.15	27.41	26.99	28.27	27.59	29.37
MnO	1.79	1.98	1.80	1.83	1.89	1.85	1.91	1.84	1.79
MgO	3.07	2.77	2.61	2.84	3.20	3.31	2.58	2.64	1.89
CaO	6.52	7.04	8.14	7.32	8.25	7.50	7.24	7.64	6.30
Na2O	5.66	5.40	4.76	5.23	4.57	5.10	5.27	5.00	5.71
K2O	1.62	1.59	1.56	1.60	1.57	1.54	1.56	1.53	1.70
F	0.640	0.738	0.735	0.624	0.830	0.644	0.681	0.526	0.424
Total	97.78	97.79	97.56	97.49	97.39	97.14	97.21	97.55	96.96
Si	6.98	6.95	6.70	6.87	6.88	6.96	6.86	6.82	7.07
Al	1.19	1.19	1.50	1.30	1.29	1.25	1.33	1.49	1.10
Ti	0.15	0.14	0.12	0.12	0.11	0.12	0.11	0.11	0.13
Fe3+	0.24	0.19	0.24	0.25	0.13	0.11	0.25	0.16	0.15
Fe2+	3.47	3.59	3.57	3.54	3.56	3.52	3.56	3.54	3.85
Mn	0.24	0.27	0.25	0.25	0.26	0.25	0.26	0.25	0.25
Mg	0.73	0.66	0.63	0.68	0.77	0.79	0.62	0.63	0.46
Ca	1.11	1.21	1.41	1.26	1.42	1.29	1.25	1.31	1.10
Na	1.75	1.68	1.49	1.63	1.43	1.59	1.65	1.55	1.80
K	0.33	0.33	0.32	0.33	0.32	0.32	0.32	0.31	0.35
F	0.3243	0.3759	0.3764	0.3189	0.4237	0.3282	0.3499	0.2676	0.2192

Sample No.	DAR 186 37	DAR 186 38	DAR 186 39	DAR 186 40	DAR 186 41	DAR 186 42	DAR 186 43	DAR 186 44	DAR 186 45
SiO2	42.87	43.22	43.10	42.74	43.68	43.27	43.05	43.07	43.42
Al2O3	6.01	5.97	5.90	6.30	5.51	5.77	5.98	5.84	5.71
TiO2	0.99	1.01	0.96	0.90	1.02	0.91	0.92	1.08	0.89
FeOT	29.86	29.68	29.86	28.85	29.89	29.81	29.86	30.01	30.16
MnO	1.79	1.66	1.68	1.78	1.83	1.90	1.98	1.93	1.87
MgO	1.70	1.68	1.68	2.36	1.64	1.51	1.62	1.26	1.37
CaO	7.38	6.08	7.01	8.11	5.67	6.59	7.01	5.83	6.15
Na2O	5.11	5.70	5.26	4.70	5.99	5.47	5.21	5.72	5.71
K2O	1.62	1.73	1.62	1.60	1.69	1.63	1.60	1.76	1.71
F	0.764	0.591	0.525	0.735	0.657	0.514	0.772	0.620	0.746
Total	97.33	96.73	97.07	97.34	96.92	96.86	97.23	96.50	96.99
Si	6.99	7.05	7.03	6.95	7.10	7.07	7.01	7.05	7.09
Al	1.16	1.15	1.14	1.21	1.06	1.11	1.15	1.13	1.10
Ti	0.12	0.12	0.12	0.11	0.12	0.11	0.11	0.13	0.11
Fe3+	0.09	0.23	0.11	0.04	0.27	0.14	0.19	0.27	0.20
Fe2+	3.98	3.82	3.96	3.88	3.80	3.93	3.88	3.84	3.92
Mn	0.25	0.23	0.23	0.25	0.25	0.26	0.27	0.27	0.26
Mg	0.41	0.41	0.41	0.57	0.40	0.37	0.39	0.31	0.33
Ca	1.29	1.06	1.23	1.41	0.99	1.15	1.22	1.02	1.08
Na	1.62	1.80	1.66	1.48	1.89	1.73	1.64	1.82	1.81
K	0.34	0.36	0.34	0.33	0.35	0.34	0.33	0.37	0.36
F	0.3950	0.3601	0.2715	0.3779	0.3401	0.2663	0.3990	0.3227	0.3866

Sample No.	DAR 186 46	DAR 186 47	DAR 186 48	DAR 187 49	DAR 187 50	DAR 187 51	DAR 187 52	DAR 187 53	DAR 187 54
SiO2	43.58	43.14	43.66	42.04	40.62	41.27	41.92	41.24	41.93
Al2O3	5.57	5.73	5.51	6.84	8.23	8.05	7.36	7.93	7.33
TiO2	0.97	1.01	1.05	0.98	1.01	1.04	1.06	0.89	1.05
FeOT	30.15	30.52	30.10	27.61	28.53	28.33	28.04	28.28	28.06
MnO	1.92	1.90	1.84	2.21	2.06	1.98	2.11	2.03	2.02
MgO	1.38	1.23	1.54	2.76	2.35	2.46	2.65	2.48	2.68
CaO	6.41	6.55	6.25	7.78	7.80	7.65	7.32	7.86	7.11
Na2O	5.47	5.38	5.72	4.78	4.77	4.86	5.13	4.76	5.26
K2O	1.60	1.61	1.57	1.59	1.60	1.59	1.61	1.55	1.65
F	0.606	0.575	0.591	0.510	0.504	0.611	0.478	0.466	0.597
Total	97.05	97.07	97.24	96.59	96.97	97.23	97.20	97.02	97.09
Si	7.10	7.04	7.10	6.84	6.58	6.66	6.76	6.67	6.77
Al	1.07	1.10	1.06	1.31	1.57	1.53	1.40	1.51	1.40
Ti	0.12	0.12	0.13	0.12	0.12	0.13	0.13	0.11	0.13
Fe3+	0.19	0.23	0.18	0.22	0.47	0.41	0.35	0.38	0.37
Fe2+	3.92	3.94	3.91	3.53	3.40	3.41	3.43	3.44	3.42
Mn	0.26	0.26	0.25	0.30	0.28	0.27	0.29	0.28	0.28
Mg	0.33	0.30	0.37	0.67	0.57	0.59	0.64	0.60	0.64
Ca	1.12	1.15	1.09	1.36	1.36	1.32	1.27	1.36	1.23
Na	1.73	1.70	1.80	1.51	1.50	1.52	1.61	1.49	1.65
K	0.33	0.33	0.33	0.33	0.33	0.33	0.33	0.32	0.34
F	0.3137	0.2981	0.3052	0.2637	0.2611	0.3143	0.2457	0.2403	0.3072

Sample No.	DAR 187 55	DAR 187 56	DAR 187 57	DAR 187 58	DAR 187 59	DAR 187 60	DAR 187 61
SiO2	40.96	40.92	42.11	40.69	42.81	41.53	41.59
Al2O3	7.93	8.13	6.98	8.58	6.70	7.39	7.60
TiO2	1.02	1.02	1.16	0.88	1.02	0.98	1.02
FeOT	28.21	28.25	27.86	28.00	27.43	27.91	28.03
MnO	2.11	2.04	2.11	2.01	2.12	2.11	2.08
MgO	2.46	2.34	2.67	2.42	2.83	2.57	2.47
CaO	7.54	7.69	7.12	8.21	6.76	7.59	7.40
Na2O	4.82	4.81	5.24	4.52	5.52	4.97	5.06
K2O	1.60	1.61	1.68	1.55	1.62	1.61	1.63
F	0.422	0.627	0.512	0.500	0.575	0.578	0.518
Total	96.65	96.81	96.93	96.86	96.81	96.66	96.88
Si	6.65	6.64	6.82	6.60	6.92	6.75	6.74
Al	1.52	1.56	1.33	1.64	1.28	1.42	1.45
Ti	0.12	0.12	0.14	0.11	0.12	0.12	0.12
Fe3+	0.47	0.39	0.28	0.36	0.23	0.29	0.32
Fe2+	3.35	3.44	3.49	3.44	3.48	3.51	3.48
Mn	0.29	0.28	0.29	0.28	0.29	0.29	0.29
Mg	0.59	0.57	0.64	0.58	0.68	0.62	0.60
Ca	1.31	1.34	1.23	1.43	1.17	1.32	1.29
Na	1.52	1.51	1.65	1.42	1.73	1.57	1.59
K	0.33	0.33	0.35	0.32	0.33	0.33	0.34
F	0.2190	0.3245	0.2636	0.2585	0.2952	0.2991	0.2672

Sample No.	DAR 187 62	DAR 187 63	DAR 187 64	DAR 187 65	DAR 188 66	DAR 188 67	DAR 188 68	DAR 188 69	DAR 188 70
SiO2	42.15	41.78	41.05	40.78	43.53	43.14	42.66	42.92	43.43
Al2O3	7.14	7.41	7.66	8.15	6.08	6.29	6.53	6.33	5.99
TiO2	0.81	0.88	0.99	0.96	1.84	1.84	1.91	1.91	1.85
FeOT	27.84	28.13	28.06	28.36	27.74	27.61	27.77	27.73	27.61
MnO	2.17	2.10	2.17	2.10	1.98	2.05	1.98	2.02	2.03
MgO	2.70	2.71	2.51	2.39	2.65	2.43	2.35	2.45	2.58
CaO	7.05	7.35	8.00	7.63	6.05	6.21	6.33	6.35	6.35
Na2O	5.22	5.07	4.69	4.90	6.12	5.91	5.79	5.71	5.71
K2O	1.56	1.57	1.57	1.63	1.61	1.59	1.63	1.59	1.57
F	0.549	0.253	0.373	0.633	0.475	0.473	0.557	0.692	0.602
Total	96.64	97.00	96.70	96.90	97.60	97.07	96.95	97.01	97.12
Si	6.82	6.75	6.68	6.61	7.00	6.98	6.91	6.94	7.01
Al	1.36	1.41	1.47	1.56	1.15	1.20	1.25	1.21	1.14
Ti	0.10	0.11	0.12	0.12	0.22	0.22	0.23	0.23	0.22
Fe3+	0.39	0.43	0.33	0.45	0.09	0.07	0.10	0.12	0.08
Fe2+	3.38	3.37	3.49	3.39	3.63	3.67	3.66	3.63	3.64
Mn	0.30	0.29	0.30	0.29	0.27	0.28	0.27	0.28	0.28
Mg	0.65	0.65	0.61	0.58	0.63	0.59	0.57	0.59	0.62
Ca	1.22	1.27	1.40	1.33	1.04	1.08	1.10	1.10	1.10
Na	1.64	1.59	1.48	1.54	1.91	1.85	1.82	1.79	1.79
K	0.32	0.32	0.33	0.34	0.33	0.33	0.34	0.33	0.32
F	0.2834	0.1303	0.1934	0.3277	0.2420	0.2424	0.2862	0.3551	0.3081

Sample No.	DAR 188 71	DAR 188 72	DAR 188 73	DAR 188 74	DAR 188 75	DAR 188 76	DAR 188 77	DAR 188 78	DAR 188 79
SiO2	43.32	43.34	43.17	41.84	43.35	42.76	43.09	43.25	43.13
Al2O3	6.14	6.23	6.30	7.07	5.94	6.54	6.12	6.13	6.14
TiO2	1.87	1.84	1.87	1.98	1.88	1.91	1.86	1.84	1.76
FeOT	27.66	27.52	27.86	28.17	27.42	27.73	27.62	27.78	27.62
MnO	2.00	2.02	2.02	1.98	2.01	1.97	2.02	2.07	2.06
MgO	2.55	2.50	2.51	2.37	2.59	2.44	2.60	2.58	2.59
CaO	6.08	6.11	6.19	6.68	6.03	6.48	6.27	6.02	6.35
Na2O	6.02	5.80	5.90	5.57	5.85	5.76	5.76	5.97	5.75
K2O	1.60	1.61	1.58	1.58	1.67	1.62	1.56	1.63	1.59
F	1.011	0.863	0.738	0.466	0.687	0.710	0.538	0.733	0.545
Total	97.24	96.97	97.40	97.24	96.74	97.21	96.90	97.27	96.99
Si	6.99	7.00	6.95	6.76	7.02	6.91	6.97	6.97	6.97
Al	1.17	1.19	1.20	1.35	1.13	1.25	1.17	1.16	1.17
Ti	0.23	0.22	0.23	0.24	0.23	0.23	0.23	0.22	0.21
Fe3+	0.09	0.11	0.15	0.26	0.09	0.07	0.14	0.17	0.12
Fe2+	3.64	3.60	3.60	3.55	3.62	3.67	3.59	3.57	3.61
Mn	0.27	0.28	0.28	0.27	0.28	0.27	0.28	0.28	0.28
Mg	0.61	0.60	0.60	0.57	0.63	0.59	0.63	0.62	0.62
Ca	1.05	1.06	1.07	1.16	1.05	1.12	1.09	1.04	1.10
Na	1.88	1.82	1.84	1.75	1.84	1.81	1.81	1.87	1.80
K	0.33	0.33	0.32	0.33	0.35	0.33	0.32	0.33	0.33
F	0.5167	0.4419	0.3772	0.2397	0.3525	0.3637	0.2762	0.3749	0.2794

Sample No.	DAR 189 80	DAR 189 81	DAR 189 82	DAR 189 83	DAR 189 84	DAR 189 85	DAR 189 86	DAR 189 87	DAR 189 88
SiO2	43.69	42.93	42.75	42.82	43.31	44.08	43.89	42.80	43.88
Al2O3	5.79	6.25	6.48	6.34	6.18	6.58	5.60	6.54	5.62
TiO2	1.26	1.21	1.09	1.24	1.08	1.21	1.37	1.09	1.33
FeOT	29.02	28.94	28.84	29.19	28.74	28.53	28.81	28.83	28.64
MnO	1.78	1.78	1.83	1.73	1.81	1.67	1.75	1.79	1.77
MgO	2.27	2.29	2.40	2.16	2.46	2.19	2.28	2.30	2.33
CaO	6.40	7.03	7.27	6.63	7.21	5.45	5.94	7.23	6.16
Na2O	5.77	5.33	5.10	5.58	5.15	6.73	5.92	5.14	5.90
K2O	1.60	1.56	1.57	1.59	1.59	1.76	1.58	1.58	1.59
F	0.827	0.467	0.602	0.829	0.740	0.475	0.810	0.872	0.880
Total	97.58	97.32	97.33	97.28	97.53	98.20	97.14	97.30	97.22
Si	7.05	6.95	6.91	6.93	6.98	7.05	7.09	6.92	7.09
Al	1.10	1.19	1.23	1.21	1.18	1.24	1.07	1.25	1.07
Ti	0.15	0.15	0.13	0.15	0.13	0.15	0.17	0.13	0.16
Fe3+	0.16	0.18	0.25	0.25	0.17	0.05	0.19	0.20	0.11
Fe2+	3.75	3.73	3.65	3.70	3.70	3.76	3.70	3.70	3.76
Mn	0.24	0.24	0.25	0.24	0.25	0.23	0.24	0.25	0.24
Mg	0.55	0.55	0.58	0.52	0.59	0.52	0.55	0.55	0.56
Ca	1.11	1.22	1.26	1.15	1.25	0.93	1.03	1.25	1.07
Na	1.80	1.67	1.60	1.75	1.61	2.09	1.85	1.61	1.85
K	0.33	0.32	0.32	0.33	0.33	0.36	0.33	0.33	0.33
F	0.4230	0.2402	0.3091	0.4266	0.3785	0.2405	0.4151	0.4480	0.4508

Sample No.	DAR 189 89	DAR 189 90	DAR 189 91	DAR 189 92	DAR 189 93	DAR 190 94	DAR 190 95	DAR 190 96	DAR 190 97
SiO2	42.77	43.16	43.26	42.74	42.87	40.73	41.51	41.22	41.10
Al2O3	6.68	6.34	6.25	6.61	6.34	7.78	7.16	7.41	7.53
TiO2	1.08	1.21	1.21	1.15	1.28	1.13	1.34	1.22	1.26
FeOT	29.06	28.95	28.99	29.11	29.23	30.06	30.00	29.70	30.00
MnO	1.77	1.78	1.71	1.77	1.70	1.49	1.48	1.47	1.45
MgO	2.24	2.23	2.33	2.17	2.09	1.67	1.68	1.79	1.63
CaO	6.73	6.16	5.89	6.63	6.74	8.72	8.24	8.77	8.23
Na2O	5.65	5.90	6.12	5.62	5.56	4.17	4.57	4.22	4.50
K2O	1.57	1.60	1.60	1.60	1.58	1.59	1.59	1.59	1.65
F	0.677	0.714	0.914	0.615	0.534	0.741	0.827	0.769	0.563
Total	97.55	97.33	97.36	97.40	97.39	97.34	97.57	97.39	97.35
Si	6.90	6.96	6.97	6.91	6.94	6.65	6.76	6.73	6.71
Al	1.27	1.21	1.19	1.26	1.21	1.50	1.38	1.43	1.45
Ti	0.13	0.15	0.15	0.14	0.16	0.14	0.16	0.15	0.15
Fe3+	0.25	0.27	0.31	0.27	0.19	0.23	0.12	0.08	0.18
Fe2+	3.66	3.63	3.60	3.66	3.77	3.88	3.96	3.98	3.91
Mn	0.24	0.24	0.23	0.40	0.30	0.10	0.00	0.00	0.00
Mg	0.54	0.54	0.56	0.52	0.50	0.41	0.41	0.44	0.40
Ca	1.16	1.06	1.02	1.15	1.17	1.52	1.44	1.53	1.44
Na	1.77	1.84	1.91	1.76	1.75	1.32	1.44	1.34	1.42
K	0.32	0.33	0.33	0.33	0.33	0.33	0.33	0.33	0.34
F	0.3471	0.3663	0.4689	0.3162	0.2746	0.3845	0.4271	0.3980	0.2915

Sample No.	DAR 190 98	DAR 190 99	DAR 190 100	DAR 190 101	DAR 190 102	DAR 190 103	DAR 190 104	DAR 190 105	DAR 190 106
SiO2	40.48	40.57	41.64	41.31	40.84	40.77	41.56	41.09	40.87
Al2O3	8.12	7.81	7.26	7.36	7.87	7.78	7.27	7.40	7.61
TiO2	1.08	1.13	0.94	1.16	1.18	1.17	0.90	1.21	1.26
FeOT	30.26	29.98	29.94	29.75	30.19	30.13	29.73	29.89	30.29
MnO	1.37	1.47	1.53	1.48	1.47	1.46	1.50	1.47	1.47
MgO	1.70	1.65	1.90	1.76	1.65	1.56	1.92	1.70	1.62
CaO	9.06	8.58	8.23	7.94	8.77	8.98	8.79	8.15	8.05
Na2O	4.11	4.30	4.54	4.66	4.14	3.95	4.38	4.52	4.58
K2O	1.55	1.59	1.57	1.59	1.58	1.57	1.51	1.65	1.62
F	0.454	0.780	0.718	0.677	0.777	0.642	0.884	0.551	0.466
Total	97.73	97.08	97.55	97.01	97.69	97.37	97.56	97.08	97.37
Si	6.59	6.64	6.76	6.75	6.64	6.66	6.77	6.72	6.66
Al	1.56	1.51	1.39	1.42	1.51	1.50	1.40	1.43	1.46
Ti	0.13	0.14	0.11	0.14	0.14	0.14	0.11	0.15	0.15
Fe3+	0.22	0.22	0.24	0.22	0.23	0.17	0.08	0.20	0.31
Fe2+	3.90	3.88	3.82	3.84	3.87	3.94	3.97	3.88	3.81
Mn	0.90	0.00	0.10	0.10	0.00	0.00	0.10	0.00	0.00
Mg	0.41	0.40	0.46	0.43	0.40	0.38	0.47	0.42	0.39
Ca	1.58	1.51	1.43	1.39	1.53	1.57	1.53	1.43	1.41
Na	1.30	1.37	1.43	1.48	1.30	1.25	1.38	1.43	1.45
K	0.32	0.33	0.32	0.33	0.33	0.33	0.31	0.34	0.34
F	0.2348	0.4059	0.3705	0.3511	0.4018	0.3330	0.4564	0.2864	0.2418

Sample No.	DAR 190 107	DAR 190 108	DAR 191 109	DAR 191 110	DAR 191 111	DAR 191 112	DAR 191 113	DAR 191 114	DAR 191 115
SiO2	40.45	41.37	39.74	41.06	42.15	39.86	42.06	43.65	41.49
Al2O3	8.20	7.46	9.19	7.80	6.47	8.41	6.45	6.76	7.27
TiO2	1.10	1.31	2.10	2.17	1.76	1.84	1.78	1.68	1.71
FeOT	30.01	30.12	29.32	30.21	30.54	30.71	30.61	30.75	30.65
MnO	1.37	1.48	1.20	1.24	1.39	1.29	1.37	1.26	1.33
MgO	1.58	1.60	1.59	1.39	1.15	1.04	1.25	1.17	1.12
CaO	8.97	8.54	10.11	8.27	7.45	7.92	7.27	5.86	6.44
Na2O	4.06	4.31	3.37	4.52	4.87	4.60	5.02	6.01	5.69
K2O	1.59	1.63	1.58	1.59	1.64	1.64	1.65	1.73	1.68
F	0.792	0.614	0.353	0.454	0.711	0.498	0.578	0.568	0.664
Total	97.33	97.82	98.20	98.25	97.42	97.31	97.46	98.87	97.38
Si	6.61	6.72	6.44	6.65	6.89	6.52	6.87	6.97	6.76
Al	1.58	1.43	1.76	1.49	1.25	1.62	1.24	1.27	1.40
Ti	0.13	0.16	0.26	0.26	0.22	0.23	0.22	0.20	0.21
Fe3+	0.17	0.13	0.00	0.06	0.05	0.31	0.11	0.16	0.26
Fe2+	3.93	3.96	3.97	4.03	4.13	3.89	4.07	3.94	3.91
Mn	0.90	0.00	0.60	0.70	0.90	0.80	0.90	0.70	0.80
Mg	0.38	0.39	0.38	0.34	0.28	0.25	0.30	0.28	0.27
Ca	1.57	1.49	1.76	1.44	1.30	1.39	1.27	1.00	1.12
Na	1.29	1.36	1.06	1.42	1.54	1.46	1.59	1.86	1.80
K	0.33	0.34	0.33	0.33	0.34	0.34	0.34	0.35	0.35
F	0.4108	0.3162	0.1810	0.2329	0.3682	0.2592	0.2991	0.2876	0.3444

Sample No.	DAR 191 116	DAR 191 117	DAR 191 118	DAR 191 119	DAR 191 120	DAR 191 121	DAR 191 122
SiO2	42.54	42.92	39.77	39.60	41.98	42.51	41.11
Al2O3	6.23	6.03	9.24	8.98	6.61	6.09	7.19
TiO2	1.85	1.95	2.17	2.20	1.81	1.80	1.95
FeOT	30.48	30.54	28.42	28.87	30.71	30.46	30.50
MnO	1.42	1.37	0.96	1.25	1.38	1.40	1.35
MgO	1.22	1.26	2.12	1.70	1.05	1.31	1.00
CaO	6.80	6.35	10.17	9.82	6.62	6.97	6.72
Na2O	5.31	5.63	3.26	3.52	5.39	5.21	5.27
K2O	1.66	1.62	1.57	1.56	1.72	1.61	1.67
F	0.671	0.698	0.609	0.585	0.694	0.860	0.542
Total	97.51	97.67	97.68	97.50	97.27	97.36	96.76
Si	6.93	6.97	6.44	6.46	6.86	6.94	6.75
Al	1.20	1.16	1.77	1.73	1.27	1.17	1.39
Ti	0.23	0.24	0.26	0.27	0.22	0.22	0.24
Fe3+	0.09	0.11	0.00	0.00	0.17	0.09	0.24
Fe2+	4.06	4.03	3.85	3.94	4.02	4.07	3.95
Mn	0.00	0.90	0.30	0.70	0.90	0.90	0.90
Mg	0.30	0.30	0.51	0.41	0.26	0.32	0.25
Ca	1.19	1.11	1.77	1.72	1.16	1.22	1.18
Na	1.68	1.77	1.02	1.11	1.71	1.65	1.68
K	0.35	0.34	0.32	0.32	0.36	0.33	0.35
F	0.3464	0.3591	0.3122	0.3014	0.3600	0.4446	0.2826

Sample No.	DAR123 N:1	DAR123 N:2	DAR123 N:3	DAR123 N:4	DAR123 N:5	DAR123 N:6	DAR123 N:7	DAR123 N:8	DAR123 N:9
SiO2	45.65	45.83	45.45	45.36	45.77	45.78	44.67	45.82	45.99
Al2O3	4.34	4.18	4.38	4.43	4.51	4.36	5.05	4.37	3.98
TiO2	1.10	1.01	1.17	1.14	1.21	1.09	1.48	0.98	0.93
ZrO2	0.351	0.413	0.395	0.354	0.375	0.344	0.428	0.377	0.383
FeOT	29.51	29.60	29.62	29.77	29.16	28.78	29.67	28.42	29.98
MnO	1.43	1.37	1.39	1.41	1.57	1.31	1.34	1.29	1.40
MgO	2.09	2.03	2.13	1.92	2.06	2.56	1.74	2.76	1.95
CaO	3.47	3.66	3.33	3.72	3.26	3.53	3.39	3.32	3.56
Na2O	7.78	7.61	7.69	7.60	7.72	7.73	7.82	7.82	7.70
K2O	1.69	1.68	1.71	1.67	1.64	1.68	1.70	1.68	1.73
F	0.489	0.464	0.254	0.520	0.628	0.673	0.482	0.521	0.624
Total	97.06	96.97	96.87	97.02	96.90	96.82	96.86	96.46	97.22
Si	7.36	7.41	7.33	7.34	7.37	7.37	7.23	7.38	7.42
Ti	0.83	0.80	0.83	0.85	0.86	0.83	0.96	0.83	0.76
Al	0.13	0.12	0.14	0.14	0.15	0.13	0.18	0.12	0.11
Zr	0.0277	0.0326	0.0312	0.0280	0.0295	0.0270	0.0339	0.0297	0.0302
Fe3+	0.20	0.15	0.32	0.19	0.25	0.19	0.22	0.23	0.17
Fe2+	3.78	3.85	3.68	3.83	3.67	3.69	3.79	3.60	3.87
Mn	0.20	0.19	0.19	0.19	0.21	0.18	0.18	0.18	0.19
Mg	0.50	0.49	0.51	0.46	0.49	0.61	0.42	0.66	0.47
Ca	0.60	0.63	0.57	0.64	0.56	0.61	0.59	0.57	0.62
Na	2.43	2.38	2.40	2.38	2.41	2.41	2.45	2.44	2.41
K	0.35	0.35	0.35	0.35	0.34	0.35	0.35	0.35	0.36
F	0.2499	0.2372	0.1303	0.2663	0.3207	0.3431	0.2472	0.2662	0.3190

Sample No.	DAR123 N:11	52246 N:27	52246 N:28	52246 N:29	52246 N:30	58270 N:2	58270 N:3	59751 N:1	59751 N:2
SiO2	45.86	44.42	45.06	45.58	45.86	41.30	42.12	45.69	45.78
Al2O3	4.36	4.23	3.95	3.45	3.70	5.61	5.77	3.13	3.14
TiO2	1.13	2.25	2.07	1.86	2.01	2.19	2.03	0.70	0.59
ZrO2	0.380	0.143	0.196	0.122	0.150	0.382	0.426	0.349	0.343
FeOT	29.39	24.87	25.07	24.73	24.51	29.32	29.06	29.63	30.97
MnO	1.35	1.29	1.38	1.35	1.37	1.29	1.21	1.19	1.23
MgO	2.08	5.22	5.29	5.49	5.53	1.61	1.89	2.56	1.72
CaO	3.12	5.33	5.76	4.92	5.63	7.51	8.04	3.42	3.61
Na2O	8.07	6.57	6.47	6.99	6.57	4.99	4.63	7.68	7.62
K2O	1.70	1.63	1.65	1.68	1.64	1.71	1.71	1.63	1.62
F	0.370	1.214	1.343	1.524	1.499	0.443	0.611	0.927	1.137
Total	97.06	95.81	96.70	96.05	96.82	95.53	96.46	95.63	96.28
Si	7.39	7.15	7.21	7.31	7.29	6.89	6.93	7.47	7.49
Ti	0.83	0.80	0.75	0.65	0.69	1.11	1.12	0.60	0.61
Al	0.14	0.27	0.25	0.22	0.24	0.28	0.25	0.09	0.07
Zr	0.0299	0.0112	0.0153	0.0096	0.0116	0.0309	0.0341	0.0279	0.0275
Fe3+	0.17	0.13	0.03	0.07	0.00	0.00	0.00	0.31	0.24
Fe2+	3.79	3.22	3.32	3.25	3.26	4.09	4.00	3.74	4.00
Mn	0.18	0.18	0.19	0.18	0.18	0.18	0.17	0.16	0.17
Mg	0.50	1.25	1.26	1.31	1.31	0.40	0.46	0.62	0.42
Ca	0.54	0.92	0.99	0.85	0.96	1.34	1.42	0.60	0.63
Na	2.52	2.05	2.01	2.17	2.03	1.62	1.48	2.44	2.42
K	0.35	0.33	0.34	0.34	0.33	0.36	0.36	0.34	0.34
F	0.1889	0.6190	0.6784	0.7736	0.7531	0.2319	0.3167	0.4814	0.5900

Sample No.	59751 N:3	59751 N:4	59751 N:5	59751 N:6	59751 N:7	59751 N:8	59751 N:9	59751 N:10	59751 N:11
SiO2	46.04	47.10	46.41	46.26	46.25	46.81	49.02	45.53	47.47
Al2O3	3.24	3.01	3.39	3.22	3.15	3.23	3.40	3.50	2.66
TiO2	0.63	0.57	0.89	0.71	0.59	0.72	0.69	0.86	0.68
ZrO2	0.326	0.237	0.301	0.319	0.340	0.190	0.126	0.230	0.158
FeOT	30.73	31.01	30.58	31.23	31.27	30.47	29.01	30.33	30.52
MnO	1.22	1.25	1.30	1.18	1.21	1.37	1.73	1.47	1.47
MgO	1.87	1.67	1.63	1.50	1.61	1.74	2.31	1.66	1.87
CaO	3.25	3.11	3.19	3.10	3.37	3.06	3.06	3.14	2.69
Na2O	7.77	8.11	7.92	7.79	7.72	7.95	7.95	7.58	8.18
K2O	1.62	1.63	1.63	1.64	1.62	1.63	1.87	1.82	1.65
F	0.688	0.856	0.704	0.804	0.750	0.835	0.821	0.782	0.729
Total	96.37	97.46	96.94	96.63	96.79	96.98	99.04	95.89	97.19
Si	7.50	7.60	7.52	7.52	7.52	7.57	7.70	7.46	7.65
Ti	0.62	0.57	0.65	0.62	0.60	0.62	0.63	0.68	0.51
Al	0.08	0.07	0.11	0.09	0.07	0.09	0.08	0.11	0.08
Zr	0.0260	0.0186	0.0238	0.0254	0.0270	0.0150	0.0096	0.0185	0.0124
Fe3+	0.31	0.14	0.15	0.28	0.27	0.18	0.00	0.31	0.21
Fe2+	3.87	4.05	4.00	3.96	3.98	3.94	3.81	3.84	3.91
Mn	0.17	0.17	0.18	0.16	0.17	0.19	0.23	0.20	0.20
Mg	0.45	0.40	0.39	0.36	0.39	0.42	0.54	0.41	0.45
Ca	0.57	0.54	0.55	0.54	0.59	0.53	0.51	0.55	0.46
Na	2.45	2.54	2.49	2.46	2.43	2.49	2.42	2.41	2.56
K	0.34	0.34	0.34	0.34	0.34	0.34	0.38	0.38	0.34
F	0.3557	0.4376	0.3613	0.4152	0.3864	0.4282	0.4076	0.4070	0.3726

Sample No.	59751 N:13	59751 N:14	59751 N:15	155053 N:16	155053 N:17	155053 N:18	155053 N:19
SiO2	47.28	46.87	46.48	47.41	45.20	46.45	46.78
Al2O3	2.64	3.00	2.99	2.11	3.17	2.31	1.99
TiO2	0.66	0.52	0.56	0.75	0.85	0.95	0.87
ZrO2	0.180	0.324	0.276	0.363	0.398	0.278	0.145
FeOT	30.76	30.97	30.80	30.71	30.71	30.93	30.71
MnO	1.20	1.17	1.18	1.44	1.41	1.37	1.41
MgO	1.68	1.74	1.77	1.43	1.20	1.27	1.38
CaO	2.65	3.04	3.11	4.02	4.58	3.89	3.93
Na2O	8.15	8.07	8.03	7.23	6.72	7.20	7.24
K2O	1.63	1.64	1.62	1.96	1.94	2.03	2.06
F	0.823	1.020	1.157	0.651	0.500	0.531	0.608
Total	96.65	97.02	96.54	97.06	95.78	96.40	96.37
Si	7.67	7.59	7.57	7.72	7.50	7.64	7.69
Ti	0.50	0.57	0.57	0.41	0.62	0.45	0.39
Al	0.08	0.06	0.07	0.09	0.11	0.12	0.11
Zr	0.0143	0.0256	0.0219	0.0288	0.0321	0.0222	0.0116
Fe3+	0.17	0.19	0.19	0.00	0.00	0.00	0.00
Fe2+	4.00	4.00	4.00	4.18	4.26	4.25	4.22
Mn	0.16	0.16	0.16	0.20	0.20	0.19	0.20
Mg	0.41	0.42	0.43	0.35	0.30	0.31	0.34
Ca	0.46	0.53	0.54	0.70	0.81	0.69	0.69
Na	2.56	2.53	2.54	2.28	2.16	2.30	2.31
K	0.34	0.34	0.34	0.41	0.41	0.43	0.43
F	0.4231	0.5235	0.5972	0.3343	0.2616	0.2755	0.3157

Sample No.	DAR164 N:2	DAR164 N:3	DAR164 N:4	DAR164 N:5	DAR164 N:6	DAR164 N:7	DAR164 N:8	DAR164 N:9	DAR164 N:10
SiO2	52.33	51.66	53.14	51.21	53.15	51.26	52.65	52.68	53.05
Al2O3	1.31	0.82	0.34	1.13	0.87	1.45	0.54	0.46	1.02
TiO2	0.09	0.04	0.04	0.07	0.05	0.25	0.06	0.10	0.11
ZrO2	0.027	0.000	0.000	0.012	0.006	0.000	0.023	0.049	0.013
FeOT	23.57	27.46	27.37	27.42	24.88	25.62	26.00	26.24	24.09
MnO	0.91	0.92	0.89	0.84	0.79	0.92	0.96	0.89	1.11
MgO	11.32	12.01	11.95	11.73	13.54	12.72	13.25	13.59	12.29
CaO	4.14	0.96	0.67	1.31	2.44	1.35	1.25	1.15	3.58
Na2O	1.33	0.22	0.19	0.43	0.35	0.43	0.29	0.19	0.52
K2O	0.17	0.14	0.07	0.16	0.06	1.08	0.04	0.04	0.12
F	0.000	0.088	0.000	0.128	0.295	0.189	0.040	0.127	0.000
Total	95.17	94.23	94.66	94.30	96.13	95.08	95.04	95.34	95.89
Si	8.01	8.04	8.18	7.98	8.01	7.90	8.06	8.04	8.03
Al	0.24	0.15	0.06	0.21	0.15	0.26	0.10	0.08	0.18
Ti	0.01	0.01	0.01	0.01	0.01	0.03	0.01	0.01	0.01
Zr	0.0020	0.0000	0.0000	0.0009	0.0005	0.0000	0.0017	0.0036	0.0010
Fe3+	0	0	0	0	0	0	0	0	0
Fe2+	3.02	3.57	3.52	3.57	3.13	3.30	3.33	3.35	3.05
Mn	0.12	0.12	0.12	0.11	0.10	0.12	0.12	0.11	0.14
Mg	2.58	2.79	2.75	2.73	3.04	2.92	3.02	3.09	2.77
Ca	0.68	0.16	0.11	0.22	0.39	0.22	0.21	0.19	0.58
Na	0.39	0.07	0.06	0.13	0.10	0.13	0.09	0.06	0.15
K	0.03	0.03	0.01	0.03	0.01	0.21	0.01	0.01	0.02
F	0.0000	0.0435	0.0000	0.0629	0.1409	0.0920	0.0191	0.0615	0.0000

Sample No.	DAR162 N:8	DAR162 N:9	DAR162 N:10	DAR162 N:11	DAR162 N:12	DAR162 N:13	DAR162 N:14	DAR162 N:15	DAR162 N:16
SiO2	53.56	50.68	51.78	53.71	53.25	53.57	53.45	52.86	51.60
Al2O3	0.31	1.51	0.99	0.32	0.48	0.19	0.24	0.43	1.78
TiO2	0.28	0.12	0.12	0.18	0.23	0.10	0.14	0.08	0.12
ZrO2	0.000	0.000	0.000	0.055	0.000	0.038	0.000	0.016	0.000
FeOT	24.44	24.06	23.69	25.55	23.92	23.79	21.53	23.48	24.59
MnO	0.53	0.88	0.73	0.42	0.48	0.43	0.71	0.68	0.50
MgO	7.23	7.62	7.48	7.18	8.14	8.21	9.53	7.98	7.25
CaO	0.88	10.41	9.31	1.23	2.46	1.38	6.29	6.13	6.46
Na2O	8.48	0.90	1.78	7.37	6.86	7.97	4.49	4.85	5.25
K2O	1.08	0.81	0.69	1.12	1.30	1.21	1.39	1.07	0.55
F	0.390	0.183	0.051	0.463	0.409	0.676	0.587	0.272	0.296
Total	96.79	96.99	96.57	97.08	97.12	96.85	97.77	97.56	98.10
Si	8.11	7.77	7.96	8.06	8.00	8.06	8.02	8.03	7.84
Al	0.06	0.27	0.18	0.06	0.08	0.03	0.04	0.08	0.32
Ti	0.03	0.01	0.01	0.02	0.03	0.01	0.02	0.01	0.01
Zr	0.0000	0.0000	0.0000	0.0041	0.0000	0.0028	0.0000	0.0012	0.0000
Fe3+	0.66	0.31	0.15	1.03	0.82	0.81	0.29	0.20	0.22
Fe2+	2.43	2.77	2.89	2.17	2.18	2.18	2.41	2.78	2.90
Mn	0.07	0.11	0.09	0.05	0.06	0.06	0.09	0.09	0.06
Mg	1.63	1.74	1.71	1.61	1.82	1.84	2.13	1.81	1.64
Ca	0.14	1.71	1.53	0.20	0.40	0.22	1.01	1.00	1.05
Na	2.49	0.27	0.53	2.14	2.00	2.33	1.31	1.43	1.55
K	0.21	0.16	0.13	0.21	0.25	0.23	0.27	0.21	0.11
F	0.1899	0.0895	0.0248	0.2246	0.1980	0.3273	0.2805	0.1314	0.1431

Sample No.	DAR162 N:17	DAR162 N:18	DAR165 N:11	DAR165 N:12	DAR165 N:13	DAR165 N:14	DAR165 N:15	DAR165 N:16	DAR165 N:17
SiO2	53.93	53.49	46.44	51.74	51.64	50.53	45.96	45.97	52.09
Al2O3	0.29	0.34	5.09	0.52	0.54	0.74	5.28	5.13	0.43
TiO2	0.06	0.09	0.38	0.43	0.16	0.20	0.91	1.59	0.43
ZrO2	0.000	0.012	0.040	0.006	0.034	0.000	0.046	0.081	0.020
FeOT	24.96	25.75	21.06	32.26	30.44	33.17	22.72	22.38	26.35
MnO	0.37	0.37	1.24	0.35	0.59	0.44	0.85	0.86	0.85
MgO	7.43	6.96	8.14	1.10	2.26	0.61	7.02	6.72	4.91
CaO	1.19	1.05	8.60	1.54	4.04	3.80	7.79	7.96	4.12
Na2O	7.44	7.65	4.53	6.61	5.45	5.08	4.76	4.53	5.16
K2O	1.05	0.79	0.96	0.54	0.60	0.59	1.38	1.40	1.03
F	0.430	0.429	0.871	0.035	0.128	0.000	0.586	0.587	0.424
Total	96.72	96.49	96.44	95.09	95.72	95.16	96.67	96.54	95.37
Si	8.10	8.07	7.23	8.25	8.22	8.15	7.19	7.21	8.16
Al	0.05	0.06	0.93	0.10	0.10	0.14	0.97	0.95	0.08
Ti	0.01	0.01	0.04	0.05	0.02	0.02	0.11	0.19	0.05
Zr	0.0000	0.0009	0.0030	0.0005	0.0027	0.0000	0.0035	0.0062	0.0016
Fe3+	0.99	1.05	0.09	0.63	0.25	0.48	0.09	0.00	0.34
Fe2+	2.14	2.19	2.64	3.67	3.80	4.00	2.88	2.93	3.11
Mn	0.05	0.05	0.16	0.05	0.08	0.06	0.11	0.11	0.11
Mg	1.66	1.57	1.89	0.26	0.54	0.15	1.64	1.57	1.15
Ca	0.19	0.17	1.43	0.26	0.69	0.66	1.31	1.34	0.69
Na	2.17	2.24	1.37	2.04	1.68	1.59	1.44	1.38	1.57
K	0.20	0.15	0.19	0.11	0.12	0.12	0.28	0.28	0.21
F	0.2089	0.2093	0.4296	0.0181	0.0649	0.0000	0.2908	0.2908	0.2116

Sample No.	DAR165 N:18	DAR165 N:19	DAR165 N:20	DAR165 N:21
SiO2	49.83	50.53	51.09	51.41
Al2O3	2.26	1.30	0.59	0.36
TiO2	0.96	0.70	0.99	0.60
ZrO2	0.053	0.024	0.017	0.000
FeOT	23.81	25.59	28.96	33.28
MnO	0.62	0.81	1.72	0.24
MgO	6.63	5.49	2.09	0.63
CaO	6.77	6.36	3.85	1.14
Na2O	4.28	4.93	5.98	6.95
K2O	1.36	1.30	0.88	0.22
F	0.275	0.588	0.307	0.065
Total	96.52	97.01	96.15	94.83
Si	7.75	7.90	8.16	8.23
Al	0.42	0.24	0.11	0.07
Ti	0.11	0.08	0.12	0.07
Zr	0.0040	0.0018	0.0013	0.0000
Fe3+	0.03	0.00	0.00	0.74
Fe2+	3.07	3.35	3.87	3.71
Mn	0.08	0.11	0.23	0.03
Mg	1.54	1.28	0.50	0.15
Ca	1.13	1.06	0.66	0.19
Na	1.29	1.49	1.85	2.16
K	0.27	0.26	0.18	0.05
F	0.1353	0.2906	0.1552	0.0333

Sample No.	DAR67 N:1	DAR67 N:2	DAR67 N:3	DAR67 N:4	DAR67 N:5	DAR67 N:6	DAR67 N:7	DAR67 N:8	DAR67 N:9
SiO2	46.71	47.26	47.08	46.76	46.60	45.66	45.42	44.67	44.33
Al2O3	4.24	4.11	4.20	4.45	4.40	4.78	5.14	5.32	5.39
TiO2	0.73	0.73	0.82	0.70	0.74	0.66	0.62	0.75	0.75
FeOT	22.26	22.42	22.46	22.63	22.68	24.69	24.84	28.10	28.22
MnO	1.12	1.08	1.07	1.01	1.05	1.15	1.10	1.28	1.23
MgO	6.88	7.11	7.12	7.06	7.16	5.56	5.47	3.19	2.94
CaO	7.65	7.72	7.60	7.71	7.72	7.20	7.37	7.32	7.42
Na2O	5.09	5.26	5.21	5.35	5.30	5.44	5.30	5.12	5.10
K2O	1.67	1.68	1.62	1.62	1.67	1.71	1.75	1.69	1.76
F	0.824	0.772	0.625	0.917	0.807	0.722	0.685	0.429	0.588
Total	96.35	97.37	97.18	97.29	97.32	96.85	97.01	97.44	97.14
Si	7.36	7.37	7.35	7.31	7.29	7.25	7.21	7.18	7.16
Al	0.79	0.76	0.77	0.82	0.81	0.90	0.96	1.01	1.03
Ti	0.09	0.09	0.10	0.08	0.09	0.08	0.07	0.09	0.09
Fe3+	0	0	0	0	0	0	0	0	0
Fe2+	2.93	2.92	2.93	2.95	2.96	3.28	3.30	3.78	3.81
Mn	0.15	0.14	0.14	0.13	0.14	0.15	0.15	0.17	0.17
Mg	1.62	1.65	1.66	1.65	1.67	1.32	1.30	0.76	0.71
Ca	1.29	1.29	1.27	1.29	1.29	1.23	1.25	1.26	1.28
Na	1.55	1.59	1.58	1.62	1.61	1.68	1.63	1.59	1.60
K	0.34	0.33	0.32	0.32	0.33	0.35	0.35	0.35	0.36
F	0.4105	0.3804	0.3084	0.4530	0.3992	0.3629	0.3442	0.2180	0.3003

Sample No.	DAR65 N:1	DAR65 N:2	DAR65 N:3	DAR65 N:4	DAR65 N:5	DAR65 N:6	DAR65 N:7	DAR65 N:8	DAR65 N:9
SiO2	53.51	53.47	53.29	53.51	53.85	53.73	53.43	53.72	53.81
Al2O3	0.10	0.09	0.12	0.11	0.09	0.11	0.10	0.15	0.08
TiO2	0.73	0.72	0.85	0.72	0.64	0.51	0.66	0.50	0.58
FeOT	21.87	22.27	21.98	21.77	21.80	21.66	21.33	21.68	21.76
MnO	0.98	1.00	0.95	1.04	1.06	1.03	1.06	1.02	1.08
MgO	7.74	7.72	7.74	7.85	8.06	7.97	8.16	8.02	8.14
CaO	1.80	2.09	2.93	2.19	1.46	1.23	1.82	1.46	1.52
Na2O	8.91	8.81	8.35	8.75	9.26	9.35	8.81	9.23	9.05
K2O	1.97	2.04	1.70	2.03	2.08	2.03	2.13	2.08	2.13
F	0.977	0.884	1.088	1.063	1.081	1.105	1.312	1.067	0.800
Total	97.61	98.21	97.91	97.97	98.30	97.62	97.50	97.86	98.15
Si	8.16	8.13	8.11	8.14	8.16	8.19	8.15	8.17	8.16
Al	0.02	0.02	0.02	0.02	0.02	0.02	0.02	0.03	0.01
Ti	0.08	0.08	0.10	0.08	0.07	0.06	0.08	0.06	0.07
Fe3+	0	0	0	0	0	0	0	0	0
Fe2+	2.79	2.83	2.80	2.77	2.76	2.76	2.72	2.76	2.76
Mn	0.13	0.13	0.12	0.13	0.14	0.13	0.14	0.13	0.14
Mg	1.76	1.75	1.76	1.78	1.82	1.81	1.86	1.82	1.84
Ca	0.29	0.34	0.48	0.36	0.24	0.20	0.30	0.24	0.25
Na	2.63	2.60	2.46	2.58	2.72	2.76	2.61	2.72	2.66
K	0.38	0.40	0.33	0.39	0.40	0.39	0.42	0.40	0.41
F	0.4714	0.4252	0.5235	0.5114	0.5180	0.5323	0.6332	0.5133	0.3839

Sample No.	DAR65 N:10	DAR65 N:11	DAR65 N:12	DAR65 N:13	DAR65 N:14	DAR65 N:15	DAR65 N:16	DAR65 N:17	DAR65 N:18
SiO2	54.00	53.70	53.83	53.66	53.76	54.18	53.26	53.55	52.92
Al2O3	0.07	0.08	0.11	0.09	0.10	0.05	0.14	0.11	0.11
TiO2	0.69	0.78	0.45	0.81	0.69	0.51	1.02	0.88	0.91
FeOT	20.95	21.90	21.36	22.19	21.76	19.72	19.91	20.27	20.18
MnO	1.15	1.09	1.00	1.01	1.04	1.21	1.28	1.24	1.21
MgO	8.37	7.91	7.94	7.96	7.94	9.33	9.13	8.65	8.74
CaO	1.69	1.67	1.20	2.02	1.68	2.80	5.07	3.68	3.97
Na2O	9.05	9.01	9.43	8.95	8.95	8.38	7.35	7.85	7.70
K2O	2.09	2.13	2.08	1.99	2.07	2.14	1.48	1.81	1.76
F	1.056	0.967	0.965	0.861	0.967	1.195	1.072	0.896	0.886
Total	98.06	98.27	97.40	98.68	97.99	98.32	98.64	98.04	97.50
Si	8.17	8.15	8.21	8.11	8.16	8.14	8.00	8.09	8.05
Al	0.01	0.01	0.02	0.02	0.02	0.01	0.03	0.02	0.02
Ti	0.08	0.09	0.05	0.09	0.08	0.06	0.11	0.10	0.10
Fe3+	0	0	0	0	0	0	0	0	0
Fe2+	2.65	2.78	2.72	2.80	2.76	2.48	2.50	2.56	2.57
Mn	0.15	0.14	0.13	0.13	0.13	0.15	0.16	0.16	0.16
Mg	1.89	1.79	1.81	1.80	1.80	2.09	2.05	1.95	1.98
Ca	0.27	0.27	0.20	0.33	0.27	0.45	0.82	0.60	0.65
Na	2.65	2.65	2.79	2.62	2.63	2.44	2.14	2.30	2.27
K	0.40	0.41	0.41	0.38	0.40	0.41	0.28	0.35	0.34
F	0.5052	0.4640	0.4652	0.4117	0.4642	0.5675	0.5091	0.4283	0.4265

Sample No.	DAR65 N:19	DAR65 N:20	DAR65 N:21	DAR66 N:42	DAR66 N:44	DAR66 N:2	DAR66 N:4
SiO2	53.40	53.72	54.93	54.84	54.48	54.43	54.78
Al2O3	0.09	0.08	0.07	0.19	0.24	0.48	0.20
TiO2	0.76	0.69	0.35	0.53	1.18	0.55	0.49
FeOT	22.37	21.69	18.02	16.63	22.03	19.55	17.02
MnO	1.00	1.07	1.19	4.78	0.66	0.99	4.06
MgO	7.75	7.91	11.03	5.56	4.67	5.92	5.90
CaO	1.97	1.85	2.57	0.01	0.00	0.00	0.00
Na2O	8.79	9.02	8.48	9.48	9.72	9.80	9.62
K2O	2.08	2.08	2.19	3.01	2.29	2.79	2.77
F	1.083	1.089	1.226	1.660	1.498	1.535	1.901
Total	98.21	98.11	98.83	95.03	95.27	94.51	94.84
Si	8.13	8.15	8.13	8.51	8.47	8.47	8.50
Al	0.02	0.01	0.01	0.03	0.04	0.09	0.04
Ti	0.09	0.08	0.04	0.06	0.14	0.06	0.06
Fe3+	0	0	0	0	0	0	0
Fe2+	2.84	2.75	2.23	2.16	2.86	2.54	2.21
Mn	0.13	0.14	0.15	0.63	0.09	0.13	0.53
Mg	1.76	1.79	2.44	1.29	1.08	1.37	1.37
Ca	0.32	0.30	0.41	0.00	0.00	0.00	0.00
Na	2.59	2.66	2.43	2.85	2.93	2.96	2.89
K	0.40	0.40	0.41	0.60	0.45	0.55	0.55
F	0.5210	0.5230	0.5737	0.8147	0.7364	0.7553	0.9329

BIOTITES

Sample No.	DAR186 N:15	DAR186 N:16	DAR186 N:17	DAR186 N:18	DAR186 N:19	DAR186 N:20	DAR186 N:21	DAR186 N:22	DAR186 N:23
SiO2	34.424	35.048	34.956	35.224	34.277	33.874	34.596	33.400	34.209
Al2O3	11.107	10.860	10.746	11.066	11.783	10.723	10.867	10.229	10.013
TiO2	3.429	2.732	2.661	2.658	2.986	3.353	3.402	3.569	1.279
FeO	34.041	34.421	35.105	34.333	33.448	34.514	34.232	34.477	36.446
MnO	1.294	1.421	1.222	1.254	1.154	1.295	1.248	1.894	2.087
MgO	1.803	1.797	1.322	1.234	1.477	1.263	1.300	1.079	0.963
CaO	0.023	0.043	0.024	0.021	0.016	0.014	0.000	0.033	0.090
Na2O	0.167	0.268	0.152	0.149	0.147	0.263	0.181	0.240	0.151
K2O	8.533	8.570	8.488	8.503	8.525	8.432	8.458	8.252	7.610
F	0.150	0.000	0.000	0.000	0.035	0.039	0.090	0.031	0.000
Cl	0.007	0.005	0.000	0.008	0.006	0.013	0.009	0.026	0.006
Total	94.978	95.165	94.676	94.450	93.854	93.783	94.383	93.230	92.854
Si	5.7578	5.8478	5.8762	5.9054	5.7726	5.7659	5.8223	5.7480	5.9338
Al	2.1896	2.1356	2.1290	2.1866	2.3388	2.1511	2.1555	2.0746	2.0471
Ti	0.4313	0.3429	0.3364	0.3352	0.3782	0.4292	0.4305	0.4620	0.1669
Fe	4.7617	4.8031	4.9353	4.8139	4.7109	4.9132	4.8181	4.9620	5.2871
Mn	0.1833	0.2009	0.1741	0.1781	0.1647	0.1867	0.1778	0.2761	0.3066
Mg	0.4495	0.4468	0.3312	0.3084	0.3709	0.3203	0.3262	0.2768	0.2489
Ca	0.0042	0.0077	0.0044	0.0037	0.0029	0.0025	0.0000	0.0060	0.0166
Na	0.0542	0.0866	0.0497	0.0483	0.0479	0.0866	0.0592	0.0801	0.0509
K	1.8207	1.8240	1.8202	1.8185	1.8314	1.8310	1.8159	1.8116	1.6839
F	0.0794	0.0000	0.0000	0.0000	0.0184	0.0209	0.0481	0.0168	0.0000
Cl	0.0020	0.0013	0.0000	0.0023	0.0018	0.0039	0.0025	0.0075	0.0017

Sample No.	DAR186 N:24	DAR186 N:25	DAR186 N:26	DAR186 N:27	DAR186 N:28	DAR186 N:29	DAR186 N:30	DAR188 N:31	DAR188 N:32
SiO2	33.997	34.376	34.379	34.404	34.953	34.495	34.941	35.014	35.457
Al2O3	10.139	10.829	10.346	10.614	10.610	11.036	11.288	11.354	10.549
TiO2	1.316	2.217	3.694	3.687	3.607	4.891	2.425	2.168	3.529
FeO	36.038	33.749	33.936	35.240	35.022	35.227	33.962	32.713	31.366
MnO	2.052	1.330	1.001	0.933	0.813	0.856	1.378	2.101	1.739
MgO	0.961	2.619	1.472	1.116	1.213	0.508	1.697	2.186	3.129
CaO	0.160	0.095	0.087	0.016	0.036	0.013	0.066	0.071	0.018
Na2O	0.149	0.212	0.203	0.234	0.223	0.210	0.306	0.123	0.283
K2O	7.707	8.392	8.364	8.469	8.276	8.452	8.334	8.664	8.456
F	0.000	0.000	0.009	0.077	0.017	0.034	0.141	0.074	0.141
Cl	0.013	0.025	0.015	0.009	0.000	0.000	0.021	0.007	0.027
Total	92.532	93.844	93.506	94.799	94.770	95.722	94.559	94.475	94.694
Si	5.9150	5.8106	5.8331	5.7912	5.8514	5.7310	5.8557	5.8584	5.8680
Al	2.0791	2.1574	2.0690	2.1058	2.0934	2.1610	2.2295	2.2390	2.0575
Ti	0.1722	0.2818	0.4713	0.4667	0.4541	0.6111	0.3056	0.2727	0.4392
Fe	5.2437	4.7709	4.8154	4.9609	4.9032	4.8946	4.7599	4.5774	4.3412
Mn	0.3023	0.1904	0.1438	0.1331	0.1153	0.1205	0.1956	0.2978	0.2438
Mg	0.2491	0.6598	0.3724	0.2799	0.3027	0.1258	0.4238	0.5453	0.7718
Ca	0.0298	0.0172	0.0158	0.0028	0.0064	0.0023	0.0118	0.0127	0.0031
Na	0.0503	0.0694	0.0669	0.0762	0.0723	0.0678	0.0994	0.0399	0.0907
K	1.7106	1.8096	1.8104	1.8186	1.7673	1.7912	1.7817	1.8493	1.7853
F	0.0000	0.0000	0.0047	0.0408	0.0090	0.0180	0.0746	0.0392	0.0738
Cl	0.0037	0.0071	0.0043	0.0026	0.0000	0.0000	0.0059	0.0021	0.0075

Sample No.	DAR188 N:33	DAR188 N:34	DAR188 N:35	DAR188 N:36	DAR188 N:37	DAR188 N:38	DAR189 N:56	DAR189 N:57	DAR189 N:58
SiO2	35.852	35.900	36.301	35.904	35.358	35.395	34.423	34.650	34.986
Al2O3	10.577	10.611	10.355	10.730	10.636	10.765	11.085	11.166	10.574
TiO2	3.583	3.593	3.652	3.545	3.425	2.881	2.037	1.471	2.054
FeO	31.377	31.328	30.991	32.430	32.247	32.545	32.640	33.414	33.002
MnO	1.675	1.715	1.714	1.829	1.773	1.814	2.074	2.005	1.903
MgO	3.106	3.126	3.263	2.429	2.471	2.631	2.776	2.949	2.794
CaO	0.000	0.014	0.010	0.000	0.034	0.009	0.135	0.047	0.084
Na2O	0.283	0.322	0.299	0.265	0.260	0.260	0.153	0.101	0.212
K2O	8.409	8.438	8.534	8.282	8.216	8.217	8.468	8.686	8.430
F	0.132	0.097	0.123	0.000	0.149	0.065	0.000	0.000	0.026
Cl	0.002	0.002	0.023	0.022	0.026	0.001	0.001	0.000	0.000
Total	94.996	95.146	95.265	95.436	94.595	94.583	93.792	94.489	94.065
Si	5.8982	5.8943	5.9428	5.8969	5.8769	5.8839	5.8076	5.8196	5.8840
Al	2.0507	2.0534	1.9980	2.0770	2.0835	2.1090	2.2041	2.2103	2.0959
Ti	0.4433	0.4437	0.4496	0.4379	0.4281	0.3602	0.2584	0.1857	0.2598
Fe	4.3169	4.3017	4.2429	4.4545	4.4826	4.5245	4.6053	4.6934	4.6417
Mn	0.2334	0.2385	0.2377	0.2545	0.2497	0.2554	0.2964	0.2853	0.2711
Mg	0.7617	0.7650	0.7961	0.5947	0.6121	0.6520	0.6981	0.7382	0.7004
Ca	0.0000	0.0024	0.0018	0.0000	0.0061	0.0017	0.0243	0.0085	0.0152
Na	0.0903	0.1026	0.0948	0.0844	0.0838	0.0840	0.0502	0.0330	0.0692
K	1.7648	1.7672	1.7821	1.7351	1.7420	1.7425	1.8224	1.8610	1.8085
F	0.0686	0.0502	0.0639	0.0000	0.0781	0.0343	0.0000	0.0000	0.0139
Cl	0.0005	0.0006	0.0065	0.0062	0.0074	0.0004	0.0002	0.0000	0.0000

Sample No.	DAR189 N:59	DAR189 N:60	DAR189 N:61	DAR189 N:62	DAR189 N:63	DAR189 N:64	DAR189 N:65
SiO2	35.188	35.258	34.555	34.972	34.316	34.289	34.706
Al2O3	10.741	10.930	10.165	10.479	11.338	11.562	10.277
TiO2	1.930	1.900	2.441	2.452	1.638	1.541	3.094
FeO	32.589	31.973	34.996	34.589	33.296	33.992	35.595
MnO	2.068	1.953	1.650	1.538	1.626	1.631	1.329
MgO	3.302	3.481	1.861	1.865	2.739	2.338	0.918
CaO	0.134	0.190	0.020	0.006	0.126	0.088	0.021
Na2O	0.230	0.146	0.281	0.175	0.122	0.087	0.219
K2O	8.327	7.734	8.338	8.497	8.447	8.419	8.145
F	0.000	0.162	0.107	0.000	0.000	0.000	0.158
Cl	0.007	0.008	0.002	0.023	0.004	0.011	0.019
Total	94.516	93.735	94.416	94.596	93.652	93.958	94.481
Si	5.8700	5.8958	5.8563	5.8834	5.8031	5.7945	5.8764
Al	2.1117	2.1540	2.0303	2.0778	2.2597	2.3027	2.0508
Ti	0.2421	0.2390	0.3111	0.3102	0.2083	0.1959	0.3940
Fe	4.5466	4.4714	4.9601	4.8664	4.7089	4.8040	5.0403
Mn	0.2922	0.2766	0.2369	0.2192	0.2330	0.2335	0.1906
Mg	0.8211	0.8675	0.4701	0.4677	0.6905	0.5889	0.2316
Ca	0.0239	0.0340	0.0037	0.0010	0.0228	0.0159	0.0038
Na	0.0743	0.0473	0.0925	0.0571	0.0399	0.0284	0.0718
K	1.7721	1.6498	1.8027	1.8236	1.8222	1.8148	1.7592
F	0.0000	0.0854	0.0574	0.0000	0.0000	0.0000	0.0848
Cl	0.0018	0.0022	0.0006	0.0064	0.0012	0.0031	0.0054

Sample No.	DAR128 N:1	DAR128 N:2	DAR128 N:3	DAR128 N:4	DAR128 N:5	DAR128 N:6	DAR128 N:7	DAR128 N:8	DAR128 N:9
SiO2	35.716	34.811	37.704	38.011	34.996	35.407	36.414	36.341	34.717
Al2O3	10.998	14.324	12.778	10.862	10.467	9.329	9.841	11.189	11.108
TiO2	3.287	2.631	2.727	2.144	2.370	2.382	2.339	4.048	4.074
FeO	31.383	29.894	25.588	29.834	30.062	26.866	29.385	29.323	32.352
MnO	3.560	2.796	2.913	3.053	3.087	3.009	2.969	2.858	2.676
MgO	1.963	1.058	2.937	4.427	4.085	6.782	4.366	3.257	0.645
CaO	0.050	0.022	0.064	0.172	0.186	0.140	0.018	0.225	0.034
Na2O	0.180	0.165	1.437	0.197	0.176	0.227	0.108	0.167	0.172
K2O	8.630	8.919	7.525	7.881	8.208	8.760	8.577	8.537	8.420
F	0.217	0.044	0.589	0.525	0.482	0.630	0.814	0.463	0.240
Cl	0.015	0.014	0.007	0.012	0.008	0.016	0.010	0.004	0.000
Total	95.999	94.678	94.269	97.118	94.127	93.548	94.841	96.412	94.438
Si	5.8749	5.7268	6.0718	6.0599	5.8540	5.9020	6.0259	5.8697	5.8274
Al	2.1321	2.7773	2.4253	2.0409	2.0635	1.8328	1.9194	2.1300	2.1975
Ti	0.4066	0.3255	0.3303	0.2571	0.2982	0.2986	0.2911	0.4917	0.5143
Fe	4.3172	4.1128	3.4461	3.9777	4.2055	3.7451	4.0666	3.9609	4.5415
Mn	0.4960	0.3896	0.3974	0.4123	0.4373	0.4249	0.4161	0.3910	0.3805
Mg	0.4813	0.2594	0.7049	1.0520	1.0186	1.6850	1.0769	0.7840	0.1614
Ca	0.0087	0.0039	0.0110	0.0293	0.0333	0.0249	0.0032	0.0390	0.0061
Na	0.0573	0.0528	0.4486	0.0610	0.0572	0.0735	0.0348	0.0523	0.0560
K	1.8109	1.8718	1.5459	1.6029	1.7515	1.8627	1.8106	1.7591	1.8030
F	0.1129	0.0230	0.3000	0.2648	0.2549	0.3323	0.4259	0.2363	0.1273
Cl	0.0043	0.0038	0.0020	0.0034	0.0023	0.0045	0.0028	0.0012	0.0000

Sample No.	DAR128 N:10	DAR128 N:11	DAR128 N:12	DAR128 N:13	DAR128 N:14	DAR128 N:15	DAR128 N:16	DAR128 N:17	DAR128 N:18
SiO2	36.301	37.274	34.160	35.560	33.781	34.958	33.361	35.047	33.645
Al2O3	9.783	9.958	10.771	10.905	11.545	11.240	11.195	10.245	10.205
TiO2	2.491	2.811	2.729	2.492	2.614	2.579	2.328	3.094	3.466
FeO	28.694	28.109	34.071	34.536	33.577	34.070	33.708	34.192	34.072
MnO	3.771	3.727	3.572	3.211	3.243	3.476	3.359	3.029	3.015
MgO	4.512	4.639	0.708	0.785	0.786	0.798	0.948	0.991	0.884
CaO	0.112	0.006	0.062	0.038	0.033	0.098	0.181	0.024	0.O47
Na2O	0.243	0.190	0.147	0.196	0.132	0.191	0.191	0.095	0.251
K2O	8.030	8.710	8.298	8.414	8.608	8.058	7.799	8.617	8.337
F	0.839	0.718	0.176	0.099	0.040	0.100	0.185	0.161	0.225
Cl	0.005	0.010	0.010	0.021	0.020	0.020	0.010	0.000	0.015
Total	94.781	96.152	94.704	96.257	94.379	95.588	93.265	95.495	94.115
Si	6.0026	6.0423	5.8009	5.9032	5.7360	5.8382	5.7418	5.8804	5.7589
Al	1.9066	1.9026	2.1558	2.1335	2.3105	2.2124	2.2708	2.0260	2.0587
Ti	0.3098	0.3427	0.3486	0.3110	0.3337	0.3240	0.3013	0.3904	0.4461
Fe	3.9680	3.8107	4.8387	4.7947	4.7681	4.7586	4.8519	4.7979	4.8774
Mn	0.5281	0.5118	0.5138	0.4515	0.4665	0.4918	0.4897	0.4305	0.4371
Mg	1.1120	1.1209	0.1791	0.1943	0.1989	0.1986	0.2431	0.2478	0.2254
Ca	0.0199	0.0010	0.0113	0.0068	0.0061	0.0175	0.0334	0.0043	0.0086
Na	0.0780	0.0597	0.0483	0.0632	0.0435	0.0618	0.0639	0.0308	0.0833
K	1.6938	1.8012	1.7977	1.7818	1.8644	1.7168	1.7123	1.8443	1.8205
F	0.4390	0.3679	0.0945	0.0520	0.0213	0.0529	0.1009	0.0855	0.1216
Cl	0.0014	0.0028	0.0028	0.0059	0.0059	0.0056	0.0030	0.0000	0.0044

Sample No.	DAR128 N:19	DAR128 N:20	DAR128 N:21	DAR128 N:22	DAR128 N:23	DAR128 N:24	DAR128 N:25	DAR128 N:26	DAR128 N:27
SiO2	35.577	35.196	34.989	35.436	35.357	34.404	34.811	35.394	35.199
Al2O3	8.845	9.929	9.514	9.284	9.675	9.990	9.771	10.304	10.284
TiO2	3.475	3.319	3.351	3.458	3.245	3.567	3.791	3.504	3.212
FeO	34.459	33.738	33.913	35.077	34.273	34.007	34.312	33.797	34.174
MnO	3.209	3.413	3.424	3.186	2.903	2.800	2.790	2.782	2.956
MgO	0.792	0.829	0.880	0.870	0.988	0.996	0.826	0.973	0.940
CaO	0.025	0.073	0.057	0.028	0.052	0.039	0.042	0.074	0.030
Na2O	0.348	0.274	0.209	0.303	0.145	0.202	0.211	0.156	0.167
K2O	8.053	7.923	8.246	8.222	8.474	8.374	8.304	8.282	8.464
F	0.145	0.142	0.138	0.091	0.083	0.150	0.180	0.310	0.179
Cl	0.000	0.008	0.000	0.012	0.010	0.004	0.020	0.006	0.000
Total	94.928	94.844	94.721	95.967	95.205	94.533	95.058	95.582	95.605
Si	6.0096	5.9250	5.9239	5.9335	5.9422	5.8349	5.8712	5.9049	5.8891
Al	1.7608	1.9700	1.8984	1.8321	1.9163	1.9969	1.9423	2.0261	2.0278
Ti	0.4414	0.4202	0.4266	0.4354	0.4102	0.4549	0.4809	0.4396	0.4042
Fe	4.8680	4.7498	4.8019	4.9120	4.8172	4.8235	4.8398	4.7155	4.7816
Mn	0.4591	0.4867	0.4911	0.4519	0.4133	0.4023	0.3985	0.3932	0.4189
Mg	0.1993	0.2081	0.2221	0.2172	0.2475	0.2517	0.2075	0.2419	0.2344
Ca	0.0045	0.0131	0.0104	0.0042	0.0093	0.0071	0.0075	0.0132	0.0054
Na	0.1138	0.0894	0.0685	0.0985	0.0472	0.0665	0.0689	0.0505	0.0540
K	1.7352	1.7016	1.7810	1.7562	1.8167	1.8118	1.7866	1.7627	1.8064
F	0.0775	0.0754	0.0737	0.0484	0.0442	0.0803	0.0960	0.1636	0.0947
Cl	0.0000	0.0023	0.0001	0.0033	0.0029	0.0012	0.0056	0.0016	0.0001

Sample No.	DAR128 N:28	DAR128 N:29	DAR128 N:30
SiO2	35.127	34.860	34.450
Al2O3	10.044	9.445	11.135
TiO2	3.501	3.645	3.050
FeO	33.950	34.768	34.307
MnO	2.906	3.025	2.468
MgO	0.884	0.814	0.858
CaO	0.049	0.035	0.008
Na2O	0.255	0.345	0.141
K2O	8.250	8.134	8.480
F	0.202	0.092	0.169
Cl	0.015	0.011	0.021
Total	95.183	95.174	95.087
Si	5.8984	5.8849	5.7946
Al	1.9877	1.8792	2.2073
Ti	0.4421	0.4627	0.3858
Fe	4.7676	4.9086	4.8260
Mn	0.4134	0.4325	0.3516
Mg	0.2212	0.2048	0.2151
Ca	0.0088	0.0064	0.0015
Na	0.0831	0.1131	0.0460
K	1.7672	1.7516	1.8196
F	0.1072	0.0492	0.0898
Cl	0.0043	0.0032	0.0061

Sample No.	DAR162 N:4	DAR162 N:5	DAR162 N:6	DAR162 N:7	DAR162 N:1	DAR162 N:1	DAR162 N:1	DAR162 N:2	DAR162 N:3
SiO2	37.3450	37.3030	36.6620	37.3960	37.8330	37.9670	37.7420	37.5480	37.3800
Al2O3	11.985	12.375	12.504	12.146	12.363	12.136	12.178	12.547	12.457
TiO2	4.204	4.111	4.100	3.682	3.277	3.073	3.762	4.143	4.064
FeO	21.595	21.370	22.980	21.950	20.376	20.513	20.547	21.302	21.133
MnO	0.111	0.131	0.363	0.192	0.177	0.182	0.184	0.196	0.193
MgO	10.045	10.548	8.983	10.402	11.737	11.799	11.469	10.596	10.650
CaO	0.000	0.000	0.000	0.000	0.000	0.000	0.034	0.031	0.038
Na2O	0.209	0.257	0.247	0.349	0.322	0.318	0.385	0.231	0.239
K2O	9.587	9.653	9.772	9.780	9.909	9.891	9.826	9.930	9.937
F	0.310	0.539	0.255	0.358	0.753	0.836	0.696	0.540	0.341
Cl	0.272	0.279	0.282	0.336	0.248	0.306	0.269	0.233	0.244
Total	95.663	96.566	96.148	96.591	96.995	97.021	97.092	97.297	96.676
Si	5.8000	5.7475	5.7206	5.7770	5.7890	5.8194	5.7745	5.7476	5.7418
Al	2.1938	2.2472	2.2995	2.2114	2.2296	2.1923	2.1960	2.2473	2.2552
Ti	0.4910	0.4764	0.4811	0.4278	0.3771	0.3542	0.4328	0.4769	0.4693
Fe	2.8049	2.7536	2.9987	2.8358	2.6075	2.6295	2.6291	2.7269	2.7148
Mn	0.0146	0.0171	0.0479	0.0251	0.0229	0.0236	0.0238	0.0255	0.0251
Mg	2.3253	2.4223	2.0892	2.3952	2.6768	2.6955	2.6156	2.4175	2.4384
Ca	0.0000	0.0000	0.0000	0.0000	0.0000	0.0000	0.0056	0.0051	0.0063
Na	0.0628	0.0768	0.0748	0.1046	0.0956	0.0946	0.1142	0.0685	0.0712
K	1.8994	1.8972	1.9452	1.9273	1.9341	1.9340	1.9178	1.9390	1.9471
F	0.1521	0.2627	0.1259	0.1749	0.3644	0.4051	0.3369	0.2614	0.1658
Cl	0.0716	0.0729	0.0745	0.0880	0.0642	0.0794	0.0697	0.0606	0.0636

Sample No.	DAR162 N:5	DAR162 N:6	DAR162 N:7	DAR162 N:8	DAR162 N:9	DAR162 N:10	DAR163 N:1	DAR163 N:2	DAR163 N:3
SiO2	37.6950	37.3590	37.6540	37.6220	37.7850	37.7670	36.8710	37.1090	36.8130
Al2O3	12.212	12.285	12.296	12.317	11.947	12.051	12.904	12.978	12.874
TiO2	3.865	4.028	3.770	3.820	4.354	3.794	2.440	2.556	2.869
FeO	20.348	22.491	21.421	21.574	21.567	20.592	22.356	22.222	22.942
MnO	0.158	0.190	0.117	0.210	0.182	0.241	0.599	0.610	0.632
MgO	11.012	9.804	10.579	10.540	10.276	10.996	9.754	9.806	9.793
CaO	0.045	0.017	0.009	0.000	0.035	0.034	0.000	0.012	0.000
Na2O	0.177	0.326	0.349	0.301	0.307	0.338	0.308	0.275	0.395
K2O	9.877	9.719	9.887	9.890	9.704	9.883	9.821	9.886	9.649
F	0.589	0.746	0.738	0.518	0.785	0.820	0.617	1.175	0.957
Cl	0.253	0.366	0.309	0.576	0.402	0.351	0.108	0.114	0.081
Total	96.231	97.331	97.129	97.368	97.344	96.867	95.778	96.743	97.005
Si	5.8038	5.7629	5.7864	5.7757	5.8017	5.8089	5.7718	5.7771	5.7210
Al	2.2161	2.2334	2.2270	2.2286	2.1621	2.1844	2.3808	2.3812	2.3579
Ti	0.4476	0.4673	0.4357	0.4410	0.5028	0.4388	0.2873	0.2992	0.3353
Fe	2.6201	2.9014	2.7530	2.7699	2.7694	2.6487	2.9268	2.8932	2.9816
Mn	0.0206	0.0248	0.0153	0.0273	0.0236	0.0313	0.0794	0.0804	0.0832
Mg	2.5273	2.2542	2.4231	2.4118	2.3517	2.5209	2.2758	2.2754	2.2683
Ca	0.0074	0.0028	0.0015	0.0000	0.0057	0.0056	0.0000	0.0019	0.0000
Na	0.0528	0.0975	0.1040	0.0897	0.0913	0.1009	0.0934	0.0829	0.1192
K	1.9399	1.9124	1.9382	1.9368	1.9007	1.9391	1.9611	1.9633	1.9128
F	0.2868	0.3640	0.3585	0.2516	0.3814	0.3987	0.3056	0.5786	0.4702
Cl	0.0660	0.0956	0.0804	0.1499	0.1045	0.0916	0.0287	0.0302	0.0214

Sample No.	DAR163 N:4	DAR163 N:5	DAR163 N:6	DAR163 N:7	DAR163 N:8	DAR163 N:9	DAR163 N:10	DAR164 N:1	DAR164 N:2
SiO2	36.7710	36.2040	36.2700	35.7310	36.2000	36.0680	35.8360	37.0530	36.8340
Al2O3	12.808	13.471	13.245	13.426	12.941	13.249	13.412	13.423	13.715
TiO2	2.603	2.651	2.672	4.571	2.943	3.328	4.592	4.911	2.011
FeO	22.949	23.258	23.498	26.935	25.407	25.857	25.469	19.502	21.506
MnO	0.650	0.643	0.640	0.712	0.728	0.471	0.684	0.130	0.150
MgO	9.666	8.815	8.837	5.255	6.955	6.660	6.171	10.642	10.693
CaO	0.042	0.000	0.002	0.004	0.005	0.008	0.034	0.026	0.028
Na2O	0.266	0.257	0.320	0.213	0.235	0.161	0.282	0.266	0.168
K2O	9.947	9.937	9.837	9.644	9.876	10.030	9.860	9.934	10.034
F	0.985	1.008	0.577	0.399	0.634	0.363	0.739	0.320	0.478
Cl	0.081	0.106	0.091	0.158	0.147	0.147	0.153	0.206	0.693
Total	96.768	96.350	95.989	97.048	96.071	96.342	97.232	96.413	96.310
Si	5.7411	5.6916	5.7022	5.6389	5.7512	5.7051	5.6324	5.6556	5.7231
Al	2.3568	2.4959	2.4542	2.4971	2.4231	2.4699	2.4844	2.4147	2.5115
Ti	0.3056	0.3135	0.3159	0.5425	0.3516	0.3959	0.5428	0.5637	0.2350
Fe	2.9965	3.0578	3.0896	3.5550	3.3757	3.4204	3.3477	2.4895	2.7944
Mn	0.0860	0.0857	0.0852	0.0951	0.0979	0.0631	0.0910	0.0168	0.0197
Mg	2.2495	2.0656	2.0708	1.2361	1.6469	1.5703	1.4457	2.4211	2.4764
Ca	0.0070	0.0000	0.0003	0.0006	0.0008	0.0013	0.0057	0.0043	0.0047
Na	0.0805	0.0783	0.0976	0.0651	0.0724	0.0495	0.0861	0.0786	0.0507
K	1.9812	1.9927	1.9729	1.9414	2.0016	2.0239	1.9769	1.9343	1.9888
F	0.4862	0.5014	0.2867	0.1990	0.3188	0.1815	0.3676	0.1543	0.2349
Cl	0.0214	0.0281	0.0244	0.0423	0.0395	0.0394	0.0409	0.0534	0.1824

Sample No.	DAR164 N:4	DAR164 N:5	DAR164 N:6	DAR164 N:9	DAR164 N:1	DAR167 N:22	DAR167 N:23	DAR167 N:24	DAR167 N:25
SiO2	37.3190	36.7110	36.1560	35.3200	36.6700	38.7080	38.2560	37.2320	37.9340
Al2O3	13.141	13.467	13.408	13.074	13.335	12.109	12.013	12.245	11.888
TiO2	3.894	4.665	3.219	4.303	4.723	2.315	2.797	3.208	3.028
FeO	21.108	21.744	23.092	21.780	20.545	17.171	17.893	22.987	19.136
MnO	0.188	0.278	0.193	0.315	0.219	0.430	0.383	0.294	0.358
MgO	10.506	9.380	9.439	8.811	9.682	14.011	13.237	9.393	12.117
CaO	0.009	0.021	0.063	1.872	0.019	0.008	0.014	0.014	0.000
Na2O	0.212	0.199	0.109	0.105	0.221	0.339	0.275	0.098	0.330
K2O	9.991	9.945	9.672	9.662	9.882	9.615	9.700	9.913	9.667
F	0.357	0.140	0.117	0.033	0.394	1.328	1.077	0.541	1.180
Cl	0.497	0.397	0.560	0.286	0.349	0.049	0.060	0.143	0.104
Total	97.222	96.947	96.028	95.561	96.039	96.083	95.705	96.068	95.742
Si	5.7096	5.6394	5.6514	5.5456	5.6667	5.8976	5.8670	5.8154	5.8647
Al	2.3695	2.4382	2.4699	2.4193	2.4287	2.1744	2.1713	2.2541	2.1662
Ti	0.4481	0.5389	0.3784	0.5080	0.5488	0.2653	0.3225	0.3768	0.3521
Fe	2.7008	2.7934	3.0185	2.8598	2.6552	2.1880	2.2949	3.0027	2.4742
Mn	0.0244	0.0362	0.0256	0.0419	0.0287	0.0554	0.0497	0.0389	0.0469
Mg	2.3959	2.1477	2.1989	2.0620	2.2302	3.1820	3.0260	2.1867	2.7921
Ca	0.0015	0.0034	0.0105	0.3149	0.0032	0.0013	0.0022	0.0023	0.0000
Na	0.0630	0.0593	0.0329	0.0321	0.0663	0.1001	0.0819	0.0298	0.0990
K	1.9499	1.9489	1.9284	1.9352	1.9481	1.8689	1.8976	1.9751	1.9066
F	0.1727	0.0679	0.0578	0.0164	0.1925	0.6398	0.5225	0.2675	0.5771
Cl	0.1288	0.1034	0.1483	0.0762	0.0914	0.0126	0.0156	0.0380	0.0271

Sample No.	DAR167 N:26	DAR167 N:27	DAR167 N:28	DAR167 N:29	DAR167 N:30	DAR167 N:31	DAR168 N:1	DAR168 N:2	DAR168 N:3
SiO2	37.8880	35.1170	36.9470	36.6990	37.9610	38.4320	37.1860	37.0000	36.6300
Al2O3	11.713	13.007	11.870	11.564	11.868	11.817	16.730	15.320	17.291
TiO2	2.942	3.998	3.193	3.615	3.023	2.759	3.564	3.513	2.853
FeO	19.978	27.418	25.822	25.462	20.628	18.023	18.838	17.904	19.110
MnO	0.329	0.254	0.286	0.374	0.418	0.344	0.147	0.153	0.154
MgO	11.631	5.381	7.330	7.276	11.270	12.995	9.295	10.145	8.792
CaO	0.031	0.000	0.010	0.025	0.000	0.010	0.019	0.008	0.008
Na2O	0.198	0.187	0.120	0.257	0.463	0.231	0.201	0.138	0.182
K2O	9.767	9.562	9.683	9.221	9.585	9.940	10.117	9.721	9.791
F	1.238	0.062	0.309	0.551	1.536	1.324	0.606	0.614	0.458
Cl	0.114	0.692	0.679	0.693	0.032	0.054	0.635	0.599	0.639
Total	95.829	95.678	96.249	95.737	96.784	95.929	97.338	95.115	95.908
Si	5.8827	5.6519	5.8580	5.8548	5.8637	5.9034	5.6141	5.6946	5.6050
Al	2.1433	2.4671	2.2180	2.1743	2.1607	2.1394	2.9769	2.7788	3.1183
Ti	0.3436	0.4838	0.3808	0.4337	0.3512	0.3187	0.4046	0.4066	0.3283
Fe	2.5941	3.6903	3.4240	3.3972	2.6647	2.3153	2.3785	2.3046	2.4455
Mn	0.0432	0.0346	0.0383	0.0505	0.0547	0.0447	0.0188	0.0200	0.0200
Mg	2.6916	1.2909	1.7323	1.7301	2.5948	2.9753	2.0917	2.3272	2.0052
Ca	0.0052	0.0000	0.0016	0.0043	0.0000	0.0016	0.0031	0.0013	0.0013
Na	0.0597	0.0582	0.0370	0.0795	0.1386	0.0689	0.0588	0.0412	0.0541
K	1.9344	1.9631	1.9586	1.8766	1.8887	1.9478	1.9484	1.9086	1.9111
F	0.6081	0.0317	0.1549	0.2778	0.7505	0.6433	0.2894	0.2988	0.2215
Cl	0.0299	0.1887	0.1826	0.1873	0.0085	0.0141	0.1624	0.1562	0.1657

FELDSPARS

Sample No.	46297 1	46297 2	46297 3	46297 4	46297 5	46297 6	46297 7	46297 8	46297 9
SiO2	69.148	68.726	67.022	68.244	66.550	66.066	67.916	66.590	65.419
Al2O3	19.830	19.549	19.240	19.235	19.705	19.251	19.525	19.681	19.216
TiO2	0.092	0.000	0.052	0.008	0.048	0.023	0.006	0.000	0.000
FeO	0.090	0.096	0.081	0.052	0.064	0.102	0.048	0.100	0.085
MnO	0.000	0.000	0.026	0.018	0.000	0.007	0.004	0.000	0.000
MgO	0.020	0.007	0.000	0.010	0.006	0.018	0.011	0.021	0.016
CaO	0.082	0.000	0.000	0.000	0.057	0.256	0.199	0.523	0.298
BaO	0.535	0.381	0.493	0.325	0.361	0.390	0.436	0.422	0.334
Na2O	4.520	4.518	4.938	4.224	5.189	5.530	2.934	6.528	5.405
K2O	5.374	7.070	6.974	8.281	6.001	8.267	9.210	5.446	7.650
Total	99.691	100.347	98.826	100.397	97.981	99.910	100.289	99.311	98.423
Si	3.044	3.035	3.018	3.032	3.005	2.979	3.026	2.982	2.982
Al	1.029	1.018	1.021	1.007	1.049	1.023	1.025	1.039	1.032
Ti	0.003	0.000	0.002	0.000	0.002	0.001	0.000	0.000	0.000
Fe	0.003	0.004	0.003	0.002	0.002	0.004	0.002	0.004	0.003
Mn	0.000	0.000	0.001	0.001	0.000	0.000	0.000	0.000	0.000
Mg	0.001	0.000	0.000	0.001	0.000	0.001	0.001	0.001	0.001
Ca	0.004	0.000	0.000	0.000	0.003	0.012	0.010	0.025	0.015
Ba	0.009	0.007	0.009	0.006	0.006	0.007	0.008	0.007	0.006
Na	0.386	0.387	0.431	0.364	0.454	0.484	0.253	0.567	0.478
K	0.302	0.398	0.401	0.469	0.346	0.476	0.524	0.311	0.445

Sample No.	46297 10	46297 11	46297 12	46297 13	46297 14	46297 15	46297 16	46297 17	46297 18
SiO2	67.603	67.315	66.772	67.187	70.000	67.178	66.640	68.943	66.431
Al2O3	19.147	19.494	18.821	19.275	19.972	19.406	19.601	19.830	19.095
TiO2	0.054	0.037	0.000	0.031	0.017	0.000	0.031	0.048	0.055
FeO	0.085	0.090	0.031	0.058	0.027	0.101	0.101	0.090	0.093
MnO	0.000	0.022	0.008	0.007	0.000	0.012	0.000	0.025	0.020
MgO	0.010	0.000	0.007	0.000	0.014	0.013	0.013	0.018	0.014
CaO	0.257	0.342	0.061	0.394	0.539	0.344	0.460	0.559	0.153
BaO	0.384	0.417	0.460	0.480	0.108	0.446	0.408	0.053	0.580
Na2O	4.825	5.660	2.516	3.194	5.761	6.238	6.392	8.329	1.633
K2O	8.332	6.595	11.146	9.708	1.455	6.155	6.207	0.296	11.805
Total	100.697	99.972	99.822	100.334	97.893	99.893	99.853	98.191	99.879
Si	3.010	3.000	3.024	3.012	3.068	2.997	2.980	3.030	3.014
Al	1.005	1.024	1.004	1.018	1.032	1.020	1.033	1.027	1.021
Ti	0.002	0.001	0.000	0.001	0.001	0.000	0.001	0.002	0.002
Fe	0.003	0.003	0.001	0.002	0.001	0.004	0.004	0.003	0.003
Mn	0.000	0.001	0.000	0.000	0.000	0.000	0.000	0.001	0.001
Mg	0.001	0.000	0.000	0.000	0.001	0.001	0.001	0.001	0.001
Ca	0.012	0.016	0.003	0.019	0.025	0.016	0.022	0.026	0.007
Ba	0.007	0.007	0.008	0.008	0.002	0.008	0.007	0.001	0.010
Na	0.417	0.489	0.221	0.278	0.490	0.540	0.554	0.710	0.144
K	0.473	0.375	0.644	0.555	0.081	0.350	0.354	0.017	0.683

Sample No.	46297 19	46297 20	46297 21	46297 22	52215 1	52215 2	52215 3	52215 4	52215 5
SiO2	67.558	66.203	65.415	66.124	67.165	67.677	66.525	66.928	66.632
Al2O3	20.042	19.125	19.453	19.359	19.302	19.228	19.974	18.624	19.283
TiO2	0.017	0.000	0.062	0.041	0.019	0.039	0.038	0.031	0.000
FeO	0.042	0.066	0.167	0.080	0.086	0.190	0.078	0.052	0.049
MnO	0.010	0.006	0.001	0.007	0.016	0.015	0.000	0.024	0.023
MgO	0.012	0.000	0.011	0.010	0.000	0.012	0.010	0.016	0.004
CaO	0.591	0.108	0.321	0.285	0.150	0.133	0.386	0.018	0.058
BaO	0.190	0.554	0.394	0.373	0.328	0.300	0.474	0.355	0.241
Na2O	8.708	2.081	5.678	6.129	6.333	6.379	9.690	2.037	6.383
K2O	2.315	11.678	7.597	7.221	7.038	6.980	2.743	12.218	6.518
Total	99.485	99.771	99.099	99.629	100.437	100.953	99.918	100.303	99.191
Si	2.9815	3.0078	2.9678	2.9780	2.9935	2.9995	2.9533	3.0275	2.9958
Al	1.0425	1.0240	1.0402	1.0276	1.0139	1.0044	1.0451	0.9929	1.0218
Ti	0.0006	0.0000	0.0021	0.0014	0.0006	0.0013	0.0013	0.0011	0.0000
Fe	0.0016	0.0025	0.0063	0.0030	0.0032	0.0070	0.0029	0.0020	0.0018
Mn	0.0004	0.0002	0.0000	0.0003	0.0006	0.0006	0.0000	0.0009	0.0009
Mg	0.0008	0.0000	0.0008	0.0007	0.0000	0.0008	0.0007	0.0011	0.0002
Ca	0.0279	0.0052	0.0156	0.0138	0.0072	0.0063	0.0183	0.0009	0.0028
Ba	0.0033	0.0099	0.0070	0.0066	0.0057	0.0052	0.0060	0.0063	0.0042
Na	0.7451	0.1834	0.4995	0.5352	0.5472	0.5482	0.8341	0.1787	0.5564
K	0.1303	0.6768	0.4397	0.4148	0.4001	0.3946	0.1554	0.7050	0.3738

Sample No.	52215 6	52215 7	52215 8	52215 9	52215 10	52215 11	52215 12	52215 13	52215 14
SiO2	66.915	68.191	67.557	67.861	67.050	67.124	67.981	66.316	64.953
Al2O3	19.237	19.401	19.243	19.457	19.356	19.309	19.410	19.957	18.779
TiO2	0.052	0.023	0.031	0.031	0.000	0.029	0.058	0.002	0.004
FeO	0.093	0.236	0.122	0.347	0.288	0.193	0.279	0.134	0.101
MnO	0.015	0.038	0.023	0.009	0.001	0.045	0.029	0.012	0.012
MgO	0.021	0.004	0.019	0.013	0.010	0.001	0.019	0.005	0.000
CaO	0.174	0.157	0.084	0.196	0.201	0.150	0.192	0.398	0.000
BaO	0.284	0.277	0.314	0.302	0.281	0.309	0.314	0.352	0.400
Na2O	6.093	6.593	6.454	7.627	7.404	6.153	6.477	11.344	0.383
K2O	6.909	6.112	6.582	3.474	5.473	6.728	4.463	0.370	14.780
Total	99.793	101.032	100.429	99.317	100.064	100.041	99.222	98.890	99.412
Si	2.9963	3.0052	3.0006	3.0093	2.9870	2.9970	3.0195	2.9498	3.0006
Al	1.0152	1.0077	1.0073	1.0169	1.0163	1.0161	1.0161	1.0462	1.0225
Ti	0.0018	0.0008	0.0010	0.0004	0.0000	0.0010	0.0019	0.0001	0.0001
Fe	0.0035	0.0087	0.0045	0.0129	0.0107	0.0072	0.0104	0.0050	0.0039
Mn	0.0006	0.0014	0.0009	0.0003	0.0000	0.0017	0.0011	0.0004	0.0005
Mg	0.0014	0.0002	0.0013	0.0009	0.0007	0.0001	0.0012	0.0003	0.0000
Ca	0.0084	0.0074	0.0088	0.0093	0.0096	0.0072	0.0092	0.0190	0.0000
Ba	0.0050	0.0048	0.0055	0.0052	0.0049	0.0054	0.0055	0.0061	0.0072
Na	0.5290	0.5633	0.5558	0.6558	0.6395	0.5326	0.5577	0.9784	0.0343
K	0.3946	0.3436	0.3729	0.1965	0.3110	0.3832	0.2529	0.0210	0.8710

Sample No.	52215 15	52215 16	52215 17	52218 1	52218 2	52218 3	52218 4	52218 5	52218 6
SiO2	64.658	65.983	68.542	66.051	66.738	67.157	64.712	66.275	65.818
Al2O3	19.088	19.326	19.842	19.331	19.333	19.445	18.595	18.974	18.961
TiO2	0.000	0.000	0.000	0.047	0.041	0.000	0.029	0.036	0.047
FeO	0.115	0.117	0.102	0.056	0.082	0.047	0.058	0.089	0.085
MnO	0.015	0.020	0.009	0.002	0.011	0.000	0.005	0.000	0.005
MgO	0.011	0.005	0.012	0.000	0.010	0.014	0.017	0.007	0.014
CaO	0.081	0.102	0.127	0.309	0.147	0.171	0.013	0.198	0.205
BaO	0.358	0.274	0.225	0.263	0.232	0.224	0.434	0.215	0.242
Na2O	4.097	3.398	3.596	6.630	6.150	8.519	1.949	6.532	6.021
K2O	11.895	10.234	6.656	6.624	7.438	4.326	12.813	6.761	7.292
Total	100.318	99.459	99.111	99.313	100.182	99.903	98.625	99.087	98.690
Si	2.9561	2.9941	3.0423	2.9771	2.9865	2.9839	2.9981	2.9924	2.9894
Al	1.0285	1.0335	1.0380	1.0269	1.0196	1.0183	1.0153	1.0097	1.0150
Ti	0.0000	0.0000	0.0000	0.0016	0.0014	0.0000	0.0010	0.0012	0.0016
Fe	0.0044	0.0044	0.0038	0.0021	0.0031	0.0017	0.0022	0.0033	0.0032
Mn	0.0006	0.0008	0.0003	0.0001	0.0004	0.0000	0.0002	0.0000	0.0002
Mg	0.0008	0.0003	0.0008	0.0000	0.0006	0.0009	0.0012	0.0005	0.0009
Ca	0.0040	0.0050	0.0060	0.0149	0.0071	0.0081	0.0007	0.0096	0.0100
Ba	0.0064	0.0049	0.0039	0.0046	0.0041	0.0039	0.0079	0.0038	0.0043
Na	0.3631	0.2989	0.3095	0.5794	0.5336	0.7339	0.1751	0.5718	0.5303
K	0.6937	0.5924	0.3768	0.3809	0.4246	0.2452	0.7573	0.3894	0.4225

Sample No.	52218 7	52218 8	52218 9	52218 10	52218 11	52218 12	52221 1	52221 2	52221 3
SiO2	63.813	62.954	67.340	65.845	65.307	65.588	67.623	68.126	68.623
Al2O3	18.466	18.342	19.454	19.116	18.761	19.288	19.073	18.908	18.963
TiO2	0.062	0.029	0.028	0.051	0.018	0.032	0.006	0.000	0.008
FeO	0.003	0.022	0.021	0.089	0.106	0.074	0.235	0.256	0.223
MnO	0.019	0.017	0.017	0.011	0.000	0.000	0.000	0.014	0.019
MgO	0.012	0.014	0.006	0.015	0.000	0.011	0.004	0.011	0.001
CaO	0.000	0.000	0.219	0.177	0.118	0.239	0.025	0.001	0.000
BaO	0.381	0.473	0.024	0.250	0.199	0.224	0.016	0.011	0.027
Na2O	0.431	0.779	10.995	6.258	5.809	7.161	11.311	11.170	11.106
K2O	15.353	14.889	0.602	7.429	7.934	6.375	0.174	0.187	0.155
Total	98.540	97.519	98.706	99.241	98.252	98.992	98.467	98.684	99.125
Si	2.9894	2.9822	2.9854	2.9799	2.9888	2.9684	3.0005	3.0130	3.0185
Al	1.0195	1.0240	1.0164	1.0196	1.0119	1.0288	0.9974	0.9856	0.9831
Ti	0.0022	0.0010	0.0090	0.0017	0.0006	0.0011	0.0002	0.0000	0.0003
Fe	0.0001	0.0009	0.0008	0.0034	0.0041	0.0028	0.0087	0.0095	0.0082
Mn	0.0007	0.0007	0.0006	0.0004	0.0000	0.0000	0.0000	0.0005	0.0007
Mg	0.0008	0.0010	0.0004	0.0010	0.0000	0.0008	0.0003	0.0007	0.0001
Ca	0.0000	0.0000	0.0104	0.0086	0.0058	0.0116	0.0012	0.0000	0.0000
Ba	0.0070	0.0088	0.0004	0.0044	0.0036	0.0040	0.0003	0.0002	0.0005
Na	0.0391	0.0716	0.9451	0.5491	0.5154	0.6284	0.9731	0.9578	0.9472
K	0.9175	0.8997	0.0341	0.4289	0.4632	0.3681	0.0099	0.0106	0.0087

Sample No.	52221 4	52221 5	52221 6	52221 7	52221 8	52221 9	52221 10	52221 11	52221 12
SiO2	68.529	67.855	67.678	67.673	68.095	67.941	69.509	68.168	67.227
Al2O3	19.000	18.815	18.999	18.994	18.961	18.868	18.922	19.043	19.147
TiO2	0.000	0.000	0.000	0.048	0.000	0.000	0.026	0.002	0.000
FeO	0.256	0.257	0.255	0.203	0.170	0.240	0.199	0.207	0.139
MnO	0.008	0.000	0.018	0.009	0.000	0.012	0.000	0.003	0.000
MgO	0.002	0.016	0.010	0.002	0.018	0.028	0.006	0.020	0.044
CaO	0.013	0.004	0.004	0.008	0.009	0.009	0.014	0.009	0.008
BaO	0.035	0.036	0.004	0.031	0.012	0.020	0.027	0.000	0.046
Na2O	10.892	11.255	11.117	11.375	10.257	10.475	9.686	11.456	11.622
K2O	0.192	0.245	0.183	0.200	0.249	0.190	0.197	0.214	0.297
Total	98.927	98.483	98.268	98.543	97.771	97.783	98.586	99.122	98.530
Si	3.0190	3.0106	3.0062	3.0016	3.0263	3.0230	3.0514	3.0051	2.9882
Al	0.9865	0.9838	0.9946	0.9929	0.9932	0.9894	0.9790	0.9894	1.0031
Ti	0.0000	0.0000	0.0000	0.0016	0.0000	0.0000	0.0009	0.0001	0.0000
Fe	0.0094	0.0095	0.0095	0.0075	0.0063	0.0089	0.0073	0.0076	0.0052
Mn	0.0003	0.0000	0.0007	0.0003	0.0000	0.0005	0.0000	0.0001	0.0000
Mg	0.0001	0.0011	0.0007	0.0001	0.0012	0.0019	0.0004	0.0013	0.0029
Ca	0.0006	0.0002	0.0002	0.0004	0.0004	0.0004	0.0007	0.0004	0.0004
Ba	0.0006	0.0006	0.0001	0.0005	0.0002	0.0003	0.0005	0.0000	0.0008
Na	0.9303	0.9682	0.9575	0.9783	0.8839	0.9037	0.8244	0.9792	1.0016
K	0.0108	0.0139	0.0104	0.0113	0.0141	0.0108	0.0110	0.0120	0.0168

Sample No.	52221 13	52221 14	52221 15	52221 16	52221 17	52221 18	52221 19	52221 20	52221 21
SiO2	67.822	67.492	66.570	66.110	68.548	67.719	66.552	67.023	72.870
Al2O3	18.819	19.203	19.248	19.381	19.208	19.152	18.941	18.824	19.505
TiO2	0.026	0.000	0.004	0.000	0.000	0.048	0.000	0.000	0.012
FeO	0.209	0.226	0.235	0.106	0.211	0.201	0.213	0.207	0.095
MnO	0.000	0.024	0.015	0.008	0.000	0.000	0.003	0.011	N.A.
MgO	0.025	0.011	0.019	0.000	0.010	0.025	0.000	0.012	N.A.
CaO	0.007	0.031	0.030	0.000	0.005	0.014	0.005	0.012	0.027
BaO	0.027	0.000	0.007	0.014	0.023	0.033	0.002	0.017	0.000
Na2O	11.803	11.819	11.853	12.040	10.948	11.805	11.601	11.202	8.008
K2O	0.160	0.157	0.178	0.212	0.207	0.150	0.307	0.325	0.147
Total	98.898	98.963	98.159	97.871	99.160	99.147	97.624	97.633	100.664
Si	3.0020	2.9870	2.9742	2.9645	3.0128	2.9906	2.9873	3.0018	3.0973
Al	0.9817	1.0017	1.0135	1.0243	0.9950	0.9968	1.0020	0.9936	0.9771
Ti	0.0009	0.0000	0.0001	0.0000	0.0000	0.0016	0.0000	0.0000	0.0004
Fe	0.0077	0.0084	0.0088	0.0040	0.0077	0.0074	0.0080	0.0077	0.0034
Mn	0.0000	0.0009	0.0006	0.0003	0.0000	0.0000	0.0001	0.0004	N.A.
Mg	0.0017	0.0007	0.0013	0.0000	0.0007	0.0017	0.0000	0.0008	N.A.
Ca	0.0003	0.0015	0.0014	0.0000	0.0002	0.0007	0.0002	0.0006	0.0012
Ba	0.0005	0.0000	0.0001	0.0002	0.0004	0.0006	0.0000	0.0003	0.0000
Na	1.0129	1.0142	1.1267	1.0468	0.9330	1.0108	1.0096	0.9728	0.6600
K	0.0090	0.0089	0.0101	0.0121	0.0116	0.0085	0.0176	0.0186	0.0080

Sample No.	52221 22	52221 23	52221 24	52221 25	52221 26	52221 27	52221 28	52221 29	52221 30
SiO2	73.168	73.622	69.487	69.430	70.147	72.575	69.432	73.041	66.480
Al2O3	19.355	19.844	19.135	19.464	19.517	19.622	20.216	19.632	18.475
TiO2	0.006	0.007	0.011	0.014	0.012	0.022	0.023	0.000	0.013
FeO	0.178	0.077	0.124	0.133	0.130	0.112	0.335	0.162	0.118
MnO	N.A.	N.A.	N.A.	N.A.	N.A.	N.A.	N.A.	N.A.	N.A.
MgO	N.A.	N.A.	N.A.	N.A.	N.A.	N.A.	N.A.	N.A.	N.A.
CaO	0.013	0.020	0.052	0.019	0.006	0.010	0.083	0.032	0.030
BaO	0.000	0.000	0.043	0.012	0.003	0.020	0.000	0.000	0.083
Na2O	8.502	8.656	11.168	9.586	9.085	9.128	8.382	8.522	3.559
K2O	0.160	0.148	0.138	0.182	0.168	0.214	0.144	0.151	11.289
Total	101.382	102.374	100.158	98.840	99.068	101.703	98.615	101.540	100.047
Si	3.0957	3.0849	3.0225	3.0377	3.0522	3.0723	3.0314	3.0863	3.0138
Al	0.9651	0.9800	0.9810	1.0037	1.0009	0.9790	1.0402	0.9777	0.9871
Ti	0.0002	0.0002	0.0004	0.0005	0.0004	0.0007	0.0007	0.0000	0.0005
Fe	0.0063	0.0027	0.0045	0.0049	0.0047	0.0040	0.0122	0.0057	0.0045
Mn	N.A.	N.A.	N.A.	N.A.	N.A.	N.A.	N.A.	N.A.	N.A.
Mg	N.A.	N.A.	N.A.	N.A.	N.A.	N.A.	N.A.	N.A.	N.A.
Ca	0.0006	0.0009	0.0024	0.0009	0.0003	0.0004	0.0039	0.0015	0.0015
Ba	0.0000	0.0000	0.0007	0.0002	0.0000	0.0003	0.0000	0.0000	0.0015
Na	0.6975	0.7033	0.9418	0.8132	0.7664	0.7492	0.7096	0.6982	0.3128
K	0.0087	0.0079	0.0077	0.0102	0.0093	0.0115	0.0080	0.0081	0.6528

Sample No.	52221 31	52221 32	77-22 1	77-22 2	77-22 3	77-22 4	77-22 5	77-22 6	77-22 7
SiO2	65.678	63.331	65.143	66.420	65.178	65.625	64.959	65.817	64.915
Al2O3	19.144	18.787	18.858	18.818	19.332	19.035	18.827	19.558	19.272
TiO2	0.032	0.009	0.034	0.000	0.042	0.046	0.048	0.071	0.040
FeO	0.150	0.080	0.091	0.012	0.176	0.165	0.184	0.094	0.114
MnO	N.A.	N.A.	N.A.	N.A.	N.A.	N.A.	N.A.	N.A.	N.A.
MgO	N.A.	N.A.	N.A.	N.A.	N.A.	N.A.	N.A.	N.A.	N.A.
CaO	0.174	0.029	0.157	0.000	0.259	0.211	0.195	0.452	0.298
BaO	0.015	0.003	0.021	0.101	0.064	0.041	0.096	0.055	0.087
Na2O	4.953	1.499	3.914	0.215	8.560	7.899	7.715	10.065	9.333
K2O	9.561	13.948	11.048	16.032	4.895	5.774	6.096	2.794	3.638
Total	99.707	97.686	99.266	101.598	98.506	98.796	98.120	98.906	97.697
Si	2.9773	2.9742	2.9817	3.0088	2.9547	2.9711	2.9687	2.9506	2.9542
Al	1.0228	1.0398	1.0173	1.0047	1.0328	1.0157	1.0140	1.0334	1.0337
Ti	0.0011	0.0003	0.0012	0.0000	0.0014	0.0016	0.0016	0.0024	0.0014
Fe	0.0057	0.0032	0.0035	0.0004	0.0067	0.0063	0.0070	0.0035	0.0043
Mn	N.A.	N.A.	N.A.	N.A.	N.A.	N.A.	N.A.	N.A.	N.A.
Mg	N.A.	N.A.	N.A.	N.A.	N.A.	N.A.	N.A.	N.A.	N.A.
Ca	0.0084	0.0015	0.0077	0.0000	0.0126	0.0102	0.0095	0.0217	0.0145
Ba	0.0003	0.0001	0.0004	0.0018	0.0011	0.0007	0.0017	0.0010	0.0016
Na	0.4353	0.1365	0.3474	0.0189	0.7523	0.6934	0.6837	0.8749	0.8235
K	0.5529	0.8356	0.6451	0.9264	0.2830	0.3335	0.3554	0.1598	0.2112

Sample No.	77-22 8
SiO2	66.392
Al2O3	19.570
TiO2	0.042
FeO	0.124
MnO	N.A.
MgO	N.A.
CaO	0.348
BaO	0.035
Na2O	9.452
K2O	3.811
Total	99.774
Si	2.9583
Al	1.0277
Ti	0.0014
Fe	0.0046
Mn	N.A.
Mg	N.A.
Ca	0.0166
Ba	0.0006
Na	0.8166
K	0.2166

Sample No.	52246 1	52246 2	52246 3	52246 4	52246 5	52246 6	52246 7	52246 8	52246 9
SiO2	68.523	68.173	68.198	67.819	68.697	68.412	68.643	67.621	68.184
Al2O3	19.082	19.224	19.163	19.207	19.270	19.168	19.190	19.160	19.078
TiO2	0.042	0.000	0.000	0.000	0.050	0.008	0.026	0.024	0.034
FeO	0.238	0.167	0.314	0.142	0.276	0.215	0.267	0.152	0.235
MnO	0.019	0.017	0.015	0.003	0.000	0.027	0.000	0.046	0.003
MgO	0.011	0.021	0.015	0.007	0.013	0.021	0.003	0.009	0.010
CaO	0.011	0.012	0.022	0.000	0.026	0.007	0.012	0.001	0.007
BaO	0.061	0.007	0.002	0.000	0.013	0.037	0.018	0.000	0.035
Na2O	11.889	12.060	11.991	11.948	12.019	11.892	11.866	11.896	12.093
K2O	0.089	0.104	0.101	0.135	0.146	0.119	0.192	0.123	0.141
Total	99.965	99.785	99.821	99.261	100.510	99.906	100.217	99.032	99.820
Si	3.000	2.991	2.993	2.991	2.994	2.997	2.999	2.989	2.994
Al	0.985	0.994	0.991	0.998	0.990	0.990	0.988	0.998	0.987
Ti	0.001	0.000	0.000	0.000	0.002	0.000	0.001	0.001	0.001
Fe	0.009	0.006	0.011	0.005	0.010	0.008	0.010	0.006	0.009
Mn	0.001	0.001	0.001	0.000	0.000	0.001	0.000	0.002	0.000
Mg	0.001	0.001	0.001	0.000	0.001	0.001	0.000	0.001	0.001
Ca	0.000	0.001	0.001	0.000	0.001	0.000	0.001	0.000	0.000
Ba	0.001	0.001	0.000	0.000	0.000	0.001	0.000	0.000	0.001
Na	1.009	1.026	1.020	1.022	1.015	1.010	1.005	1.020	1.030
K	0.005	0.006	0.001	0.008	0.008	0.007	0.011	0.007	0.008

Sample No.	52246 10	52246 11	52246 12	52246 13	52246 14	52246 15	52246 16	52246 17	52246 18
SiO2	65.055	64.551	65.028	65.121	65.419	65.136	68.316	65.247	68.227
Al2O3	18.750	18.209	18.563	18.236	18.534	18.001	19.021	18.420	19.039
TiO2	0.076	0.061	0.020	0.018	0.006	0.020	0.000	0.000	0.020
FeO	0.167	0.153	0.121	0.173	0.106	0.123	0.197	0.174	0.279
MnO	0.008	0.013	0.017	0.002	0.010	0.001	0.000	0.023	0.008
MgO	0.017	0.000	0.017	0.017	0.032	0.004	0.014	0.004	0.016
CaO	0.000	0.000	0.000	0.000	0.000	0.000	0.000	0.000	0.009
BaO	0.060	0.027	0.036	0.079	0.057	0.048	0.020	0.067	0.008
Na2O	2.394	1.114	2.029	1.110	2.087	0.616	11.895	1.496	11.821
K2O	13.619	15.135	13.648	14.631	13.007	14.955	0.108	14.152	0.160
Total	100.146	99.263	99.479	99.387	99.258	98.904	99.571	99.583	99.587
Si	2.981	2.998	2.994	3.009	3.006	3.022	3.002	3.004	2.999
Al	1.013	0.996	1.007	0.993	1.004	0.984	0.985	1.000	0.986
Ti	0.003	0.002	0.001	0.001	0.000	0.001	0.000	0.000	0.001
Fe	0.006	0.006	0.005	0.007	0.004	0.005	0.007	0.007	0.010
Mn	0.000	0.000	0.001	0.000	0.000	0.000	0.000	0.001	0.000
Mg	0.001	0.000	0.001	0.001	0.002	0.000	0.001	0.000	0.001
Ca	0.000	0.000	0.000	0.000	0.000	0.000	0.000	0.000	0.000
Ba	0.001	0.000	0.001	0.001	0.001	0.001	0.000	0.001	0.000
Na	0.213	0.100	0.181	0.099	0.186	0.055	1.013	0.134	1.008
K	0.796	0.896	0.802	0.863	0.762	0.885	0.006	0.831	0.009

Sample No.	52246 19	52246 20	52246 21	52246 22	52246 23	52246 24	52246 25	52246 26	52246 27
SiO2	67.972	68.344	68.151	65.262	65.631	64.965	64.426	68.411	67.767
Al2O3	19.249	19.079	19.148	19.080	18.119	18.004	18.186	19.137	19.258
TiO2	0.018	0.006	0.004	0.039	0.026	0.035	0.014	0.000	0.042
FeO	0.161	0.283	0.079	0.154	0.230	0.180	0.124	0.334	0.228
MnO	0.000	0.000	0.024	0.020	0.016	0.014	0.000	0.024	0.005
MgO	0.021	0.011	0.000	0.020	0.020	0.007	0.000	0.022	0.004
CaO	0.008	0.027	0.038	0.000	0.010	0.000	0.000	0.022	0.015
BaO	0.000	0.003	0.037	0.062	0.055	0.049	0.052	0.037	0.003
Na2O	11.706	11.835	11.639	2.360	4.809	0.626	0.540	11.626	11.765
K2O	0.152	0.194	0.454	13.098	9.446	15.494	15.500	0.149	0.135
Total	99.287	99.782	99.574	100.095	98.362	99.374	98.842	99.762	99.222
Si	2.994	2.999	2.998	2.981	3.012	3.013	3.004	3.000	2.989
Al	0.999	0.987	0.993	1.027	0.980	0.984	0.999	0.989	1.001
Ti	0.001	0.000	0.000	0.001	0.001	0.001	0.000	0.000	0.001
Fe	0.006	0.010	0.003	0.006	0.009	0.007	0.005	0.012	0.008
Mn	0.000	0.000	0.001	0.001	0.001	0.000	0.000	0.001	0.000
Mg	0.001	0.001	0.000	0.001	0.001	0.000	0.000	0.001	0.000
Ca	0.000	0.001	0.002	0.000	0.000	0.000	0.000	0.001	0.001
Ba	0.000	0.000	0.001	0.001	0.001	0.001	0.001	0.001	0.000
Na	1.000	1.007	0.993	0.209	0.428	0.056	0.049	0.989	1.006
K	0.009	0.011	0.026	0.763	0.553	0.917	0.922	0.008	0.008

Sample No.	52246 28	52246 29	52246 30	52246 31	52246 32	52246 33	52246 34	52246 35	59751 1
SiO2	68.115	68.060	67.930	67.219	67.678	67.906	64.013	64.118	62.732
Al2O3	19.276	19.191	19.228	19.157	19.278	19.331	18.505	18.371	18.800
TiO2	0.014	0.000	0.024	0.030	0.020	0.000	0.023	0.056	0.041
FeO	0.258	0.403	0.293	0.307	0.304	0.115	0.186	0.166	0.105
MnO	0.009	0.000	0.000	0.000	0.000	0.003	0.002	0.019	0.000
MgO	0.024	0.000	0.001	0.019	0.019	0.012	0.020	0.014	0.026
CaO	0.022	0.013	0.013	0.000	0.035	0.009	0.000	0.000	0.017
BaO	0.048	0.022	0.016	0.034	0.058	0.000	0.076	0.051	1.648
Na2O	11.909	12.003	12.010	11.971	12.003	11.966	1.426	1.422	0.797
K2O	0.113	0.158	0.176	0.126	0.109	0.165	14.704	14.490	14.637
Total	99.788	99.850	99.691	98.863	99.504	99.507	98.955	98.707	98.803
Si	2.990	2.989	2.987	2.982	2.983	2.988	2.981	2.989	2.958
Al	0.997	0.993	0.996	1.001	1.001	1.002	1.016	1.009	1.045
Ti	0.000	0.000	0.001	0.001	0.001	0.000	0.001	0.002	0.001
Fe	0.010	0.015	0.011	0.011	0.011	0.004	0.007	0.007	0.004
Mn	0.000	0.000	0.000	0.000	0.000	0.000	0.000	0.001	0.000
Mg	0.002	0.000	0.000	0.001	0.001	0.001	0.001	0.001	0.002
Ca	0.001	0.001	0.001	0.000	0.002	0.000	0.000	0.000	0.001
Ba	0.001	0.000	0.000	0.001	0.001	0.000	0.001	0.001	0.030
Na	1.013	1.022	1.024	1.030	1.026	1.021	0.129	0.129	0.073
K	0.006	0.009	0.010	0.007	0.006	0.009	0.874	0.862	0.880

Sample No.	59571 2	59751 3	59751 4	59751 5	59751 6	59751 7	59751 8	59751 9	59751 10
SiO2	63.164	62.468	65.781	68.562	68.133	68.466	68.398	64.188	68.197
Al2O3	18.748	18.565	19.026	19.166	19.164	19.405	19.284	18.371	19.102
TiO2	0.053	0.031	0.008	0.000	0.018	0.032	0.020	0.023	0.000
FeO	0.115	0.201	0.107	0.279	0.219	0.105	0.211	0.128	0.245
MnO	0.000	0.003	0.007	0.008	0.007	0.000	0.003	0.034	0.004
MgO	0.014	0.016	0.008	0.017	0.015	0.018	0.014	0.007	0.004
CaO	0.000	0.403	0.014	0.010	0.006	0.014	0.000	0.000	0.005
BaO	1.744	1.367	0.447	0.054	0.013	0.000	0.026	0.009	0.045
Na2O	0.759	0.750	8.695	11.029	11.785	11.747	11.764	1.047	11.456
K2O	14.456	14.745	5.531	0.108	0.179	0.084	0.219	15.141	0.118
Total	99.053	98.549	99.624	99.233	99.539	99.871	99.939	98.948	99.176
Si	2.967	2.955	2.965	3.013	2.996	2.995	2.995	2.990	3.004
Al	1.038	1.035	1.011	0.993	0.993	1.000	0.995	1.009	0.992
Ti	0.002	0.001	0.000	0.000	0.001	0.001	0.001	0.001	0.000
Fe	0.005	0.008	0.004	0.010	0.008	0.004	0.008	0.005	0.009
Mn	0.000	0.000	0.000	0.000	0.000	0.000	0.000	0.001	0.000
Mg	0.001	0.001	0.001	0.001	0.001	0.001	0.001	0.000	0.000
Ca	0.000	0.020	0.001	0.000	0.000	0.001	0.000	0.000	0.000
Ba	0.032	0.025	0.008	0.001	0.000	0.000	0.000	0.000	0.001
Na	0.069	0.069	0.760	0.939	1.005	0.996	0.999	0.095	0.979
K	0.866	0.890	0.318	0.006	0.010	0.005	0.012	0.900	0.007

Sample No.	59751 11	59751 12	59751 13	59751 14	59751 15	59751 16	59751 17	59751 18	59751 19
SiO2	68.072	63.573	64.064	68.160	68.014	67.873	62.597	61.687	62.729
Al2O3	19.479	18.606	18.271	19.265	19.236	19.252	18.973	19.112	18.662
TiO2	0.026	0.000	0.051	0.014	0.030	0.000	0.008	0.096	0.016
FeO	0.125	0.155	0.157	0.310	0.290	0.233	0.139	0.116	0.169
MnO	0.000	0.000	0.005	0.006	0.000	0.000	0.013	0.000	0.038
MgO	0.008	0.010	0.007	0.014	0.004	0.006	0.005	0.000	0.020
CaO	0.004	0.000	0.000	0.029	0.004	0.000	0.000	0.000	0.000
BaO	0.011	0.649	0.097	0.016	0.046	0.024	2.052	2.138	1.417
Na2O	11.546	0.890	0.830	11.729	11.737	12.019	0.837	0.693	0.650
K2O	0.155	15.007	15.283	0.125	0.123	0.117	14.425	14.535	14.879
Total	99.426	98.890	98.765	99.668	99.484	99.524	99.049	98.377	98.580
Si	2.991	2.976	2.993	2.993	2.993	2.988	2.951	2.934	2.963
Al	1.009	1.027	1.006	0.997	0.998	0.999	1.054	1.071	1.039
Ti	0.001	0.000	0.002	0.000	0.001	0.000	0.000	0.003	0.001
Fe	0.005	0.006	0.006	0.011	0.011	0.009	0.005	0.005	0.007
Mn	0.000	0.000	0.000	0.000	0.000	0.000	0.000	0.000	0.001
Mg	0.000	0.001	0.000	0.001	0.000	0.000	0.000	0.000	0.001
Ca	0.000	0.000	0.000	0.001	0.000	0.000	0.000	0.000	0.000
Ba	0.000	0.012	0.002	0.000	0.001	0.000	0.038	0.040	0.026
Na	0.984	0.081	0.075	0.999	1.001	1.026	0.077	0.064	0.060
K	0.009	0.896	0.911	0.007	0.007	0.007	0.867	0.882	0.897

Sample No.	59751 20	59751 21	59751 22	59751 23	59755 1	59755 2	59755 3	59755 4	59755 5
SiO2	67.686	67.891	67.423	67.453	68.489	72.939	67.442	67.487	69.350
Al2O3	19.300	19.159	19.074	19.199	19.864	19.509	19.134	18.958	20.056
TiO2	0.000	0.006	0.000	0.020	0.011	0.000	0.001	0.023	0.028
FeO	0.236	0.269	0.301	0.242	0.352	0.307	0.368	0.385	0.406
MnO	0.015	0.026	0.000	0.013	N.A.	N.A.	N.A.	N.A.	N.A.
MgO	0.018	0.010	0.000	0.012	N.A.	N.A.	N.A.	N.A.	N.A.
CaO	0.000	0.020	0.000	0.011	0.012	0.015	0.020	0.010	0.013
BaO	0.0190	0.0230	0.0000	0.0110	0.0000	0.0490	0.0400	0.0000	0.0490
Na2O	11.8520	11.9180	11.9460	11.7110	9.5740	8.4130	11.9160	11.9150	11.3980
K2O	0.211	0.124	0.103	0.120	0.133	0.136	0.193	0.135	0.140
Total	99.337	99.446	98.847	98.792	98.435	101.368	99.114	98.913	101.440
Si	2.9855	2.9908	2.9887	2.9885	3.0139	3.0888	2.9851	2.9910	2.9873
Al	1.0033	0.9947	0.9965	1.0025	1.0302	0.9737	0.9981	0.9903	1.0182
Ti	0.0000	0.0002	0.0000	0.0007	0.0004	0.0000	0.0000	0.0008	0.0009
Fe	0.0087	0.0099	0.0112	0.0090	0.0129	0.0109	0.0136	0.0143	0.0146
Mn	0.0006	0.0010	0.0000	0.0005	N.A.	N.A.	N.A.	N.A.	N.A.
Mg	0.0012	0.0006	0.0000	0.0008	N.A.	N.A.	N.A.	N.A.	N.A.
Ca	0.0000	0.0009	0.0000	0.0005	0.0006	0.0007	0.0009	0.0005	0.0006
Ba	0.0003	0.0004	0.0000	0.0002	0.0000	0.0008	0.0007	0.0000	0.0008
Na	1.0136	1.0179	1.0267	1.0060	0.8169	0.6908	1.0226	1.0239	0.9519
K	0.01190	0.00700	0.00580	0.00680	0.00750	0.00730	0.01090	0.00760	0.00770

Sample No.	59755 6	59755 7	155053 1	155053 2	155053 3	155053 4	155053 5	155053 6	155053 7
SiO2	68.356	69.156	67.711	67.692	68.192	68.634	64.061	64.107	63.823
Al2O3	20.022	19.750	19.238	19.226	19.351	19.383	18.337	18.287	18.388
TiO2	0.005	0.012	0.006	0.000	0.022	0.000	0.021	0.012	0.047
FeO	0.428	0.455	0.142	0.129	0.146	0.199	0.115	0.258	0.117
MnO	N.A.	N.A.	0.000	0.003	0.012	0.018	0.019	0.020	0.019
MgO	N.A.	N.A.	0.030	0.028	0.023	0.012	0.008	0.013	0.025
CaO	0.013	0.013	0.015	0.008	0.013	0.013	0.000	0.000	0.000
BaO	0.1100	0.0000	0.0230	0.0000	0.0170	0.0150	0.0400	0.0260	0.0480
Na2O	12.0990	12.0610	11.7960	11.7000	11.2740	11.8420	0.6860	1.0710	0.4850
K2O	0.172	0.168	0.122	0.147	0.126	0.174	15.590	15.039	15.830
Total	101.205	101.615	99.083	98.933	99.176	100.290	98.877	98.833	98.782
Si	2.9659	2.9833	2.9902	2.9922	3.0001	2.9946	2.9912	2.9910	2.9864
Al	1.0239	1.0041	1.0013	1.0016	1.0034	0.9967	1.0091	1.0056	1.0140
Ti	0.0002	0.0004	0.0002	0.0000	0.0007	0.0000	0.0007	0.0004	0.0017
Fe	0.0155	0.0164	0.0052	0.0048	0.0054	0.0073	0.0045	0.0101	0.0046
Mn	N.A.	N.A.	0.0000	0.0001	0.0005	0.0006	0.0008	0.0008	0.0008
Mg	N.A.	N.A.	0.0020	0.0019	0.0015	0.0008	0.0006	0.0009	0.0018
Ca	0.0006	0.0006	0.0007	0.0004	0.0006	0.0006	0.0000	0.0000	0.0000
Ba	0.0019	0.0000	0.0004	0.0000	0.0003	0.0003	0.0007	0.0005	0.0009
Na	1.0178	1.0087	1.0100	1.0028	0.9617	1.0018	0.0621	0.0969	0.0440
K	0.00950	0.00920	0.00690	0.00830	0.00710	0.00970	0.92860	0.89510	0.94490

Sample No.	155053 8	155053 9	155053 10	155053 11	155053 12	155053 13	155053 14	155053 15	155053 16
SiO2	64.030	67.483	67.998	63.944	64.096	67.859	67.785	63.297	64.135
Al2O3	18.301	19.173	19.176	18.527	18.308	19.250	19.088	18.290	18.284
TiO2	0.000	0.000	0.000	0.031	0.019	0.000	0.000	0.037	0.037
FeO	0.238	0.126	0.166	0.137	0.192	0.112	0.111	0.092	0.211
MnO	0.022	0.005	0.037	0.018	0.000	0.000	0.013	0.009	0.022
MgO	0.000	0.009	0.005	0.000	0.019	0.006	0.014	0.010	0.023
CaO	0.000	0.019	0.021	0.000	0.000	0.001	0.000	0.000	0.008
BaO	0.0450	0.0000	0.0120	0.0430	0.0080	0.0090	0.0120	0.0730	0.0000
Na2O	0.8920	11.7780	11.3590	0.9340	0.8190	11.8670	11.8370	0.5980	0.9580
K2O	15.484	0.143	0.237	15.357	15.498	0.123	0.152	15.640	15.087
Total	99.012	98.736	99.011	98.991	98.959	99.227	99.012	98.046	98.765
Si	2.9886	2.9905	3.0008	2.9820	2.9905	2.9918	2.9956	2.9843	2.9926
Al	1.0067	1.0014	0.9974	1.0183	1.0067	1.0003	0.9942	1.0163	1.0055
Ti	0.0000	0.0000	0.0000	0.0011	0.0007	0.0000	0.0000	0.0013	0.0013
Fe	0.0093	0.0047	0.0061	0.0054	0.0075	0.0041	0.0041	0.0036	0.0082
Mn	0.0009	0.0002	0.0014	0.0007	0.0000	0.0000	0.0005	0.0004	0.0009
Mg	0.0000	0.0006	0.0004	0.0000	0.0013	0.0004	0.0009	0.0007	0.0016
Ca	0.0000	0.0009	0.0010	0.0000	0.0000	0.0000	0.0000	0.0000	0.0004
Ba	0.0008	0.0000	0.0002	0.0008	0.0001	0.0002	0.0002	0.0013	0.0000
Na	0.0808	1.0120	0.9719	0.0845	0.0741	1.0145	1.0143	0.0547	0.0866
K	0.92190	0.00810	0.01340	0.91360	0.92240	0.00690	0.00860	0.94070	0.89800

Sample No.	155053 17	155053 18	155053 19	155053 20	155053 21	155053 22	155053 23	155053 24	155053 25
SiO2	68.146	67.663	67.903	67.830	63.185	63.726	64.162	67.355	67.353
Al2O3	19.295	19.223	19.334	19.281	18.459	18.293	18.248	19.257	19.325
TiO2	0.018	0.018	0.000	0.000	0.045	0.023	0.000	0.010	0.038
FeO	0.127	0.028	0.127	0.134	0.149	0.103	0.224	0.153	0.116
MnO	0.000	0.026	0.002	0.003	0.055	0.012	0.005	0.043	0.000
MgO	0.012	0.006	0.014	0.014	0.017	0.001	0.013	0.000	0.009
CaO	0.013	0.006	0.027	0.000	0.044	0.000	0.000	0.003	0.075
BaO	0.0290	0.0000	0.0050	0.0350	0.0030	0.0080	0.0250	0.0020	0.0000
Na2O	11.8700	11.9380	11.6580	11.5600	0.9300	0.8210	0.8190	11.6890	11.6160
K2O	0.122	0.179	0.145	0.171	14.859	15.256	15.365	0.107	0.145
Total	99.632	99.087	99.215	99.028	97.746	98.243	98.861	98.619	98.677
Si	2.9926	2.9890	2.9921	2.9943	2.9786	2.9907	2.9946	2.9878	2.9854
Al	0.9986	1.0008	1.0041	1.0032	1.0256	1.0118	1.0038	1.0068	1.0096
Ti	0.0006	0.0006	0.0000	0.0000	0.0016	0.0008	0.0000	0.0003	0.0013
Fe	0.0047	0.0010	0.0047	0.0050	0.0059	0.0040	0.0087	0.0057	0.0043
Mn	0.0000	0.0010	0.0001	0.0001	0.0022	0.0005	0.0002	0.0016	0.0000
Mg	0.0008	0.0004	0.0009	0.0009	0.0012	0.0001	0.0009	0.0000	0.0006
Ca	0.0006	0.0003	0.0013	0.0000	0.0022	0.0000	0.0000	0.0001	0.0036
Ba	0.0005	0.0000	0.0001	0.0006	0.0001	0.0001	0.0005	0.0000	0.0000
Na	1.0106	1.0225	0.9960	0.9895	0.0850	0.0747	0.0741	1.0054	0.9983
K	0.00680	0.01010	0.00810	0.00960	0.89360	0.91330	0.91480	0.00610	0.00820

Sample No.	155053 26	155053 27	155053 28	155053 29	155053 30	155053 31	155053 32	155053 33	155053 34
SiO2	63.858	63.681	63.557	63.737	68.287	67.651	63.791	63.574	67.330
Al2O3	18.369	18.479	18.466	18.415	19.441	19.268	18.290	18.304	19.367
TiO2	0.043	0.049	0.060	0.037	0.022	0.000	0.072	0.000	0.000
FeO	0.097	0.093	0.102	0.165	0.149	0.121	0.087	0.194	0.158
MnO	0.002	0.026	0.019	0.000	0.035	0.000	0.000	0.009	0.000
MgO	0.018	0.008	0.015	0.020	0.010	0.015	0.000	0.000	0.004
CaO	0.000	0.000	0.000	0.000	0.015	0.020	0.000	0.000	0.008
BaO	0.0480	0.0290	0.0570	0.0230	0.0170	0.0000	0.0010	0.0490	0.0700
Na2O	0.7070	0.7820	0.5620	0.7940	11.6860	11.7210	0.5610	0.7130	11.8450
K2O	15.639	15.619	15.731	15.562	0.124	0.171	15.870	15.472	0.134
Total	98.781	98.766	98.569	98.753	99.786	98.967	98.672	98.315	98.916
Si	2.9866	2.9799	2.9807	2.9824	2.9920	2.9902	2.9883	2.9870	2.9816
Al	1.0125	1.0191	1.0207	1.0155	1.0039	1.0037	1.0098	1.0136	1.0108
Ti	0.0015	0.0017	0.0021	0.0013	0.0007	0.0000	0.0025	0.0000	0.0000
Fe	0.0038	0.0036	0.0040	0.0065	0.0055	0.0045	0.0034	0.0004	0.0059
Mn	0.0001	0.0010	0.0007	0.0000	0.0013	0.0000	0.0000	0.0004	0.0000
Mg	0.0013	0.0006	0.0010	0.0014	0.0007	0.0010	0.0000	0.0000	0.0003
Ca	0.0000	0.0000	0.0000	0.0000	0.0007	0.0010	0.0000	0.0000	0.0004
Ba	0.0009	0.0005	0.0011	0.0004	0.0003	0.0000	0.0000	0.0009	0.0012
Na	0.0641	0.0709	0.0511	0.0721	0.9927	1.0045	0.0509	0.0649	1.0170
K	0.93300	0.93240	0.94110	0.92890	0.00690	0.00960	0.94830	0.92740	0.00760

Sample No.	155053 35
SiO2	67.872
Al2O3	19.368
TiO2	0.000
FeO	0.147
MnO	0.000
MgO	0.013
CaO	0.006
BaO	0.0050
Na2O	11.8980
K2O	0.136
Total	99.445
Si	2.9872
Al	1.0046
Ti	0.0000
Fe	0.0054
Mn	0.0000
Mg	0.0009
Ca	0.0003
Ba	0.0001
Na	1.0153
K	0.00760

N°4 DAR87	N°5 DAR87	N°6 DAR87		
68.401	47.653	51.802	[illegible]	[illegible]
[illegible]	43.281	41.142	[illegible]	[illegible]
[illegible]	2.420	0.975	[illegible]	[illegible]
[illegible]	0.366	0.443	[illegible]	[illegible]
[illegible]	0.042	0.038	[illegible]	[illegible]
[illegible]	0.158	[illegible]	[illegible]	[illegible]
[illegible]	[illegible]	[illegible]	[illegible]	[illegible]
[illegible]	[illegible]	[illegible]	[illegible]	[illegible]
[illegible]	[illegible]	[illegible]	[illegible]	[illegible]
[illegible]	[illegible]	0.164	[illegible]	0.272
[illegible]	[illegible]	[illegible]	[illegible]	[illegible]
[illegible]	[illegible]	[illegible]	[illegible]	[illegible]
[illegible]	[illegible]	0.007	[illegible]	[illegible]
[illegible]	[illegible]	[illegible]	[illegible]	[illegible]
[illegible]	[illegible]	[illegible]	[illegible]	[illegible]
[illegible]	[illegible]	[illegible]	[illegible]	[illegible]

Sample No.	N:1 DAR67	N:2 DAR67	N:3 DAR67	N:4 DAR67	N:5 DAR67	N:6 DAR67	N:7 DAR67	N:8 DAR67	N:9 DAR67
CaO	52.845	52.996	52.948	50.401	47.653	51.802	52.844	50.138	50.743
P2O5	41.964	42.007	41.939	39.722	43.261	41.142	42.062	38.971	39.881
SiO2	0.144	0.290	0.253	1.675	2.420	0.975	0.284	2.130	1.433
FeO	0.215	0.310	0.352	0.389	0.956	0.447	0.207	0.326	0.313
MnO	0.028	0.000	0.030	0.000	0.042	0.039	0.034	0.000	0.000
MgO	0.001	0.000	0.000	0.000	0.158	0.000	0.008	0.000	0.014
SrO	3.091	3.065	2.881	2.833	1.880	2.570	2.927	2.043	2.740
La2O3	0.260	0.277	0.302	1.348	0.851	0.897	0.282	1.746	1.240
Ce2O3	0.254	0.365	0.417	2.054	1.506	1.189	0.341	2.619	1.759
Pr2O3	0.013	0.058	0.000	0.203	0.181	0.154	0.113	0.272	0.159
Nd2O3	0.089	0.128	0.196	0.637	0.536	0.350	0.121	0.926	0.557
Sm2O3	0.019	0.035	0.000	0.083	0.083	0.089	0.055	0.022	0.084
Cl	0.001	0.000	0.017	0.011	0.000	0.007	0.000	0.013	0.001
F	4.441	3.698	4.618	4.492	5.276	3.955	3.466	3.530	3.405
O=F	1.870	1.557	1.944	1.891	2.221	1.665	1.459	1.486	1.434
Total	101.494	101.670	102.009	101.956	102.583	101.954	101.285	101.250	100.861

Sample No.	N:10 DAR67	N:11 DAR67	N:12 DAR67	N:1 DAR67	N:2 DAR67	N:5 DAR67	N:6 DAR67	N:7 DAR67	N:2 DAR67
CaO	51.836	52.183	53.209	50.848	52.476	53.092	50.418	52.365	53.210
P2O5	40.859	41.564	42.302	40.053	41.691	42.208	39.446	41.025	41.578
SiO2	0.815	0.588	0.125	1.456	0.655	0.181	1.842	0.827	0.172
FeO	0.321	0.375	0.229	0.256	0.262	0.142	0.279	0.153	0.169
MnO	0.000	0.008	0.014	0.000	0.026	0.027	0.000	0.007	0.003
MgO	0.001	0.006	0.000	0.016	0.005	0.000	0.000	0.000	0.000
SrO	2.694	2.921	3.401	2.736	2.940	2.740	2.213	1.906	2.979
La2O3	0.846	0.512	0.239	1.273	0.572	0.332	1.530	0.859	0.265
Ce2O3	1.044	0.688	0.239	1.785	0.681	0.473	2.288	1.302	0.373
Pr2O3	0.033	0.100	0.050	0.205	0.108	0.186	0.174	0.163	0.000
Nd2O3	0.254	0.183	0.063	0.559	0.170	0.149	0.717	0.433	0.113
Sm2O3	0.099	0.033	0.046	0.052	0.035	0.007	0.102	0.119	0.039
Cl	0.005	0.003	0.000	0.022	0.005	0.000	0.013	0.001	0.002
F	3.444	3.642	3.353	3.535	3.435	4.091	3.799	3.677	3.994
O=F	1.450	1.533	1.412	1.488	1.446	1.722	1.600	1.548	1.681
Total	100.802	101.274	101.857	101.309	101.616	101.905	101.222	101.288	101.214

Sample No.	N:3 DAR67	N:4 DAR67	N:5 DAR67	N:6 DAR67	N:7 DAR67	N:8 DAR67	N:11 DAR67	N:12 DAR67	N:13 DAR67
CaO	51.611	52.265	52.639	51.795	50.600	47.984	52.850	51.792	49.040
P2O5	39.380	40.659	41.293	40.333	38.834	36.298	42.089	41.173	38.151
SiO2	1.406	0.560	0.225	0.770	1.809	3.213	0.144	0.746	2.575
FeO	0.304	0.224	0.235	0.284	0.336	0.411	0.310	0.287	0.318
MnO	0.000	0.056	0.001	0.000	0.000	0.000	0.036	0.000	0.002
MgO	0.021	0.001	0.000	0.001	0.000	0.000	0.000	0.015	0.011
SrO	2.260	2.956	2.354	2.801	2.049	1.043	2.935	2.864	1.793
La2O3	1.226	0.523	0.390	0.705	1.496	2.799	0.272	0.757	2.055
Ce2O3	1.551	0.679	0.533	0.998	2.411	4.220	0.344	0.999	3.274
Pr2O3	0.058	0.074	0.059	0.113	0.206	0.273	0.079	0.145	0.293
Nd2O3	0.329	0.237	0.214	0.342	0.737	1.433	0.118	0.324	1.055
Sm2O3	0.020	0.053	0.062	0.042	0.111	0.250	0.050	0.056	0.138
Cl	0.000	0.011	0.002	0.000	0.009	0.003	0.000	0.013	0.000
F	3.304	3.915	4.145	4.161	3.720	3.982	4.718	4.559	4.333
O=F	1.391	1.648	1.745	1.752	1.566	1.676	1.986	1.919	1.824
Total	100.079	100.564	100.408	100.593	100.752	100.233	101.962	101.811	101.214

Sample No.	N:14 DAR67	N:1 DAR65	N:2 DAR65	N:3 DAR65	N:4 DAR65	N:5 DAR65	N:6 DAR65	N:7 DAR65	N:8 DAR65
CaO	51.019	50.425	53.325	50.622	49.610	52.851	52.829	51.733	48.817
P2O5	40.589	39.321	41.667	40.026	39.331	41.774	41.756	40.685	37.715
SiO2	1.420	1.624	0.954	0.639	2.129	0.543	0.496	0.318	2.213
FeO	0.601	0.086	0.069	0.079	0.063	0.048	0.029	0.062	0.067
MnO	0.018	0.000	0.000	0.000	0.000	0.000	0.007	0.002	0.000
MgO	0.096	0.000	0.000	0.000	0.013	0.000	0.001	0.002	0.000
SrO	2.807	1.531	1.398	1.632	1.466	1.394	1.375	1.530	1.496
La2O3	0.798	1.486	0.469	0.785	1.616	0.563	0.519	0.643	1.936
Ce2O3	1.102	2.476	0.868	1.234	2.776	0.906	0.818	0.951	3.387
Pr2O3	0.155	0.169	0.065	0.111	0.189	0.047	0.197	0.123	0.309
Nd2O3	0.372	0.877	0.310	0.462	0.908	0.356	0.332	0.317	1.217
Sm2O3	0.114	0.123	0.093	0.056	0.173	0.043	0.038	0.094	0.190
Cl	0.007	0.009	0.006	0.006	0.006	0.000	0.014	0.010	0.010
F	4.501	3.751	3.645	4.400	4.045	4.604	5.357	5.182	4.836
O=F	1.895	1.579	1.535	1.852	1.703	1.938	2.255	2.182	2.036
Total	101.704	100.300	101.334	98.200	100.622	101.192	101.513	99.469	100.157

Sample No.	N:9 DAR65	N:10 DAR65	N:11 DAR65	N:12 DAR65	N:13 DAR65	N:14 DAR65	N:1 DAR65	N:2 DAR65	N:3 DAR65
CaO	53.208	52.362	46.345	49.898	50.223	52.958	51.072	49.193	53.612
P2O5	41.306	41.172	35.024	39.286	39.063	41.674	40.084	38.663	42.080
SiO2	0.433	0.803	4.076	1.567	1.776	0.464	1.350	2.128	0.354
FeO	0.065	0.035	0.074	0.000	0.031	0.000	0.051	0.055	0.028
MnO	0.015	0.000	0.000	0.000	0.000	0.000	0.000	0.000	0.002
MgO	0.000	0.000	0.000	0.010	0.000	0.002	0.000	0.018	0.004
SrO	1.370	1.461	1.316	1.512	1.477	1.372	1.608	1.482	1.132
La2O3	0.454	0.831	2.902	1.585	1.452	0.454	1.237	1.834	0.369
Ce2O3	0.779	1.387	4.959	2.545	2.500	0.783	1.913	3.010	0.572
Pr2O3	0.071	0.183	0.421	0.281	0.292	0.102	0.196	0.239	0.048
Nd2O3	0.284	0.531	1.750	0.923	0.871	0.323	0.625	1.069	0.223
Sm2O3	0.002	0.109	0.324	0.169	0.125	0.081	0.122	0.228	0.074
Cl	0.008	0.006	0.016	0.011	0.007	0.005	0.021	0.020	0.004
F	5.313	5.082	4.718	5.097	4.925	5.599	3.006	3.530	4.028
O=F	2.237	2.140	1.986	2.146	2.073	2.357	1.266	1.486	1.696
Total	101.073	101.823	99.937	100.740	100.670	101.459	100.019	99.984	100.834

Sample No.	N:4 DAR65	N:5 DAR65	N:6 DAR65	N:10 DAR65	N:11 DAR65	N:12 DAR65	N:13 DAR65	N:14 DAR65	N:15 DAR65
CaO	50.965	49.015	51.147	52.315	48.744	51.050	52.750	54.050	52.882
P2O5	40.573	38.223	40.892	41.421	38.075	40.408	41.583	42.181	41.565
SiO2	1.169	2.374	4.040	0.601	2.912	1.304	0.931	0.376	0.301
FeO	0.041	0.019	0.071	0.094	0.057	0.080	0.109	0.018	0.001
MnO	0.007	0.000	0.017	0.010	0.000	0.000	0.001	0.010	0.000
MgO	0.000	0.008	0.000	0.008	0.012	0.008	0.012	0.000	0.000
SrO	1.629	1.433	1.380	1.543	1.383	1.516	1.549	1.041	1.554
La2O3	1.173	1.853	0.500	0.630	2.183	1.177	0.656	0.349	0.651
Ce2O3	1.981	3.106	0.753	1.098	3.701	1.858	1.191	0.615	0.971
Pr2O3	0.074	0.381	0.113	0.121	0.305	0.162	0.187	0.038	0.176
Nd2O3	0.711	1.123	0.292	0.430	1.343	0.630	0.441	0.222	0.363
Sm2O3	0.137	0.168	0.081	0.050	0.205	0.081	0.060	0.018	0.091
Cl	0.006	0.006	0.003	0.013	0.002	0.027	0.000	0.009	0.006
F	4.654	4.410	4.647	4.742	5.136	4.192	4.749	4.336	4.038
O=F	1.959	1.857	1.956	1.996	2.162	1.765	1.999	1.825	1.700
Total	101.162	100.261	101.981	101.079	101.896	100.728	102.220	101.435	100.898

Sample No.	N:16	DAR65
CaO		50.227
P2O5		38.505
SiO2		2.140
FeO		0.062
MnO		0.000
MgO		0.000
SrO		1.424
La2O3		1.644
Ce2O3		2.791
Pr2O3		0.209
Nd2O3		0.946
Sm2O3		0.158
Cl		0.020
F		4.092
O=F		1.723
Total		100.495

Sample No.	N:1 DAR162	N:2 DAR162	N:4 DAR162	N:5 DAR162	N:6 DAR162	N:7 DAR162	N:1 DAR162	N:2 DAR162	N:3 DAR162
CaO	54.954	52.306	55.167	54.295	55.033	54.714	55.273	54.846	54.755
P2O5	41.997	41.505	42.140	41.585	42.144	42.254	42.362	41.933	42.047
SiO2	0.454	2.272	0.420	0.454	0.192	0.175	0.185	0.393	0.311
FeO	0.054	0.079	0.111	0.103	0.101	0.095	0.057	0.106	0.116
MnO	0.027	0.037	0.057	0.048	0.062	0.053	0.015	0.044	0.035
MgO	0.000	0.015	0.020	0.008	0.001	0.001	0.000	0.001	0.004
SrO	0.023	0.057	0.041	0.041	0.040	0.073	0.053	0.046	0.065
La2O3	0.137	0.198	0.208	0.219	0.177	0.191	0.527	0.132	0.158
Ce2O3	0.463	0.436	0.501	0.553	0.393	0.463	0.963	0.448	0.459
Pr2O3	0.061	0.039	0.177	0.156	0.058	0.016	0.220	0.112	0.143
Nd2O3	0.243	0.207	0.245	0.254	0.244	0.260	0.391	0.261	0.270
Sm2O3	0.045	0.058	0.106	0.060	0.047	0.053	0.048	0.014	0.092
Cl	0.071	0.053	0.112	0.014	0.081	0.072	0.088	0.092	0.193
F	3.679	5.064	2.497	6.999	4.273	5.222	4.696	3.953	5.131
O=F	1.549	2.132	1.051	2.947	1.799	2.198	1.977	1.664	2.160
Total	100.660	100.193	100.750	101.843	101.047	101.443	102.901	100.718	101.619

Sample No.	N:4 DAR162	N:5 DAR162	N:6 DAR162	N:7 DAR162	N:8 DAR162	N:9 DAR162	N:1 DAR163	N:2 DAR163	N:3 DAR163
CaO	55.066	54.835	55.405	54.609	54.559	54.663	55.300	54.934	55.329
P2O5	42.221	41.932	42.318	42.224	41.753	41.583	42.479	42.105	42.539
SiO2	0.431	0.455	0.244	0.385	0.640	0.451	0.284	0.561	0.193
FeO	0.057	0.109	0.176	0.079	0.051	0.106	0.047	0.037	0.032
MnO	0.041	0.058	0.042	0.054	0.002	0.028	0.027	0.046	0.033
MgO	0.011	0.006	0.027	0.000	0.002	0.022	0.000	0.001	0.000
SrO	0.078	0.057	0.077	0.062	0.039	0.039	0.050	0.062	0.055
La2O3	0.270	0.174	0.134	0.297	0.351	0.251	0.264	0.341	0.242
Ce2O3	0.583	0.433	0.323	0.591	0.870	0.679	0.482	0.786	0.598
Pr2O3	0.058	0.031	0.172	0.110	0.143	0.139	0.109	0.132	0.109
Nd2O3	0.304	0.245	0.215	0.295	0.497	0.357	0.232	0.287	0.209
Sm2O3	0.057	0.081	0.044	0.087	0.100	0.065	0.036	0.026	0.070
Cl	0.114	0.050	0.003	0.104	0.000	0.059	0.021	0.015	0.024
F	4.183	4.987	3.619	4.091	5.129	4.818	4.525	4.475	4.407
O=F	1.761	2.100	1.524	1.722	2.159	2.028	1.905	1.884	1.855
Total	101.714	101.351	101.275	101.267	101.977	101.231	101.952	101.922	101.986

Sample No.	N:4 DAR163	N:6 DAR163	N:7 DAR163	N:8 DAR163	N:1 DAR163	N:2 DAR163	N:3 DAR163	N:4 DAR163	N:5 DAR163
CaO	55.038	55.482	54.721	50.381	54.626	53.694	54.476	54.681	54.068
P2O5	42.023	42.189	41.349	37.713	41.592	40.571	42.096	42.272	41.260
SiO2	0.356	0.312	0.666	2.766	0.533	1.004	0.307	0.339	0.962
FeO	0.052	0.115	0.134	0.259	0.046	0.039	0.060	0.019	0.006
MnO	0.027	0.032	0.016	0.000	0.016	0.031	0.069	0.021	0.007
MgO	0.000	0.000	0.001	0.000	0.000	0.000	0.003	0.009	0.000
SrO	0.062	0.066	0.098	0.084	0.057	0.025	0.060	0.082	0.047
La2O3	0.297	0.296	0.495	1.438	0.471	0.570	0.272	0.386	0.535
Ce2O3	0.607	0.595	1.009	3.185	0.964	1.288	0.541	0.689	1.120
Pr2O3	0.149	0.149	0.080	0.444	0.155	0.166	0.094	0.224	0.039
Nd2O3	0.216	0.242	0.362	1.416	0.393	0.541	0.232	0.293	0.437
Sm2O3	0.056	0.099	0.066	0.291	0.064	0.090	0.043	0.091	0.086
Cl	0.009	0.007	0.014	0.029	0.023	0.003	0.019	0.017	0.010
F	5.557	4.563	4.675	5.751	3.829	4.125	5.401	4.346	4.143
O=F	2.339	1.921	1.968	2.421	1.612	1.737	2.274	1.830	1.744
Total	102.109	102.226	101.718	101.336	101.158	100.409	101.399	101.640	100.975

Sample No.	N:6 DAR163	N:8 DAR163	N:9 DAR163	N:10 DAR163	N:11 DAR163	N:2 DAR164	N:3 DAR164	N:4 DAR164	N:5 DAR164
CaO	55.183	55.124	54.555	53.144	54.884	54.914	55.141	55.129	54.618
P2O5	42.105	42.243	41.666	40.317	41.890	41.293	42.167	42.039	42.328
SiO2	0.267	0.282	0.542	1.359	0.486	1.818	0.355	0.446	0.294
FeO	0.065	0.043	0.038	0.040	0.002	0.103	0.044	0.089	0.145
MnO	0.028	0.028	0.012	0.051	0.032	0.062	0.052	0.072	0.054
MgO	0.022	0.020	0.000	0.000	0.004	0.020	0.003	0.013	0.022
SrO	0.065	0.063	0.061	0.075	0.074	0.053	0.081	0.054	0.025
La2O3	0.296	0.341	0.489	0.791	0.368	0.060	0.051	0.047	0.089
Ce2O3	0.589	0.660	0.942	1.678	0.724	0.140	0.229	0.231	0.212
Pr2O3	0.131	0.058	0.168	0.154	0.065	0.056	0.036	0.122	0.070
Nd2O3	0.252	0.249	0.318	0.650	0.260	0.121	0.122	0.201	0.205
Sm2O3	0.057	0.088	0.118	0.157	0.095	0.078	0.030	0.078	0.084
Cl	0.009	0.019	0.000	0.026	0.006	0.278	0.246	0.353	0.130
F	4.073	4.159	4.006	3.900	5.207	4.755	3.055	3.659	5.010
O=F	1.715	1.751	1.687	1.642	2.192	2.002	1.286	1.540	2.109
Total	101.426	101.627	101.228	100.700	101.905	101.749	100.325	100.996	101.176

Sample No.	N:6 DAR164	N:7 DAR164	N:9 DAR164	N:10 DAR164	N:11 DAR164	N:12 DAR164	N:13 DAR164	N:1 DAR165	N:2 DAR165
CaO	54.797	55.312	55.398	55.028	55.158	54.667	54.901	54.215	53.902
P2O5	42.351	42.572	42.617	42.236	42.719	42.182	42.432	41.387	41.092
SiO2	0.226	0.481	0.376	0.546	0.169	0.254	0.142	0.507	0.801
FeO	0.180	0.290	0.421	0.072	0.220	0.040	0.098	0.062	0.035
MnO	0.084	0.045	0.093	0.081	0.064	0.107	0.110	0.062	0.025
MgO	0.003	0.008	0.036	0.003	0.018	0.008	0.000	0.010	0.008
SrO	0.062	0.051	0.056	0.065	0.029	0.055	0.071	0.040	0.105
La2O3	0.136	0.059	0.117	0.057	0.086	0.069	0.099	0.357	0.409
Ce2O3	0.240	0.253	0.228	0.208	0.176	0.341	0.294	0.855	0.972
Pr2O3	0.102	0.071	0.035	0.156	0.131	0.116	0.110	0.126	0.191
Nd2O3	0.241	0.226	0.195	0.189	0.170	0.249	0.266	0.424	0.401
Sm2O3	0.031	0.125	0.064	0.102	0.035	0.112	0.110	0.055	0.093
Cl	0.118	0.149	0.068	0.200	0.250	0.358	0.391	0.007	0.010
F	4.932	2.825	3.007	3.597	4.098	4.408	4.449	4.430	3.382
O=F	2.076	1.189	1.266	1.514	1.725	1.856	1.873	1.865	1.424
Total	101.427	101.277	101.445	101.028	101.599	101.110	101.601	100.671	100.003

Sample No.	N:3 DAR165	N:4 DAR165	N:5 DAR165	N:6 DAR165	N:7 DAR165	N:8 DAR165	N:9 DAR165	N:10 DAR165	N:11 DAR165
CaO	53.661	53.911	53.170	53.723	52.103	53.640	54.212	54.272	54.245
P2O5	40.915	41.247	40.773	41.346	39.585	41.012	41.226	41.631	41.133
SiO2	0.868	0.798	1.082	0.783	1.622	0.709	0.703	0.729	0.595
FeO	0.057	0.047	0.020	0.051	0.113	0.071	0.000	0.033	0.057
MnO	0.054	0.046	0.033	0.059	0.029	0.091	0.003	0.034	0.002
MgO	0.000	0.006	0.016	0.000	0.000	0.003	0.001	0.004	0.000
SrO	0.027	0.028	0.035	0.031	0.021	0.058	0.034	0.068	0.052
La2O3	0.467	0.432	0.401	0.488	0.844	0.508	0.492	0.348	0.384
Ce2O3	1.209	0.983	1.031	1.177	1.924	1.024	1.025	0.833	0.853
Pr2O3	0.234	0.079	0.225	0.140	0.228	0.245	0.128	0.189	0.142
Nd2O3	0.631	0.488	0.496	0.558	0.966	0.527	0.515	0.468	0.437
Sm2O3	0.152	0.129	0.119	0.154	0.238	0.090	0.122	0.046	0.079
Cl	0.002	0.004	0.020	0.006	0.025	0.015	0.016	0.004	0.001
F	3.322	3.980	4.859	4.444	4.600	4.410	3.844	4.083	3.914
O=F	1.399	1.676	2.046	1.871	1.937	1.857	1.618	1.719	1.648
Total	100.200	100.502	100.232	101.090	100.361	100.546	100.701	101.023	100.247

Sample No.	N:12 DAR165	N:13 DAR165	N:14 DAR165	N:1 DAR167	N:2 DAR167	N:3 DAR167	N:4 DAR167	N:6 DAR167	N:7 DAR167
CaO	53.856	53.994	54.196	54.300	54.284	54.322	54.608	54.192	54.148
P2O5	41.260	41.373	41.434	41.441	41.611	41.342	41.524	41.263	41.354
SiO2	0.711	0.622	0.604	0.745	0.580	0.736	0.640	0.781	0.695
FeO	0.030	0.041	0.008	0.060	0.152	0.261	0.100	0.066	0.032
MnO	0.083	0.051	0.047	0.068	0.042	0.080	0.050	0.079	0.068
MgO	0.000	0.000	0.010	0.000	0.000	0.000	0.000	0.013	0.018
SrO	0.017	0.058	0.040	0.046	0.054	0.044	0.048	0.032	0.064
La2O3	0.440	0.404	0.415	0.240	0.235	0.294	0.250	0.108	0.192
Ce2O3	0.905	0.923	0.862	0.726	0.569	0.755	0.628	0.353	0.459
Pr2O3	0.192	0.133	0.153	0.171	0.157	0.114	0.059	0.112	0.043
Nd2O3	0.493	0.495	0.426	0.393	0.353	0.442	0.419	0.311	0.342
Sm2O3	0.131	0.102	0.125	0.122	0.071	0.106	0.092	0.134	0.064
Cl	0.012	0.012	0.023	0.007	0.011	0.001	0.002	0.022	0.004
F	4.160	4.325	3.985	3.608	3.925	3.485	3.499	4.166	3.682
O=F	1.751	1.821	1.678	1.519	1.652	1.467	1.473	1.754	1.550
Total	100.899	100.711	100.649	100.409	100.392	100.515	100.446	99.879	99.614

Sample No.	N:8 DAR167	N:9 DAR167	N:10 DAR167	N:11 DAR167	N:12 DAR167	N:1 DAR168	N:2 DAR168	N:3 DAR168	N:4 DAR168
CaO	54.342	53.954	53.950	54.381	54.141	54.706	53.646	53.776	53.370
P2O5	41.166	40.328	41.143	41.382	41.184	42.391	42.152	41.999	40.215
SiO2	1.019	1.089	0.820	0.644	0.925	0.438	0.067	0.351	2.200
FeO	0.067	0.073	0.067	0.093	0.069	0.214	0.292	0.238	0.255
MnO	0.053	0.065	0.051	0.063	0.045	0.272	0.377	0.333	0.089
MgO	0.000	0.002	0.006	0.000	0.005	0.026	0.021	0.026	0.001
SrO	0.060	0.017	0.054	0.053	0.043	0.017	0.038	0.052	0.057
La2O3	0.169	0.325	0.260	0.155	0.193	0.171	0.099	0.048	0.339
Ce2O3	0.454	0.817	0.728	0.568	0.560	0.212	0.266	0.229	1.429
Pr2O3	0.104	0.142	0.245	0.074	0.088	0.052	0.040	0.140	0.217
Nd2O3	0.366	0.471	0.426	0.372	0.376	0.127	0.184	0.231	1.194
Sm2O3	0.111	0.115	0.085	0.099	0.113	0.005	0.032	0.120	0.181
Cl	0.000	0.032	0.031	0.006	0.026	0.059	0.133	0.066	0.032
F	3.850	4.285	3.905	3.828	4.294	3.786	4.629	4.873	3.913
O=F	1.621	1.804	1.644	1.612	1.808	1.594	1.949	2.052	1.647
Total	100.140	99.910	100.128	100.106	100.255	100.883	100.025	100.432	101.843

Sample No.	N:5 DAR168	N:6 DAR168	N:7 DAR168	N:8 DAR168	N:9 DAR168	N:10 DAR168	N:11 DAR168	N:12 DAR168	N:13 DAR168
CaO	54.582	52.761	53.629	53.981	54.448	53.533	55.233	51.432	54.798
P2O5	42.344	39.222	40.475	40.277	41.047	40.539	42.000	38.265	42.287
SiO2	0.151	1.396	1.013	1.561	0.753	0.802	0.341	3.227	0.331
FeO	0.082	0.050	0.059	0.055	0.099	0.099	0.061	0.074	0.198
MnO	0.109	0.067	0.031	0.020	0.046	0.028	0.025	0.007	0.115
MgO	0.006	0.007	0.004	0.000	0.008	0.000	0.000	0.012	0.003
SrO	0.076	0.099	0.054	0.075	0.226	0.147	0.141	0.089	0.066
La2O3	0.139	0.817	0.542	0.471	0.553	0.567	0.127	1.113	0.090
Ce2O3	0.336	1.733	1.057	0.959	1.092	1.065	0.258	2.281	0.311
Pr2O3	0.167	0.099	0.170	0.145	0.010	0.199	0.119	0.252	0.202
Nd2O3	0.189	0.764	0.423	0.435	0.417	0.446	0.152	0.861	0.182
Sm2O3	0.078	0.143	0.093	0.117	0.012	0.079	0.052	0.101	0.107
Cl	0.074	0.004	0.014	0.011	0.014	0.009	0.000	0.022	0.057
F	3.878	4.963	4.414	5.742	4.186	7.822	5.845	5.921	4.607
O=F	1.633	2.089	1.858	2.417	1.762	3.293	2.461	2.493	1.940
Total	100.579	100.036	100.122	101.431	101.152	102.043	101.893	101.164	101.415

Sample No.	N:14	DAR168	N:15	DAR168	N:16	DAR168
CaO		55.063		53.506		53.157
P2O5		41.846		41.770		41.757
SiO2		1.606		0.104		0.349
FeO		0.159		0.280		0.295
MnO		0.008		0.428		0.405
MgO		0.000		0.028		0.020
SrO		0.042		0.055		0.070
La2O3		0.000		0.089		0.128
Ce2O3		0.020		0.291		0.339
Pr2O3		0.139		0.010		0.029
Nd2O3		0.019		0.201		0.291
Sm2O3		0.066		0.082		0.068
Cl		0.009		0.117		0.109
F		4.230		4.923		4.120
O=F		1.781		2.073		1.735
Total		101.428		99.812		99.403

APPENDIX 2

X-ray fluorescence analysis

2.1 Analytical techniques

(a) Major element analysis using fused discs

70 samples were analysed for major elements on fused discs. 0.75g of weighed sample, dried for several hours in an oven at 120^{oc}, is mixed with 5.3333 times the measured weight of Johnson and Matthey Spectroflux 105. This is then placed in an oven at 1100^{oc} for 20 minutes. Any weight loss on cooling is made up by adding further Spectroflux. The sample is then re-melted over a meker burner and formed into a disc using a graphite mould. Analyses were carried out on a Phillips PW1400 X-ray spectrometer fitted with a rhodium tube, and calibrated using USGS standards. Selected samples were analysed at intervals to test for precision and accuracy for both major and trace elements.

(b) Trace element analysis using pressed powder pellets

The same 70 samples were analysed for 18 trace elements (Zn, Cu, Ni, Rb, Sr, Y, Zr, Nb, Ba, U, Th, Pb, Ti, V, Cr, La, Ce, Nd). Samples are prepared by adding 1.5g of Bakelite binding agent to 8.5g of dried sample powder and the mixture is shaken for a period of 10-15 minutes to ensure homogenisation. The sample is then formed into disc-shaped pellets by applying a load pressure of 20 tons in a hydraulic press. Finally, the pellets are cured overnight in an oven at 120^{oc}. Analyses were carried out on a Phillips PW1400 X-ray spectrometer.

2.2 Data tables

All the major and trace element analyses carried out by the author and used in the thesis are listed on the following pages. The whole-rock analyses of unaltered magmatic syenites used in the thesis were taken from Chambers (1976) [see Chapter 7 for reference] and are not listed here. Also given is a comparison of La, Ce and Nd analyses from XRF and ICP methods.

Comparison of XRF and ICP analyses for La, Ce and Nd.

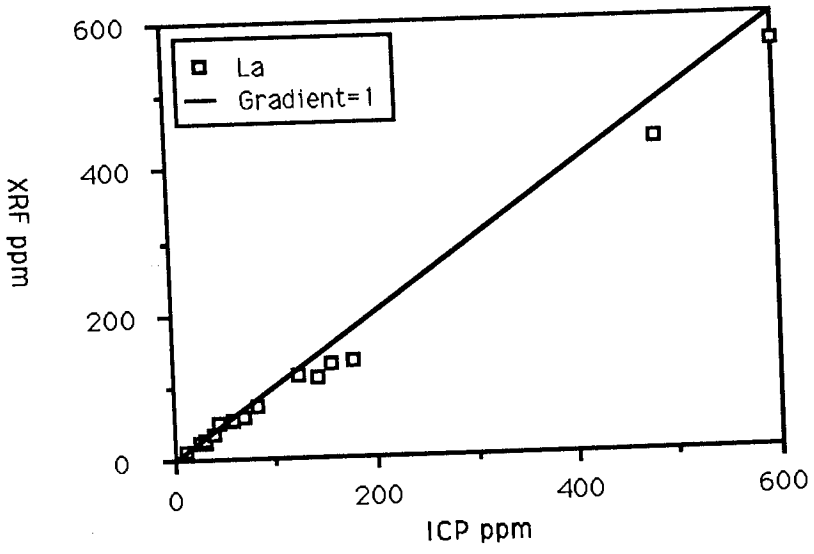

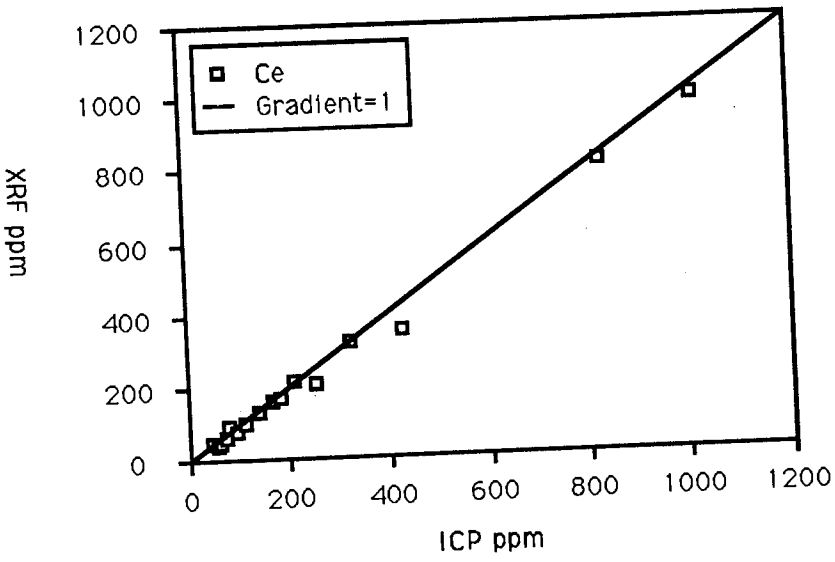

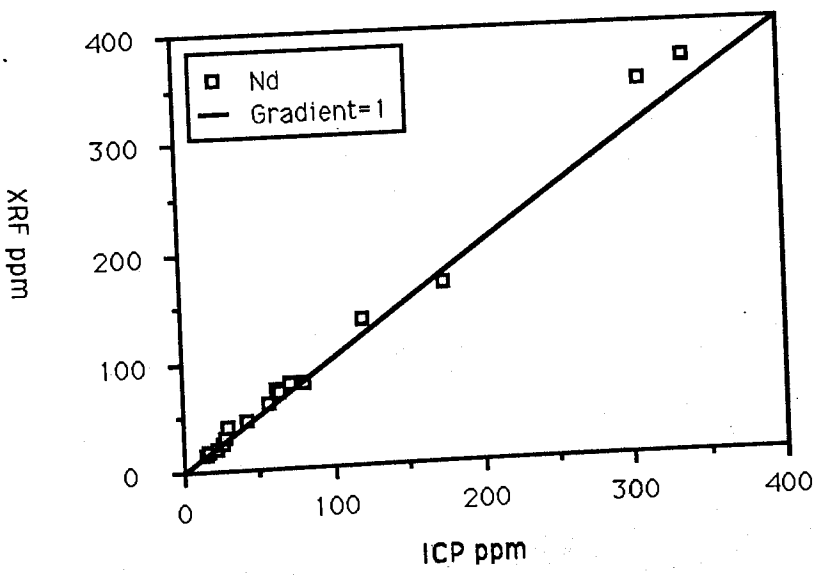

Sample No.	DAR138	DAR139	DAR140	DAR141	DAR142	DAR143	DAR144	DAR185	DAR186
SiO2	56.681	57.941	55.408	55.348	56.678	57.450	56.110	56.867	55.906
TiO2	0.562	0.645	0.344	0.322	0.340	0.406	0.565	0.373	0.302
Al2O3	18.223	17.924	18.970	18.707	19.166	19.520	19.401	19.000	19.040
Fe2O3	6.924	7.656	6.771	6.847	7.302	7.026	5.546	7.394	6.907
MnO	0.248	0.269	0.243	0.269	0.276	0.223	0.177	0.273	0.270
MgO	0.438	0.465	0.215	0.196	0.187	0.193	0.593	0.242	0.178
CaO	2.199	2.311	1.562	1.527	1.619	1.511	1.762	1.655	1.513
Na2O	6.185	6.902	8.609	8.572	8.574	7.939	7.741	7.861	8.043
K2O	5.810	5.942	5.573	5.512	5.650	6.063	5.960	5.705	5.770
Total	97.270	100.055	97.695	97.300	99.792	100.331	97.855	99.370	97.929
Zn	205	171	204	235	219	130	87	231	183
Cu	9	8	8	3	5	4	8	6	4
Ni	18	22	23	16	24	22	22	25	20
Pb	206	189	273	286	277	228	208	287	280
Sr	286	252	57	68	61	71	354	98	39
Y	78	60	84	112	105	58	62	118	87
Zr	913	598	1140	1523	1496	744	371	1650	1138
Nb	214	162	217	297	281	134	117	323	223
Ba	1133	1023	218	204	203	265	1099	315	126
U	2	1	3	7	4	3	1	5	4
Th	13	9	13	19	18	6	3	16	12
Pb	13	12	13	23	20	10	5	26	21
TiO2	4746	5356	2856	2561	2773	2871	4922	2955	2113
V	-2	2	4	-1	2	4	2	0	-2
Cr	22	18	6	8	-3	22	23	11	21
La	126	121	117	165	144	70	56	159	127
Ce	295	291	281	371	330	177	159	374	300
Nd	141	137	131	164	146	90	81	162	139

Sample No.	DAR187	DAR188	DAR189	DAR190	DAR191	DAR241	DAR242	DAR243	DAR248
SiO2	55.279	55.511	55.311	57.235	57.046	54.693	56.416	55.559	56.731
TiO2	0.338	0.396	0.371	0.359	0.341	0.170	0.384	0.355	0.354
Al2O3	18.548	18.566	18.699	19.522	19.730	20.148	19.179	18.730	19.087
Fe2O3	7.013	6.845	6.918	7.330	6.556	5.361	7.439	7.533	7.468
MnO	0.277	0.295	0.267	0.249	0.225	0.191	0.279	0.255	0.277
MgO	0.215	0.264	0.275	0.204	0.229	0.156	0.296	0.279	0.203
CaO	1.623	1.528	1.650	1.611	1.607	1.067	1.769	1.775	1.632
Na2O	7.646	7.835	8.071	7.640	8.008	9.851	8.084	8.118	8.156
K2O	5.496	5.578	5.498	6.194	6.033	5.175	5.741	5.611	5.636
Total	96.435	96.818	97.060	100.344	99.775	96.812	99.587	98.215	99.544
Zn	253	250	239	165	146	182	143	164	213
Cu	2	3	3	4	2	4	7	6	3
Ni	20	18	17	20	15	20	19	25	19
Pb	280	281	275	264	249	337	245	287	265
Sr	95	151	114	74	56	48	84	74	65
Y	132	120	118	58	60	58	34	42	96
Zr	1924	1748	1782	684	845	1299	611	825	1318
Nb	359	334	344	182	257	231	187	229	264
Ba	254	408	295	243	210	167	313	282	219
U	6	5	4	3	3	5	2	2	5
Th	23	20	21	12	10	16	9	14	16
Pb	30	25	26	13	14	24	4	10	16
TiO2	2734	3187	2871	2715	2832	1192	3242	2933	2701
V	1	3	5	5	5	4	3	3	0
Cr	-2	-2	12	6	-2	3	-8	0	15
La	186	170	163	110	116	99	92	103	137
Ce	425	378	376	266	277	206	230	250	322
Nd	182	166	161	129	139	79	114	119	142

Sample No.	DAR249	DAR250	DAR251
SiO2	55.275	54.967	55.659
TiO2	0.372	0.372	0.351
Al2O3	18.443	18.574	19.018
Fe2O3	7.418	7.291	6.833
MnO	0.274	0.289	0.245
MgO	0.202	0.221	0.193
CaO	1.603	1.576	1.655
Na2O	7.902	8.079	7.083
K2O	5.429	5.404	5.179
Total	96.918	96.773	96.216
Zn	214	278	193
Cu	5	3	4
Ni	16	15	12
Rb	275	266	230
Sr	45	67	81
Y	87	124	88
Zr	1241	1777	1114
Nb	236	347	215
Ba	154	222	198
U	6	6	6
Th	17	23	17
Pb	15	29	15
TiO2	2969	2957	2715
V	0	2	4
Cr	-3	-4	-3
La	154	174	142
Ce	351	387	330
Nd	155	168	148

Sample No.	DAR105	DAR106	DAR107	DAR115	DAR116	DAR118	DAR123	DAR127	DAR232
SiO2	54.287	53.687	53.736	54.740	55.017	57.076	54.839	54.528	56.864
TiO2	0.230	0.341	0.266	0.573	0.240	0.402	0.216	0.286	0.241
Al2O3	18.665	17.910	20.051	18.066	20.220	19.225	20.582	19.756	15.796
Fe2O3	6.874	7.986	7.063	7.464	4.895	6.823	4.733	5.796	10.550
MnO	0.250	0.299	0.197	0.276	0.150	0.234	0.145	0.213	0.377
MgO	0.180	0.239	0.170	0.527	0.131	0.487	0.170	0.226	0.257
CaO	1.558	1.641	1.633	1.778	1.294	1.732	1.332	1.899	0.945
Na2O	9.091	7.983	8.089	7.778	9.204	7.604	9.847	8.181	5.811
K2O	5.390	5.281	5.457	5.642	5.770	5.790	5.483	5.236	6.605
Total	96.525	95.367	96.662	96.844	96.921	99.373	97.347	96.121	97.446
Zn	138	146	115	161	89	140	89	75	217
Cu	1	1	2	17	1	36	4	7	16
Ni	20	11	17	15	22	14	17	15	22
Pb	408	364	366	359	347	265	317	280	273
Sr	40	118	23	288	53	345	38	198	167
Y	148	134	15	107	13	83	23	101	49
Zr	4202	3641	433	1149	447	811	598	2080	762
Nb	313	354	129	289	72	214	95	234	165
Ba	101	398	60	1050	144	1047	112	145	123
U	1	2	0	4	-0	2	3	1	5
Th	3	0	2	11	2	6	4	5	22
Pb	8	7	4	8	4	4	5	5	34
TiO2	1593	2777	1982	5168	1897	4007	1563	1914	1751
V	2	3	2	-2	2	2	2	-2	13
Cr	11	17	13	3	5	1	-2	16	20
La	131	128	16	133	17	97	27	103	90
Ce	320	291	41	352	42	247	67	233	176
Nd	134	107	21	165	18	118	25	93	63

Sample No.	DAR235	DAR236	DAR237	DAR239	52246	59751	155053
SiO2	55.728	56.203	56.566	56.736	53.770	54.29	54.98
TiO2	0.264	0.317	0.476	0.452	0.590	0.29	0.39
Al2O3	19.601	20.874	19.126	19.113	20.140	19.08	20.58
Fe2O3	6.742	5.232	7.220	6.564	5.450	6.36	6.62
MnO	0.276	0.207	0.233	0.207	0.220	0.23	0.26
MgO	0.247	0.281	0.469	0.262	0.520	0.24	0.24
CaO	1.367	1.257	1.773	1.513	1.780	1.86	1.66
Na2O	6.117	7.370	7.309	5.682	9.330	9.17	8.40
K2O	5.742	5.483	6.276	6.244	5.820	5.30	6.08
Total	96.084	97.224	99.448	96.773	97.620	96.820	99.210
Zn	198	149	114	121	149	123	178
Cu	4	0	3	4	4	1	7
Ni	13	18	18	15	3	6	3
Pb	260	219	259	211	257	386	228
Sr	248	188	209	159	108	61	52
Y	56	76	23	50	63	84	62
Zr	1211	812	343	489	956	3045	1039
Nb	227	205	132	159	205	299	280
Ba	145	133	884	408	207	220	83
U	6	6	0	2	4	0	6
Th	22	24	4	9	19	0	16
Pb	21	22	4	10	27	7	37
TiO2	2051	2462	4361	3623	N.A.	N.A.	N.A.
V	2	2	3	2	0	0	0
Cr	11	12	21	16	0	0	0
La	107	132	59	93	125	88	126
Ce	227	271	153	217	N.A.	N.A.	N.A.
Nd	91	111	73	105	N.A.	N.A.	N.A.

Sample No.	DAR70	DAR71	DAR72	DAR73	DAR74	DAR76	DAR77	DAR79	DAR162
SiO2	72.924	74.290	72.587	72.670	73.106	73.239	74.286	74.247	63.692
TiO2	0.149	0.144	0.143	0.153	0.167	0.143	0.148	0.131	0.444
Al2O3	14.053	14.201	13.995	14.329	13.897	14.221	14.223	14.326	17.888
Fe2O3	1.305	1.470	1.319	1.313	1.421	1.280	1.439	1.515	3.895
MnO	0.051	0.053	0.054	0.046	0.064	0.045	0.032	0.067	0.082
MgO	0.352	0.354	0.416	0.401	0.603	0.419	0.389	0.354	1.155
CaO	1.637	1.864	1.351	1.187	1.880	1.024	1.088	1.548	2.695
Na2O	4.137	4.126	4.029	4.025	4.037	3.695	3.548	3.885	5.802
K2O	4.204	4.129	4.412	4.441	3.540	4.769	5.103	4.423	3.662
Total	98.812	100.631	98.306	98.565	98.715	98.835	100.256	100.496	99.315
Zn	33	33	39	38	45	34	26	32	79
Cu	4	5	6	2	2	5	8	2	5
Ni	46	41	49	48	60	49	36	38	21
Pb	157	150	164	159	165	170	177	150	134
Sr	359	352	348	342	360	332	318	343	852
Y	10	10	10	8	12	9	8	12	26
Zr	84	84	81	81	88	79	85	83	374
Nb	10	10	12	9	12	11	9	10	58
Ba	520	461	527	531	376	570	557	562	1761
U	4	5	5	2	4	4	3	4	6
Th	10	7	9	9	8	9	10	12	8
Pb	32	31	38	29	34	28	29	32	29
TiO2	1348	1381	1299	1465	1486	1426	1368	1123	5039
V	17	14	14	13	28	18	16	14	42
Cr	16	5	18	28	12	29	25	34	50
La	13	13	15	14	22	17	15	15	52
Ce	26	28	31	21	35	31	27	24	102
Nd	13	13	15	11	19	15	14	14	46

Sample No.	DAR163	DAR164	DAR165	DAR167	DAR168	DAR169	DAR172	DAR175	DAR178
SiO2	57.214	66.428	68.640	66.644	70.238	65.737	63.653	56.545	61.643
TiO2	0.367	0.339	0.244	0.381	0.238	0.103	0.794	1.000	0.631
Al2O3	19.227	16.783	15.289	14.796	15.934	18.532	18.068	18.703	15.993
Fe2O3	4.557	3.117	2.245	3.620	1.994	1.127	8.823	5.661	4.623
MnO	0.122	0.059	0.081	0.063	0.045	0.031	0.059	0.166	0.082
MgO	1.057	1.042	0.399	1.211	0.636	0.373	0.216	1.054	2.457
CaO	2.646	2.382	0.910	1.760	1.313	0.371	0.492	3.144	2.984
Na2O	5.323	4.569	5.238	4.565	3.719	5.274	1.729	5.891	4.588
K2O	5.749	4.378	5.581	4.051	5.536	7.357	2.382	4.532	3.850
Total	96.262	99.097	98.627	97.091	99.653	98.905	96.216	96.696	96.851
Zn	137	61	65	70	38	22	200	120	83
Cu	5	3	6	13	2	1	16	12	6
Ni	12	21	27	23	29	29	50	20	24
Pb	192	124	166	129	167	180	121	90	131
Sr	580	649	132	435	427	168	203	1465	889
Y	30	12	41	15	39	28	11	31	35
Zr	533	176	416	175	123	68	184	664	164
Nb	109	9	86	10	10	9	10	110	12
Ba	1309	1279	957	1807	1387	294	532	2480	1504
U	5	3	7	4	4	6	1	3	5
Th	10	7	12	9	11	18	9	5	7
Pb	24	16	54	21	20	27	16	23	25
TiO2	4277	3889	2491	5000	2871	797	7969	10187	7234
V	32	39	7	42	22	17	123	13	81
Cr	7	31	7	20	22	11	136	16	46
La	60	26	74	35	110	11	23	54	101
Ce	131	48	157	60	209	80	84	115	199
Nd	60	26	71	30	79	16	27	55	82

Sample No.	DAR179	DAR279	DAR280	DAR281
SiO2	66.147	73.255	78.133	72.786
TiO2	0.333	0.148	0.058	0.189
Al2O3	15.763	13.877	13.321	15.172
Fe2O3	2.534	1.108	0.557	1.718
MnO	0.056	0.034	0.016	0.039
MgO	1.320	0.621	0.092	0.514
CaO	1.465	0.950	0.354	1.247
Na2O	6.472	4.063	3.225	4.275
K2O	5.494	4.638	5.729	4.150
Total	99.584	98.694	101.485	100.090
Zn	48	24	13	37
Cu	1	2	3	11
Ni	17	39	51	35
Pb	200	153	198	171
Sr	133	411	177	388
Y	13	24	9	16
Zr	173	80	27	95
Nb	9	15	6	13
Ba	201	443	258	635
U	5	8	9	4
Th	4	12	7	10
Pb	8	33	37	24
TiO2	2815	1181	393	1865
V	19	17	4	20
Cr	17	11	32	18
La	9	14	2	19
Ce	27	25	-1	41
Nd	20	17	2	18

DAR324	DAR325
73.473	73.473
0.150	0.196
14.192	15.231
1.366	1.905
0.061	0.059
0.311	0.550
1.264	1.118
3.891	3.962
4.056	4.399
98.764	100.893
29	37
0	5
57	37
160	169
289	415
12	15
93	99
12	11
469	737
7	4
22	10
35	27
1299	2002
11	21
38	32
22	23
46	42
17	20

Sample No.	DAR52	DAR53	DAR62	DAR63	DAR64	DAR65	DAR67	DAR291	DAR294
SiO2	57.624	45.924	78.878	73.322	70.296	58.518	49.834	98.880	90.096
TiO2	2.949	5.438	0.139	0.135	0.121	0.522	0.277	0.194	0.647
Al2O3	10.734	13.511	18.015	17.154	16.945	6.784	1.880	1.084	2.951
Fe2O3	16.181	17.489	0.933	1.273	1.638	9.826	17.684	1.218	2.885
MnO	0.346	0.917	0.004	0.013	0.024	0.425	0.811	0.020	0.090
MgO	5.869	1.990	0.046	0.084	0.144	1.772	5.375	0.084	0.350
CaO	1.213	2.787	0.072	0.103	0.270	9.636	19.356	0.189	0.943
Na2O	1.316	2.436	0.297	3.251	7.000	6.116	2.283	0.063	1.032
K2O	0.763	2.604	2.111	2.460	2.020	0.669	0.420	0.176	1.362
Total	96.995	93.096	100.495	97.795	98.458	94.268	97.920	101.908	100.356
Zn	151	176	8	14	25	103	422	22	79
Cu	65	48	-2	0	3	69	16	3	18
Ni	527	510	36	25	69	38	26	198	117
Pb	70	91	95	117	80	23	23	4	54
Sr	129	730	98	162	466	1046	2003	20	57
Y	36	76	12	19	12	102	109	15	27
Zr	315	660	84	88	92	371	670	133	391
Nb	76	182	9	9	9	50	125	33	79
Ba	255	20821	172	295	659	85	68	54	221
U	4	8	4	4	4	2	8	2	4
Th	10	19	10	11	6	50	58	7	12
Pb	14	23	6	9	74	14	12	8	24
TiO2	32734	65810	1193	1158	1153	4611	2539	1719	5859
V	660	269	23	16	17	156	210	20	68
Cr	301	451	23	10	14	39	-20	27	42
La	60	117	19	14	18	436	562	49	82
Ce	161	224	38	24	27	809	984	92	138
Nd	83	142	16	12	17	345	372	41	48

APPENDIX 3

Inductively coupled plasma spectrometry (ICPS)

3.1 Experimental methods

16 samples were analysed for 12 rare earth elements (La, Ce, Pr, Nd, Sm, Eu, Gd, Dy, Ho, Er, Yb, Lu) in the Department of Geology, Royal Holloway and Bedford New College (RHBNC).

0.5g of rock powder is digested to dryness in a mixture of 4ml $HClO_4$ and 15ml HF in a platinum crucible. 5ml of conc.HCl is added to dissolve the residue. This solution is filtered and the filtrate collected in a beaker. The filter paper and the platinum crucible are thoroughly rinsed with distilled water. The filter paper is then ignited at 800^{oc}, after which 5 pellets of NaOH are added. This is re-heated at 800^{oc} for half-an-hour and the resultant mixture is dissolved in approximately 5ml distilled water plus 3ml conc.HCl. This solution is added to the original filtrate and made up to approximately 100ml with distilled water.

The sample is then passed through a resin column. When the sample has passed through, the column is eluted with 450ml of 1.7N HCl and his portion is discarded. 600ml of 4.0N HCl are then passed through the column and the eluted portion is saved. This is evaporated to dryness.

The sample is re-dissolved in 5ml of HNO_3 and analysed in an ICP spectrometer. Blank and standard compositions were analysed to test for machine precision and 'clean' sample preparation.

3.2 Data tables

Full data tables of all the analyses carried out are given on the following page.

REE	155073	155095	DAR115	DAR105	DAR65	DAR67	DAR291	DAR325	DAR324
La	147.90	93.50	177.70	155.70	483.40	599.20	44.70	29.30	24.90
Ce	320.20	197.40	426.50	324.80	828.90	1012.80	77.80	55.20	46.50
Pr	40.46	25.00	54.25	38.10	93.89	109.25	9.62	7.15	5.92
Nd	132.90	82.20	175.50	120.20	309.40	338.20	29.70	21.50	16.70
Sm	22.10	13.32	29.68	23.13	45.89	45.80	4.49	3.36	2.54
Eu	1.95	3.84	3.30	1.61	10.67	12.30	0.64	0.68	0.54
Gd	17.02	10.14	23.10	20.82	32.79	31.41	3.66	3.24	2.51
Dy	14.12	7.77	19.92	24.13	19.49	18.62	2.50	2.49	1.83
Ho	2.85	1.56	4.05	5.39	3.80	3.74	0.53	0.56	0.42
Er	8.73	5.00	12.51	17.97	11.32	11.74	1.97	2.33	1.96
Yb	6.92	3.62	10.21	17.32	7.97	7.70	0.95	1.72	1.49
Lu	1.08	0.58	1.55	2.65	1.32	1.09	0.16	0.30	0.28

REE	DAR169	DAR168	DAR167	DAR165	DAR164	DAR163	DAR162
La	10.10	143.60	38.20	81.90	29.90	69.70	58.70
Ce	90.50	251.00	71.00	163.50	59.80	138.00	109.80
Pr	4.24	26.99	8.95	20.01	7.88	17.24	13.38
Nd	14.40	80.20	28.10	64.40	25.10	56.20	42.20
Sm	4.45	10.99	4.08	10.33	3.82	8.92	6.29
Eu	0.78	1.40	1.27	1.61	1.00	1.57	1.32
Gd	4.56	8.46	3.60	8.52	3.44	7.30	5.44
Dy	4.24	6.23	2.62	6.63	2.23	5.65	4.10
Ho	0.94	1.27	0.56	1.38	0.48	1.16	0.87
Er	3.63	4.37	2.18	4.62	1.96	3.92	3.24
Yb	3.13	2.74	1.40	3.45	1.19	2.80	2.39
Lu	0.51	0.42	0.23	0.53	0.21	0.44	0.40

APPENDIX 4

Fluid Inclusion Results

A table of homogenisation temperatures and freezing (last melting of ice) temperatures are given overleaf.

Quartz Th = homogenisation temperatures for fluid inclusions in quartz grains from the granite-gneiss and the quartzite.

Fluorite Th = homogenisation temperatures for fluid inclusions in fluorite from veins cutting unit SN5 of the North Qoroq centre.

Tm = Temperature of last melting of ice, Quartz and Fluorite as above.

Quartz Th	Fluorite Th	Quartz Tm	Fluorite Tm
108	163	-4	0
158	173	-3	0
105	213	-6	0
136	313	-3	0
98	314	0	0
145	346	-2	0
213	362	-7	-1
206	384	-6	-1
251	321	-5	-1
215	359	-5	-2
239	96	-8	-2
264	136	-3	-3
207	113	-5	0
233	114	-5	0
240	150	-2	0
247	147	-4	0
262	149		0
171	150		0
189	242		0
144	257		0
218	115		
270	160		
240	143		
172	220		
254	151		
257	204		
226	212		
168	229		
297	240		
232	232		
235	422		
160	318		
203	333		
267	357		
161	306		
188	318		
202	334		
248	289		
293	292		
227	337		
260	361		
279	139		
	105		
	118		
	120		
	154		
	161		
	169		
	170		
	123		
	134		
	138		
	113		
	156		
	157		
	162		
	160		
	152		
	156		
	132		
	273		

APPENDIX 5

Computer programming

During the thesis considerable time was devoted to the development of computer programmes to aid in the recalculation of whole-rock and mineral data. Programmes were written to recalculate the structural formulae of sodic pyroxenes (normalising to 4.00 cations and 6.00 anions), to recalculate whole-rock analyses to a 100 oxygen standard cell and to calculate Xn-Fv relationships for whole-rock XRF analyses for both major and trace elements. The programmes were written in either FORTRAN-77 on the VAX-VMS mainframe or in BBC BASIC on a BBC microcomputer. Listings of these programmes are given below.

The major programming task undertaken, though, was the automation of the Aston University Cambridge Instruments Microscan 5 electron microprobe. A combined software/hardware package was purchased by the Geology department from Cambridge Microanalysis Consultants Ltd but this was found not to work. Numerous problems were encountered and eventually the package of programmes was almost entirely re-written. Due to copyright reasons it is considered advisable not to list these programmes here as, despite the fact that they are 80% written by myself, copyright still rests with Microanalysis Consultants Ltd. A brief summary is given overleaf of some of the problems encountered and the solutions found.

Re-programming of the electron microprobe

Problem	Solution
1. ZAF corrections were not on-line because standard data was stored only in variables and hence deleted in chaining the correction programmes. Analyses were run in batches but memory restrictions meant that the biggest batch possible was ~6 full silicate analyses.	All standard data is now stored in permanent files which are read selectively for the phase definition required. Corrections are fully on-line after each analysis though the option to run a batch still remains and the theoretical upper limit is ~30 analyses.
2. Once a phase had been defined the only way to add or subtract elements was to re-define the whole phase which also entailed re-reading the standards.	The programme now recognises phase names such as 'PYRO' and recalculates the analysis to the appropriate no. of oxygens. The phases can be re-defined at any time by adding or subtracting any element.
3. Reading the standards involved manually peaking-up using control keys on the computer and watching the meter reading of x-ray counts.	This option is retained but an automatic peaking-up procedure is available scans across the peak angle and determines the new peak position.
4. If more than one count was done, the routine was to count peak, +ve bkgd, -ve bkgd/peak, +ve bkgd, -ve bkgd etc. This increases both analysis time and spectrometer wear.	The counting system is now peak, peak, peak/+ve bkgd, +ve bkgd, +ve bkgd/-ve bkgd, -ve bkgd, -ve bkgd. The count sorting programmes were re-written to sort the new format of data input.

Programme to recalculate sodic pyroxenes

BBC BASIC

```
   10 MODE0:VDU19,0,4,0,0,0:U%=0:Z%=0
   20 PRINT"                  ----------------------------------------"
   30 PRINT"                  Sodic pyroxene recalculation programme.":PRINT"
          ----------------------------------------"
   40 PRINT'"  Calculates Fe3+ by normalising to a stoichiometry of 4 cations an
d 6 anions."
   50 @%=&20406
   60 DIM OX(8),A$(1),A(9),MX%(9),MB(9),T(9),S%(9),CTN(9),U(9),U1(9),BB(9),FB(10
),RCO(10)
   70 IF U%=1 THEN CLS
   80 IF Z%=1 THEN F$=G$:GOTO 110
   90 INPUT''"Is data on file (Y/N) ",E$:IF E$="N" THEN GOTO 140
  100 INPUT'"Input the filename ",F$
  110 FILE=OPENIN(F$)
  120 REPEAT
  130 INPUT£FILE,A$,R1,R2,R3,R4,R5,R6,R7,R8,R9:GOTO 260
  140 INPUT'"How many analyses do you have ",Q%
  145 *DELETE":0.PXTEMP"
  150 SS%=OPENOUT("PXTEMP")
  160 PRINT"Input the analyses in the following format : "
  170 PRINT"Sample No.,SiO2,TiO2,Al2O3,FeO,MnO,MgO,CaO,Na2O,ZrO2"
  180 FOR I%=1 TO Q%:INPUT A$,R1,R2,R3,R4,R5,R6,R7,R8,R9:PRINT£SS%,A$,R1,R2,R3,R
4,R5,R6,R7,R8,R9:NEXT
  190 CLOSE£SS%
  200 INPUT'"Input filename for data (not more than 7 characters) ",G$
  210 SS%=OPENIN("PXTEMP")
  220 I2%=OPENOUT(G$)
  230 REPEAT:INPUT£SS%,A$,R1,R2,R3,R4,R5,R6,R7,R8,R9:PRINT£I2%,A$,R1,R2,R3,R4,R5
,R6,R7,R8,R9:UNTIL EOF£SS%:CLOSE£SS%:CLOSE£I2%
  240 INPUT'"Do you wish to process this data now (Y/N) ",V$:IF V$="N" THEN END
  250 Z%=1:GOTO 70
  260 OX(1)=R1:OX(2)=R2:OX(3)=R3:OX(4)=R5:OX(5)=R6:OX(6)=R7:OX(7)=R8:OX(8)=R9
  270 VDU2:PRINT'"* * * * * * * * * * * * * * * * * * * * * *"':VDU3
  280 VDU2:PRINT"Pyroxene recalculation by normalisation to 4 cations and 6 anio
ns"
  290 VDU2:VDU 1,27,1,69:PRINT'A$:VDU 1,27,1,70:VDU3
  300 DATA OX(1),OX(2),OX(3),R4,OX(4),OX(5),OX(6),OX(7),OX(8)
  310 RESTORE 300:FOR I%=1 TO 9:READ A(I%):NEXT I%
  320 DATA 60,80,102,72,71,40,56,62,107
  330 RESTORE 320:FOR I%=1 TO 9:READ MX%(I%):NEXT I%
  340 FOR I%=1 TO 9:MB(I%)=A(I%)/MX%(I%):NEXT I%
  350 DATA 2,2,3,1,1,1,1,1,2
  360 RESTORE 350:FOR I%=1 TO 9:READ S%(I%):NEXT I%
  370 FOR I%=1 TO 9:CTN(I%)=MB(I%)*S%(I%):NEXT I%
  380 DATA 2,2,1.5,1,1,1,1,0.5,2
  390 RESTORE 380:FOR I%=1 TO 9:READ T(I%):NEXT I%
  400 V=6/(CTN(1)+CTN(2)+CTN(3)+CTN(4)+CTN(5)+CTN(6)+CTN(7)+CTN(8)+CTN(9))
  410 FOR I%=1 TO 9:U(I%)=V*CTN(I%):NEXT I%
  420 FOR I%=1 TO 9:U1(I%)=U(I%)/T(I%):NEXT I%
  430 AB=4/(U1(1)+U1(2)+U1(3)+U1(4)+U1(5)+U1(6)+U1(7)+U1(8)+U1(9))
  440 FOR I%=1 TO 9:BB(I%)=AB*U1(I%):NEXT I%
  450 DB=(6-(AB*6))*2
  460 EB=BB(4)-DB
  470 IF EB<0 PROCHOLE
  480 DATA BB(1),BB(2),BB(3),EB,DB,BB(5),BB(6),BB(7),BB(8),BB(9)
  490 RESTORE 480:FOR I%=1 TO 10:READ FB(I%):NEXT I%
  500 @%=&2040A
```

```
510 XX=FB(7)/(FB(4)+FB(6)+FB(7)+FB(9))*100
520 YY=(FB(4)+FB(6))/(FB(4)+FB(6)+FB(7)+FB(9))*100
530 ZZ=FB(9)/(FB(4)+FB(6)+FB(7)+FB(9))*100
540 RCN=(FB(4)/(FB(4)+FB(5)))*R4
550 RCM=((FB(5)/(FB(4)+FB(5)))*R4)*1.1113
560 DATA OX(1),OX(2),OX(3),RCN,RCM,OX(4),OX(5),OX(6),OX(7),OX(8)
570 RESTORE 560:FOR I%=1 TO 10:READ RCO(I%):NEXT I%
580 WW=RCO(1)+RCO(2)+RCO(3)+RCO(4)+RCO(5)+RCO(6)+RCO(7)+RCO(8)+RCO(9)+RCO(10)
590 VDU 2
600 PRINT
610 PRINT"SiO2   "RCO(1)"       Si   "FB(1)
620 PRINT"TiO2   "RCO(2)"       Ti   "FB(2)
630 PRINT"Al2O3  "RCO(3)"       Al   "FB(3)
640 PRINT"FeO    "RCO(4)"       Fe2  "FB(4)
650 PRINT"Fe2O3  "RCO(5)"       Fe3  "FB(5)
660 PRINT"MnO    "RCO(6)"       Mn   "FB(6)
670 PRINT"MgO    "RCO(7)"       Mg   "FB(7)
680 PRINT"CaO    "RCO(8)"       Ca   "FB(8)
690 PRINT"Na2O   "RCO(9)"       Na   "FB(9)
700 PRINT"ZrO2   "RCO(10)"       Zr   "FB(10)
710 PRINT
720 PRINT"Total  "WW
730 PRINT
740 PRINT "Di= "XX
750 PRINT
760 PRINT "Hd= "YY
770 PRINT
780 PRINT "Ac= "ZZ
790 PRINT
800 VDU 3
810 UNTIL EOF£FILE
820 CLOSE£FILE
830 INPUT"DO YOU WISH TO PROCESS MORE DATA ",P$
840 U%=1:IF Z%<>0 THEN Z%=0
850 IF P$="Y" THEN GOTO 70
860 GOTO 950
870 DEFPROCHOLE
880 VDU2:VAC=(BB(4)+(DB/2))-(BB(4)*1.5):VAC=6-VAC
890 VDU 1,27,1,69:PRINT'"WARNING":VDU 1,27,1,70
900 PRINT"Insufficient Fe to normalise to 6 oxygens - all Fe treated as Fe3+"
910 IF VAC>5.95 PRINT"Analysis normalises to "VAC" oxygens"
920 IF VAC=5.95 PRINT"Analysis normalises to "VAC" oxygens"
930 IF VAC<5.95 PRINT"Bad analysis or element missing - oxygen < 5.95atoms"
940 EB=0:DB=BB(4):VDU3:ENDPROC
950 CHAIN"MENU":END
```

Programme to recalculate XRF whole-rock major element analyses to a 100 oxygen cell

BBC BASIC

```
10 REM PROGRAM TO CALCULATE CATIONS PER 100 OXYGENS FROM XRF
15 MODE0:VDU19,0,4,0,0,0:Z%=0
20 DIM A$(11),B$(1),R$(10)
30 DATA Si,Ti,Al,Fe,Mn,Mg,Ca,Na,K ,P ,Z
40 FOR I=1 TO 10:READ A$(I):NEXT I
65 @%=&01020206
70 VDU2:PRINT"XRF Analyses recalculated to a 100-oxygen cell":PRINT:PRINT
80 PRINT"     ","     "A$(1),"     "A$(2),"     "A$(3),"     "A$(4),"     "A$(5),"
"A$(6),"     "A$(7),"     "A$(8),"     "A$(9),"     "A$(10)
90 VDU3:CLS
95 PRINT'"                                                    ":PRINT"
                XRF recalculation to a 100 oxygen cell":PRINT"
   ----------------------------------------"
100 @%=&00020206
110 DIM MW(10),OX(10),MP(10),O(10),AP(10),C(10),X(10),CAT(10)
120 RESTORE 140
121 IF Z%=1 THEN CLS
130 INPUT'''"Input label ",B$
140 DATA 60,80,102,160,71,40,56,62,94,142
150 FOR I=1 TO 10
160 READ MW(I)
170 NEXT I
200 PRINT''"Input oxide wt.% in the following order ;":PRINT"SiO2,TiO2,Al2O3,F
e2O3,MnO,MgO,CaO,Na2O,K2O,P2O5":PRINT'"Press <CR> after each oxide."
205 DATA SiO2,TiO2,Al2O3,Fe2O3,MnO,MgO,CaO,Na2O,K2O,P2O5
206 FOR I=1 TO 10:READ R$(I):NEXT I
210 FOR I=1 TO 10
220 PRINT R$(I);:PRINTTAB(6)"";:INPUT OX(I)
230 NEXT I
240 FOR I=1 TO 10
250 MP(I)=OX(I)/MW(I)
260 NEXT I
270 DATA 2,2,3,3,1,1,1,1,1,5
280 FOR I=1 TO 10
290 READ O(I)
300 NEXT I
310 FOR I=1 TO 10
320 AP(I)=MP(I)*O(I)
330 NEXT I
340 REM CALCULATE CONVERSION FACTOR
350 Z=AP(1)+AP(2)+AP(3)+AP(4)+AP(5)+AP(6)+AP(7)+AP(8)+AP(9)+AP(10)
360 W=100/Z
370 FOR I=1 TO 10
380 C(I)=W*AP(I)
390 NEXT I
400 DATA 0.5,0.5,0.67,0.67,1,1,1,2,2,0.4
410 FOR I=1 TO 10
420 READ X(I)
430 NEXT I
440 FOR I=1 TO 10
450 CAT(I)=C(I)*X(I)
460 NEXT I
465 PRINT:PRINT
470 VDU2
480 PRINT B$,CAT(1),CAT(2),CAT(3),CAT(4),CAT(5),CAT(6),CAT(7),CAT(8),CAT(9),CA
T(10)
490 VDU3
500 INPUT'"MORE DATA PROCESSING ",Q$
510 Z%=1:IF Q$="Y" THEN GOTO 120
520 ELSE GOTO 530
530 END
```

Programme to calculate Xn-Fv relations for trace elements

BBC BASIC

```
   10 REM PROGRAM TO CALCULATE MASS BALANCE RELATIONS OF TRACE ELEMENTS USING
GRESENS(1967) GENERAL METASOMATIC EQUATION
   20 MODE0:VDU19,0,4,0,0,0:Z%=0
   30 DIM AW%(15),EL$(15),PPM(15),AWE%(15),B$(3),A(3),PPM2(15),WT2(15),XN(15),WT
(15),OX(15),OX2(15)
   40 RESTORE 300:FOR I%=1 TO 15:READ AW%(I%):NEXT
   50 RESTORE 310:FOR I%=1 TO 15:READ EL$(I%):NEXT
   60 RESTORE 320:FOR I%=1 TO 15:READ AWE%(I%):NEXT
   70 RESTORE 330:FOR I%=1 TO 3:READ B$(I%):NEXT
   80 PRINT'SPC(15)"**Composition-volume programme for trace elements**"
   90 INPUT''"Input sample label ",A$
  100 IF Z%=1 PROCINPUT:GOTO 140
  110 PRINT'"Input trace element contents in ppm values."
  120 PRINT"Enter the composition of the protolith first and the metasomite seco
nd"
  130 FOR I%=1 TO 15:line=VPOS:PRINT EL$(I%);:PRINTTAB(3)"";:INPUT PPM(I%);:PRIN
TTAB(10,line) EL$(I%);:INPUT PPM2(I%):NEXT
  140 FOR I%=1 TO 15:WT(I%)=PPM(I%)/10000:WT2(I%)=PPM2(I%)/10000:NEXT
  150 FOR I%=1 TO 15:OX(I%)=WT(I%)*(AW%(I%)/AWE%(I%)):OX2(I%)=WT2(I%)*(AW%(I%)/A
WE%(I%)):NEXT
  160 PRINT"Volume factor and densities for calculations"
  170 FOR I%=1 TO 3:PRINT B$(I%);:INPUT A(I%):NEXT
  180 FOR I%=1 TO 15:XN(I%)=100*(A(1)*(A(3)/A(2))*OX2(I%)-OX(I%)):NEXT
  190 VDU2:@%=&20308:IF Z%=0 VDU1,27,1,69:PRINT'"MASS BALANCE RELATIONS OF TRACE
 ELEMENTS":VDU1,27,1,70:PRINT"(Xn values in g/100g*100 derived from the general
metasomatic equation          of Gresens[Chem.Geol.Vol.2 1967 p47-65])"
  200 VDU1,27,1,69:PRINT'A$,"     FV=";:@%=&20205:PRINT A(1):VDU1,27,1,70:@%=&20
308:PRINT SPC(5);:FOR I%=1 TO 8:PRINT EL$(I%),SPC(5);:NEXT:PRINT
  210 FOR I%=1 TO 8:PRINT XN(I%);:NEXT:PRINT''
  220 PRINT SPC(5);:I%=9:REPEAT:PRINT EL$(I%),SPC(5);:I%=I%+1:UNTIL I%=16:PRINT
  230 I%=9:REPEAT:PRINT XN(I%);:I%=I%+1:UNTIL I%=16:PRINT:VDU3
  240 INPUT'"MORE DATA PROCESSING (Y/N) ",C$:IF C$="Y" THEN Z%=1:INPUT"Same samp
les, different volume factor (Y/N) ",F$:IF F$="Y" THEN GOTO 160
  250 IF C$="Y" THEN CLS:GOTO 90
  260 END
  270 DEFPROCINPUT:INPUT"Same protolith (Y/N) ",D$:IF D$="Y" THEN PRINT"Input th
e ppm values of the new metasomite":FOR I%=1 TO 15:PRINT EL$(I%);:PRINTTAB(3)"";
:INPUT PPM2(I%):NEXT
  280 IF D$="N" THEN PRINT"Input the ppm values - protolith first, metasomite se
cond":FOR I%=1 TO 15:line=VPOS:PRINT EL$(I%);:PRINTTAB(3)"";:INPUT PPM(I%);:PRIN
TTAB(10,line) EL$(I%);:INPUT PPM2(I%):NEXT
  290 ENDPROC
  300 DATA 81,80,75,186,104,226,123,266,153,270,264,223,182,152,326
  310 DATA "Zn","Cu","Ni","Rb","Sr","Y ","Zr","Nb","Ba","U ","Th","Pb","V ","Cr"
,"La"
  320 DATA 65,64,59,170,88,178,91,186,137,238,232,207,102,104,278
  330 DATA "FV ","Density of protolith  ","Density of metasomite "
```

```
C                              COMP.VOL
C
C
C
C        PROGRAMME WRITTEN BY D.A.RAE, ASTON UNIVERSITY, JUNE 1967,
C      TO CALCULATE DENSITY FROM X.R.F. WHOLE ROCK ANALYSES OR MINERAL
C      ANALYSES (AFTER THE METHOD OF BOTTINGA & WEILL [AM.J.SCI.,1970]).
C      THESE RESULTS ARE THEN APPLIED TO THE GENERAL METASOMATIC
C      EQUATION OF GRESENS [CHEM.GEOL.,1967] AND VALUES FOR Fv AND Xn
C      ARE CALCULATED.
C
C
      PARAMETER(MMAX=1000)
      REAL OX(10,MMAX),AW(10),VO(10),EX(10)
      DIMENSION AO(10),AF(10),VT(10),XM(10),XV(10),BO(10),BF(10),YM(10),
     1YV(10),XN(10),CB(10),CA(10),FVC(10)
      REAL XMS,XVS,YMS,YVS,D1,D2,B,C,DD
      CHARACTER*40 INFILE,OFILE
      CHARACTER*9 NAME(MMAX)
      CHARACTER*5 EL(11)
      INTEGER K,L,M,N
      DATA AW,VO,EX,EL/60.09,74.90,101.96,159.68,71.85,70.94,40.30,56.1
     1,61.93,94.20,26.00,21.00,37.96,52.00,12.30,14.00,11.60,16.30,28.1
     2,46.00,0.000009,0.00024,0.000026,0.000025,0.00016,0.0024,0.0021,
     30.00018,0.00024,0.00030,'SiO2','TiO2','Al2O3','Fe2O3','FeO','MnO',
     4'MgO','CaO','Na2O','K2O','FV'/
C
C      **EXPLANATION OF ARRAYS LISTED ABOVE**
C
C      ARRAY OX CONTAINS THE OXIDE WT% FROM THE ANALYSES.THE ORDER OF OX-
C      IDES IN OX IS AS FOLLOWS ; 1=SIO2,2=TIO2,3=AL2O3,4=FE2O3,5=FEO,6=
C      MNO,7=MGO,8=CAO,9=NA2O,10=K2O.
C      ARRAY AW CONTAINS THE MOLECULAR WEIGHTS OF THE OXIDES
C      ARRAY VO CONTAINS THE PARTIAL MOLAR VOLUME OF EACH OXIDE AT A REF-
C      ERENCE TEMPERATURE OF 1400C
C      ARRAY EX CONTAINS THE THERMAL EXPANSION COEFFICIENTS OF EACH OXIDE
C      AT 1400C
C      ARRAY VT CONTAINS THE PARTIAL MOLAR VOLUMES OF EACH OXIDE AT TEMP-
C      ERATURE T
C      ARRAYS (A,B)O CONTAIN THE NO. OF MOLES OF EACH OXIDE
C      ARRAYS (A,B)F CONTAIN THE MOLE FRACTIONS OF EACH OXIDE
C
C
      WRITE(5,1)
    1 FORMAT(' *D.A.RAE COMPOSITION/VOLUME PROGRAMME'/' *NAME OF INPUT F
     1ILE?')
      READ(5,2)INFILE
    2 FORMAT(A40)
      OPEN(UNIT=10,FILE=INFILE,STATUS='OLD')
      WRITE(5,3)
    3 FORMAT(/' *HOW MANY ANALYSES DO YOU HAVE?')
      READ(5,4)M
    4 FORMAT(I4)
      DO 20 J=1,(MMAX-(MMAX-M))
      READ(10,5)NAME(J),(OX(I,J),I=1,10)
    5 FORMAT(1H ,A9,10(1X,F6.3))
   20 CONTINUE
      WRITE(5,6)
    6 FORMAT(/' *NAME OF OUTPUT FILE?')
      READ(5,2)OFILE
```

```
      OPEN(UNIT=13,FILE=OFILE,STATUS='NEW')
  101 WRITE(5,8)
    8 FORMAT(/' *INPUT TEMPERATURE (FOR USE IN DENSITY CALCULATIONS)')
      READ(5,4)K
      K=1400-K
  102 WRITE(5,9)
    9 FORMAT(/' *ANALYSIS NO. OF PROTOLITH?')
      READ(5,4)L
      WRITE(5,10)
   10 FORMAT(/' *ANALYSIS NO. OF METASOMITE?')
      READ(5,4)N
      WRITE(13,7)NAME(L),NAME(N)
    7 FORMAT(///'     PROTOLITH : 'A9'          METASOMITE : 'A9)
      WRITE(13,17)(EL(I),I=1,11)
   17 FORMAT(/1X,5(2X,A5),1X,6(2X,A5))
C
C     **END OF INPUT - CALCULATE DENSITY OF PROTOLITH**
C
      DO 50 I=1,10
      AO(I)=OX(I,L)/AW(I)
   50 CONTINUE
      B=AO(1)+AO(2)+AO(3)+AO(4)+AO(5)+AO(6)+AO(7)+AO(8)+AO(9)+AO(10)
      DO 56 I=1,10
      AF(I)=AO(I)/B
      VT(I)=VO(I)*(1-(EX(I)*K))
      XM(I)=AF(I)*AW(I)
      XV(I)=AF(I)*VT(I)
   56 CONTINUE
      XMS=XM(1)+XM(2)+XM(3)+XM(4)+XM(5)+XM(6)+XM(7)+XM(8)+XM(9)+XM(10)
      XVS=XV(1)+XV(2)+XV(3)+XV(4)+XV(5)+XV(6)+XV(7)+XV(8)+XV(9)+XV(10)
      D1=XMS/XVS
C
C     **DENSITY OF PROTOLITH CALCULATED - NOW CALCULATE METASOMITE**
C
      DO 55 I=1,10
      BO(I)=OX(I,N)/AW(I)
   55 CONTINUE
      C=BO(1)+BO(2)+BO(3)+BO(4)+BO(5)+BO(6)+BO(7)+BO(8)+BO(9)+BO(10)
      DO 57 I=1,10
      BF(I)=BO(I)/C
      YM(I)=BF(I)*AW(I)
      YV(I)=BF(I)*VT(I)
   57 CONTINUE
      YMS=YM(1)+YM(2)+YM(3)+YM(4)+YM(5)+YM(6)+YM(7)+YM(8)+YM(9)+YM(10)
      YVS=YV(1)+YV(2)+YV(3)+YV(4)+YV(5)+YV(6)+YV(7)+YV(8)+YV(9)+YV(10)
      D2=YMS/YVS
C
C     **END OF DENSITY CALCULATIONS - APPLY D TO GRESENS EQUATION**
C
  103 WRITE(5,11)
   11 FORMAT(/' *WHAT VOLUME FACTOR DO YOU WANT TO USE?')
      READ(5,12)FV
   12 FORMAT(F4.2)
      DD=D2/D1
      DO 51 I=1,10
      CB(I)=OX(I,N)/100
      CA(I)=OX(I,L)/100
      IF(CB(I). EQ. 0) GO TO 106
      FVC(I)=CA(I)/(DD*CB(I))
  106 XN(I)=100*(FV*DD*CB(I)-CA(I))
```

```
51   CONTINUE
     WRITE(13,13)(XN(I),I=1,10),FV
13   FORMAT(1H ,11(1X,F5.2))
     WRITE(5,14)
14   FORMAT(/' *FURTHER RUN (DIFFERENT VOLUME FACTOR) REQUIRED ON SAME
    1 SAMPLES?'/' 0=NO ; 1=YES')
     READ(5,*)X
     IF(X. GT. 0) GO TO 103
     K=1400-K
     WRITE(13,18)K,D1
18   FORMAT(/'      TEMPERATURE (DEG.CENT.) : 'I4'       D(P) : 'F4.2)
     WRITE(13,19)D2
19   FORMAT('                                              D(M) : 'F4.2)
     WRITE(13,24)
24   FORMAT(/'  VOLUME FACTORS FOR ZERO MASS CHANGE OF EACH ELEMENT')
     WRITE(13,21)
21   FORMAT('    Si     Ti     Al     Fe3+   Fe2+   Mn     Mg     Ca     Na
    1    K')
     WRITE(13,22)(FVC(I),I=1,10)
22   FORMAT(1H ,10(1X,F5.3))
     WRITE(5,15)
15   FORMAT(/' *FURTHER APPLICATION OF GRESENS EQUATION WITH DIFFERENT
    1 SAMPLES?'/' 0=NO ; 1=YES')
     READ(5,*)Y
     IF(Y. GT. 0) GO TO 102
     WRITE(5,16)
16   FORMAT(/' *DO YOU WISH TO RUN CALCULATIONS AT A DIFFERENT TEMPERAT
    1URE?'/' 0=NO ; 1=YES')
     READ(5,*)Z
     IF(Z. GT. 0) GO TO 101
     STOP
     END
```